A study of the atmospheric corrosion of mediaeval stained glass windows in the United Kingdom

Paula Jayne Mills

D Phil Thesis

University of York

Department of Physics

1995

Abstract

In excess of two hundred specimens of mediaeval stained glass have been analysed to obtain information on their degradation. The chemical composition of the glasses and of any decay products present were determined using electron-probe micro analysis, diffuse reflectance Fourier transform infrared spectroscopy and x-ray powder diffraction.

This thesis outlines the previous work in this field and provides data for future investigations. The data collected statistically enhances the previous studies and provides evidence for and against the hypotheses in this area.

In addition to this evidence is given to suggest that the orientation of the window is an important factor in the degradation, probably due to wind direction. Also the amount of magnesia present in the glass is more fundamental to understanding the degradation than previously thought.

Contents

List of Tables

List of Figures

Acknowledgements

This work was funded by the Engineering and Physical Science Research Council.

Thanks go to the following people/organisations/councils for making the specimens of glass used in this study available. Mr J. Malleson (Fairford), Revd. P. J. C. Clements (Stanford), Very Revd. Dr. M. Higgins (Ely), Redundant Churches Fund (Fledborough), Mr. R. W. Read, Mr. G. Cook and Revd. G. A. Spencer (Heckington) and Revd. A. J. L. Hodgson (Checkley). Mr. Keith Barley of Barley Studios is thanked for making the glass from Meysey Hampton available and for supplying this and all other specimens from his workshop. I am also indebted to him and Peter Gibson for their advice and support throughout this study.

Mr. Steve Moehr kindly carried out the sample preparation. My sincere thanks to Dave Coulthard and Steve Lawson for getting me out of many a pickle with the equipment. Cheers to all the other technicians (too numerous to list) for their invaluable help. Thank you to Alan Gebbie for printing the thousand or so photographs.

I would like to thank Prof. M. R. D. Seaward and Dr. H. G. M. Edwards of the University of Bradford for their help and advice on the identification of the biological growths found on some specimens and also for proof reading the sections written thereof. (Special mention to Alistair Fitter and Anita for sending me to such helpful men).

Mr. R. Girling performed the Raman spectroscopy on the glass samples with organisms on them. A special mention to Steve, Tom, Rob and Karl for being there (sarcasm excepted).

Thanks go to Al Cox for suggesting this work, supporting it, being helpful and I hope you enjoy your retirement.

Finally I would like to thank Ian for encouraging me in the final stages and without whom it would never have been completed.

Declaration

I declare that this thesis is my own work and that the work contained within this volume was performed by myself alone.

Where work by other persons is incorporated in the interpretation of the results obtained, such work is cited.

The work presented here has not been published in any form although two papers are in press:

- P. J. Mills and G. A. Cox *Analytical Studies of Weathered Medieval Stained Glass in England*: Proceedings of Archaeometry 1994.

- P. J. Mills and G. A. Cox *Medieval Windows: What can chemical analyses tell us?*: Proceedings of Archaeological Sciences 1995.

Abbreviations

LRMH Laboratoire des Recherches des Monuments Historiques

EDTA Ethylene DiamineTetraacetic Acid

ICG International Conference on Glass

IIC International Institute of Conservation

D Durable

IP Isolated Pits

MP Merged Pits

TP Totally Pitted

U Uniformly weathered/crusted

EPMA Electron-Probe MicroAnalysis

EDS Energy Dispersive Spectroscopy

WDS Wavelength Dispersive Spectroscopy

ESF European Science Foundation

SEM Scanning Electron Microscope

ZAF matrix corrections for atomic number, absorption and fluorescence

SCB Stanford

ELY Ely

FAI Fairford

GMH Meysey Hampton

LHE Heckington

CHK Checkley

FB/FL Fledborough

FTIR Fourier Transform InfraRed spectroscopy

DRIFT Diffuse Reflectance Infrared Fourier Transform spectroscopy

SIMS Secondary Ion Mass Spectrometry

NAA Neutron Activation Analysis

AAS Atomic Absorption Spectroscopy

XRD X-Ray Diffraction analysis

XRF X-Ray Fluorescence analysis

ASTM American Society for the Testing of Materials

Γ_{LM} Group of glasses with low magnesia content

Γ_{HM} Group of glasses with high magnesia content

NBO number of Non-Bridged Oxygen atoms

ΔG Free energy of hydration

Chapter 1

Introduction

At the beginning of the twentieth century relatively little was known about the deterioration of glass or enamels. In 1917 W. E. S. Turner published a bibliography of the then previous works; it contained 95 references. Turner, as head of a glass technology department, was involved in a great many studies in the 1920s, covering such topics as chemical durability and physical properties. This work was followed in the 1930s by theoretical models of Zachariasen and Warren [144, 140, 141, 41, 104] for the structure of glass. Since the second World War the number of researchers studying glass and its deterioration has increased greatly.

1.1 Atmospheric Corrosion of Glass

One of the major reasons for studying the atmospheric attack of glass is for the preservation and restoration of Europe's heritage of stained glass windows. Several studies have been carried out in the UK, mostly centered on York Minster [36, 35, 58, 59, 105, 57, 103]. The remaining studies have principally taken place on the Continent of Europe, in France [15, 112, 111, 30], Germany [56, 72, 46, 48, 128] and Austria [5, 6, 129, 130, 131, 132] with additional work in America [21, 22, 23].

It has been established that the presence of water on the surface of glass is a key factor in its destruction. Douglas and Isard [43] showed that unless water was present, even very high proportions of sulphur dioxide will not attack the glass network. Recent work at the Deutsches Museum, Munich, has involved the monitoring of both humidity and temperature of the surrounding environment in the hope of establishing the influence these have on deterioration [49, 48, 50]. Results indicate that cycles of condensation and drying are more damaging than a constant high humidity [99, 101].

Contrary to popular belief, the smaller the amount of water present the greater the deterioration

[102]. If excess water is present, and remains present, it is possible for the extracted alkali to be diluted and hence little harm done. However, humidity is a good promoter of moss and lichen growth, which in turn can lead to corrosion of glass which might otherwise be resistant. This is because they harbour moisture at the surface and could therefore cause damage [90].

Over the last few decades there has been great concern as to whether the acceleration of atmospheric corrosion is due to air pollution. This has been very hard to substantiate, and many now believe that damage, subsequent to the second World War was caused not by air pollution but poor storage during the War [104]. In a recent paper by Cox and Cooper [32] evidence was presented which indicates that poorly durable mediaeval glasses had deteriorated prior to the increase in sulphur dioxide levels associated with the development of heavy industry. They have shown that glass which was buried in the sixteenth century had visible signs of atmospheric decay. This is distinguishable from the subsequent decay in the archaeological environment and highlights the fact that sulphur dioxide in natural occurring amounts is sufficient to explain the formation of sulphates as decay products.

Generally an alkaline solution is formed on glass as a result of water leaching out alkali and/or alkaline earth ions from the bulk glass. Sulphur dioxide, carbon dioxide and other gases may then react with this solution to form salts. The hypothesis as to the ensuing mechanism is that water reacts with glass to form hydroxides, which are then converted to carbonates by atmospheric carbon dioxide; these are subsequently changed into sulphates [41, 109, 128]. These salts are referred to as the corrosion, or weathering, products and are generally the insoluble salts that have remained after the water has evaporated or drained off the surface. Usually, the products are calcite, gypsum or syngenite [56, 15, 112, 58, 59], although several others have been reported. Gypsum and syngenite are usually found together in a form of weathering known as is crusting [14, 111].

There have been many studies which consider other types of environment. Work in America in recent years has centered on artificial corrosion, although Brill carried out a substantial amount of research on glass deterioration at the Corning Museum [21, 22, 23]. One of the areas looked at was *crizzling*. This is a common occurrence in glasses which are deficient in lime but have excess alkali. It manifests itself as reduced transparency due to crazing of the surface. Brill discovered that crizzling develops when the 'sick' glasses are stored in an atmosphere of less than 20% relative humidity.

1.2 Groundwater Corrosion

In 1863 Brewster [18] discovered the reason for the iridescent nature of the crust on an excavated glass. He noted that the crust was laminated in structure, the separation of layers being of the

order of the wavelength of light. Thus the iridescence was due to interference.

One of the most interesting theories put forward in this area was that the "time of burial could be found by counting the number of layers in the corrosion crust" [24, 21, 79]. This has since been disproved [93, 101]. Layer formation is now reasonably well understood. If the pH of the leachant is greater than 9 then network dissolution occurs [45], until the solubility of the oxides in solution reaches their limit. When this limit is exceeded, new phases may be precipitated, which regulate the pH and eH (oxidation potential) of the solution at the corrosion front in a cyclic manner. The crust formed is porous in nature and therefore allows the leachant to diffuse through it. In a glass which contains inhomogeneous regions or inclusions, the layers formed are not necessarily parallel to the glass surface [93, 106, 34].

W. von Geilmann, in 1956, studied many examples of excavated window glass, proving that a particularly deep form of corrosion was initiated by old cracks in the glass [55]. Similar findings were obtained and reviewed by Newton [94, 95]. Geilmann identified particularly high levels of manganese(Mn) in glass from the 10th to 18th centuries, in part due to the use of beechwood ash and partly due to deliberate addition. He also studied more than 100 ancient glasses and identified a high phosphorus content, again due to the use of wood ash. In his non-archaeological studies he was led to the suggestion that syngenite is converted to gypsum if there is a large amount of water present [56].

The layer structure that forms due to the action of groundwater is not usually regular, and often it is distorted by surface inhomogeneities. Cox *et al.* found inclusions or "plugs", many of which on chemical analysis contained areas rich in manganese [34, 37]. The crust formed is generally of inorganic compounds, though non-crystalline. A related topic is that of underwater corrosion [33] which produces a similar laminated structure, but the inclination for plug formation has not so far been observed on such samples. Underwater corrosion involves continuous replacement of surrounding water and hence the "in contact" solution is unable to become saturated although the solution in the reaction zone can attain saturation. Any crystalline products that result due to decay are probably not derived from the glass.

1.3 Artificial Environments

The benefits of simulation are clearly apparent in the case of nuclear waste disposal glasses, since, glass in which highly radioactive waste is to be stored must be known to be incredibly durable over a period of time like 10^4 years. Therefore to be practical, the time taken for the experiments must be reduced. This is done by elevating the temperatures, using different pH's, *etc.*.

This field of glass research that has boomed since the 1960s, with the majority of the work occuring

in Europe, the USA and Japan [64]. It is in part responsible for the increased attention being paid to glass of archaeological origin. The latter provides information on real case studies of underground corrosion, enabling a comparison to be made of accelerated testing against the results of natural corrosion, thus enabling mathematical models to be devised.

1.4 Thesis Outline

In this study the aim was to investigate the extent of decay of '*in-situ*' mediaeval stained glass windows in the United Kingdom. In carrying out such a study it was hoped that the following aspects could be considered:

- Correlation between extent of decay within the different geographical regions of the country. This would involve glass of similar chemical composition being found in different churches.
- Correlation between the extent of decay and window orientation. This requires that the glass in the windows analysed, be of the same composition and has never been moved or the panels reversed, for example, when it was restored.
- Relationship between the chemical composition of the glass and the decay products found.
- The development of the decay process. This involves comparing the decay of different types of glass, perhaps from different centuries.
- Determine whether sulphur dioxide is one of the primary attacking agents. This would not be by experimentation, but through the observation of the distribution of sulphur, probably in the form of sulphates, on the natural surface and in depth profile.

In chapter 2 what is meant by the term glass will be discussed and a critique will be given of previous work in the area of glass corrosion. The various hypotheses on glass structure will be dealt with. Results from other investigations on mediaeval glass will be presented.

In chapter 3 an outline of the theory and practice of electron probe micro-analysis will be given. This technique was used to determine the chemical composition of the glasses. The instrumentation is described and a brief summary of the results obtained (more detailed data are given in Appendix B). Also the location of the churches from which the window glass was obtained is given, with an associated background.

This is followed by two separate chapters detailing the techniques used to identify the decay products. The first is the application of diffuse reflectance infrared spectroscopy; the latter is that of x-ray powder diffraction. The data collected using both methods are given in detail in Appendix C; summaries and calibration information are given in the separate chapters.

Some of the glass analysed was investigated in a purely topographical manner. This formed the basis of the morphological study that was carried out on "sacrificable" samples from two of the churches and is covered in chapter 6.

The results are analysed in a more thorough manner in chapters 7 and 8. Here the data have been examined using the software package SPSS (Statistical software Package for the Social Scientist). It is also used as a means of testing previous hypotheses and models. Chapter 7 details the more analytical work whereas chapter 8 contains the environmental aspects such as biodeterioration.

The final chapter gives a comparison of this work to the previous studies, lists the conclusions and suggests how this study could be followed.

Chapter 2

Corrosion of Glass

An understanding of the nature of glass is needed in order to comprehend the deterioration processes. It is essential, therefore, to make clear what is meant by the term "glass". Glass is commonly used to refer to the fusion product of inorganic materials where crystallisation has not taken place [109], though this is not necessarily the case. In this study "a glass" is a material formed from silica, alkali and lime.

In antiquity there was no understanding of the chemistry of glassmaking, indeed science of the day was based upon there being only four elements. As a result, mediaeval glass has many components and in many cases is inhomogeneous. The most important literary evidence of mediaeval glass-making procedures is the treatise *De Diversis Artibus* written in the twelfth century by a monk known as Theophilus [63]. This states

> '...take two parts of the ashes and a third part sand...mix them...put them on an upper hearth so that they may be fritted'.

This illustrates the true art of the glassmaker - being able to create a transparent solid substance from buckets of powder which could vary in origin and content depending on the reliability of supply. It also shows that the process involved only two ingredients, sand and ash. The ash in the mediaeval period being rich in potassium and phosphorus indicates that wood was the source (beech ash being the most common). It was possible to produce a range of colours from the glass melt by altering the furnace conditions and Theophilus gives details. These colour changes can be understood by consideration of the redox reaction of iron and manganese (and other elements). Glass-makers of the period also added metal oxides to the melt to produce other colours [126, 51].

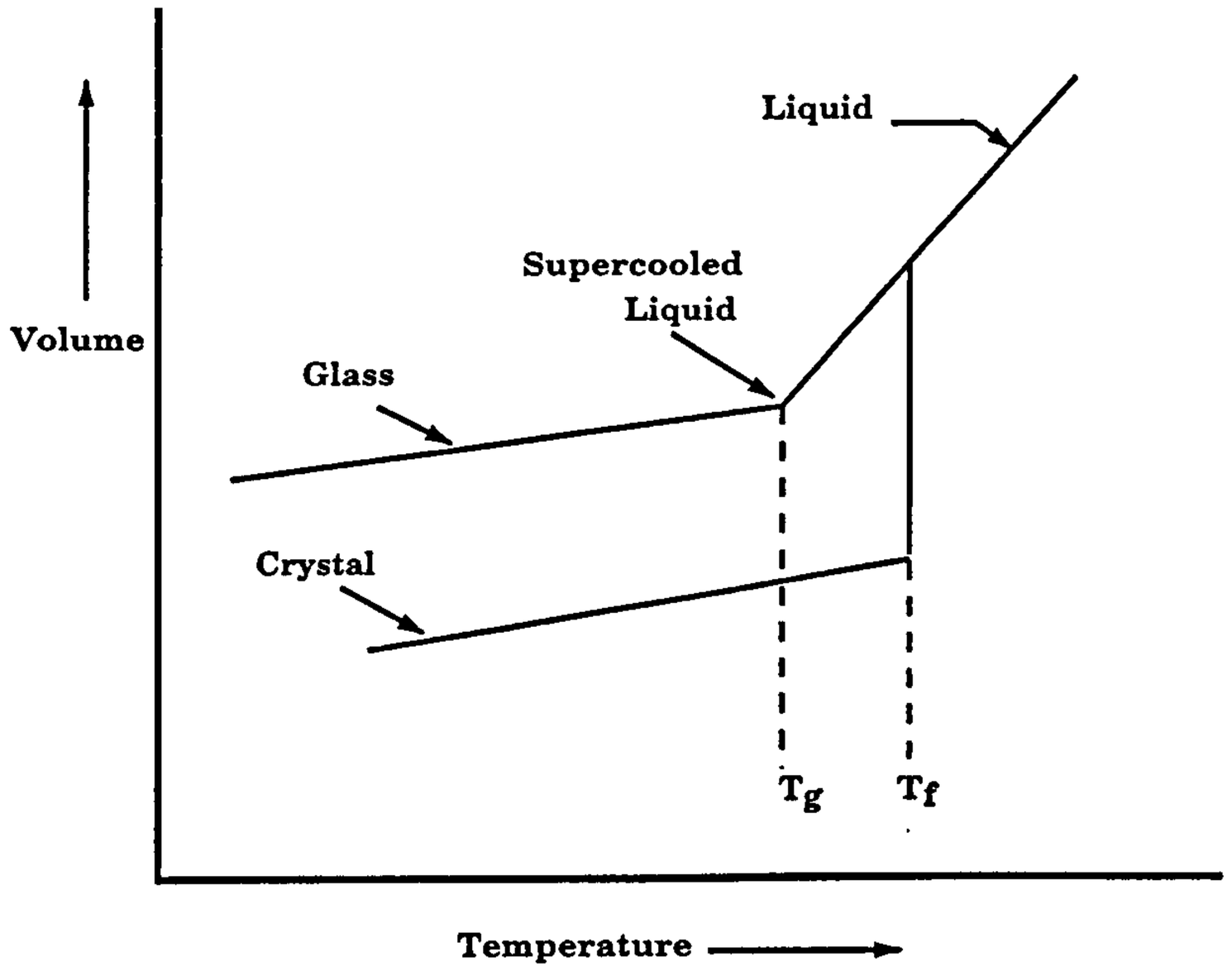

Figure 2.1: Schematic diagram of the relationship between the glassy, liquid and solid states for the temperature dependence of specific volume.

2.1 Structure of Glass

When a liquid cools its volume changes. At a temperature T_f (freezing point) the volume decreases substantially and crystallisation normally occurs. As the temperature is reduced further, the volume continues to diminish, but with a different temperature gradient. Figure 2.1 shows the deviation of the volume-temperature relationship for both crystalline and vitreous materials. When a liquid cools to form a glass, crystallisation does not occur at T_f. However, at a temperature T_g the viscosity of the melt is such that it is said to be a solid. Thus, at T_g the liquid has become a glass; this temperature is called the transformation temperature. It is more usual to refer to the transformation *range* of the melt, as the change in viscosity is gradual and thus does not occur at a fixed temperature. The temperature at which the glass was melted determines the homogeneity of the non-crystalline structure.

There are several characteristics which separate glasses and crystals:

1. X-ray and electron diffraction studies indicate that glasses do not exhibit long-range periodic order, *ie.* they have an infinite unit cell with an infinite number of atoms therein.
2. Glasses are similar in structure to liquids, *ie.* amorphous and isotropic.
3. Glasses do not have a sharp melting point, *ie.* no discontinuity in any physical property.
4. Glasses will not cleave in preferential directions.

Any liquid can in principle form a glass if cooled sufficiently quickly and brought below the transformation range. For a material to be a good glass former its rate of crystallisation must be very slow with respect to the rate of cooling. There is as yet no general empirical hypothesis to explain glass formation, but there are those with limited application.

2.1.1 Goldschmidt's Model

A simple ionic oxide, $A_M O_N$, exhibits a correlation between the relative size of A and O and its ability to form a glass [60, 109]. If an oxide can form a glass, then the ratio of ionic radii, $R_A : R_O$ is in the range 0.2 to 0.4. The co-ordination number of ionic compounds is known to be dictated by R_A/R_O and thus the geometrical arrangement is restricted. This lead Goldschmidt to propose that a tetrahedral configuration was a prerequisite of glass formation. However, the bonding in a glass is not (purely) ionic and therefore this rule does not always apply.

2.1.2 Zachariasen's Random Network Theory

This was developed from the ideas of Goldschmidt and was the first model to be universally accepted . Zachariasen postulated that the atoms in the glass must form a three-dimensional network [144]. The diffraction studies (of the time) showed that this network was not periodic or symmetrical, as is the case for crystals. He thus proposed the following set of rules:

1. The number of oxygen atoms surrounding the ion A must be small (three or four), *ie.* a small co-ordination number for the cation.

2. No oxygen ion may be linked to more than two atoms of A.

3. The oxygen polyhedra share corners with each other, not edges or faces.

4. At least three corners of each polyhedron must be shared by other polyhedra.

The above criteria are satisfied by A_2O_3, AO_2 and A_2O_5. Warren [140, 141] took this model and used it to interpret x-ray diffraction patterns of glasses. Figure 2.2 illustrates an imaginary two dimensional oxide, A_2O_3, in the crystalline and vitreous forms [109].

There are, however, limitations to this theory: it only represents an average structure and can say nothing about the local distribution of the ions. This theory is the basis for the classification of glass-forming oxides as network *formers, modifiers* and *stabilisers.* The network former in ancient glasses is silica, (although in other glass types it can be oxides of boron, lead or phosphorus). This three-dimensional network of tetrahedra with the silicon ion surrounded by four oxygen ions. This would of course give the chemical formulae SiO_4 if it were not for the fact that the four oxygen

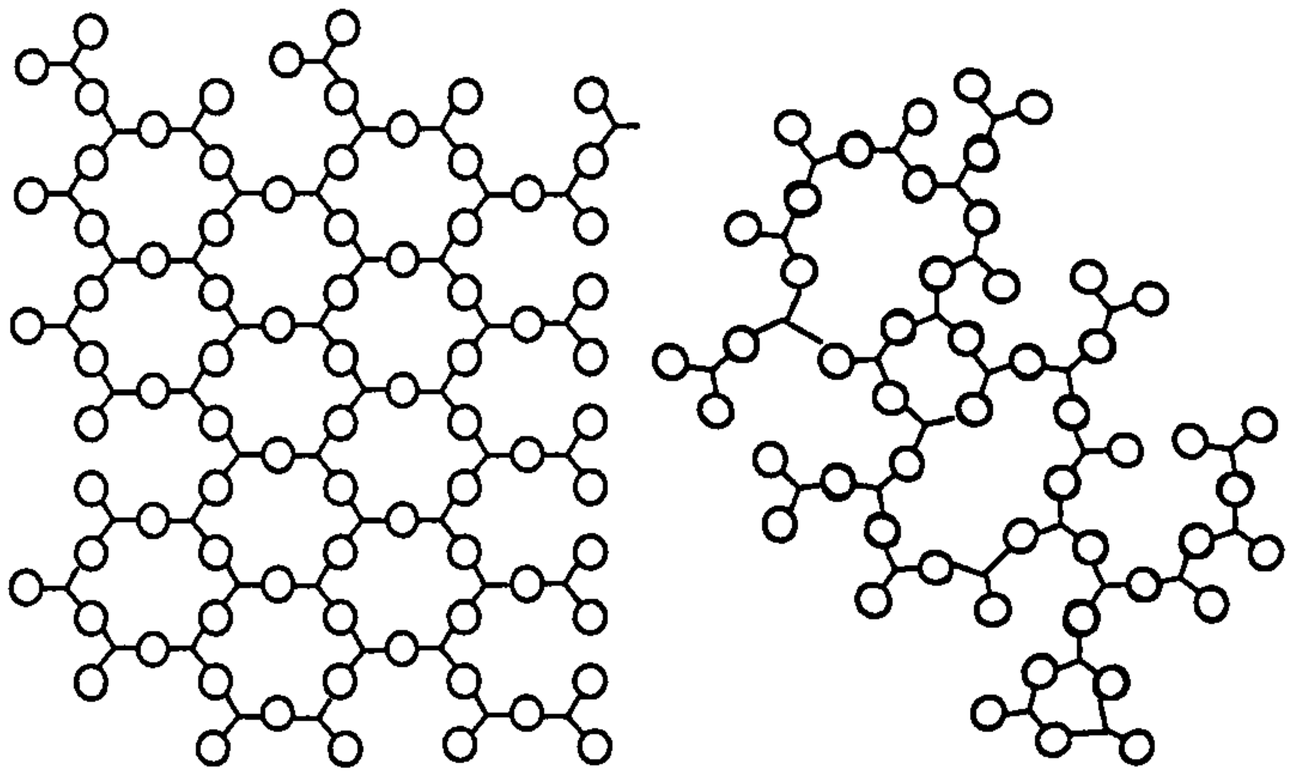

(a) Regular (b) Irregular

Figure 2.2: Schematic two-dimensional representation of the structure of (a) a hypothetical crystalline compound A_2O_3, and (b) the glassy form of the same compound.

ions are shared by two silicon ions to give the chemical formula of SiO_2. A network modifier is an ion which breaks the siloxane bonds which form the network. Figure 2.3 is a more realistic representation of a glass [135]. The network formers are black spots within triangles, which are surrounded by three oxygen ions. An oxygen ion can be either *bridging* or *non-bridging*. A bridging ion is one which is shared between two of the shaded triangles and hence forms part of the network. A non-bridging ion belongs to only one of the triangles and has a residual negative charge (as the valency of the oxygen is unsatisfied). The charge is neutralised by the positive charge of the "modifying" cations.

The modifier may have one or more positive charges, *ie.* be mono- or di-valent. A monovalent ion is usually an alkali ion, for example, sodium or potassium. These ions are quite mobile. This mobility means that the ions can be easily removed from the network, thus lowering the durability of the glass. The advantage of such is the lowering of the melting point. A divalent ion is more strongly bound to the glass structure and therefore is less mobile. However, they can neutralise two of the charged oxygen ions and hence forge new links in the network. A network stabiliser can be a former or a modifier; they are usually tri-valent ions. Alumina (Al_2O_3) is the most important stabiliser when considering ancient glass.

2.1.3 Alternative Hypotheses

Stevels developed the idea of using non-bridging oxygen ions to define a structure parameter, 'Y factor' [135]. As the number of network modifiers increases, the Y factor decreases. For a silica

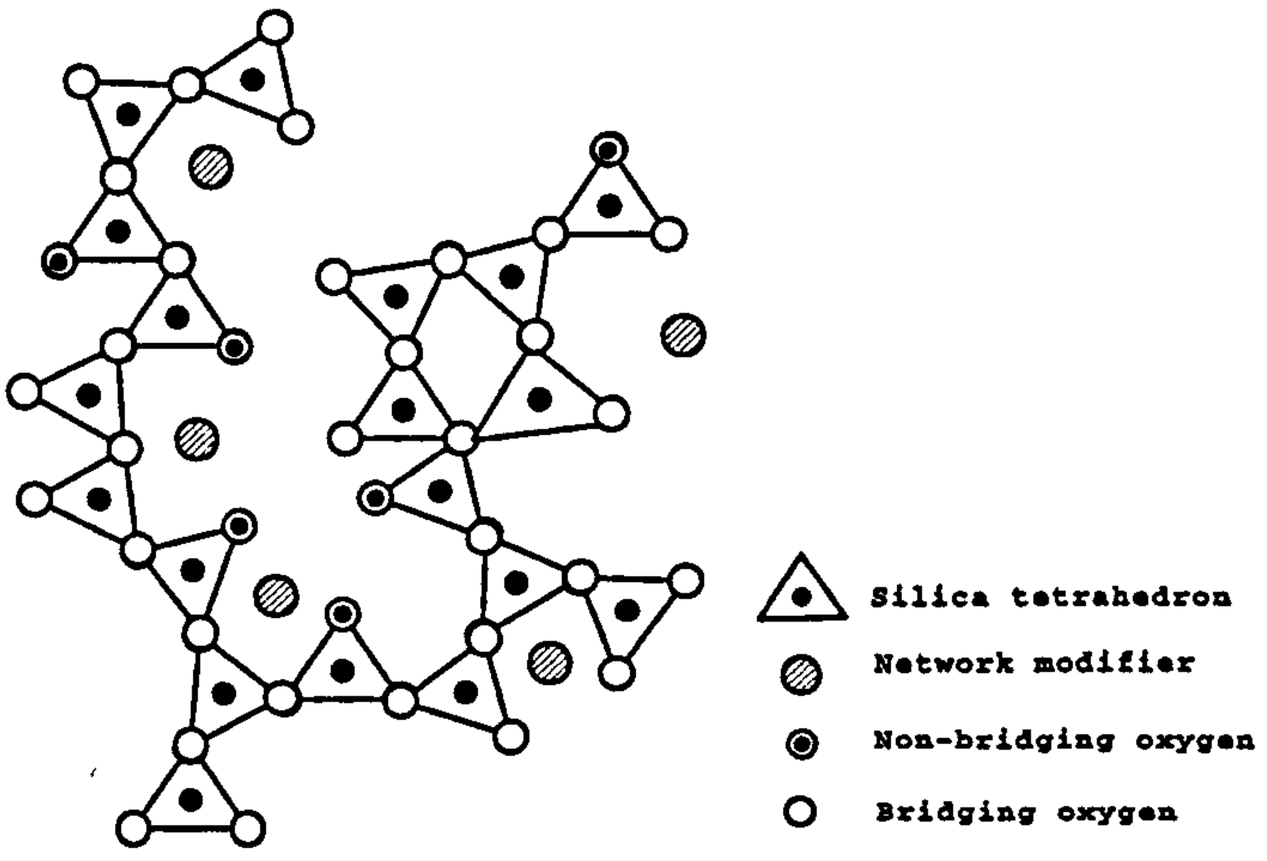

Figure 2.3: Schematic representation of a glass network.

glass Y=4, but for $A_2O.SiO_2$, Y=2. A strict interpretation of Zachariasen's theory suggests that glasses with Y<3 do not exist. Stevels, however, succeeded in forming glasses with Y below 2, which are now called invert glasses.

A Russian school developed a glass formation theory called "the crystallite hypothesis". This commenced with the work of Lebedev [120, 128, 121]. It is based on the idea that a glass is made up of small crystalline domains (crystallites) which have an ordered structure within themselves, but together give an overall random structure. There is no longer any support for this hypothesis as diffraction studies have reduced the possible size of the crystallite to be of the order of a silica tetrahedron.

Despite this, the theory has had some successes and in conjunction with Zachariasen's should form a good base for an overall theory of glass structure.

2.2 Mechanisms of Glass Decay

The alkali ions present in glass are prone to extraction if the glass surface is brought into contact with an aqueous solution [109]. The resistance of glass to such attack is known as "chemical durability" and, if water and atmospheric gases or soil are present, the type of decay is said to be *weathering*. The extraction of alkali leaves a silica-rich, leached layer at the surface, often termed a hydrogen glass. The thickness of this layer depends upon environmental conditions such as pH, time the leaching solution is in contact *etc.*

Charles proposed a possible mechanism for this aqueous attack on glass [27].

1. Penetration of a proton from the water into the silica network, replacing an alkali ion :

$$\equiv Si - OR + H_2O \rightleftharpoons \equiv Si - OH + R^+ + OH^- \tag{2.1}$$

2. The hydroxyl ion in solution disrupts the siloxane bonds:

$$\equiv Si - O - Si \equiv + OH^- \rightleftharpoons \equiv Si - OH + \equiv Si - O^- \tag{2.2}$$

3. The non-bridging oxygen formed in equation 2.2 interacts with a molecule of water giving an hydroxyl ion which is free to repeat the previous process:

$$\equiv Si - O^- + H_2O \rightleftharpoons \equiv Si - OH + OH^- \tag{2.3}$$

The first equation, however, is thermodynamically improbable. Thus, an alternative hypothesis was put forward by Scholze [127, 128].

$$\equiv Si - O - Si \equiv + H_2O \rightarrow \equiv Si - OH + HO - Si \equiv \tag{2.4}$$

This is an auto-condensation reaction which is well known to apply to vitreous silica. Analogously, Scholze states that the dissolution of silicate glasses in alkaline solution is expressed by:

$$\equiv Si - O - Si \equiv + OH^- \rightarrow \equiv Si - OH + \equiv Si - O^- \tag{2.5}$$

and

$$\equiv Si - O^- + H_2O \rightarrow \equiv Si - OH + OH^- \tag{2.6}$$

If the solution is acidic then:

$$\equiv Si - O^- Na^+_{(g)} + H^+_{(l)} \rightleftharpoons \equiv Si - OH_{(g)} + Na^+_{(l)} \tag{2.7}$$

ie. an ion-exchange reaction takes place.

Ernsberger concluded that the proton transportation could not occur by an ion-exchange mechanism and instead advocated that the proton is diffusely transported as part of a water molecule [46]. This is the more favourable explanation, since the field intensity of a lone proton is too great to exist in condensed matter.

Douglas and Isard [43] investigated alkali extraction from a soda-lime-silicate glass. They were able to prove that the amount of sodium removed from a glass varies as the square root of time, thus indicating a diffusion process [1]. If this were correct, then it should be experimentally demonstrable, as the rate of extraction would be related to the electrical conductivity. Douglas and Isard assumed that below the softening temperature of glass, the silica network ions were fixed in position and the sodium ions were able to move from a site to a neighbouring one on acquiring a definite activation energy, E. Therefore, the passage of electric current through the glass would be

solely due to sodium ions. In order for the glass to maintain electrical neutrality a contra-diffusion of hydrogen ions must occur, or else an electric double-layer would form, rapidly bringing the process to a halt [119].

They performed several experiments in which the electrical conductivity was measured as a function of time. The result for aqueous leachants was that the rate-controlling process was indeed diffusion. However, the mathematics of double-diffusion illustrates that should the sodium ions be considerably slower than the hydrogen ions, the apparent diffusion constant is approximately twice that of sodium, giving a discrepancy factor of three between theory and experiment. They deduced that this meant not all the sodium ions were involved in diffusion, in agreement with other authors' observations, such as Lyle [84].

Douglas and El-Shamy [42] studied the leaching rates of powdered glasses in aqueous solutions. They looked at both soda-lime and potash-lime silicates, and concluded that:

- For short time periods and low temperatures the amount of alkali, Q, leached out was proportional to the square root of time.
- For long time periods and high temperatures the amount leached varied linearly with time.

This gives the overall equation:

$$Q = a\sqrt{t} + bt \tag{2.8}$$

where Q is the amount of alkali extracted, t is the time and a and b are empirical constants.

2.3 Factors Affecting the Durability

The chemical durability of a glass is conventionally taken to mean the resistance of glass towards attack by aqueous solution and atmospheric agents. There have been many methods established to measure the durability of glasses, though they can only indicate the *relative* durability.

2.3.1 Surface Area

The importance of surface area exposed to high humidity or aqueous solutions has been known for some time, namely that large panes of glass should not be stored face to face in damp conditions [97]. In durability studies it is usual first to grind the glass to a size such that its surface area is proportional to its weight [109].

The surface area exposed is needed to calculate the surface area to volume ratio (SA/V). Dimbleby and Turner [40] were led to the suggestion that the amount of alkali removed from the glass varies

with the SA/V ratio. The reason for this was later found to be due to the pH change and not the actual SA/V [45].

Sanders *et al.* [125] carried out an experiment which led them to the following classification of glass surfaces:

Type I surface is extremely thin, though no significant change in composition has occurred.

Type II surface is one which has its silica network intact, but has been leached of alkali.

Type IIIA surface has a double protective film due to the presence of aluminium or phosphorus oxide in the glass.

Type IIIB surface is multilayered. The multiple protective layers are of oxides, hydroxides and hydrated silicates, but this is only found with complex nuclear waste glass.

Type IV has a silica-rich film though not sufficient to protect the underlying glass; this is due to rather low silica content. Most mediaeval glass is of this type.

Type V is soluble and can have a marked ability to form pits.

2.3.2 Temperature

As most experimental corrosion studies are carried out at elevated temperatures, the dependence of durability on temperature must be known. According to Paul [109], workers have likened the temperature dependence to the Arrhenius equation:

$$A = B \exp(\frac{-E}{RT}) \tag{2.9}$$

A being the specific reaction rate changing with temperature T; B a constant; E the activation energy and R the universal gas constant.

The equation is difficult to apply as both reaction constants, a (activity constant) and K (equilibrium constant), are temperature dependent:

$$Q = Kt^a \tag{2.10}$$

where Q is again the amount of alkali extracted and t the time.

2.3.3 Nature of Leaching Solution

El-Shamy studied the effect of frequency of leachant replacement [44]. In the depolymerisation reactions of silica the essential step is the breaking of the siloxane bond, Si-O-Si. Budd [26]

investigated the nucleophilic-electrophilic attack of the silica network. He concluded that acids such as hydrochloric and hydroiodic will attack the bridging oxygen atoms as well as the silicon atoms, though the latter type of attack is almost negligible. Hydrofluoric acid however, attacks both strongly.

An alkali-silicate glass, in pure water, changes the pH depending upon the alkali concentration and the alkali-silica ratio. The result of many investigations shows that silicate glasses are particularly susceptible to decay when the pH is above 9. That is, the rate of extraction of silica from a glass increases with the pH of a solution above this pH level. The thermodynamic prediction of this was verified by El-Shamy *et al.* [45]. The conclusions were:

pH less than 9, alkali and silica extraction at constant rate and independent of pH.

pH greater than 9, alkali extraction decreases but silica extraction increases with increasing pH.

If the lime content is greater than 10mol%, then the rate of alkali extraction will increase rapidly with decreasing pH below 13. The extraction of silica is opposite in manner to that of alkali.

2.3.4 Glass Composition

This is indeed the major factor affecting glass durability. The rate of alkali extraction will decrease when the amount of alkali in the glass has decreased. The diminishment of ionic radius has a similar effect, as does a decrease in the amount of silica, in comparison to alkali, in the glass.

Several studies of glasses, with simple binary/ternary compositions in contact with various solutions and at different temperatures have been carried out, especially in the field of nuclear waste disposal glasses. These cannot as yet be readily compared to the natural corrosion of complex glasses, as binary glasses are far removed from mediaeval glasses.

The addition of lime to a binary glass (sodium silicate) can have a profound effect on the durability. If the amount added is less than 10mol%, then the time taken to extract a certain amount of soda is increased [109]. If the amount added exceeds that limit, then there is no difference in extraction time from that of the ordinary binary glass.

As defined earlier glass is made up of a silica network with modifiers, stabilisers and formers [104]. A network former has the same role as silica, a modifier will break up the silica network forming ionic bonds and a stabiliser can take either role. If the silica content falls below about 60mol%, then the decay that occurs is more likely to be crusting [119]. There has not yet been a study into the effect that the trace elements present have on the deterioration. It is, however, generally thought that the elements introduced as colourants, whether purposefully or not [98], play little or no part in the decay process.

A simple theory for the prediction of relative durability was put forward by Illife and Newton [67, 68]. This was welcomed initially as it provided a means of estimating the durability on a purely compositional basis, via the number of network formers and network modifiers. The simplicity of this theory is its weak point, ie. the assumption that all components can be placed into one of three categories ('SiO_2','RO','R_2O'). In this theory there is no way of accounting for the different effect sodium and potassium have on the durability (soda glass being approximately twice as durable as a potash glass, all other components being the same).

An alternative theory of data reduction is based on thermodynamics. The essential feature is that the more positive the free energy of hydration then the more durable the glass. This was developed by Paul [108] in 1977 to predict the durability of glass, though Jantzen and Plodinec [69] took it a step further to link it to glass structure and the number of non-bridged oxygen ions.

Mixed alkali effect

Gradual substitution of one alkali ion by a different alkali ion can lead to a binary glass displaying non-linear behaviour in some properties. It is usual to refer to this effect when substituting some of the alkali ions with other alkali ions, or reducing the silica content to incorporate the alkali ions of a different type. A dramatic effect is seen in the variation of electrical conductivity when, say, a soda-silicate glass has some soda replaced by potash (see Figure 2.4 taken from page 162 of [128]) - the conductivity increases very rapidly. This change in conductivity arises out of the change in ion mobility. Ion mobility is a key factor in the dissolution of the silica network and therefore one should expect a change in the durability of a glass as result.

For instance, the durability is affected to the extent that a glass with 3mol% K_2O and 12mol% Na_2O will be twice as durable as one with 15mol% Na_2O (this is an effect due to both alkalis being present and should not to be confused with the earlier statement that soda glass is more durable than potash glass).

The *mixed alkali effect* is only measurable when the total alkali content is about 10mol%; it also decreases with temperature and is not limited to alkalis. The latter would suggest that the effect be renamed the *mixed oxide effect* [128].

2.3.5 Phase Separation

The phase structure of glasses has a significant effect on their physical properties. The addition of oxides to the glass melt, or heat treatment during melting, can alter the magnitude of phase separation within a glass. The addition of alumina to a soda-lime-silica glass reduces its tendency

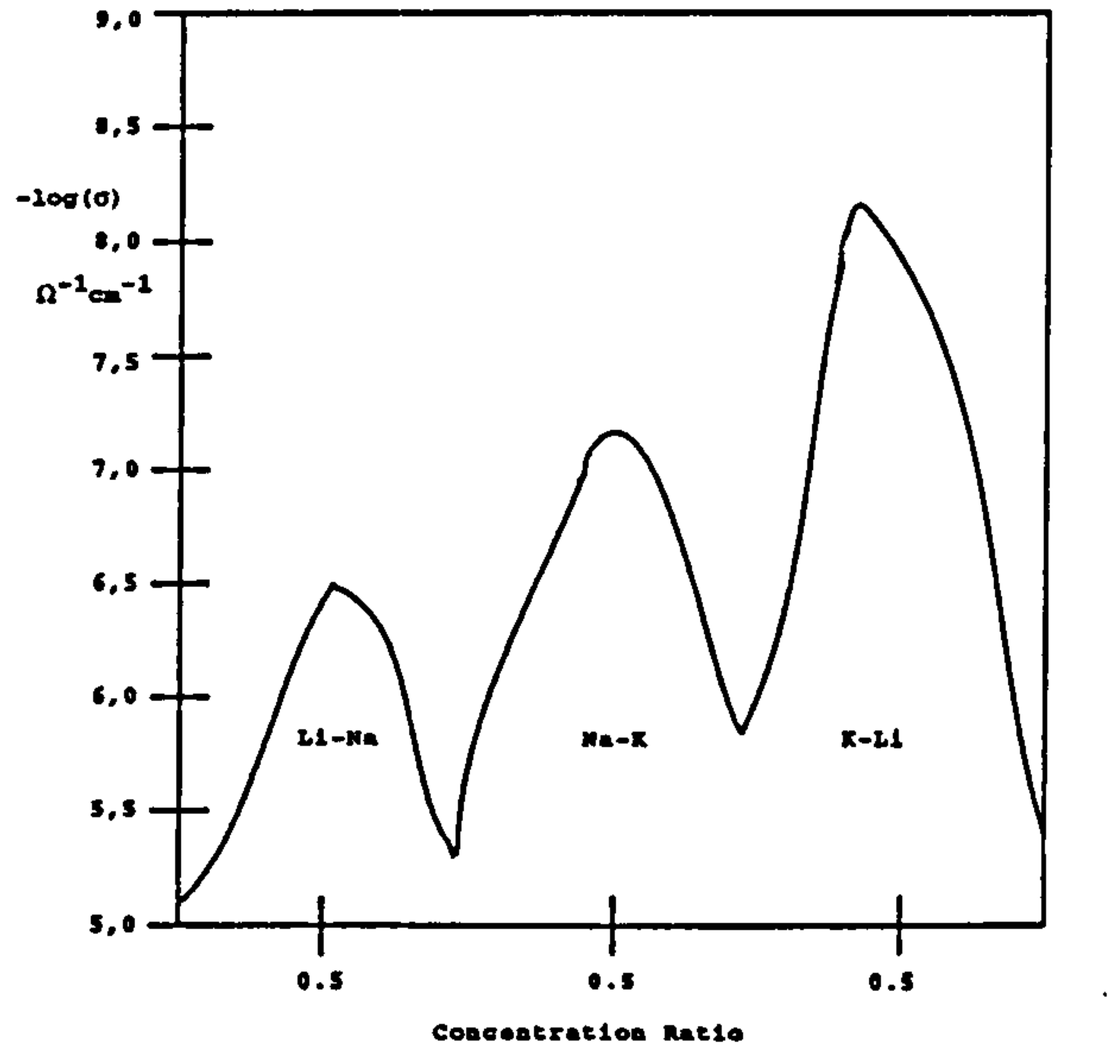

Figure 2.4: Illustration of the influence of the mixed alkali effect on electrical conductivity in an alkali-silicate glass.

to phase separate. Various studies have been carried out to investigate phase separation of multi-component glasses and these are reviewed by Doremus [41].

2.3.6 Other Factors

There are two more factors to be mentioned, though neither of great importance. It has long been known that solarisation of mediaeval glasses can and does occur. The overall effect this has is a change of colour; a tint development. The other factor is a more modern aspect - vibration. It is thought that shock waves set up by aircraft flying at Mach number 1, or above, can cause damage to stained glass windows. The flying of supersonic aircraft at low altitudes was permissible in 1954 but is now forbidden.

Another manifestation of deterioration is the development of dark inclusions within the glass. These are due to the solarisation of manganese. Mueller [92] advocates that dissolving the Mn compounds in an acid medium revitalises the glass. This will only work if the compounds are at the surface.

2.4 Atmospheric Attack

There are an infinite number of decay types observed although they are generally categorised as the following [111]:

unweathered surfaces are those that are apparently undecayed. The glass remains smooth and shiny in appearance, even though the outer layers have been chemically altered.

pitting is the formation of small circular craters in the surface. These can remain isolated or increase in size and number until they merge. This could ultimately lead to holes in the glass, or an overall thinning of the glass making it much more fragile.

crusting is when the surface becomes coated with an opaque layer of crystalline corrosion products. This usually occurs when the lime content is high and the silica content low.

It has been found that pitted glasses have gypsum and calcite as the major corrosion products, whereas on crusted glasses syngenite is also present [112, 58, 59, 132]. It is also possible that amorphous hydrated silica may be present. Figure 2.5 illustrates the forms; biological corrosion *eg.* due to lichen is represented in Figure 8.1.

Chen *et al.* [28] performed controlled experiments on sodium disilicate glasses, varying the temperature and humidity; this was similar to the earlier study by Sanders and Hench [124]. The results indicated that sodium ions were drawn out of the bulk glass. When at the surface, the alkali ions (and alkaline earth ions, such as Ca^{2+}, would also have been leached had they been present) can react with atmospheric gases such as carbon dioxide and sulphur dioxide. Protons or hydronium ions from the water replace the alkali ions in the glass.

2.4.1 Studies carried out in Britain

Cox *et al.* studied mediaeval glass from York Minster (YM) in 1977 [36]. The glass analysed in the study (more than 200 pieces) was from the 12th to 15th centuries, with two samples from the sixteenth. In order to broaden their investigation they included glass from the cathedrals of Ely, Canterbury and Coventry, along with another Yorkshire church (Thornhill). The individual sample totals from each site, except YM, were insufficient to draw any conclusive proof of climatic variations affecting the corrosion.

They classified the samples by corrosion type from unweathered to surface fractured. The glasses were analysed quantitatively using energy-dispersive x-ray fluorescence (XRF) and the conclusions included the now well-documented fact that mediaeval glasses with a silica content in excess of 60mol% will not weather appreciably. They found that pitted glasses could have less than 60mol% 'SiO_2' and crusted glasses generally have 'R_2O' above 13mol%, if the 'SiO_2' is greater than 60mol%. They also noted that the later the glass (within the Middle Ages), then the smaller the amount of magnesia within the glass; a drop from 8 to 11mol% to only 5.7 to 4.5mol%.

Further research into the YM glasses was undertaken in 1986 by Gillies and Cox [58, 59]. This

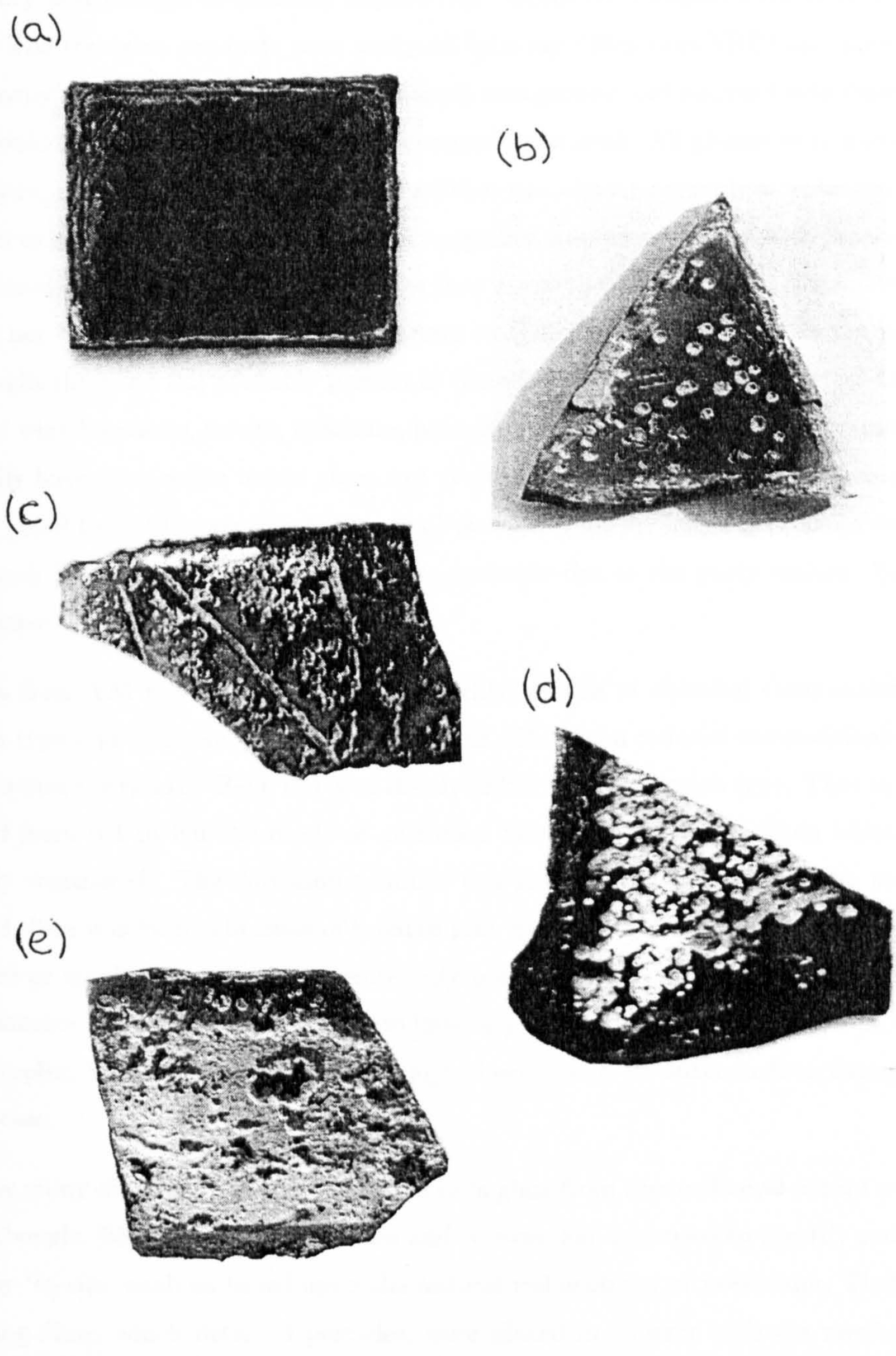

Figure 2.5: Photographs illustrating forms of decay: (a) durable (b) isolated pitting (c) merged pits (d) totally pitted and (e) uniformly weathered.

detailed study of over 60 pieces from the Minster was supplemented by 8 and 10 samples from Canterbury and Carlisle cathedrals, respectively. Again the samples were 12th to 14th century in date. The corrosion products were analysed by x-ray diffraction(XRD) and atomic absorption spectroscopy(AAS). The actual glass had a small area ground and polished with diamond paste, so that it could be analysed by XRF, to give compositional data. All glasses were found to be of the potash type, except one from Canterbury, and that was almost certainly a replacement piece. The major decay products were mainly gypsum, syngenite, and an unusually high proportion of silica. The explanation for the presence of silica was that it was the remains of the silica network, however this had not been reported by any other group at the time. It was stated in the papers, that it was thought the silica was probably present in the other analyses, but unreported. Other minerals identified were bassanite, calcite, epsomite, palmerite and barytes. Some of these minerals did not necessarily have their origin in the glass, but could instead have been due to external agents such as putty (used to seal the glass to the leading) or wash from the building. Calcite was likely to be due to wash from the building, palmerite was probably due to the putty sealant. Barytes was an isolated case.

The data from YM was analysed more thoroughly; graphs of chemical composition versus both corrosion type and corrosion product were plotted. The mean reduced compositions of the glasses suggested that the ratio of 'R_2O/RO' was closely linked to the corrosion type. That is, as 'R_2O/RO' increased from 0.4 to 0.6 the mode of corrosion became more severe; from isolated pitting to uniformly weathered. The corrosion product was found to be linked with the mode of decay. Hydrated silica was formed in cases of isolated pits, gypsum/bassanite/calcite was present in cases of merged or totally pitted and syngenite only present if the sample were uniformly weathered. The uncommon products did not appear to have any link with composition or mode of decay. One of the samples, YM499, had evidence of biological activity on its outer surface, though this was an isolated case.

An earlier study discovered that durable blue soda glass from the mediaeval period was not as rare as once thought [35]. Prior to this Hudson and Newton [66] had tried to identify soda and potash glasses by '*in-situ*' analysis based upon the natural radioactivity of potassium. That is, radiation monitoring films, which detect β particles, were placed in contact with the mediaeval glass. If left for a long enough period (two months) the film could be developed and would provide useful data on the decay of ^{40}K isotope (the radioactive isotope of potassium which occurs naturally as 0.0118% of K and has a half life of 1.28×10^9years). Thus a soda glass would give a different result to a potash glass. They detected only three blue soda glasses. The result of the Cox and Gillies work indicated that much more of the durable blue glass was soda based, and that it probably contained recycled Roman glass.

In 1988 Fuchs and Newton [105] analysed twelve samples of YM glass by electron-probe microanal-

ysis (EPMA), which were to be used subsequently in the testing of protective resins. Each sample was half-coated in a particular resin so as to leave the other half exposed to the environment and enable more accurate comparisons. In order to assess the weathering that occurred they did not use Illife and Newton's triangular diagram but the more recent Free Energy of Hydration (ΔG) method. ΔG is calculated from the chemical composition. The composition must be expressed in terms of molar percentage oxide and then each component is assumed to be related to an amount of silicate rather than oxide. The energy of hydration for the silicate is found from tables [69] and multiplied by the molar percent present in the glass. These individual values are summed to give the total ΔG. The overall outcome of the study was that ΔG values was a significant predictor for durability [105].

2.4.2 Studies carried out in Germany and Austria

A group of workers at the Deutsches Museum [49, 48, 50] performed an extensive study of stained glass within the Federal Republic of Germany. The aim of the study was to investigate the condition of preservation of German stained glass and at the same time compile an atlas which could be used to enhance study of the nature and extent of glass decay. Various panes from 45 different locations were included in the "damage atlas". There were no general means of selecting the panes for documentation, other than they were those which were 'out for restoration' during the period 1977-80. A one-year study of the temperature, relative humidity and rates of emission of gases (SO_2, Cl^{-1} and F^{-1}) was carried out at half of the chosen sites. The major corrosion products identified were gypsum, syngenite, silica and calcite. Their work has recently been published with added colour-coded diagrams [49, 50]. The conclusions were:

- Glass from the same original glass-workshop decays differently depending on the location.
- Mediaeval glass is more decayed than either Roman/Saxon or Renaissance (post fifteenth century) glass.
- Air pollution and high humidity accelerate corrosion.

In 1986 Fitz studied air pollutants and whether they attack glass [48](this formed part of the Deutsches Museum work). In laboratory experiments Fitz found that when the relative humidity is below 20%, then even high amounts of SO_2 do not result in corrosion. He also found that there was a correlation between the emission rates of acid pollutants and the state of preservation of the glass. His conclusion was that air pollution is responsible for the increase in the degradation of stained glass within the last century.

W. von Geilmann performed many glass studies, but one particularly relevant investigation was of non-excavated ancient glass [56]. He found the essential products to be a mixture of silica and

potassium/calcium sulphates. The latter is the double sulphate, syngenite $K_2Ca(SO_4)_2.2H_2O$, identified by XRD. He also stated that increased pollution was the reason for the observed increase in decay. In a study of early glass, he attempted to correlate the chemical composition of the glasses to the composition of various wood-ashes with little success [55].

Ferrazzini [100] reported that inhomogeneities and surface cracks on the glass led to rapid local deterioration. This work was reported by Newton [95] at the Kyoto ICG Congress. Ferrazzini is also noted for the hypothesis that the ion exchange process, (invoked to explain the corrosion mechanism) is due to a "tunnelling effect". This, however, has no supporting evidence.

Marschner has done a great deal of work on the testing of protective resins as well as on the morphology of glass deterioration [88]. She is credited with the discovery that pits form initially as small defects below the surface, which grow upwards to the surface and then spread until they eventually cover the entire surface and hence form a crust of decay products (the natural surface having been eaten away). The decay products were identified as gypsum and syngenite by the "mapping" of the various elements in cross-section (see section 6 for details of this method).

This leaves two major authors to be mentioned, Bacher and Schreiner. Bacher was a firm believer that Austrian glass corroded differently to that anywhere else on the Continent of Europe. He found that glass '*in-situ*' in Austria corroded by forming an opaque crust on its surface. So sure was he of this 'unique' aspect of the Austrian atmosphere, that when visiting the 'tiny Parish church of Kirby Wharfe, Yorkshire' [5](which had had some Austrian glass installed relatively recently) he was surprised to see that the glass had continued to corrode in the same manner. This mystery was solved when *crusted* samples of glass were identified at York Minster; thus it was not due to the Austrian atmosphere, but the glass composition [36]. Bacher was one of the many to speak against the theory that air pollution or humidity are the sole causes of external degradation of stained glass.

Schreiner [129, 130, 131, 132] analysed a limited number of mediaeval glasses (window and vessel) using Scanning Electron Microscopy (SEM), Secondary Ion Mass Spectrometry (SIMS) and Neutron Activation Analysis (NAA). He advocates an ion-exchange mechanism and claims that since beechwood ash has 0.1–0.5wt% Fe and Mn, then glass made from this can be any colour other than red, without the need for added colourants, by manipulating the furnace environment. He concluded that the below-surface inhomogeneities, as well as atmospheric attack, were the reason for the particular type of deterioration, ie. pitting, crusting. Even in the cases of "apparently unweathered" surfaces, he found a large depletion of network modifiers and an increase in hydrogen near the surface.

2.4.3 Studies carried out in France

Most of the French work has been based at the Laboratoire des Recherches des Monuments Historiques (LRMH), with an associated group at Laboratoire de Chimie Appliquée de l'Etat Solide. The head of the LRMH is Jean-Marie Bettembourg and most of their work is published under his name or the collective title of LRMH. His (their) major findings were related to the protection of stained glass. In 1976 he announced that sulphur dioxide in the air did not attack glass, but the corrosion products already formed thereon [13]. In 1980 he more aggressively stated that moisture was the key attacking agent and emphasised the need for protection. Many cleaning methods and protective coatings were tested and developed by Bettembourg. Two solutions (A and B) were developed at LRMH. They are sodium salts of EDTA (ethylene diaminetetraacetic acid) which dissolved the adhered sulphates from the glass surface [14]. These solvents were said not to damage the underlying glass and thereby left the surface intact. Subsequent to cleaning, the glass would need a protective coating to prevent further damage.

In 1976 Bauer [10] investigated numerous cleaning methods, including the two solutions put forward by Bettembourg. The tests looked at the ability of the solution to remove the corrosion products whilst not damaging the underlying glass. Solution A (10% $Na_2S_2O_3.5H_2O$ and 5% $Na_4P_2O_7.10H_2O$) passed the tests but, solution B (3% EDTA and 3% NH_4HCO_3) failed as it tended to loosen the paintwork. The Bettembourg solutions were tested alongside other methods such as airbrasive and acid polishing. Bettembourg, in 1974, presented a paper at the IIC congress in which he gave details of an external glazing experiment carried out at Saint Père de Chartres. Condensation and humidity were found to be very important, especially if the gap between the original window and its glazing was not ventilated [16].

In 1975 LRMH worked in association with Perez-y-Jorba [113] to analyse mediaeval French glass using a variety of techniques. The results from XRD analysis revealed thirteen different crystalline phases:

- gypsum
- syngenite
- quartz α and β, these are obviously of external origin as the transition from glass network to crystalline quartz is energetically unfavourable.
- calcite
- 5 unidentified
- 3 unidentified, which were specific to d'Evreux grisaille.

The most frequent corrosion products were the hydrated sulphates with syngenite appearing if the base glass had more than 16% potassium oxide by weight. They also showed that glass composition was the predominant factor affecting corrosion and was directly related to the morphology of the corrosion. That is, whether the pits formed initially, progress to merging and then to the uniform crusting of the glass depends upon the composition.

Perez-y-Jorba *et al.* [111, 110] studied the effects of micro-organisms on mediaeval glass. The resulting biological corrosion was characterised by concentric striations at evenly spaced intervals and calcium oxalate was a decay product. Chemical analysis showed that there was an associated migration of calcium and phosphorus. A problem they discovered was that the type of bacteria affects the decay that results, and hence the products. That is, ferro-bacteria will metabolise manganese whereas sulpho-bacteria localises sulphur and iron.

Recent excavations in France have improved the number of glass 'wares' (vessel and window glass) available for analysis. These glasses have been analysed to obtain chemical compositional data (they date from the 10th to the 18th century), but no information is given on the state of preservation [9].

Very recently the LMRH have collaborated with Libourel and some German workers to look at the deterioration of glass at Saint-Gatien de Tours and Sainte-Catherine d'Oppenheim. No detailed information has been published, though the preliminary data confirms all previously respected hypotheses [82].

Chapter 3

Electron-Probe Microanalysis

The technique of electron-probe microanalysis is possibly the most established method of glass analysis although the more modern techniques of neutron activation analysis and inductively coupled plasma mass spectrometry are gaining popularity. It must be noted however, that these techniques provide different information.

This technique allows non-destructive analysis of a sample to a spatial resolution of the order of 1μm. Essentially, the technique uses a highly collimated energetic beam of electrons to cause ionisation of the specimen. The specimen is then identifiable from the characteristic x-rays that are emitted (see section 3.1.1). The result of this interaction can be detected either by an energy dispersive or a wavelength dispersive spectrometer [123]. Energy dispersive spectrometry (EDS) became an acceptable alternative to the wavelength dispersive type (WD) with the advent of scanning electron microscopes. This was principally because WD spectrometers were not usable as an attachment to a scanning electron microscope. The energy dispersive detector, based upon a lithium drifted silicon, Si(Li), solid state device, has the advantages that it can be placed close to the specimen, rapidly evaluates the elemental constituents and, except for minor losses, every photon that is incident at the detector will produce a measurable pulse [123].

The two instruments have very different resolutions: WDS offers high resolution, 5-10keV at Mn$K\alpha$, whereas EDS is only capable of 140eV [61]. ED spectrometers were first used for purely qualitative analysis of specimens, that is the identification of the elements present. Later, detectors were improved to enable quantitative analysis to be undertaken. Another feature of EPMA is the ability to form compositional maps of a surface from the emitted x-rays. This will be explained in more detail in section 6.2.

3.1 The Scanning Electron Microscope

The scanning electron microscope (SEM) is one of the most versatile instruments available for the examination and analysis of the microstructure of solids [61]. It comprises of an electron gun, a condenser lens system and a detector/display mechanism. Such a system produces a focussed electron beam and allows the surface topography to be seen. This type of microscopy is a near surface technique in that it excites atoms within the first few microns of the surface.

A very fine beam of electrons (often called a probe) is focussed on the surface of the sample, which is within an evacuated chamber. The focussing is done electromagnetically and the probe is scanned across the surface, approximately fifty times a second. The two principal ways in which the electron beam can interact with the surface are:

- To produce secondary electrons which are detected and the resulting signals displayed to give an image of the surface on the monochrome screen.
- To produce x-rays which are detected by the energy-dispersive x-ray analyser, enabling qualitative identification and quantitative compositional information.

In this study the equipment used was a Cambridge Instruments scanning electron microscope (model 90B) with a Link Systems x-ray analyser (model AN10000). Figure 3.1 gives the schematic diagram for the arrangement of the detectors and the electron-optics of the equipment. The operating conditions were determined from the amalgamation of the software recommendations and the practicalities of the machine. An acceleration voltage of 15kV was chosen because this is sufficient to excite all the elements of interest [61] and is low enough that the absorption of emitted x-rays is minimised (see section 3.1.1). The working distance was 15mm, which was a compromise of the required depth of field for photographs and the magnification necessary for a small, homogeneous area to be analysed. The beam current was measured after the first data collection in each qualitative analysis. It was usually found to be 0.7nA, corresponding to a count rate of the order of 2000cps and a total wt% oxide between 96 and 103%.

3.1.1 Electron-atom Interactions

It is possible to obtain considerable information about a compound or surface by looking at what happens when subatomic particles or radiation are incident on a sample. This equipment uses electrons, although x-rays, neutrons and photons will also give useful information of different kinds. In order to discuss how an electron interacts with an atom it is first necessary to clarify what is meant by an atom.

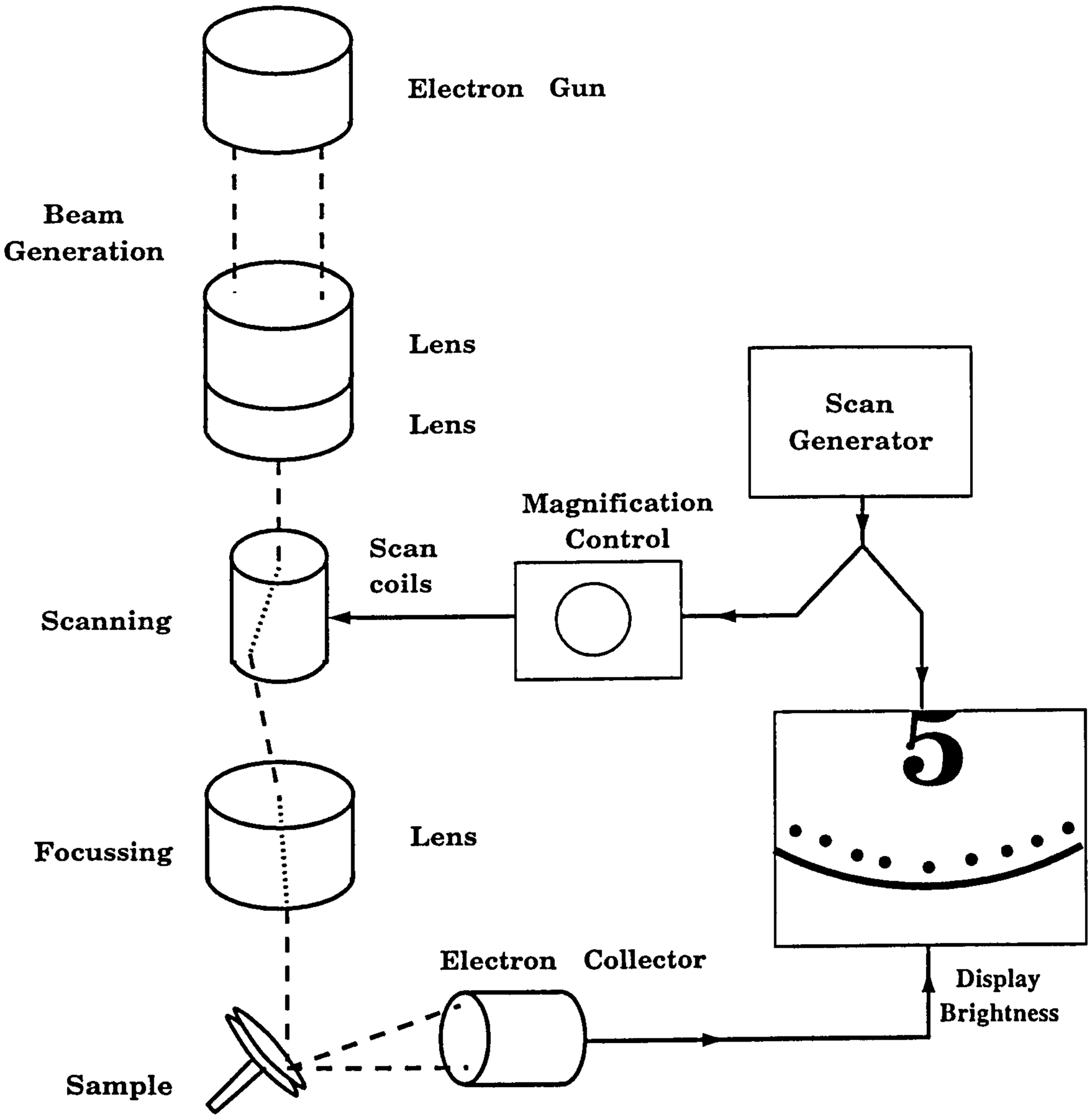

Figure 3.1: Schematic diagram of the electron-optics and detectors in the SEM.

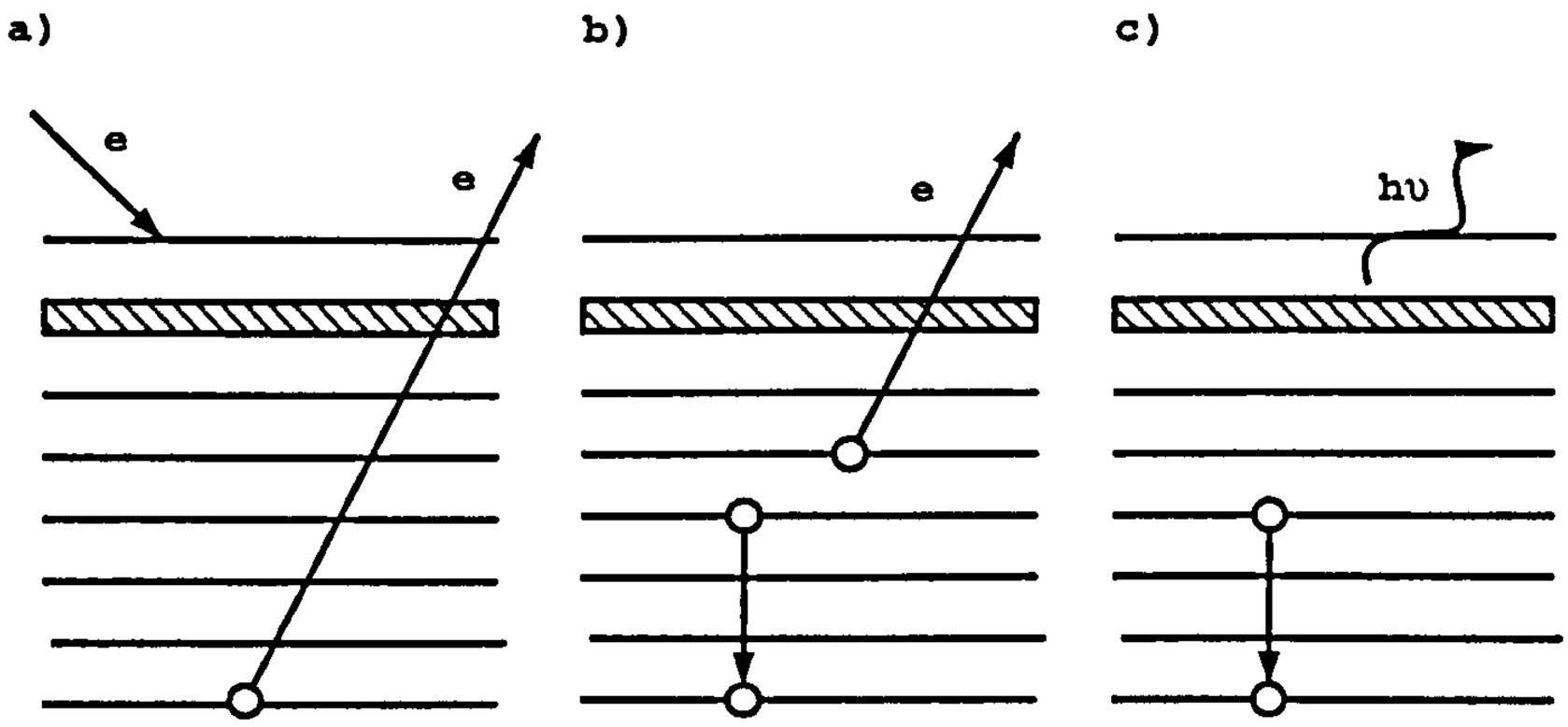

Figure 3.2: Schematic diagram of electron-atom interactions. a) The emission of an electron from an inner shell b) the Auger process and c) the emission of an x-ray photon.

It is usual to refer to the Bohr model of the atom and the semi-classical idea of electron shells. These shells are labelled K, L, M *etc.* outwards from the nucleus (this is for historical reasons) and correspond to the principal quantum number $n = 1, 2, 3$ *etc.* These are subdivided into orbitals governed and labelled by the angular momentum quantum number l (which are in turn further divided and labelled by the magnetic quantum number m). The electron also has a spin quantum number s, and according to the Pauli exclusion principle no two electrons can have the same set of quantum numbers. Thus every element has a different electronic configuration.

When an electron interacts with an atom it causes the atom to become excited. That is, a hole is created in an electron shell, which is illustrated in a) of Figure 3.2. Figure 3.2 then illustrates the way in which an atom can de-excite itself: it can emit a photon and/or an electron. For x-ray emission, the energy of the x-ray is determined by the difference in energies of the two electron shells involved. For example, a K-shell hole when filled by an L-electron will give a photon of energy, of magnitude $(E_K - E_L)$. There are selection rules which govern the electron transitions for x-ray emission [12] and produce the characteristic line spectra.

Competing with this is the *Auger process.* This is when the decay of the excited state results in the emission of an electron from an outer orbital, (Figure 3.2b) and the transition of another to fill the electron hole (formed by excitation) [122]. To use this process requires ultra high vacuum technology.

Glass Corrosion

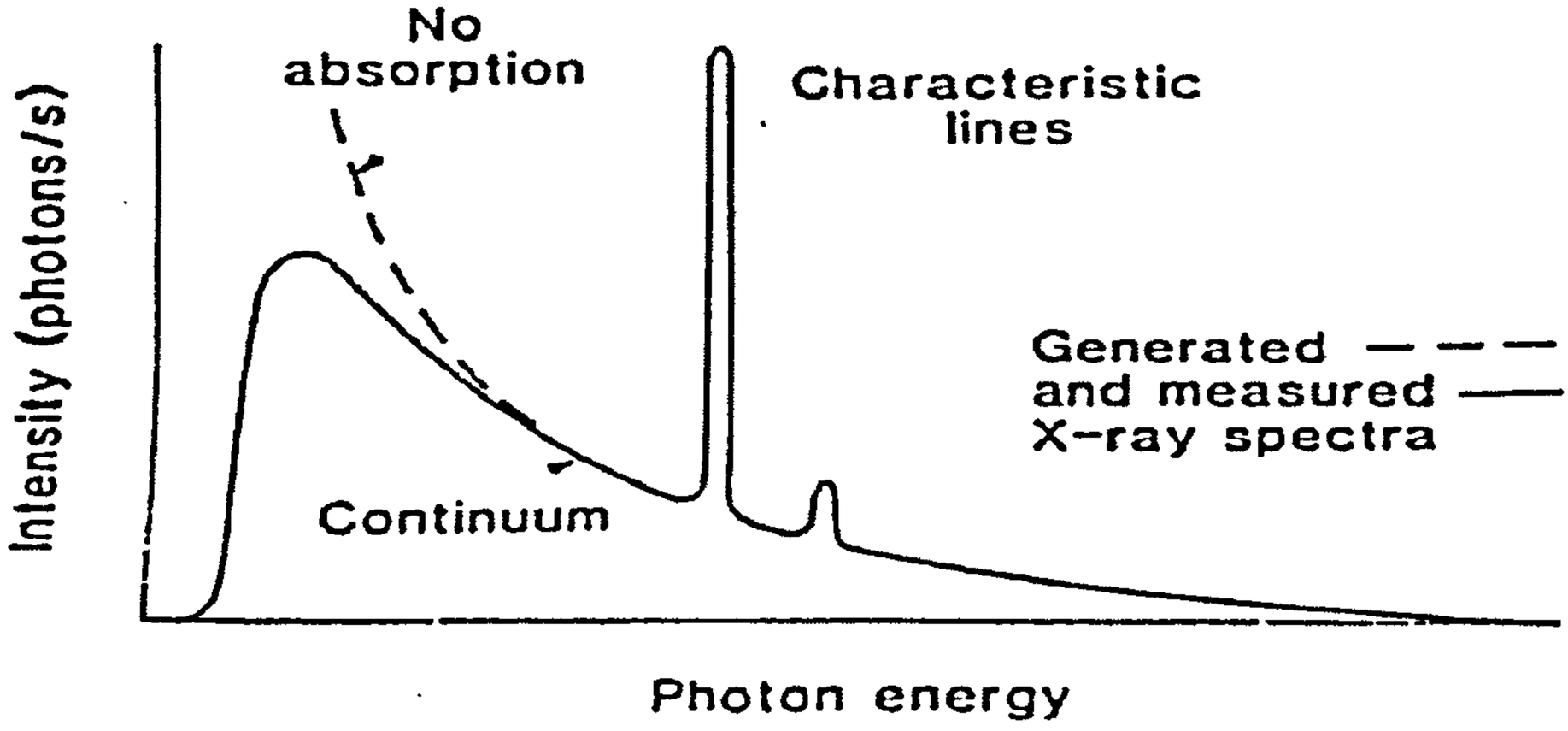

Figure 3.3: Schematic diagram of the relationship between the background and characteristic line spectra for x-rays

3.2 The ZAF Software

It was found by Moseley [123] that characteristic x-ray frequencies are linearly related to the atomic number of the emitting element. There are very specific equations which express this relationship depending upon the type of spectrum i.e. K, L, M *etc.* The energy-dispersive x-ray analyser collects the data and the output is in the form of a series of peaks, superimposed upon a background (see Figure 3.3). The photon energy at which the peaks appear gives an indication of the elements present, though certain peaks will overlap e.g., Kβ with Lα. A specific case relevant to this analysis is the Mn Kβ overlapping the Fe Kα. This type of analysis is *semi-quantitative*, unless deconvolution of peaks is carried out.

The data may be further processed by ZAF software to give quantitative results. The name comes from "atomic number (Z)", "absorption (A)" and "fluorescence (F)" corrections which are individually calculated. The atomic number correction allows for the stopping power. This takes into account the difference in the rate of loss of energy in a specimen to that in a standard. Since not all the energy of the incident electron is given up to the target, a backscatter factor is also needed and is incorporated in the atomic number correction.

The absorption correction is needed because the photons emitted from one element, due to electron interactions, can be absorbed by another lighter element. As such, this factor depends upon the penetration depth of the electrons, the photon energy and the elements present in the specimen. This is the largest of the three factors. Absorption occurs when the photon energy is greater than the binding energy of a particular shell; it is most likely when the energy gap is small. This effect

follows an exponential law so the deeper into the sample that the x-rays are generated then the greater the loss due to absorption. as a result the sample orientation is very important.

Finally, the fluorescence correction allows for the x-rays emitted from one atom being absorbed by another. This is the least important factor and affects the data by implying a higher concentration of the lighter elements. If these matrix effects were not allowed for, then the calculated elemental concentrations would be incorrect. The exact algorithm of the software was not known as the ZAF system is a commercial package, though a general outline may be given.

The elemental concentration is first estimated by ratioing the measured net intensity of the x-rays from the sample to that of the pure element or compound of known composition. This is why standards are needed for the analyser to be properly calibrated. The standards must be measured under identical conditions to those to be used for analysis, i.e. same acceleration voltage, surface orientation and condition. The ratio of the measured intensity to that emitted by the pure element is known as the *k-ratio* and it is this that the ZAF program uses as a basis:

$$C = \frac{k}{ZAF} \tag{3.1}$$

where C is the concentration, Z, A and F the appropriate correction factors and k is as described above. The derivation of the above equation is given in Appendix A.2.

An iterative procedure is then used to obtain the weight concentration values, since $k = CZAF$ cannot be used directly; all of the correction factors are functions of concentration. There are various methods of iteration that can be and are used. The principle depends upon the repeated application of equation 3.1 to evaluate the weight percent concentration. The process halts when the end point is reached:

$$\frac{(C_j - C_{j-1})^2}{C_j^2} \leq 0.00001 \tag{3.2}$$

where C_j is the value after the j^{th} iteration. The above can be generalised to a 0.3% relative difference between C_j and C_{j-1}. The procedure is performed for each element and the iteration only halts when the criteria are met for all elements in the specimen.

3.2.1 Angular Dependence Analysis

On initialising the ZAF program several parameters must be set. These include:

tilt is the angle, in degrees, between the specimen and the incident electron beam.

elevation is the angle between the x-ray detector and the horizontal plane.

azimuth is the angle between the direction of tilt and the line between the x-ray detector and the probe spot as viewed from the electron beam.

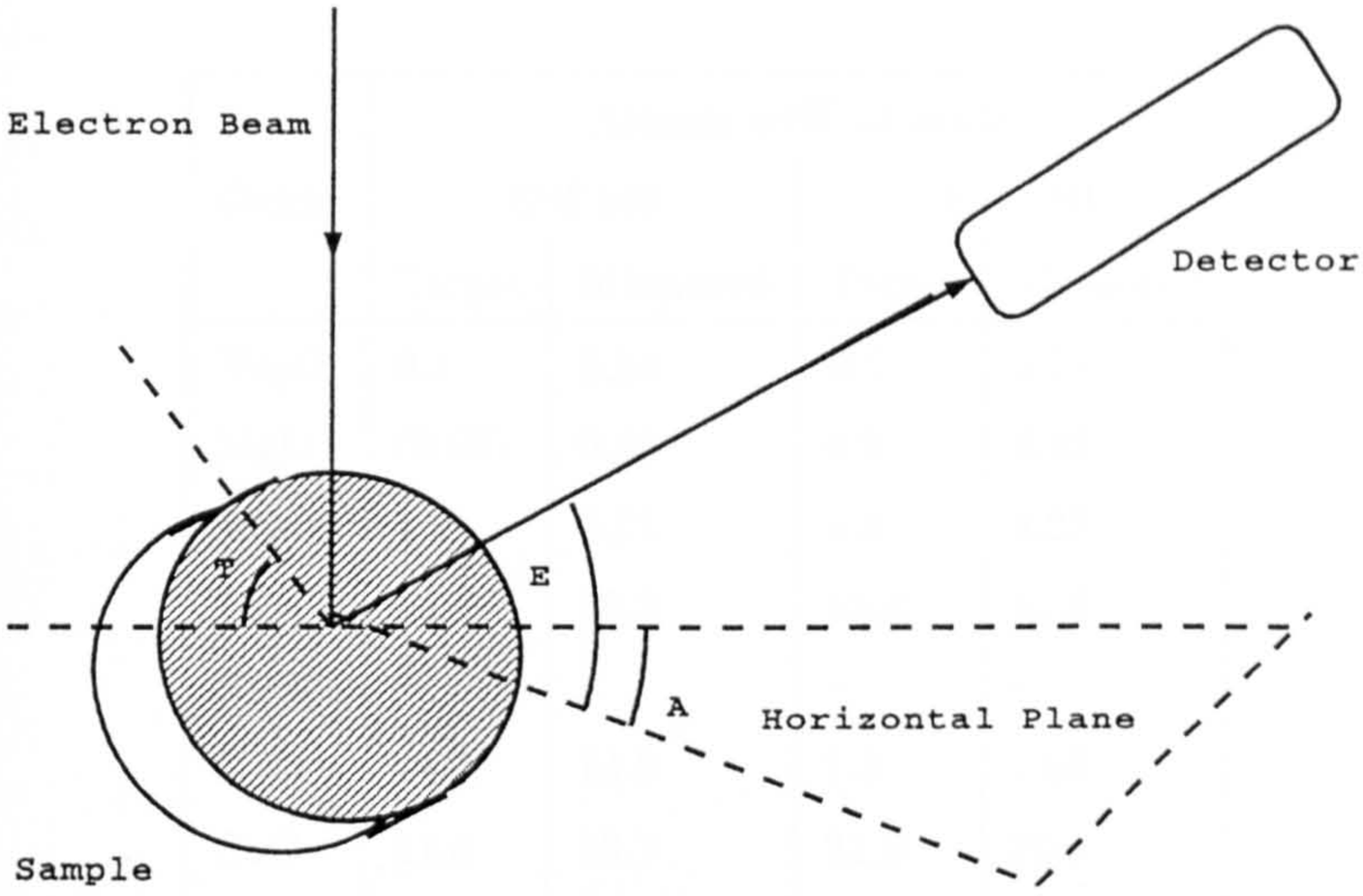

Figure 3.4: Schematic diagram of the orientation of the sample with respect to the SEM and x-ray detectors.

The above are generally set to $45°, 0°, 33°$ respectively (see Figure 3.4).

Experiments were carried out to establish how accurately the tilt and azimuth must be known (the elevation is zero as the two detectors are horizontal). The surface could be made parallel to the base and therefore the controls enabled positioning. Since the actual glass samples would naturally be uneven and the ground and polished flat would not necessarily be at 45°, orientation by the controls alone would be inaccurate.

Test One: Variation of the Tilt angle

The European Science Foundation (ESF) produce standard glasses to enable work from different laboratories to be compared with each other and for standardising equipment. There are a range of glass types available and in order to enable analysis of tilt variation two simulated mediaeval glasses were chosen and embedded in resin. Two samples were deemed necessary so as to establish that any angular dependence found was not just a coincidence. ESF76-C-149 and ESF77-C-150 (referred to as ESF149 and ESF150 from now on) were chosen, one was a soda glass the other a potash type. Table 3.1 gives the full chemical composition of the two ESF glasses, both from actual analysis and data provided by the ESF. As the glasses were embedded in resin, it was possible to ensure that the surface was parallel to the carousel and hence the azimuthal angle was not affected.

ZAF calculations were performed on both samples in 5° steps between 20° and 70°. For each angle the chemical composition was determined ten times and the mean calculated from this. Sample ESF150 was analysed in greater detail between 39° and 51° (one degree steps). This second analysis

Oxide	Atomic wt% of oxide			
	ESF149		ESF150	
	Target	Measured	Target	Measured
Na_2O	0.1	0.14	9.5	9.17
MgO	(0.05)	0.06	6.6	6.43
Al_2O_3	4.2	3.71	4.3	4.23
SiO_2	56.8	59.2	55.4	57.8
P_2O_5	–	–	–	–
K_2O	14.3	14.8	1.5	1.60
CaO	21.5	19.7	21.9	20.1
MnO	1.8	1.49	–	–
Fe_2O_3	–	–	0.3	0.34
CuO	0.91	0.71	–	–
PbO	–	0.26	–	0.09

Table 3.1: Composition of the ESF simulated mediaeval glasses used in the testing of angular dependence.

Element	ESF 149			ESF150		
	2σ at 45°	Difference (40-45°)	Difference (45-50°)	2σ at 45°	Difference (40-45°)	Difference (45-50°)
Na_2O	1.9×10^{-3}	7.7×10^{-4}	5.1×10^{-4}	3.6×10^{-3}	2.7×10^{-3}	4.4×10^{-3}
MgO	2.3×10^{-3}	3.5×10^{-4}	8.6×10^{-4}	3.5×10^{-3}	2.1×10^{-3}	3.1×10^{-3}
Al_2O_3	1.1×10^{-3}	2×10^{-4}	1×10^{-5}	1.6×10^{-3}	4.6×10^{-4}	3.2×10^{-4}
SiO_2	6.9×10^{-3}	2.4×10^{-3}	5×10^{-3}	6.5×10^{-3}	1.6×10^{-3}	2.5×10^{-3}
P_2O_5	–	–	–	3×10^{-4}	8.3×10^{-5}	1.8×10^{-5}
K_2O	2.3×10^{-3}	6×10^{-4}	1.9×10^{-3}	1.2×10^{-3}	4.8×10^{-4}	2.8×10^{-5}
CaO	3.9×10^{-3}	2.5×10^{-3}	2.5×10^{-3}	3.4×10^{-3}	5.8×10^{-3}	5.9×10^{-3}
MnO	2.0×10^{-3}	6.6×10^{-4}	2.1×10^{-4}	1.4×10^{-3}	4.4×10^{-5}	2.5×10^{-4}
Fe_2O_3	3.2×10^{-4}	1.3×10^{-4}	9.5×10^{-5}	8.5×10^{-4}	1.1×10^{-4}	4.1×10^{-5}
CuO	4.6×10^{-3}	1.6×10^{-4}	4.7×10^{-4}	2.1×10^{-3}	1.8×10^{-4}	2.4×10^{-4}
PbO	7.2×10^{-4}	5.2×10^{-5}	1.5×10^{-4}	6.8×10^{-4}	6.5×10^{-5}	5.4×10^{-5}

Table 3.2: Comparison of the errors in mean molar percent of an element at 45° to the difference of the mean molar percent at 40° and 50° with respect to 45° tilt.

was to give more information on the region in which the approximate 'flat polishing' was expected to fall.

The variation in the values obtained across the $20-70°$ range was clearly dependent upon the element. The greater the amount of oxides present, then the smaller the variation (10% in Si wt%; 50% in Na wt%). Figures 3.5 and 3.6 show the effect of altering the angle of tilt on the measured molar concentration of three of the oxides of interest (lime, silica and potash). The symbols are larger than the errors introduced through averaging the results. Table 3.2 shows that the variation in the measured molar percent of an element at the tilt angle of 45° is comparable or greater than the difference between the mean molar percentages (at 40° *wrt* to 45° and 50° *wrt* to 45°) for all elements in both ESF glasses. Figure 3.7 illustrates the more detailed region of $39-51°$, which was only studied for the sample ESF150. Overall, the view was taken that if the tilt angle was known to within ± 5 degrees, then the analyses would be within acceptable experimental error, introduced by the counting statistics.

Test Two: Variation in the Azimuthal angle

Another sample of the glass ESF149 was chosen for use in this test. Instead of embedding this sample, it was treated as a non-destroyable specimen. A small region, at an edge, was ground and polished at 45° to the horizontal. The angle of the polished face to the upper surface was orientated using the controls on the SEM since the surface was parallel to the base. The azimuthal angle was varied through 15°, either side of an arbitrary starting point. This starting point was when the line of intersection of the polished flat to the upper surface appeared as a straight line parallel to the bottom of the viewing screen on the SEM. The rotate dial was then used to vary the sample position with respect to the x-ray detector.

Figure 3.8 illustrates the variation of the value of the same three oxides as earlier, with azimuthal changes. Again the results confirmed the expected i.e. the sample was correctly orientated when the line of intersection appeared as a horizontal line on the screen. When the sample is turned away from the x-ray detector the concentration of the various elements decreases and vice versa. Thus a general guideline as to the correct positioning of the specimens had been established.

3.2.2 Consequences of the Angular Dependence

The tests carried out show that if the tilt angle was correct to $\pm 5°$ degrees and the line of intersection was positioned as mentioned earlier, the data resulting are a correct representation of the elemental composition of the specimen (within experimental error). However, it was considered that some means of measuring the angle and achieving consistency between samples was necessary.

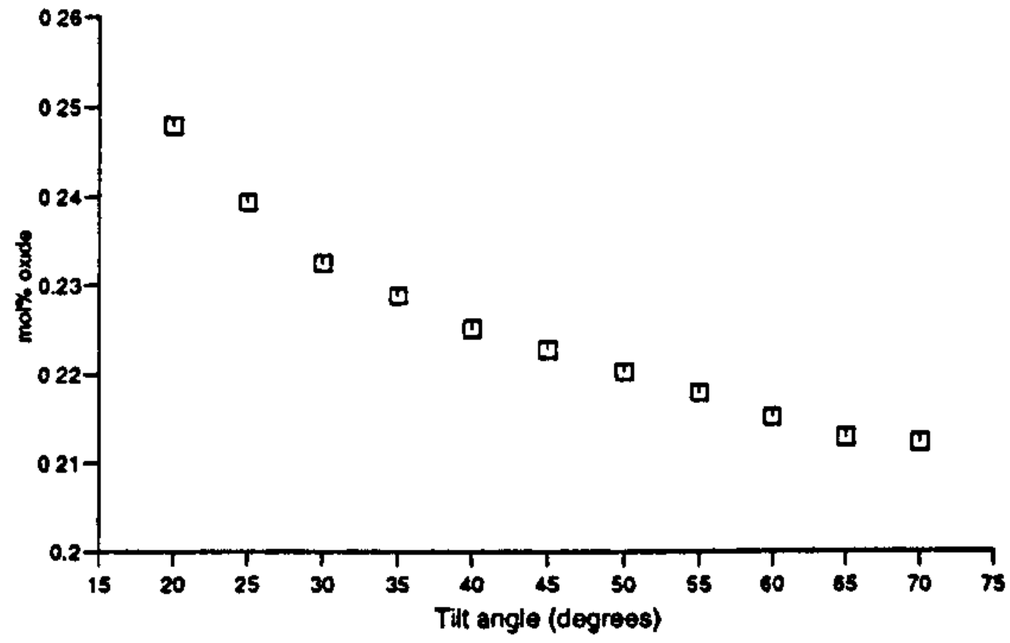

(a) lime

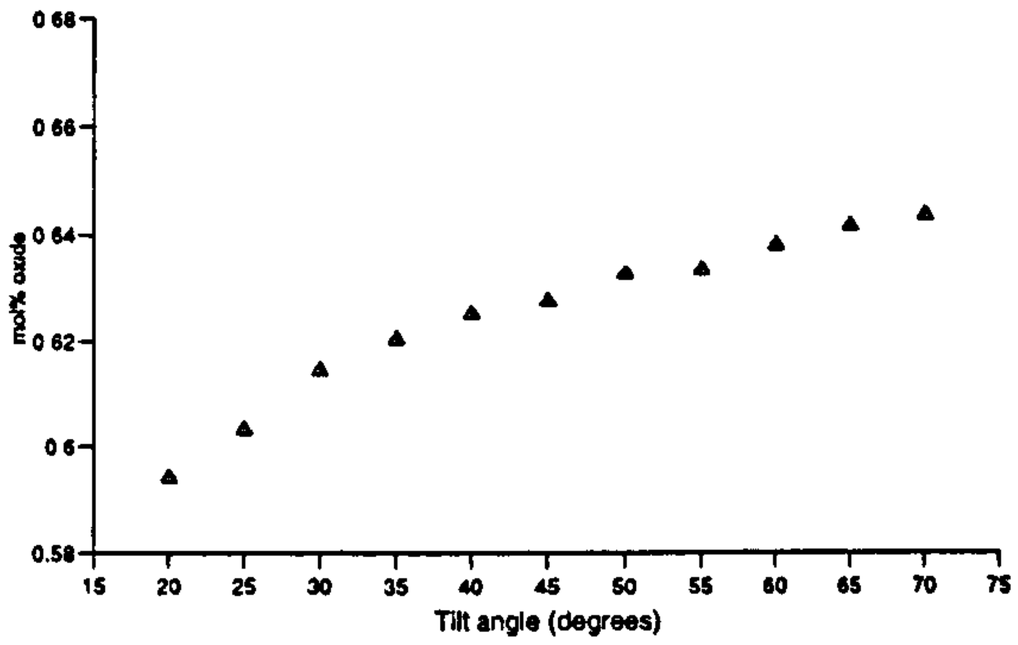

(b) silica

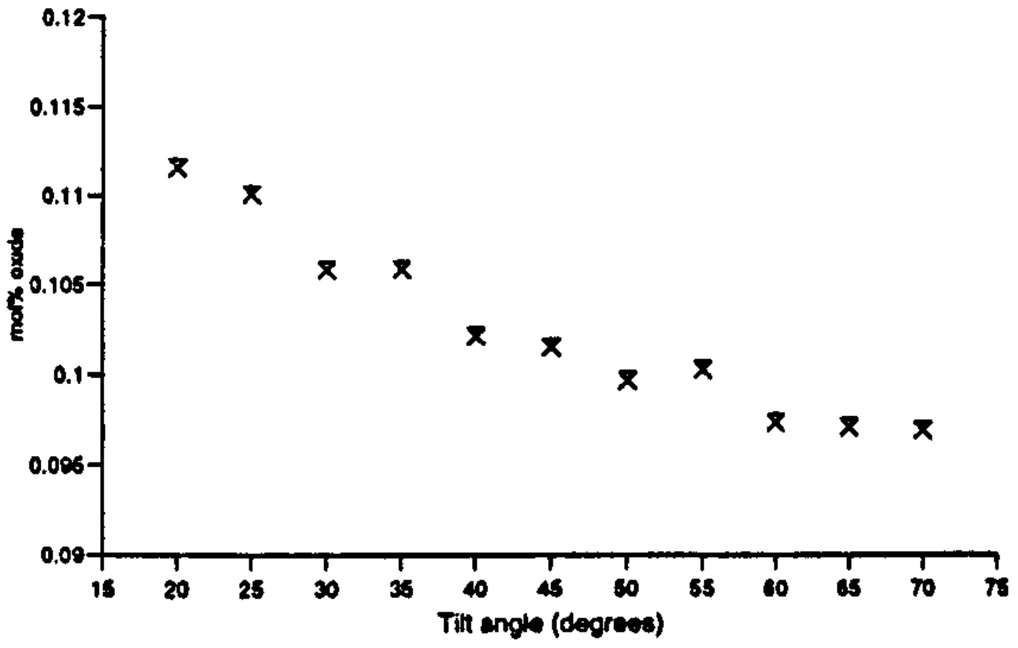

(c) potash

Figure 3.5: Graphical illustration of the variation of measured concentrations of the elemental oxides in ESF149 for the angles of tilt between 20° to 70°.

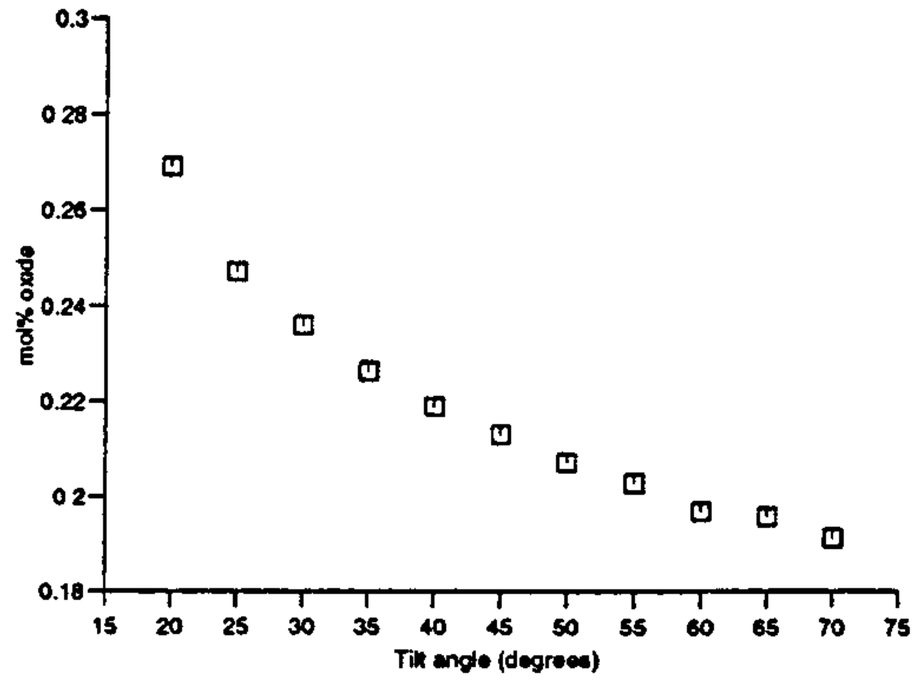

(a) lime

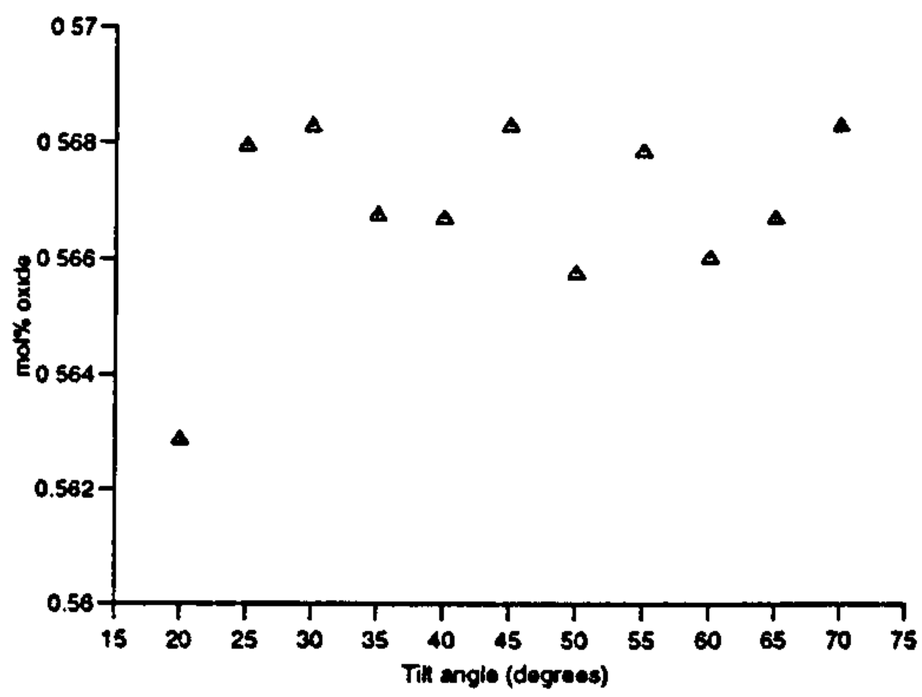

(b) silica

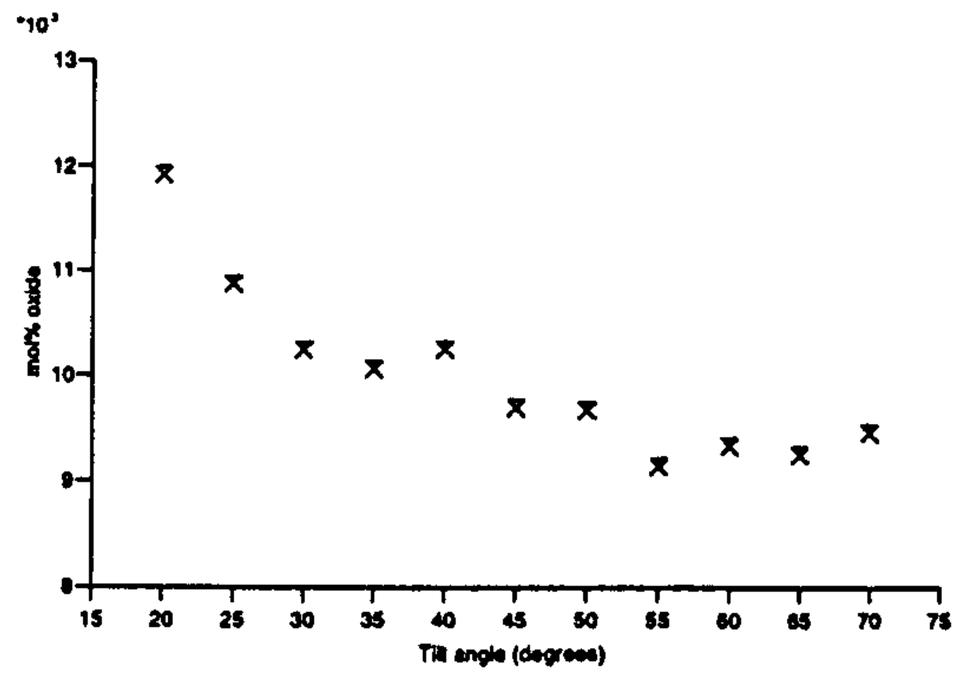

(c) potash

Figure 3.6: Graphical illustration of the variation of measured concentrations of the elemental oxides in ESF150 for the angles of tilt between 20° to 70°.

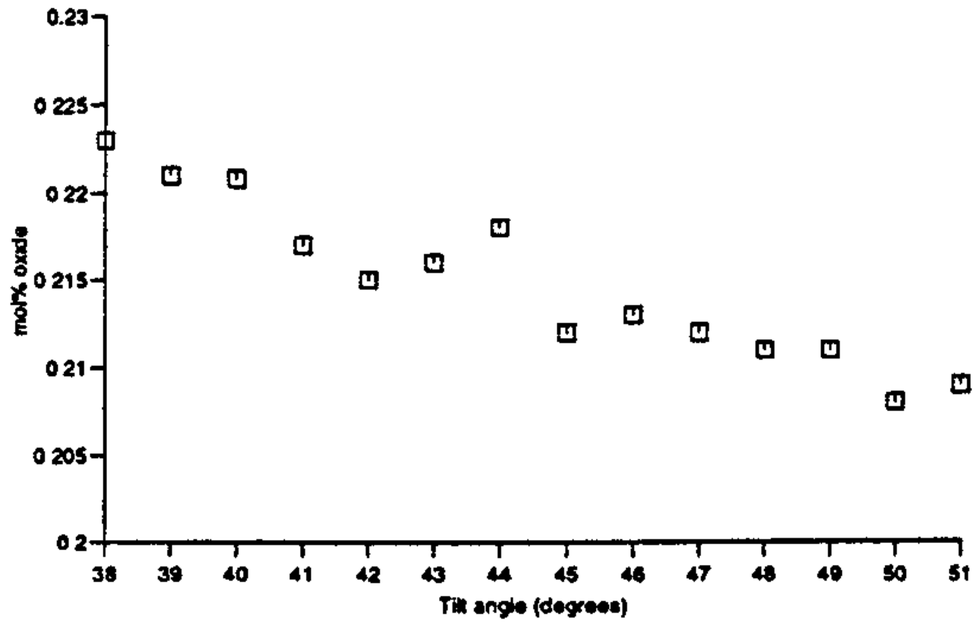

(a) lime

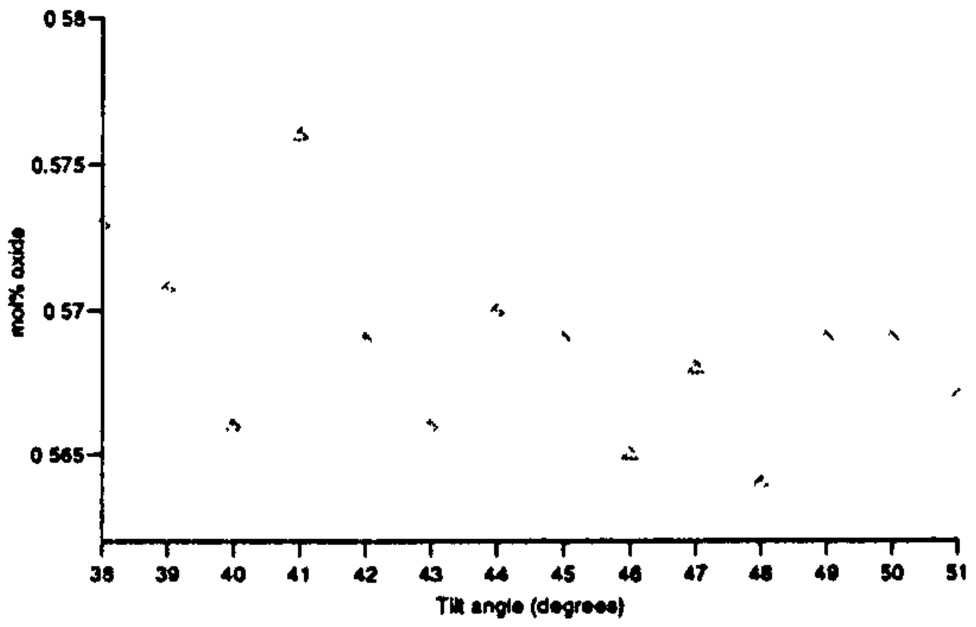

(b) silica

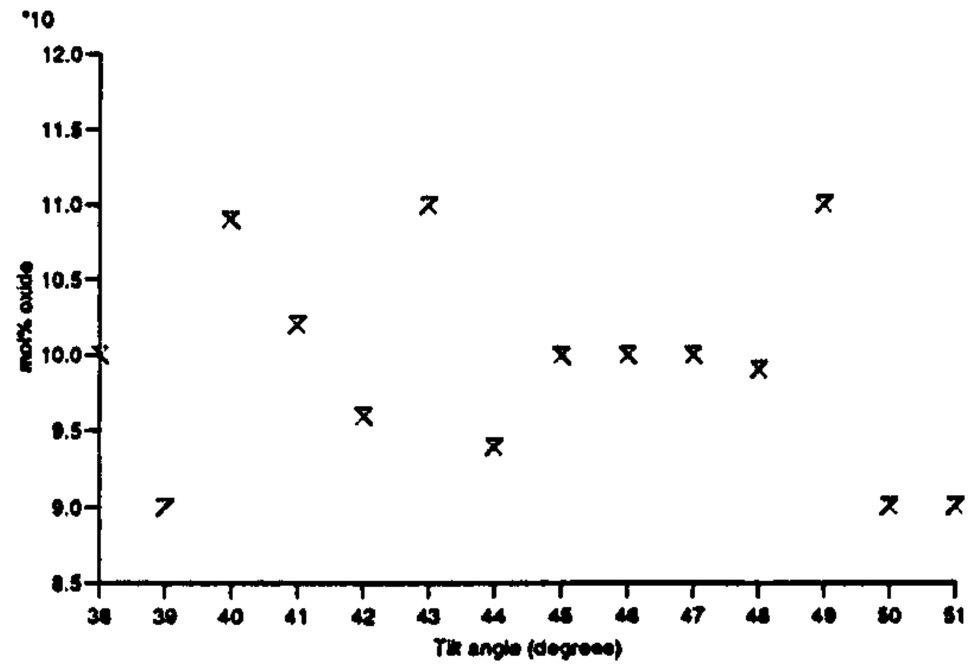

(c) potash

Figure 3.7: Graphical illustration of the variation of measured concentrations of the elemental oxides in ESF150 in the detailed region of 39° to 51°.

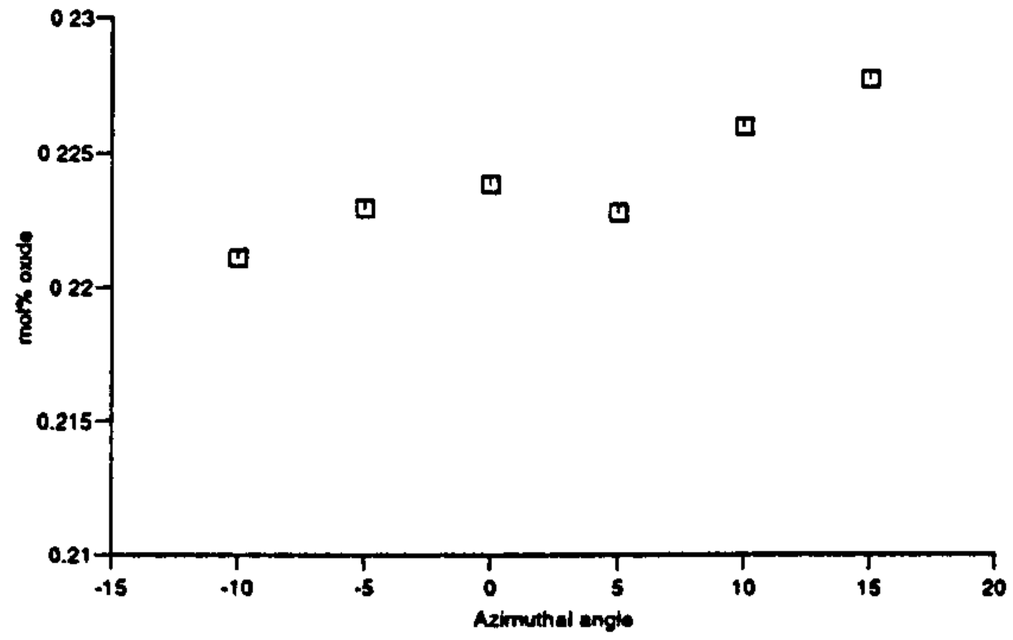

(a) lime

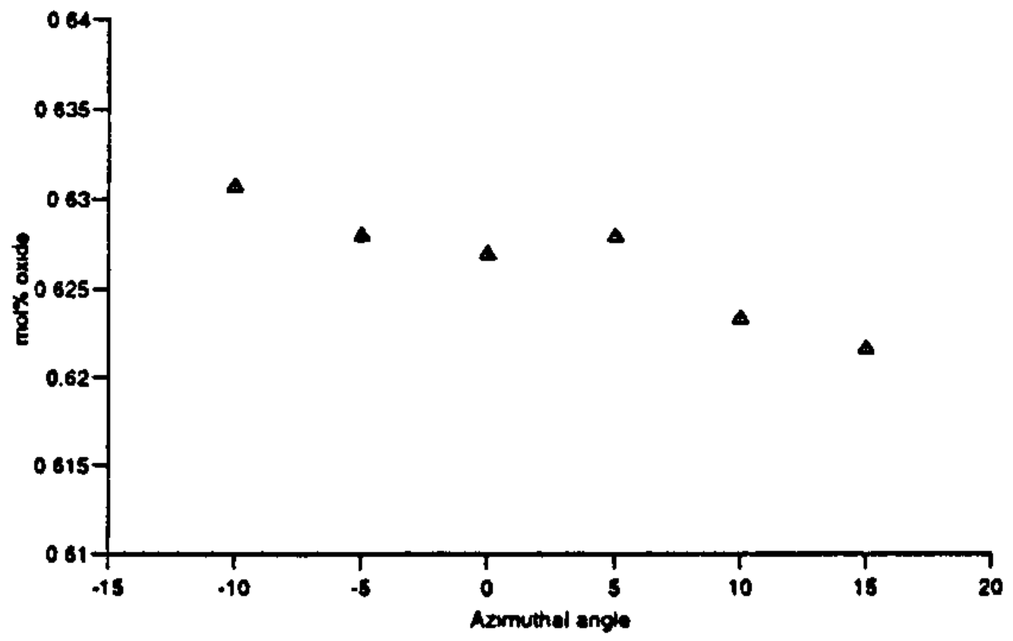

(b) silica

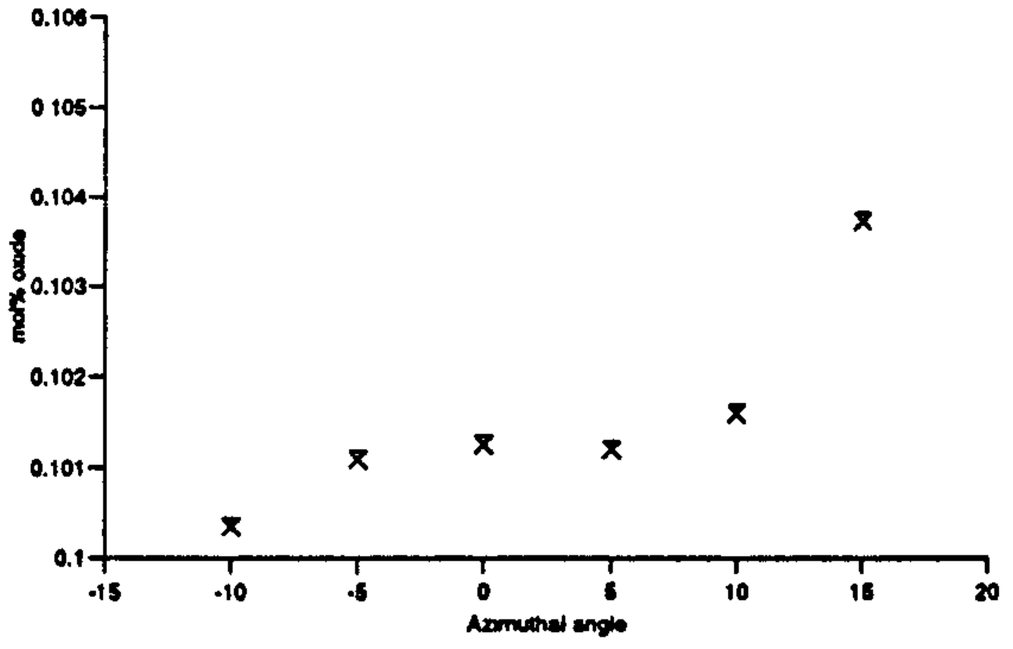

(c) potash

Figure 3.8: Graphical illustration of the variation of measured concentrations of the elemental oxides in ESF149 with azimuthal angle.

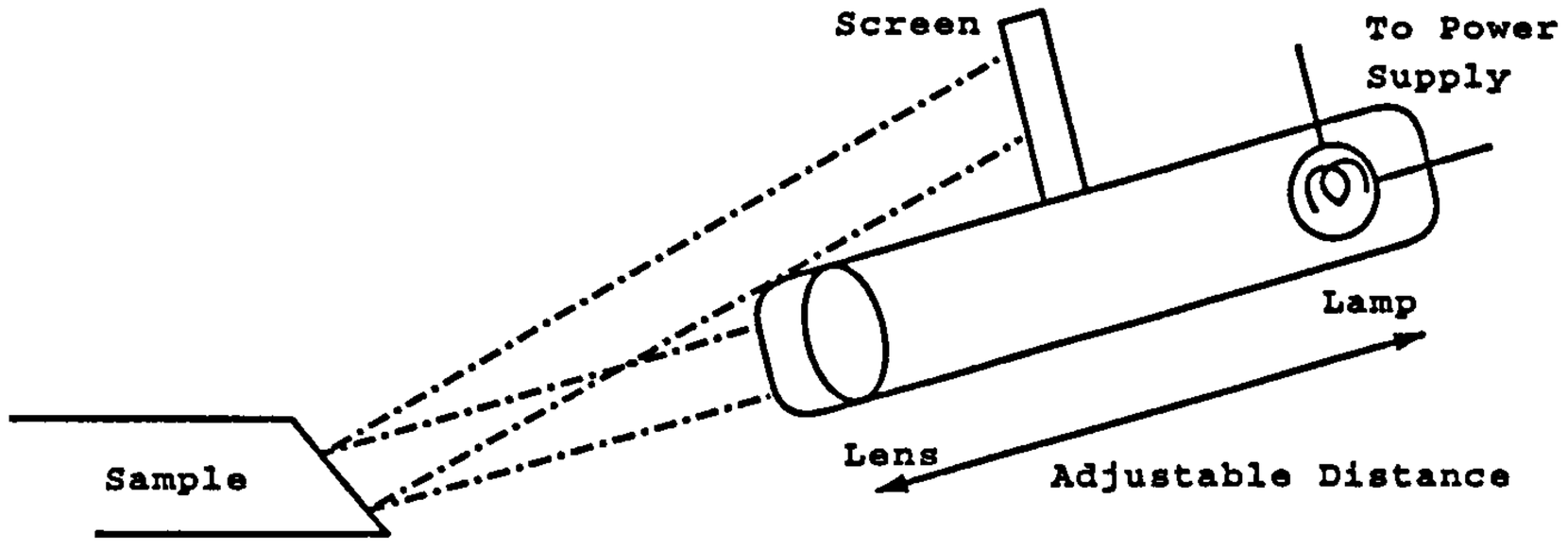

Figure 3.9: Schematic diagram of the goniometer.

The steps taken were:

1. The design and production of two supporting jigs for the grinding and polishing wheels. These were necessary because polishing at a different angle to that of the ground flat produced rounding of the edges and the area was no longer a flat plane. Also it ensured that the flats on individual samples would be self-consistent.

2. The design and construction of a device to ensure that the tilt = 45° and azimuth = 33° (the angle between the two detectors was 33° and therefore if the sample was in line with the SEM detector it would also be at 33° to the x-ray detector). The goniometer consisted of a small bulb connected to a 6v supply, a microscope eyepiece of X4 magnification and a ground glass screen. The whole body was mounted on a support, to allow vertical movement, which was attached to the SEM door via a base plate. The goniometer was first orientated using an embedded sample whose surface was flat, parallel and as reflective as the sample to be analysed. The goniometer was correctly aligned when the bright spot was in the centre of the target region on the ground screen. The sample was then mounted on the carousel and moved until the bright spot returned to the correct position.

3. Each sample was orientated, as mentioned above, before analysis. In order to do so the sample first had to be mounted. A simple mount was made to enable the samples to be fixed and coated with carbon. The carbon coating was essential to remove charge build up from the surface.

3.3 Analyses

Each of the 206 samples of glass was analysed using the above method. Obviously the size of the chamber limited the size of the specimen (though in general this was not a problem). In all cases the sample composition was obtained by collecting a spectrum from a livetime of 100 seconds. This

Oxide	Molar mass factor	Oxide	Molar mass factor
SiO_2	0.60	Na_2O	0.62
K_2O	0.942	MgO	0.403
CaO	0.560	Al_2O_3	1.02
Fe_2O_3	1.597	P_2O_5	1.419
MnO	0.71	CuO	0.795
PbO	2.07	S	0.321
Cl	0.35		

Table 3.3: The factors for converting weight percentages to molar percentages.

time period was selected because it produced adequate counts in the profile spectra for the selected elemental oxides [83] and is the manufacturers recommended value. To further reduce errors five spectra were collected and the composition determined as an average. This average composition was then normalised to give a weight percent total of 100. This was then converted from the weight percentages of oxide to molar percentages: conversion is necessary because the oxides do not exhibit an effect based upon the weight of the molecules but by the number of molecules. Table 3.3 contains the conversion factors for each of the oxides. The composition is obtained by dividing the weight percent oxide by the appropriate factor and then rescaling the overall amounts so that the total is again 100%. The average weight and molar percentages for each specimen are contained within the tables of Appendix C. Also contained within these tables are the values of the free energy of hydration, the number of non-bridged oxygen atoms and the ternary co-ordinates.

3.3.1 Free Energy of Hydration, ΔG

The value of the free energy of hydration (ΔG) gives an indication of the chemical durability if the following assumptions are applied:

1. The mechanism of decay is directly related to the stoichiometry of the solid.
2. The amount of silica extracted is a function of the mol% of silica present in the glass.
3. The release of silica is a function of the number of non-bridged oxygen atoms (NBO).
4. The dynamic exchange reactions at the glass-solution interface can be described in terms of thermodynamic equilibria.

The value is calculated assuming that glass is a homogeneous mixture of structural units such as K_2SiO_3 [69]. Table 3.4 gives the free energy of hydration values for the relevant silicates and oxides

Component	ΔG, kcalmol^{-1}	Component	ΔG, kcalmol^{-1}
$Na_2O.SiO_2$	-28.815	$P_2O_5^*$	10.010
$MgSiO_3$	-13.888	SiO_2	5.589
K_2SiO_3	-41.735	Al_2O_3	3.040
$CaSiO_3$	-16.116	$MnSiO_3$	-14.871
$FeSiO_3$	-14.609	Fe_2O_3	15.500

Table 3.4: Table containing the values of the free energy of hydration for various silicates and oxides when they react with water.

(P_2O_5 is asterixed because this value was obtained through personal communication with Dr. G. Cooper). This factor is multiplied by the molar percent of the respective oxide present in the glass and the individual values are summed to give the total ΔG of the glass.

However, the calculation for the ΔG value for iron oxide and silica is more involved. Determination of the iron oxide value requires a knowledge of the amount of manganese oxide present. This is due to the redox reaction between iron and manganese that means the iron may be in one or both oxidation states. It was taken that iron(II)oxide was present if MnO $<$ 0.002 mol%, iron(III)oxide if MnO $>$ 0.009 mol% and that an equal mixture of iron(II) and (III)oxides were present in all other cases [31]. Silica is altered because some of the ΔG values in the table 3.4 are silicate values. The molar percentage of these oxides (Na_2O, K_2O, MnO, MgO, CaO, FeO) must be subtracted from the mol% silica values before the ΔG_{Si} is evaluated. If the molar value of silica becomes negative then it is assumed to be zero.

3.3.2 Non-bridged Oxygens

The number of non-bridged oxygens atoms is linked to the durability in the same way as the ΔG value, and it reflects the amount of distortion to the glass network as a result of the modifying ions. To calculate the quantity it is assumed that every mole[cule] of mono- and di-valent oxide contributes two NBO atoms [69]. Every mole of trivalent oxide, however, creates two BO atoms. The NBO total is then calculated as:

$$NBO = \frac{2(X - Y)}{M} \tag{3.3}$$

where M is the molar oxide sum, X is the sum of the mol% of monovalent and divalent ions with Y as the sum of the trivalent oxides.

3.3.3 Ternary Co-ordinates

The first of the ternary co-ordinates is 'SiO_2', which is the amalgamation of the network formers present in the glass:

$$'SiO_2' = SiO_2 + 2Al_2O_3 + 2Fe_2O_3 \tag{3.4}$$

The alumina and iron oxide are included because not only can they form part of the network but also immobilise a network modifier:

$$Al_2O_3 + Na_2O \rightarrow 2AlO_2^- + 2Na^+ \tag{3.5}$$

Therefore the alumina and iron oxide must also be subtracted from the alkaline network modifiers, 'R_2O':

$$'R_2O' = Na_2O + K_2O - Al_2O_3 - Fe_2O_3 \tag{3.6}$$

The final ternary co-ordinate is composed of the divalent network modifiers, 'RO':

$$'RO' = CaO + MgO + MnO + FeO + CuO + PbO \tag{3.7}$$

It must be noted when using the co-ordinate reduction, if the glass contains a measurable amount of lead oxide then the assumptions made are not valid and therefore this method no longer correctly represents the reduced composition.

3.3.4 The Samples

The samples chosen for this investigation were, in general, the most corroded ones from each of the panels available from the various churches. There were, however, certain limiting factors:

The location - it was not possible to select glass from the entire bank of stained glass in Britain as only glass that was scheduled to be restored during the three year time span of this research project could be considered.

The number - the length of time that the windows were to be in the restorers workshop affected the length of time available for the analyses, and hence the number of specimens that could be investigated.

The size - the individual pieces of glass had to fit within the SEM chamber, and therefore no samples were larger than 15cm by 6cm.

The colour - the same distribution of colour was taken from each location where possible.

Site	County	Masonry	Window Orientation	Number of Samples
Stanford	Northants.	Attleborough	unknown	6
Fledborough	Notts.	Limestone	north	6
Fledborough	Notts.	Limestone	south	8
Ely	Cambs.	Barnack	unknown	13
Meysey Hampton	Gloucs.	Limestone	unknown	19
Heckington	Lincs.	Limestone	unknown	25
Checkley	Staffs.	White Hollington	south	32
Checkley	Staffs.	White Hollington	north	34
Fairford	Gloucs.	Limestone	north	22
Fairford	Gloucs.	Limestone	south	44

Table 3.5: A brief summary of the information concerning masonry and sample size from each location.

As a consequence of the above constraints, glass from seven churches was investigated: Fledborough (FLD), Stanford (SCB), Ely (ELY), Meysey Hampton (GMH), Heckington(LHE), Checkley (CHK) and Fairford (FAI). Figure 3.10 shows the geographical location of these churches and York. It can be seen that they are all inland sites in the midland and southern regions of the United Kingdom. This distribution is somewhat indicative of the general spread of mediaeval glass - as it was imported into this country and generally only installed in the more wealthy regions. A brief summary of the churches and their backgrounds is given in section 3.3.5. All but one of the churches were of fourteenth century glazing, the exception being Fairford which was sixteenth. Three of the churches had both north- and south-facing windows available for inspection and for one of these, FAI, the windows are strongly believed to have remained in their original panels and orientations. A comparison of two churches (Fairford and Checkley) was presented at Archaeological Sciences (1995). The total number of samples from each location varied considerably (see table 3.5).

Aside from the effect of the location and orientation of the glass, it was also possible to investigate the correlation between the decay product and the chemical composition. The details of these comparisons will be given in chapter 7.

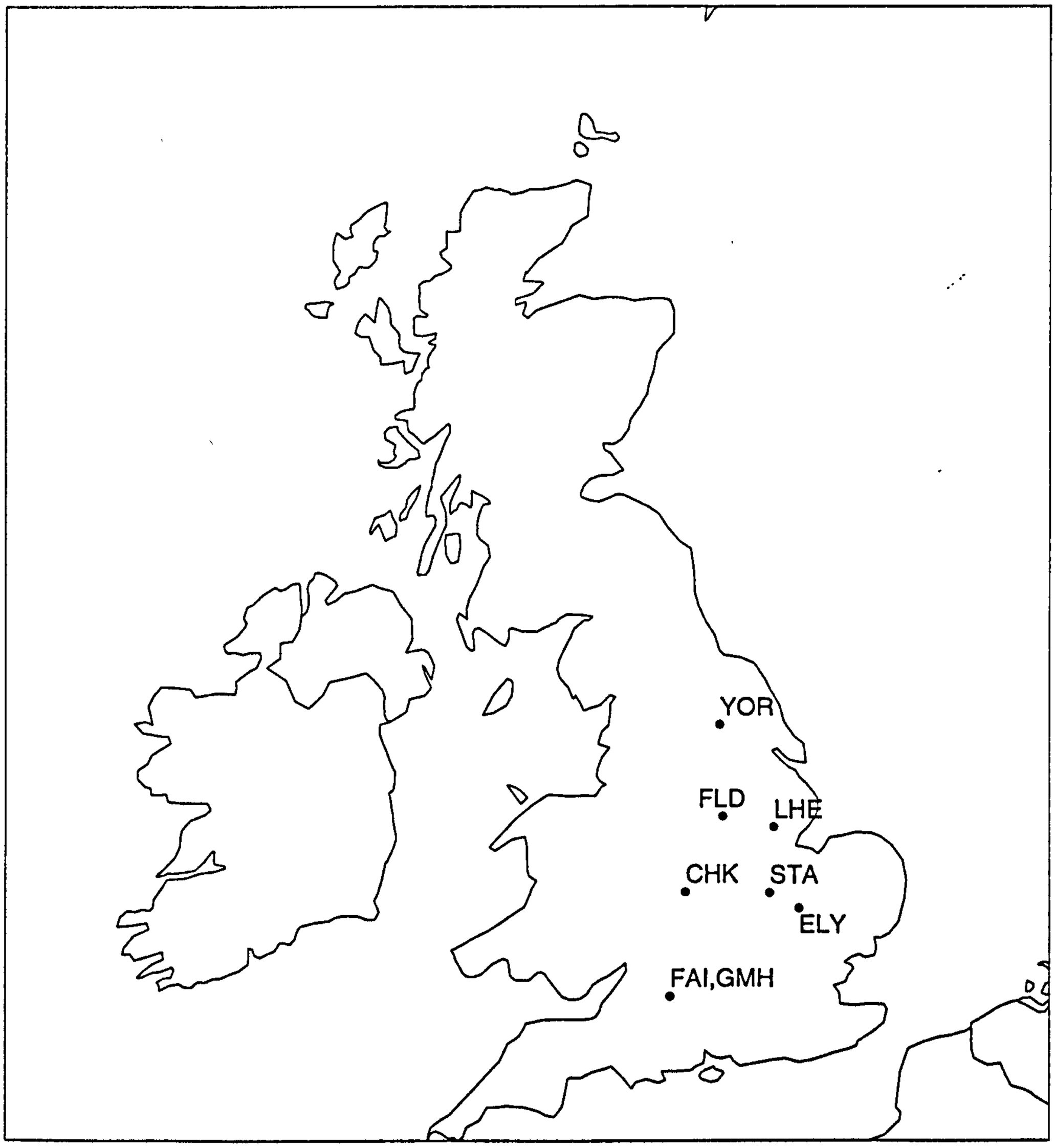

Figure 3.10: The location of the churches from which the specimens were obtained. YOR=York, FLD=Fledborough, LHE=Heckington, CHK=Checkley, STA=Stanford, ELY=Ely, FAI=Fairford and GMH=Meysey Hampton.

3.3.5 Location

Stanford-upon-Avon

The glazing in this church, dates from @ 1320 and the specimens chosen were 6 colourless border pieces (samples are labelled as SCB) from a chancel panel [116]. All samples had a thick crust, although these appeared in general as though this could have originated from external sources, such as wash from the building. One sample in particular had a markedly different appearance (SCB6). It had a shiny, but hard and fine, crust similar to that produced on etching. The use of artificially distressing glass when replacing it was popular in Victorian times so that it blended in with the surrounding pieces. The chemical composition of this piece was also so different that it would suggest this piece is a Victorian replacement, as suspected from its appearance. The church itself is erected out of Attleborough stone, which is mainly limestone. Subsequent masonry repair has been carried out using a combination of ironstone and limestone.

Ely

The thirteen specimens from Ely cathedral (sample labelled as ELY) had been in storage for approximately 20 years at the Stained Glass Museum in Ely. They were originally removed by the workers of Dennis King's workshop. Unfortunately, during this period the identifying labels had been misplaced, and therefore, little information was available on the samples [115]. They were from the Lady Chapel glazing, which dates from the fourteenth century and some of them had been investigated by other workers [3, 36]. The cathedral itself is built from Barnack stone.

Fledborough

St. Gregory's church, Fledborough, is uncommonly rich in fourteenth century stained glass [114]. The church is built from limestone and therefore any calcite identified as a corrosion product could actually be due to wash from the building. Fourteen pieces were selected in total: three from a large north panel, three from a north tracery light and the remaining from two south traceries. The former, labelled FLE, were large colourless specimens that were slightly decayed. The samples from the traceries were labelled FB followed by N or S, depending on the orientation. The north traceries were covered in green algae, whereas the southern ones were rendered opaque by decay products.

Meysey Hampton

This small parish church has some fragments of thirteenth century glazing, but is mainly fourteenth [139]. This church is situated approximately six miles from Fairford and is built of the same limestone. A total of 19 pieces (labelled as GMH) were taken as representative of the most deteriorated glass whilst still reflecting the spread of colours available. This church is situated approximately 6miles from Fairford church and therefore would be useful when comparing the local climate of the churches. Unfortunately this fact could not be used as the glasses were of different dates.

Heckington

This is one of the grandest churches in Lincolnshire [118]. It is built of Ancaster stone, which is the local limestone. Twenty-five specimens (labelled as LHE) were selected from this fourteenth century church. This glass was last cited as being in the west window, although the length of time in this glazing position is unknown.

Checkley

St. Mary's church, Staffordshire, underwent extensive glass restoration coincidental with this study and therefore a substantial sample size was analysable. The glazing is late fourteenth century whereas the church was originally built in the thirteenth century but practically rebuilt in the seventeenth century [117]. Thirty-four samples (labelled as CHK) were selected from the north-facing panels, and a further thirty two from the south-facing panels. As with the Fledborough glass, the north-facing material had a coating of green algae, whilst the south facing glass was rendered opaque by decay products. It was built from White Hollington stone.

Fairford

St. Mary's church, Gloucestershire, is one of the most renowned in England. It was built of Cotswold limestone between 1500 and 1532; the glazing scheme is contemporary with this. The glazing is unusually complete, with ancient glass in all of its twenty eight windows [87]. Art historians are confident that the scheme has not been altered or moved since its installation. There is a marked difference in the extent of decay between the north- and south-facing windows. The north-facing glass has suffered extensive loss of paint detail, but is otherwise fine; the south-facing has up to 2mm of crust on the surface. This difference meant that the number of samples chosen from each orientation was very different with an associated different label: 22 from the north (FAI) and 44 from the south (FAS). The total number of samples, therefore, being equal to that taken

from Checkley i.e. 66. This was so that a direct comparison between these two churches could be undertaken.

Glass Corrosion

Chapter 4

Infrared Reflection Spectroscopy

The infrared region of the electromagnetic spectrum extends over the frequency range 10–20000cm^{-1} (though the range used, in this study, for diffuse reflectance Fourier transform infrared spectroscopy (DRIFT) was 400–4000cm^{-1}). Infrared spectroscopy is an important tool for obtaining chemical information as all compounds absorb IR radiation of specific wavelengths depending on the nature of the compound. For this reason it may be used to identify the functional groups present in a pure compound or a mixture. The development of Fourier transform spectroscopy (FTIR) provided a means of almost instantaneously recording the whole IR spectrum; previously the response at each part of the spectrum had to be collected separately. The earlier method was particularly inefficient if the spectrum contained only one or two peaks as most of the time was spent recording background noise [8].

A special application of FT-IR is in the analysis of powders through diffuse reflectance, usually abbreviated to DRIFT. The usual method of wavelength dispersive IR analysis involves making potassium bromide (KBr) disks, though this requires a reasonable amount of sample, the addition of a dilutent (KBr) in the correct ratio and is subject to difficulties in preparation. As the amount of sample was limited not only by what was present on the surfaces but also by what was removable, DRIFT analysis was chosen. For DRIFT no dilutent is needed, no preparation is required beyond obtaining the sample and the sample is reusable.

4.1 IR Absorption

A molecule can absorb radiation of frequency ν by undergoing one or more transitions [4, 12]. These transitions can be of three types and are dependent on the properties of the molecule. In order for *rotational* transitions to occur the molecule must possess a permanent electric dipole moment;

for *vibrational* transitions to occur there must be a change in the dipole moment. The other type of transition is electronic, in which the net dipole moment changes on the electron redistribution. Otherwise the transition is forbidden. All types of transitions are governed by quantum mechanical selection rules.

In the case of classical rotation, for a rigid rotor:

$$E = \frac{1}{2} I_{xx} \omega_x^2 \tag{4.1}$$

where E is energy, I_{xx} is the moment of inertia and ω_x is the angular velocity, which becomes in quantum mechanics

$$E_{JK} = hcBJ(J+1) + hc(A-B)K^2 \tag{4.2}$$

where J is 0,1,2 *etc.* and K is 0 to $\pm J$ with

$$A = \frac{h}{8\pi^2 c I_{para}} \tag{4.3}$$

and

$$B = \frac{h}{8\pi^2 c I_{perp}} \tag{4.4}$$

The selection rules which apply are

$$\Delta J = \pm 1 \tag{4.5}$$

and

$$\Delta K = 0 \tag{4.6}$$

For vibration we have the harmonic oscillator equation

$$E_\nu = \frac{(\nu + \frac{1}{2})h\omega}{2\pi} \tag{4.7}$$

where

$$\omega = (\frac{k}{\mu})^{\frac{1}{2}} \tag{4.8}$$

as the simplest expression for the energy of vibration. The selection rule for transitions between the vibrational states is

$$\Delta\nu = \pm 1 \tag{4.9}$$

but for a diatomic molecule this becomes

$$\Delta\nu = 1 \tag{4.10}$$

where ν is the vibrational quantum number [138, 12].

The above is for diatomic molecules only and unfortunately most of the functional groups that are to be considered through absorption spectroscopy are polyatomic, which makes the analysis more

complex. For example, water can be identified through IR absorption in the following three regions: $3652cm^{-1}, 1595cm^{-1}$ and $3756cm^{-1}$. These are due to three different vibrational modes (stretch, bend and asymmetric stretch). Usually both vibration and rotation occur, therefore one expects to see a complex spectrum with the rotation superimposed on to the vibration. The rotation of molecules is restricted in solids leading to a broadening of the rotational bands, such that in IR spectra only vibrational information is measurable.

The observed vibrational spectra increase in complexity with the number of functional groups present. This can result in misinterpretation of spectra, eg. the sulphate and silica bands overlap in the $1100cm^{-1}$ region because the sulphate stretch mode is at $1105cm^{-1}$ and the Si-O stretch mode occurs around $1080cm^{-1}$ depending on the bond strength. This also means that only the major component and possibly one or two others may be identified by DRIFT analysis.

4.2 FT-IR Spectroscopy

Infrared spectrometers are based upon the Michelson interferometer (MI), which was originally designed to detect the ether wind. The simplest form of MI, is two mutually perpendicular mirrors, one of which is movable(Figure 4.1).

4.2.1 Instrumentation

Spectrometers are made up of various components (see Figure 4.1):

The source is a form of filament, either Nernst or globar. This is maintained at red/white heat by an applied electric current.

The monochromator guides and focuses the beam.

The detector will work either by sensing the heating effect of the radiation or by the photoconductivity of it. The most common type is the mercury cadmium telluride (MCT) detector which operates at liquid nitrogen temperatures.

The sample can be solid, liquid or gas although each have inherent problems. Solids are particularly difficult to examine due to reflection and scatter.

Consider a monochromatic radiation source, as the movable mirror is scanned through the position of equidistance the resultant output changes due to interference. At the equidistance position constructive interference occurs producing a maximum and minima occurs when the path difference

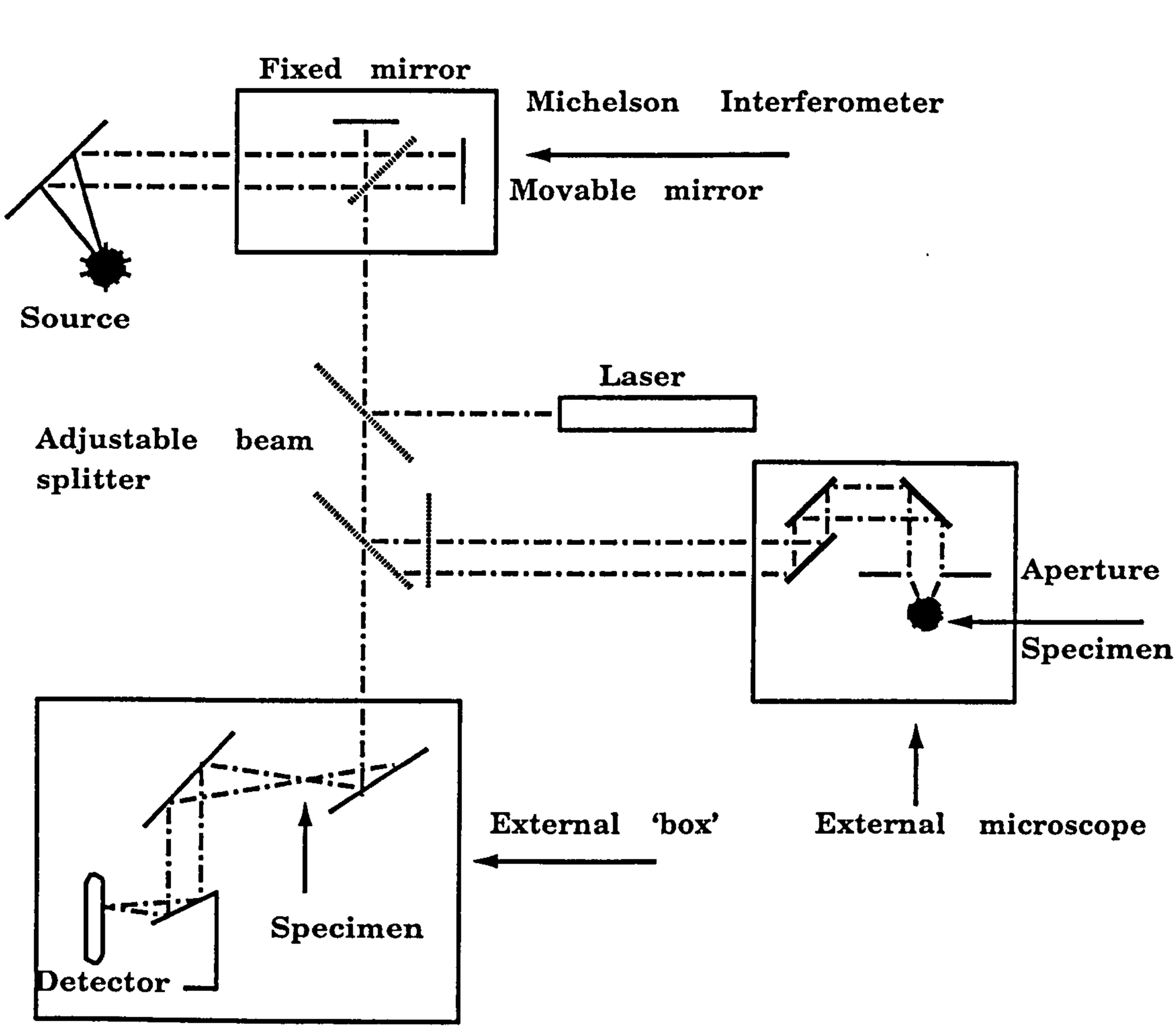

Figure 4.1: Schematic diagram of the major parts within the FT-IR spectrometer.

Glass Corrosion

is $\lambda/2$ [62]. The output can be considered as two parts, a constant d.c. component and a modulated a.c. component.

$$I'(\delta) = 0.5I(\nu)(1 + \cos 2\pi\delta\nu) \tag{4.11}$$

where $I'(\delta)$ is the intensity of the detected signal, $I(\nu)$ is the intensity of the source and δ is the retardation. It is the modulated component that is referred to as the interferogram. In practice, the amplitude of the interferogram is also dependent on the detector response, beam splitter efficiency and the characteristics of the amplifier. The spectrum is then derived from the interferogram by taking the Fourier transform of $I'(\delta)$. In the case of monochromatic radiation this is trivial. A sample emitting two or more frequencies will appear to the detector as the sum of the waves and the interferogram will be the resultant of the individual interferograms for each frequency. This gives a complex spectrum for transformation, though a computer will perform these calculations in seconds. It is in this manner that FT-spectroscopy has speeded up data collection by as much as a factor of 1000.

4.3 Theory of Diffuse Reflectance Infrared Fourier Transform Spectroscopy

Initial use of diffuse reflectance as a potentially quantitative technique dates as far back as the 1920s [52]. When radiation is reflected from a surface it is both specular and diffuse. Diffuse reflectance measurements must have the specular reflections minimised, perhaps by the introduction of a dilutent. The amount of light reflected is measured with the aid of a suitably modified transmission spectrophotometer. The output is in terms of percent reflected. Several theories of diffuse reflectance have been suggested, Kubelka-Munk being the the least general but most used. The following is a brief summary of the theory with the complete derivation of the Kubelka-Munk equation in appendix A.1.

4.3.1 Kubelka-Munk Theory in brief

The theory developed assumes the diffuse reflectance is from an infinitely thick opaque layer and yields the following equation:

$$\frac{k}{s} = \frac{(1 - R'_\infty)^2}{2R'_\infty} \tag{4.12}$$

where k is the molar absorption coefficient, s the scattering coefficient and R'_∞ is the absolute reflectance. It is more usual however, to work with R_∞, defined as:-

$$R_\infty = \frac{R'_{\infty sample}}{R'_{\infty standard}} \tag{4.13}$$

The standard chosen being either magnesium oxide or barium sulphate. This renders the Kubelka-Munk equation as:-

$$F(R_\infty) \equiv \frac{(1-R_\infty)^2}{2R_\infty} = \frac{k}{s} \tag{4.14}$$

and the wavelength component of the scattering coefficient is made negligible by ensuring the particle size is large compared to the wavelength used.

When the reflectance of a sample diluted by the presence of a non or low absorbing powder is measured against the pure powder, k may be replaced by $2.30\epsilon C$. Where C is the molar concentration and ϵ is the extinction coefficient. A straight-line relationship between C and $F(R_\infty)$ is only observed when the sample is weakly absorbing and the grain size is relatively small.

4.4 Practical Aspects

The analysis was performed using a Mattson Galaxy 6020 instrument, comprising of a globar source, a He-Ne laser to provide a reference beam, and a DRIFT attachment placed in the external chamber (see Figure 4.1). This was a correctly aligned set of mirrors which allowed the diffuse reflected beam to be focussed. DRIFT has one major drawback: it has a very low energy throughput. This means that the throughput must be maximised, via tuning, a simple process involving a height adjustment of the sample pedestal.

The computer attachment enables various parameters to be set, such as resolution, spectrum type and number of scans. It is essential that the same parameters be used when collecting both background and sample spectra. For the analysis, the small pedestal was covered with a small piece of aluminised silicon carbide (SiC) paper. This was necessary to hold the powder in place. The presence of the SiC paper on the pedestal means that it must be included when taking a background spectrum, and must be free from contamination. It is good practice to take background spectra throughout the data collection, as room temperature and other properties may vary (recalibration every five spectra was found to be more than adequate). A small amount of sample powder was placed on a piece of SiC paper and lightly brushed to remove any excess (with a clean paintbrush for example). This was necessary as too much sample will cause the peaks to be truncated.

The collected spectrum was set to be of type 'single beam (sbm)', this was ratioed with the background (bkg) spectrum and then converted into a diffuse reflectance (drt) spectrum for the purpose of interpretation. Purging the system removes the effect of atmospheric water and carbon dioxide since these are particularly active in the IR region and can mask other more relevant peaks. The background ratioing removes any remaining atmospheric effects such as the reflectivity of the paper. The conversion was done computationally using Kubelka-Munk equations, thus the results are in KM units. The (drt) spectrum is a derived absorbance spectrum from the collected

Parameter	Value/Description
Number of scans	500
Resolution	8 cm^{-1}
Gain	20
Detector	standard MCT detector
Start wavenumber	450cm^{-1}

Table 4.1: Summary of the parameters used in DRIFT analysis of the weathering products.

reflectance spectrum [89]. It is possible from this spectrum to identify constituent functional groups of the sample.

4.4.1 Application and Calibration

The DRIFT analysis of several mineral compounds (those listed in section 5.2.2) was carried out so that a library of spectra would be available for comparison when the unknowns were analysed.

Whilst taking the 'calibration' mineral spectra, an auxiliary investigation into parameter settings was carried out. The following background effects were looked at:

- Does the size and grade of the SiC paper affect the results?
- Does the purging system work properly?
- How much sample is needed?

The conclusions were that the purging was in correct working order and that the amount of specimen needed depended upon the compounds present. The size of paper onto which the powder was placed did not matter but the grade of the paper needed to be greater than 100μm. This latter point is because otherwise the particle size of the paper would be of the order of the wavelength of the radiation and hence interference would result. The paper used was 600μm. Several spectra were taken for each unknown with gradually diminishing amounts of powder until the spectra were unsaturated.

Throughout the data collection the parameters for computational control were fixed as indicated in Table 4.1.

These parameters were chosen to give the optimal spectrum for the equipment available and the time limitations. The resolution of the equipment is related to the mirror movement, x, by

$$\delta\nu = \frac{1}{x_{max}} \tag{4.15}$$

For this galaxy FTIR spectrometer, the highest resolution available is $1cm^{-1}$; that used for the study was not the limit of the machine. The resolution affects the signal to noise ratio *(s/n)*, therefore, the higher the resolution the longer the recording time must be for the same ratio. The relationship between the *s/n* ratio and number of scans follows a square root dependence (Fellget's advantage [8]), which means that there is a limit to the effectiveness of increasing the number of scans. For the chosen resolution the number of scans required was not large. The gain was selected to give the largest amplitude without clipping the interferogram.

The sample analysis involved removing a small amount of the crust or powder from the glasses. Initially it was hoped that crust removal would not be necessary for this analysis; unfortunately effects due to the glass underlying the corrosion products proved very difficult to remove from the spectra. There was also a problem with the size of glass sample that would fit within the DRIFT attachment. This latter restriction would have resulted in a vast reduction in the possible number of glass samples that could be analysed. Generally the amount of powder needed for this analysis is extremely small; it was found that the powder removed for XRD was more than adequate to enable both techniques to be used. DRIFT was performed on the powder first since no 'background' is mixed in with the powder, enabling its re-use. The DRIFT analysis allowed the minerals to be identified directly using the 'library' of mineral spectra collected. If the library had not been stored, then the analysis would only have identified the functional groups present in the powder and the ensuing interpretation would have taken much longer.

4.4.2 Interpretation

All of the glass specimens that had removable decay products were analysed in the previously mentioned manner. In some cases more than one sample of powder was removed, especially in those cases where both surfaces had deteriorated. Also, when present, the putty from the window leading was analysed to enable clarification of non-decay products in the samples where this was not obvious.

Figure 4.2 illustrates the type of diffuse reflectance spectra obtained from an unknown and the comparable reference spectra of the minerals. This particular data is from GMH14 (outer surface) and the products are clearly silica and calcite. A complete table of the results is given in Appendix B where the compounds identified by DRIFT have been combined with those from XRD.

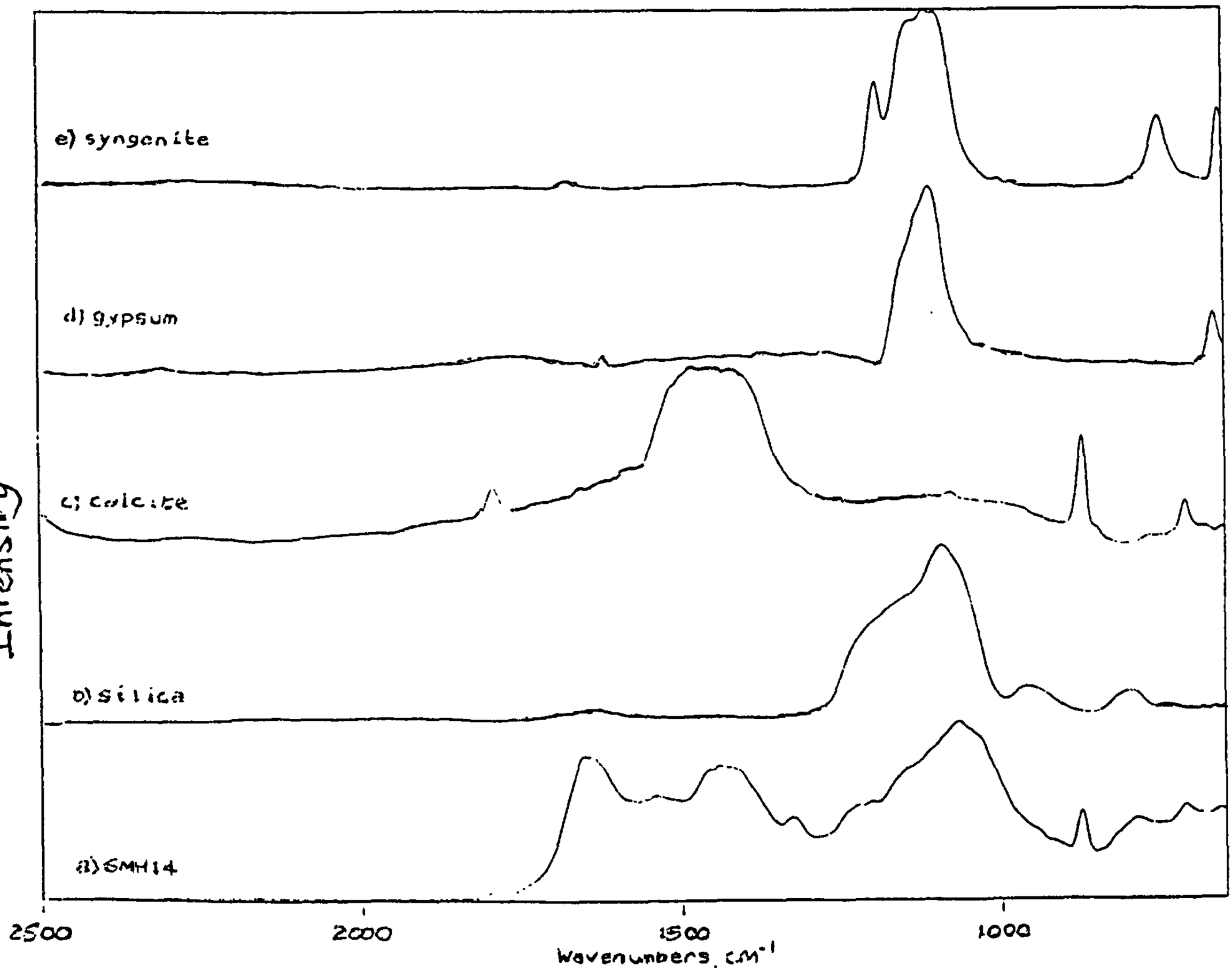

Figure 4.2: An example of the (drt) spectra obtained for a) GMH14 (outer surface) b) silica c) calcite d) gypsum e) syngenite

Chapter 5

X-Ray Diffraction : Theory and Practice

5.1 X-Ray Diffraction Theory

It was Laue who first suggested that a crystal might behave towards x-rays in the same way that a diffraction grating does to ordinary light [80, 134]. In 1912 Friedrich, Knipping and Laue [80, 53, 71] performed an experiment to show this. X-rays were emitted from a metallic target on bombardment with electrons; these were then collimated and fired at a specimen. The crystal chosen was zinc blende. On passing through the sample the x-rays hit a photographic plate which on development gave a central bright spot as well as some surrounding fainter spots. This indicated that there was more than one direction through which the crystal selectively diffracted x-rays.

The explanation of the above was published in 1913 by W.L.Bragg [17]. He inferred that so long as a crystal had a structure that was repetitive in three dimensions, it was possible to draw sets of parallel planes in which the atoms were arranged the same way. These planes have been called Bragg planes.

When monochromatic x-rays (of wavelength λ) fall upon Bragg planes (at an angle θ with a plane separation of d), each atom acts as a scatterer. Generally, the scattered waves from each plane are out of phase with each other and destructive interference results. However, if the Bragg equation (equation 5.1) is satisfied, then constructive interference occurs and a relatively intense beam is reflected from the surface.

$$2d \sin\theta = n\lambda \tag{5.1}$$

It is very rare, however, for only one beam to emerge from a crystal, and hence most x-ray diffraction

patterns are complex. Importantly, any non-crystalline powder will not give a distinctive set of x-ray diffraction lines, but a broad diffuse band.

5.2 Experimental Methods of X-Ray Diffraction

Of the various methods available for performing x-ray diffraction the powder method was selected. This has the advantage that the sample is finely ground thus eliminating the need for a single crystal. The x-ray source is monochromatic eg., Cu Kβ. Since the specimen is a powder it must be contained within a vessel, such as a thin capillary tube. As this was the method of analysis chosen, further details about it are given in the next section.

5.2.1 Practical Aspects

The technique of x-ray powder diffraction was used to identify the compounds present in the weathering crusts. This was done using the Debye-Scherrer method [81, 39, 38]. A powder camera was used in conjunction with an x-ray generator. The Cu Kβ radiation was removed by a nickel filter, making the analysing radiation Cu Kα; average wavelength, 1.5418Å. This produces doublets at high angle diffraction, since the difference between the two component wavelengths is highlighted. This type of analysis requires that the corrosion products be easy to remove from the glass' surface; in some cases this was not possible , *ie.* when the weathering that had occurred was only shallow pitting. The removed crust was then finely ground, under acetone, mixed with a quick setting adhesive and rolled into a thin rod. This method of mounting was found to be superior to placing the ground powder in a fine capillary tube, since less scattering resulted from the amorphous glue than the glass [35]. By comparing the interatomic spacing values from the resulting diffraction patterns with the American Society for Testing and Materials (ASTM) powder diffraction file and card index, the compounds present were identified.

5.2.2 Calibration

Prior to commencing the analysis of the corrosion products it was necessary to calibrate the equipment. Initially some "known" specimens were analysed by placing them in fine capillary tubes. The chosen "standards" were aluminium oxide (alumina), Al_2O_3 and lithium fluoride, LiF. The resulting diffraction patterns were then used to calculate the interatomic spacings, ie. the *d*-values. The measured values and the expected values were then compared.

As can be seen from Table 5.1 the maximum error in the values was:

$$\delta = \pm 0.06\mathring{A} \tag{5.2}$$

Powder	d-values /Å			Error /Å
	Direct Scale	Measured	ASTM	Meas. to ASTM
Al_2O_3	1.34	1.35	1.39	- 0.04
	1.98	2.04	1.98	+0.06
	2.45	2.49	2.45	+ 0.04
Al_2O_3	1.35	1.35	1.39	- 0.04
	2.10	2.04	1.98	+0.06
	2.48	2.49	2.45	+ 0.04
LiF	2.25	2.28	2.33	- 0.05
	1.95	1.97	2.01	- 0.04
	1.39	1.40	1.42	- 0.02
LiF	2.25	2.28	2.33	- 0.05
	1.96	1.97	2.01	- 0.04
	1.40	1.40	1.42	- 0.02

Table 5.1: Interatomic spacing values evaluated during the calibration of the x-ray camera.

However, on closer examination it was noted that aluminium oxide, Al_2O_3 has five possible phases at room temperature and therefore was not a good "standard". This left an error of the order of $0.04\mathring{A}$ which was thought to be due to a slight broadening of the diffraction lines by the width of the capillary tube. In order to test whether the capillary tube itself was affecting the results the LiF was repeated as a rolled Durafix rod.

As can be seen from Table 5.2 the results were not improved, the error remains of the same order. The LiF in Durafix was repeated, giving identical results. This suggested that the error was systematic and a constant offset of the equipment.

A calibration plot was drawn enabling all further calculated d-values to be corrected. The measured d-values of LiF were plotted against the expected values from the ASTM file. An important point to note is that the plot was only valid for d-values between 1 and 3.5 Å, ie. the range over which LiF diffraction lines exist (therefore uncorrected values have an associated asterisk).

To test the method of correction two samples were analysed, a known (precipitated calcium carbonate) and a blind test specimen. The latter was correctly identified as syngenite. The corrected results match the expected ones remarkably well, to within 0.01 Å, and are given in Table 5.3.

As a follow up to the calibration of the camera, several pure minerals were analysed so that a library of their x-ray diffraction patterns was readily available. This facilitated identification of possible compounds present, by enabling a direct comparison of a pure mineral's x-ray lines with the those on the x-ray diffraction pattern of an unknown. The minerals chosen were in compliance

LiF Type	Measured d Å	ASTM d Å	Error /Å
Capillary	2.28	2.33	-0.05
	1.97	2.01	- 0.04
	1.40	1.42	- 0.02
Capillary	2.28	2.33	-0.05
	1.97	2.01	-0.04
	1.40	1.42	-0.02
Durafix	2.25	2.33	-0.08
	1.95	2.01	-0.06
	1.39	1.42	-0.03

Table 5.2: Interatomic spacing values for LiF.

Mineral	d-value Å		
	Experimental	Corrected	ASTM
$CaCO_3$	3.76	3.88 ± 0.02	3.86
	2.95	3.03 ± 0.03	3.04
	2.44	2.50 ± 0.02	2.49
	2.24	2.30 ± 0.02	2.28
	2.08	2.13 ± 0.03	2.10
	1.87	1.92 ± 0.01	1.91
	1.82	1.86 ± 0.01	1.87
	1.58	1.60 ± 0.01	1.60
$K_2Ca(SO_4)_2$	2.79	2.85 ± 0.03	2.86
	3.09	3.18 ± 0.03	3.17
	5.59	5.59*	5.71
	2.68	2.75 ± 0.03	2.74
	2.79	2.85 ± 0.03	2.83
	9.64	9.64*	9.49
	4.48	4.62 ± 0.03	4.62
	3.26	3.36 ± 0.03	3.35

Table 5.3: Interatomic spacing calculation by correction for syngenite and calcite.

Glass Corrosion

with those that had previously been identified on atmospherically corroded glass [58, 59]. They were :

- Syngenite, $K_2Ca(SO_4)_2).H_2O$
- Calcite, $CaCO_3$
- Gypsum, $CaSO_4.2H_2O$
- Epsomite, $MgSO_4.7H_2O$
- Anhydrite Calcium Sulphate, $CaSO_4$
- Hydrated Silica Gel, $SiO_2.xH_2O$
- Bassanite, $CaSO_4.1/2H_2O$
- Quartz (although this is probably of external origin).

In addition, Durafix was analysed so that the area of the x-ray diffraction patterns that could be affected by the halo, due to the amorphous glue, could be identified. All the corrected d-values for the above minerals agreed with the ASTM values within experimental error, provided the d-value of the line was in the correct region, ie., between 1 and 3.5 Å. Fortunately, most of the intense characteristic lines occurred within this region.

5.3 Interpretation

All of the unknown powders were mixed with Durafix glue to enable the powder diffraction analysis to be carried out. The actual samples were placed in a Debye-Scherrer camera attached to an x-ray generator (40kV, 20mA, CuKα) and exposed for up to fourteen hours, depending upon the amount of specimen available and the mineral type. Figure 5.1 shows the type of patterns obtained. The first diffraction pattern is of the unknown powder from SCB3 and is followed by the patterns produced by calcite, bassanite, gypsum and syngenite. It can be seen that the products are calcite and gypsum.

In most of the cases the high-angle diffraction lines were impossible to obtain (due to absorption by the sample and the fact that increasing the exposure time also increases the background, thus weak lines) and therefore identification was by direct comparison of the unknown with the mineral patterns. The only mineral that could not be identified by these means was silica gel. This was due to the broad, scattered band produced by the glue masking any effect produced by amorphous silica. The complete list of data is contained in Appendix B, although in this table the silica has been identified by DRIFT only.

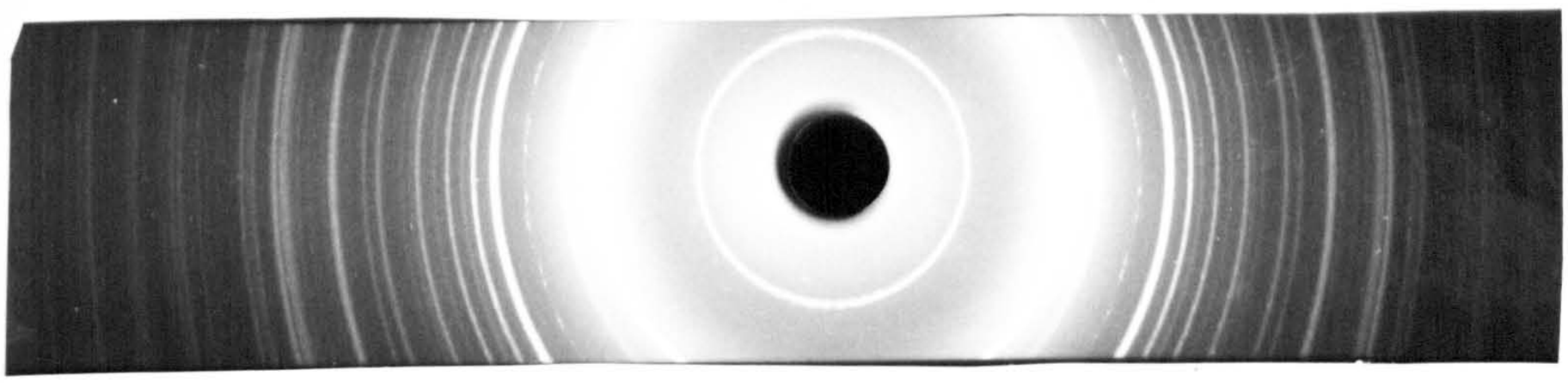

Figure 5.1: An example of the x-ray diffraction patterns obtained for a) SCB3 (outer surface) b) calcite c) bassanite d) gypsum e) syngenite

Chapter 6

Morphology Studies

The topography of corroded glass specimens varies enormously and therefore it was felt that a thorough study of this variation was called for. The samples were easily divided into three broad categories; 'unchanged', 'pitted' and 'crusted'. An initial investigation was carried out using an optical microscope at X21 magnification and these categories were compared to see if further division was necessary. Figures 6.1, 6.2 and 6.3 show the variation observed between the crusted and pitted types.

Figure 6.1 illustrates glass with isolated pit; it can be seen that pits are 'altered' regions (the grey areas of 6.1a with clear edges and marked centers. In 6.1a and more clearly in 6.1b, a white deposit can be seen in the center. This is the decay product. Surrounding the product are the pit walls. In 6.1b conchoidal fractures are observed around the rim.

Figure 6.2 contains micrographs of specimens with merged pits and there appears to be no visual distinction between those pits that merge and those that remain isolated. In the sample in 6.2b the decay products are more crystalline.

Figure 6.3 highlights the crusted surface. In both examples the remnants of pits can be discerned. The first micrograph is of a sample which had a hard white crust, whilst the other is of the soft orange crust as mentioned in Appendix C.

The optical micrographs of samples with biological growths on them are shown in Figure 8.1 in section 8.1. Photographs of the durable specimens have not been included as they convey little information.

Further investigation of the topography required observation in a scanning electron microscope. This in turn meant that they had to be coated with either carbon or a metal, eg. aluminium. Following this study the coating would need to be removed without damaging the underlying

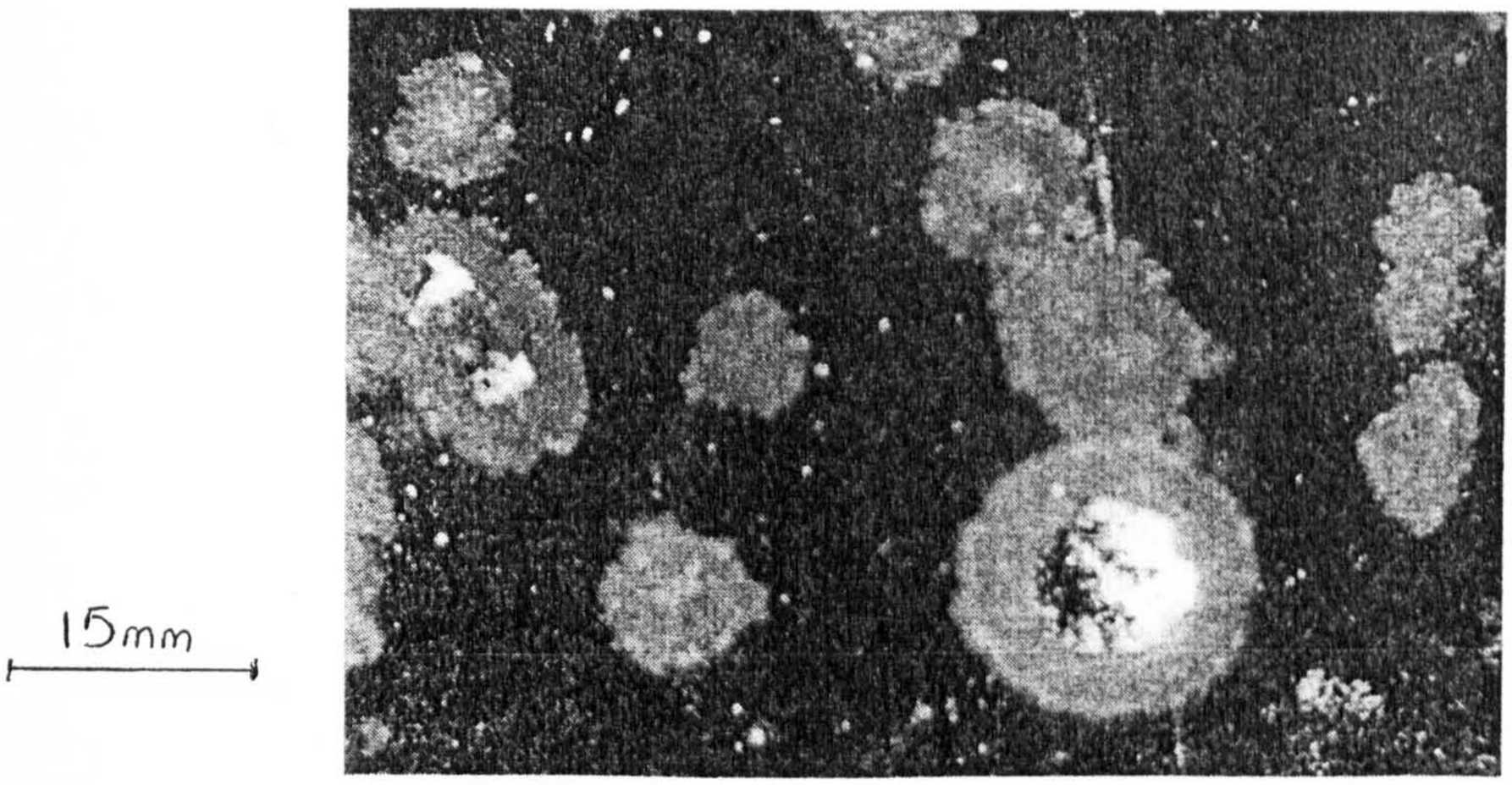

Figure 6.1: Optical micrographs of isolated pits at X21.a) the surface of CHK4S showing several pits and b) the surface of CHK27N a large isolated pit.

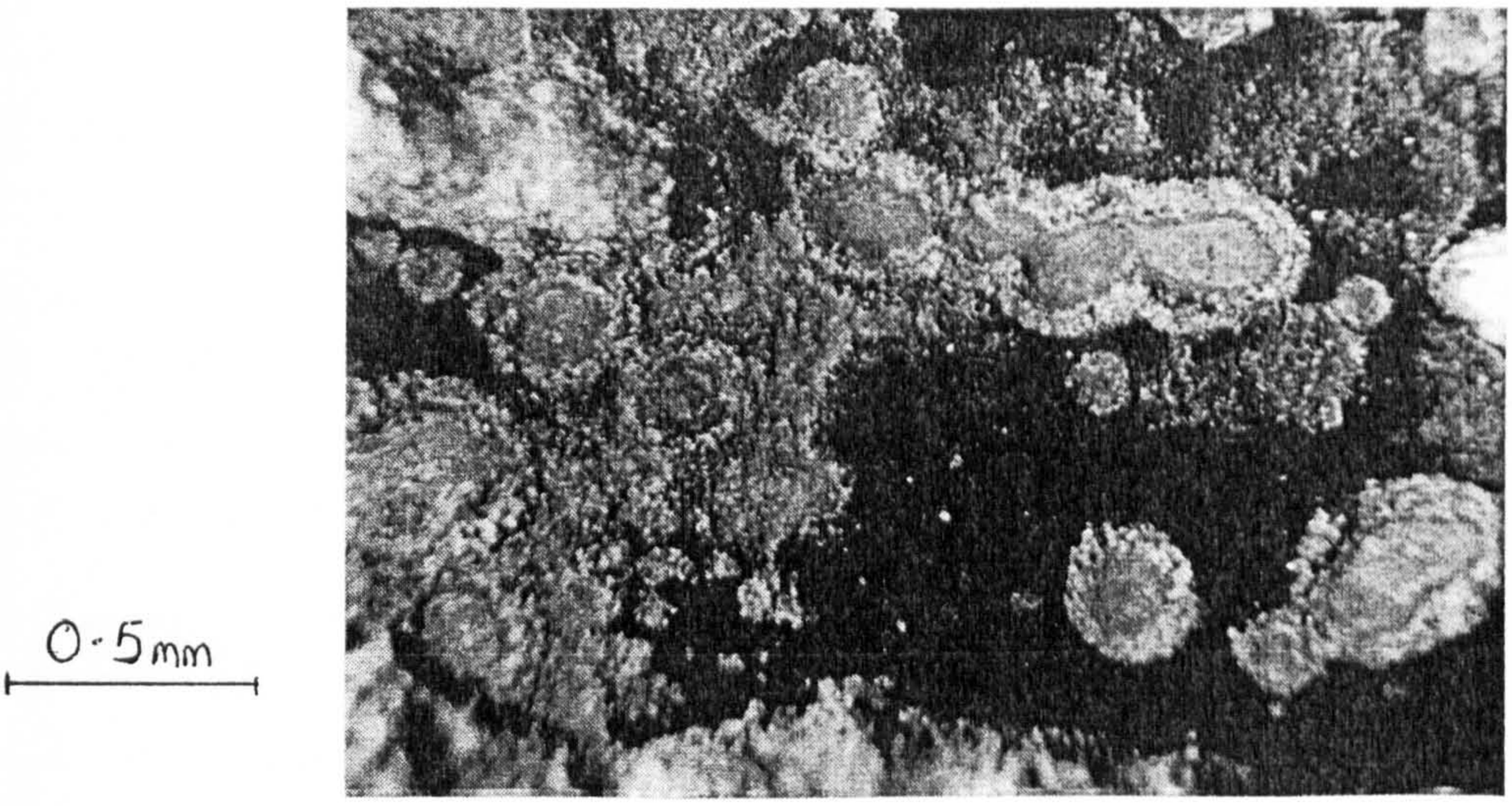

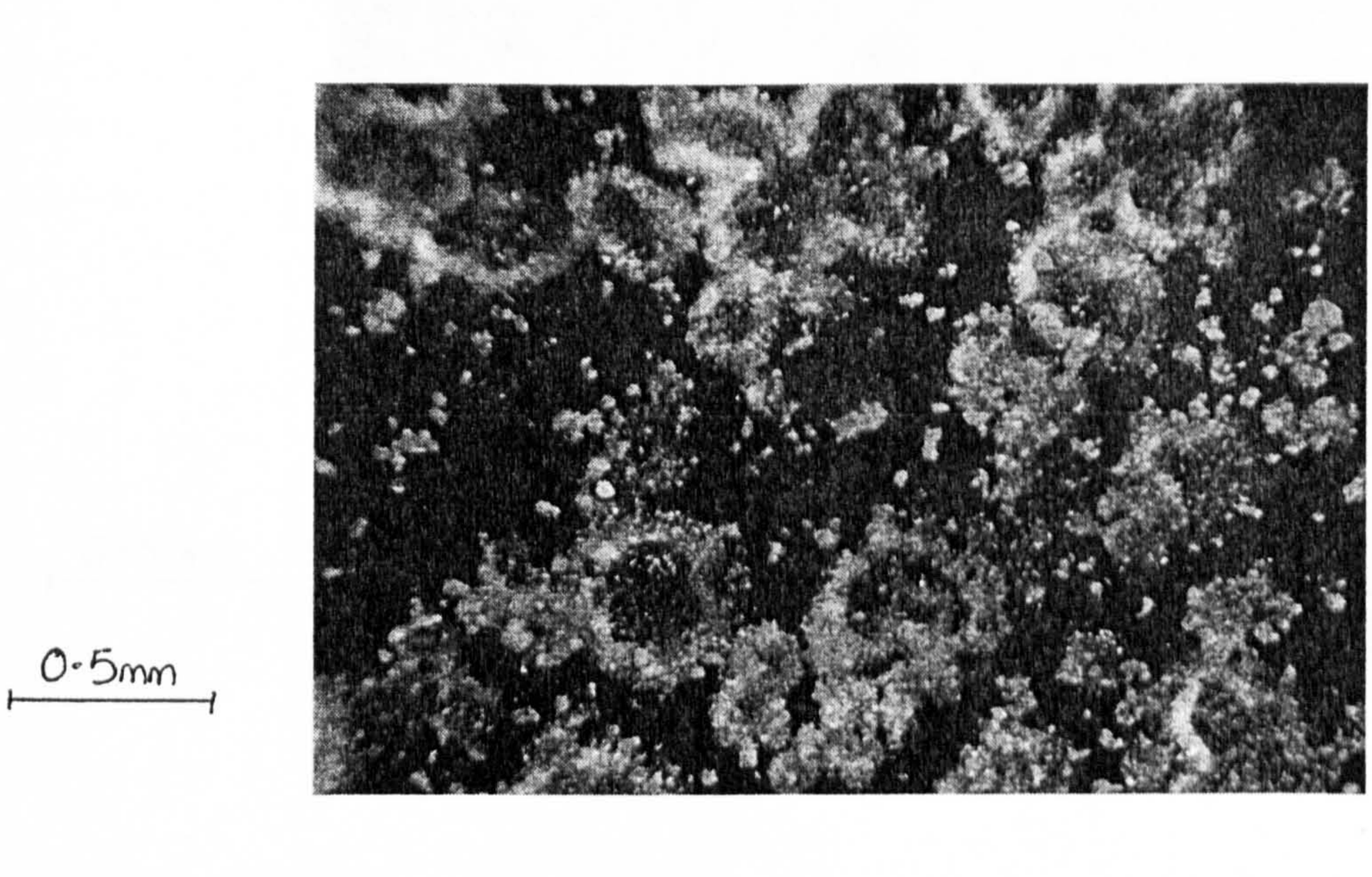

Figure 6.2: Optical micrographs of merged pits. a) the surface of CHK5S and b) the surface of LHE2 which has a rougher surface.

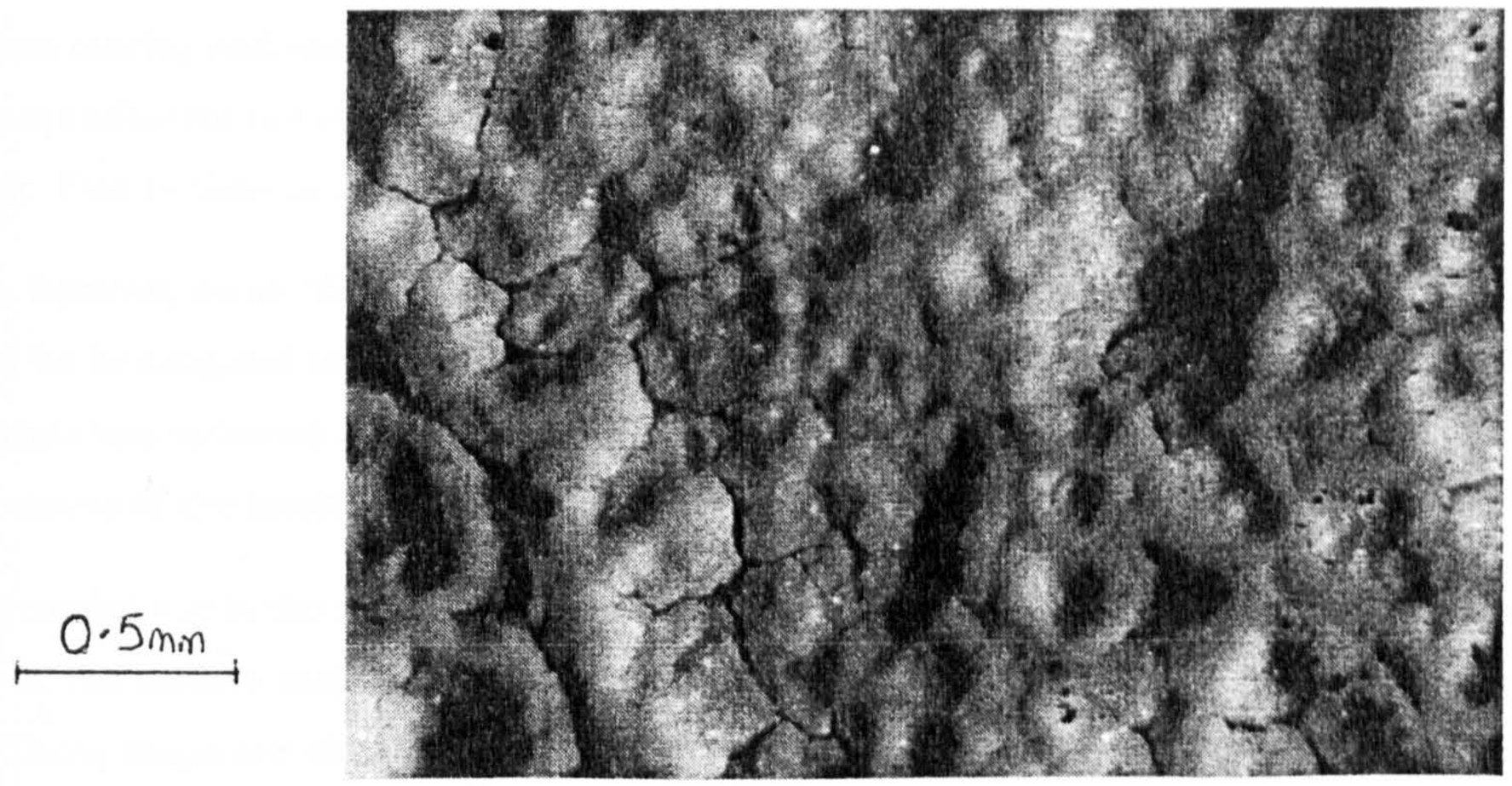

Figure 6.3: Optical micrographs of the crust. a) the surface of FAI64, a white hard crust and b) the surface of CHK21S, a soft, orange, powdery crust.

Glass Corrosion

surface. In order to minimise this risk only a small number of samples were investigated in this way. Coating with aluminium gave much better micrographs although it affected the compositional data obtained. This was because the aluminium layer would be detected as well as the aluminium present in the glass, resulting in an incorrect alumina content. Thus the samples were first analysed with a carbon coating and then re-photographed with an aluminium one present. The coat layer was much more adherent to the rougher surfaces; in all cases the majority of the surface was masked from coating. Due to time constraints only a limited number of samples were examined.

There were, however, some "donated samples" from two of the churches - Stanford and Fairford, which could be investigated thoroughly as they did not have to be returned. The background of these fragments was unknown and they will be referred to as the 'sacrificable' pieces from now on. During the course of the investigation the samples were destroyed.

The studies carried out in the SEM involved using the 'dot mapping' facility. That is, micrographs were taken of the surface and then subsequent 'maps' of the same area were taken for selected elements. These maps are obtained by setting a window on the spectrum, so that the signal observed on the screen of the SEM is only due to the emitted x-rays of a certain element. Thus a light area on a micrograph is due to the presence of a given element and a dark area the absence. A problem with this, was that the emission of x-rays was affected by the surface topography. Normally in chemical analysis the surface effects are removed by polishing the sample. The detected signal and hence the 'map', was angle dependent. As this was clearly inappropriate the angle at which the area was presented to the detector was varied and several micrographs taken. In the case of particularly deep pits, however, it was very difficult to get a signal from the sides and/or bottom; these show up as dark areas for all elements. The intensity of the map depends on the length of exposure as well as the element concerned. This is discussed in chapter 3.

The sacrificable samples enabled the study to be taken a step further; the distribution of the elements by depth could be investigated. The samples were first looked at 'as received' then embedded in resin and cross-sectioned. The surface exposed was then finely polished (using diamond paste to 1μm finish) and carbon coated.

The results obtained for each investigation will now be discussed separately, in sections 6.1 and 6.2.

6.1 Returnable Samples

This study was commenced towards the end of the available time and hence specimens from only a few of the churches were investigated in this manner. These were glasses from Checkley, Ely and Fairford. A complete analysis of the Fairford glass was curtailed due to lack of time. The

specimens considered were ELY 5, 8, 13; FAI 60; CHK 5N, 26N, 27N, 31N; CHK 1S, 4S, 18S, 20S, 21S, and 29S. The comparability of the compositions of all the specimens will be discussed in section 7.1.1 and it can be shown that these samples represent the spread of compositions found. They also reflect all of the manifestations of decay that were observed. Figures 6.4 and 6.5 show the corrosion types MP and U respectively.

Figure 6.4 shows a pit which is approximately 2mm in diameter. The SEM image highlights the difference in detecting signals from the edges of the pit and the rest of the surface. The contrast was too strong because the carbon coat was not continuous and therefore there was occasional charge build up. A good correlation between calcium and sulphur is seen at the bottom of the pit. The silicon distribution is quite different, being very intense at the pit boundary. This is expected, as the boundary should be deficient in modifiers and be mainly the remnants of the network. The distribution for potassium was the same as that for calcium and this would indicate in the present context that the pit contained syngenite. This was found to be the case when the products were analysed by XRD/DRIFT.

Figure 6.5 shows a crusted sample. The SEM image shows no specific feature and thus the dot maps have a random distribution. The silicon map is very different to that for calcium and/or sulphur. The calcium is markedly more intense, particularly in the lower right, than the sulphur, which could suggest that two calcium salts were present. This agrees with the XRD/DRIFT analysis of the products which shows them to be calcite and gypsum. Figure 6.6 is the dot map for potassium for the same sample. This is included to illustrate the type of dot map obtained from the base glass. It correlates very well with the silicon distribution.

6.2 Donated Sacrificable Fragments

The donated fragments came from the churches Stanford and Fairford. They were generally pieces smaller than $4cm^2$ in area and were of assorted colours. More pieces were provided from Fairford than from Stanford, but as with the full size samples (which were returned) from Fairford they were mainly durable. This meant that there were limited areas of interest on these samples. The samples will be considered together, but the Stanford samples produced the more interesting results. Only the Stanford fragments were analysed in cross-section due to time constraints.

Figure 6.7 shows the fragments from Stanford in the "as received" state; the samples from Fairford were comparable in size but less deteriorated. Figures 6.8, 6.9 and 6.10 show the more detailed morphology of the Stanford samples. Similar images were obtained for the Fairford fragments, but are not included. As can be seen from Figure 6.7 the Stanford fragment labelled L is more interesting from a corrosion point of view and therefore the most important sample for this study.

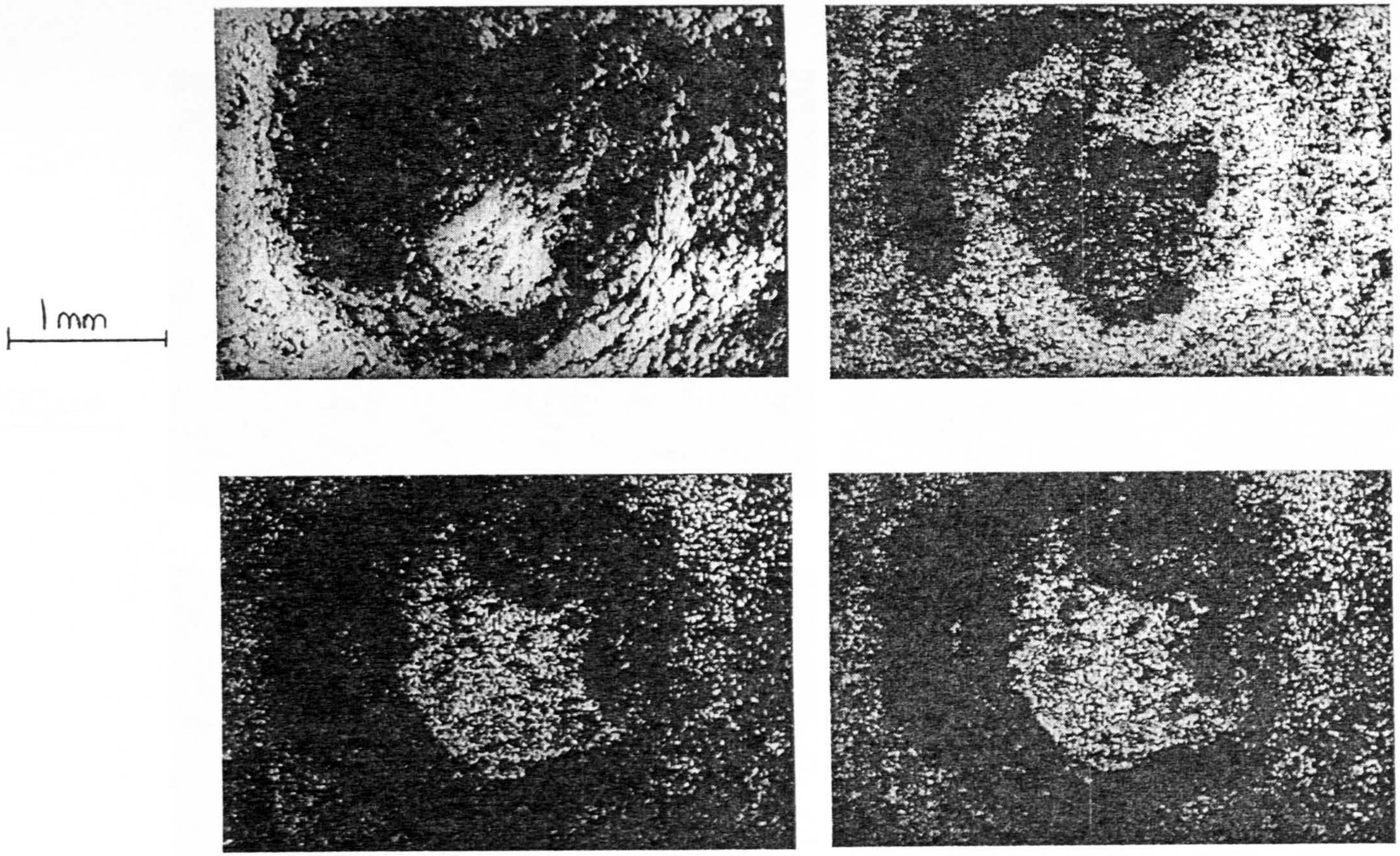

Figure 6.4: Electron micrographs of CHK29S. This sample had merged pits across the surface. a) the secondary electron image b) the dot map for silicon c) dot map for calcium and d) dot map for sulphur.

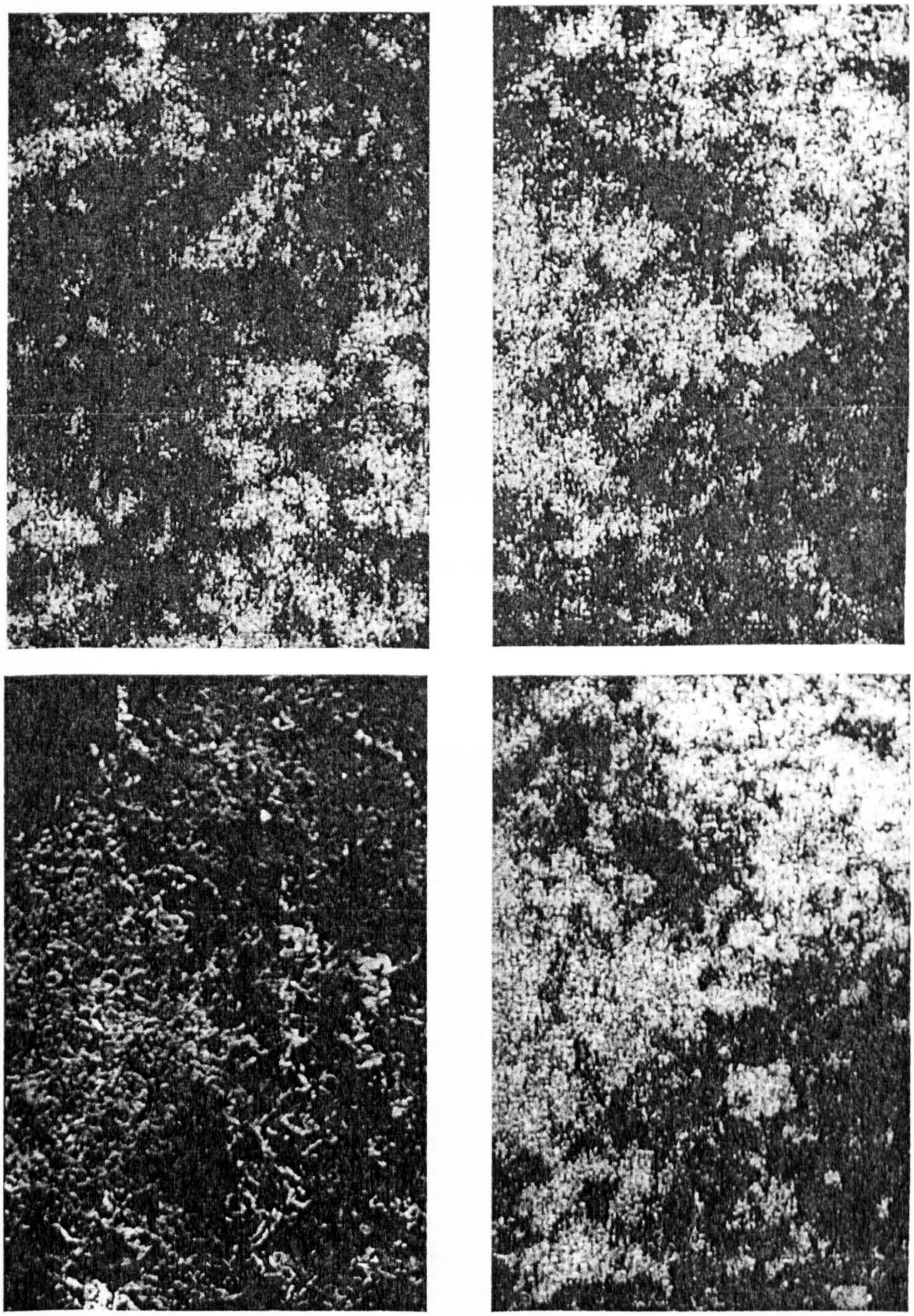

Figure 6.5: Electron micrographs of CHK18S. This sample had a crusted surface. a) the secondary electron image b) the dot map for silicon c) dot map for calcium and d) dot map for sulphur.

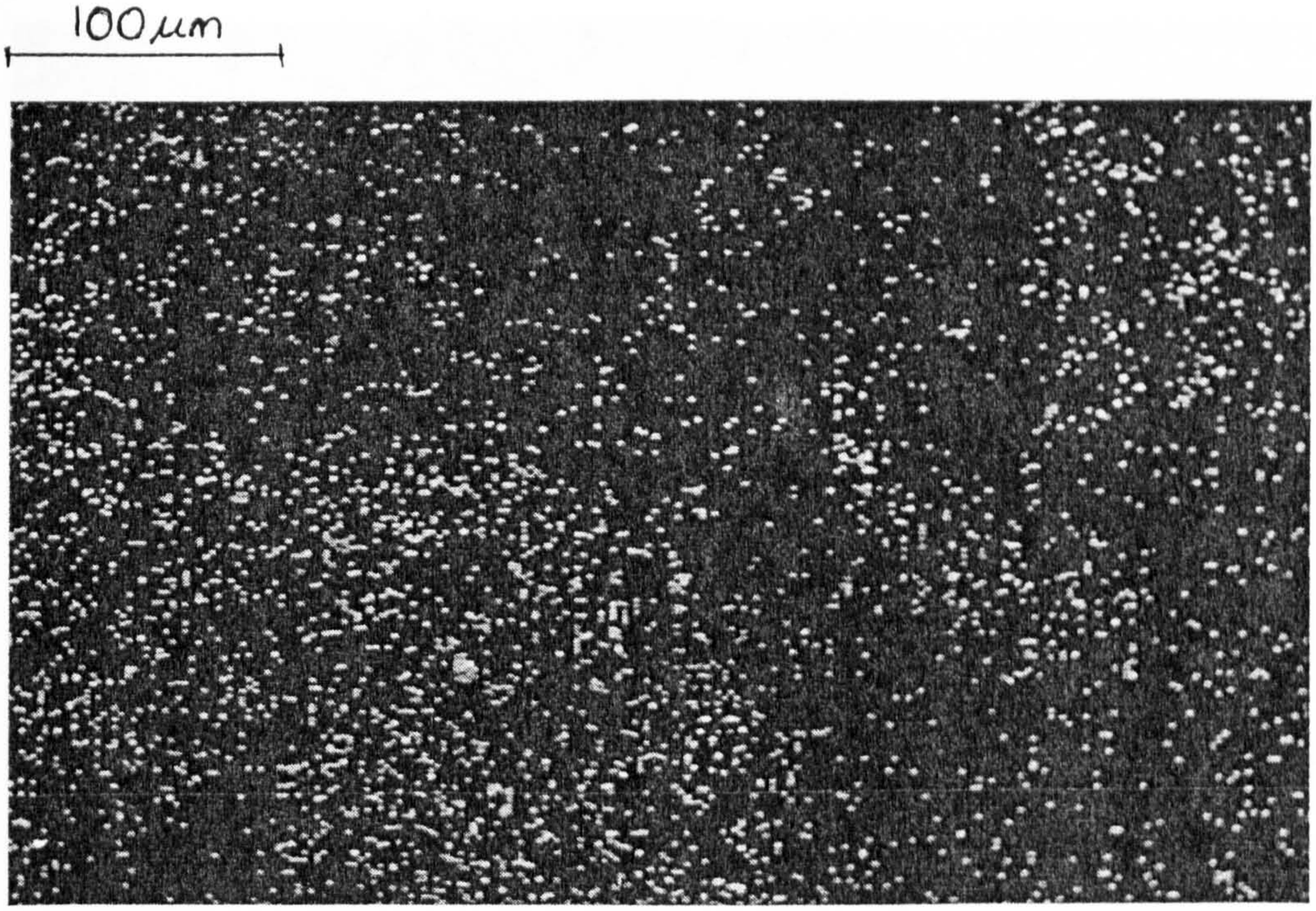

Figure 6.6: Elemental distribution map for potassium for the sample CHK18S.

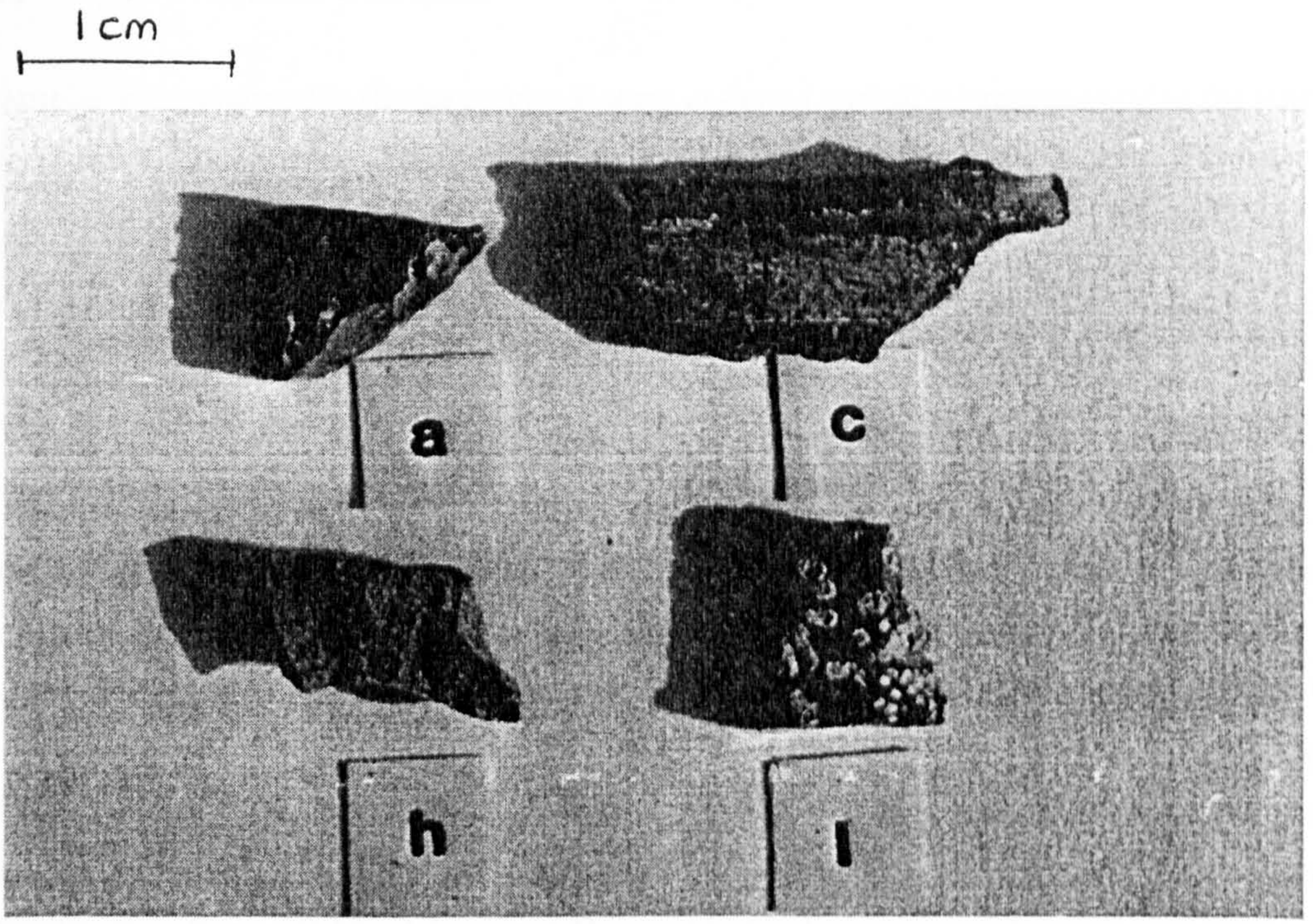

Figure 6.7: Photograph of the Stanford fragments.

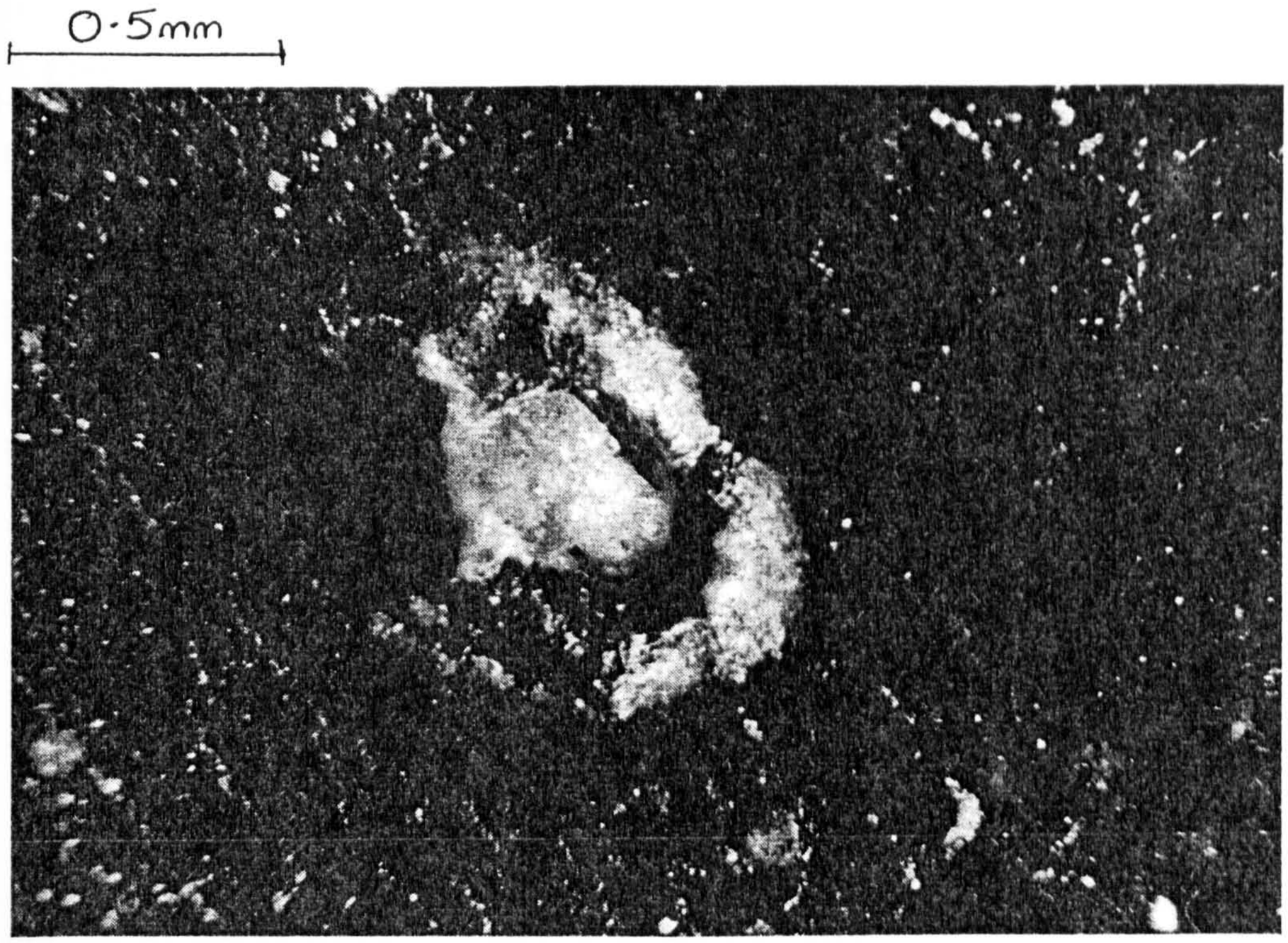

Figure 6.8: Optical micrograph of Stanford fragment A.

6.2.1 The Natural Surface

All samples were analysed in the 'as received' state under an optical microscope and in the scanning electron microscope. Subsequently they were embedded in resin blocks and cross-sectioned.

As the samples Stanford A and Stanford C had no products on the surface, the dot maps produced did not convey useful data. Stanford fragment H had some crusted regions, close to the painted areas. The dot maps of this area are given in Figure 6.11. The maps appear to indicate a correlation between the distribution of calcium and sulphur. These two species are in anti-correlation with silicon.

Stanford fragment L showed a similar correlation, see Figure 6.12. In this set of images, however, the sulphur signal is much more intense than that for calcium. There were no other cations that correlated with sulphur which would explain this discrepancy. Thus the difference must have been due to the difference in exposure time and the irregularity of the surface. Figure 6.13 shows the dot maps produced of the natural surface of Fairford fragment A. Here there is no apparent pattern to the calcium and sulphur distributions but these are obviously negatively correlated with the arrangement of silicon. Fairford fragment B gave identical results, but fragment M gave a more marked correlation of calcium and sulphur.

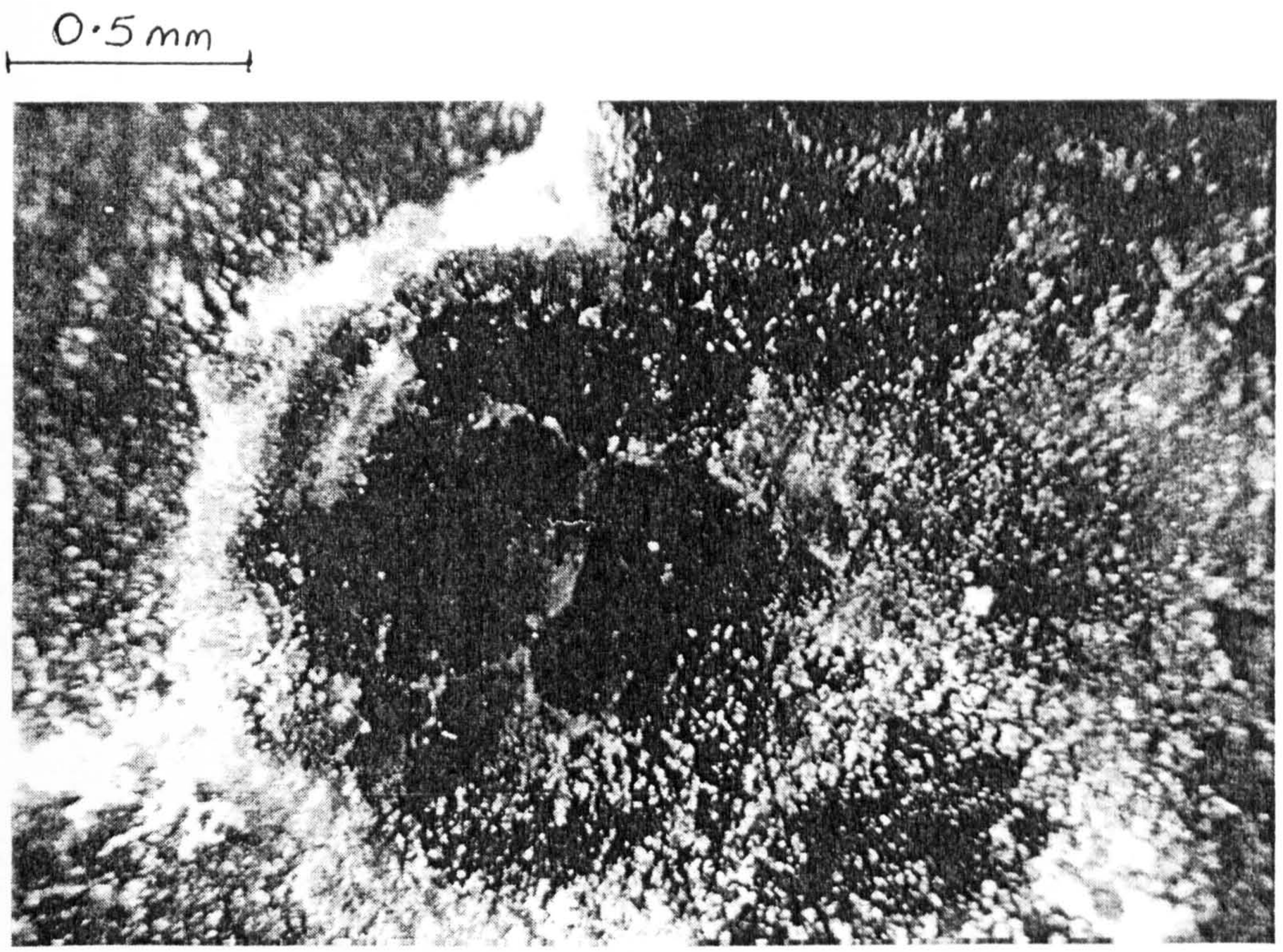

Figure 6.9: Optical micrograph of Stanford fragment C.

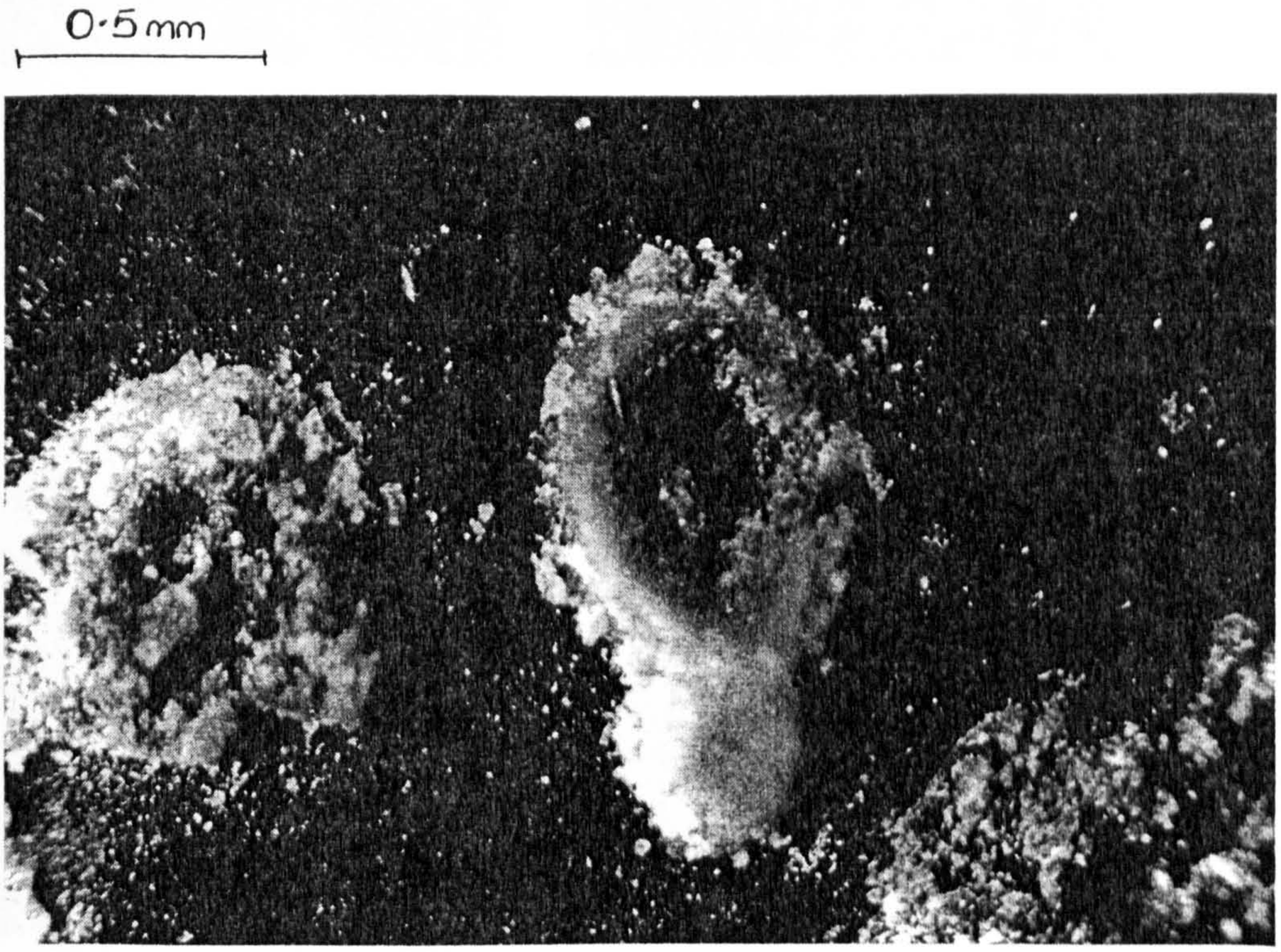

Figure 6.10: Optical micrograph of Stanford fragment L.

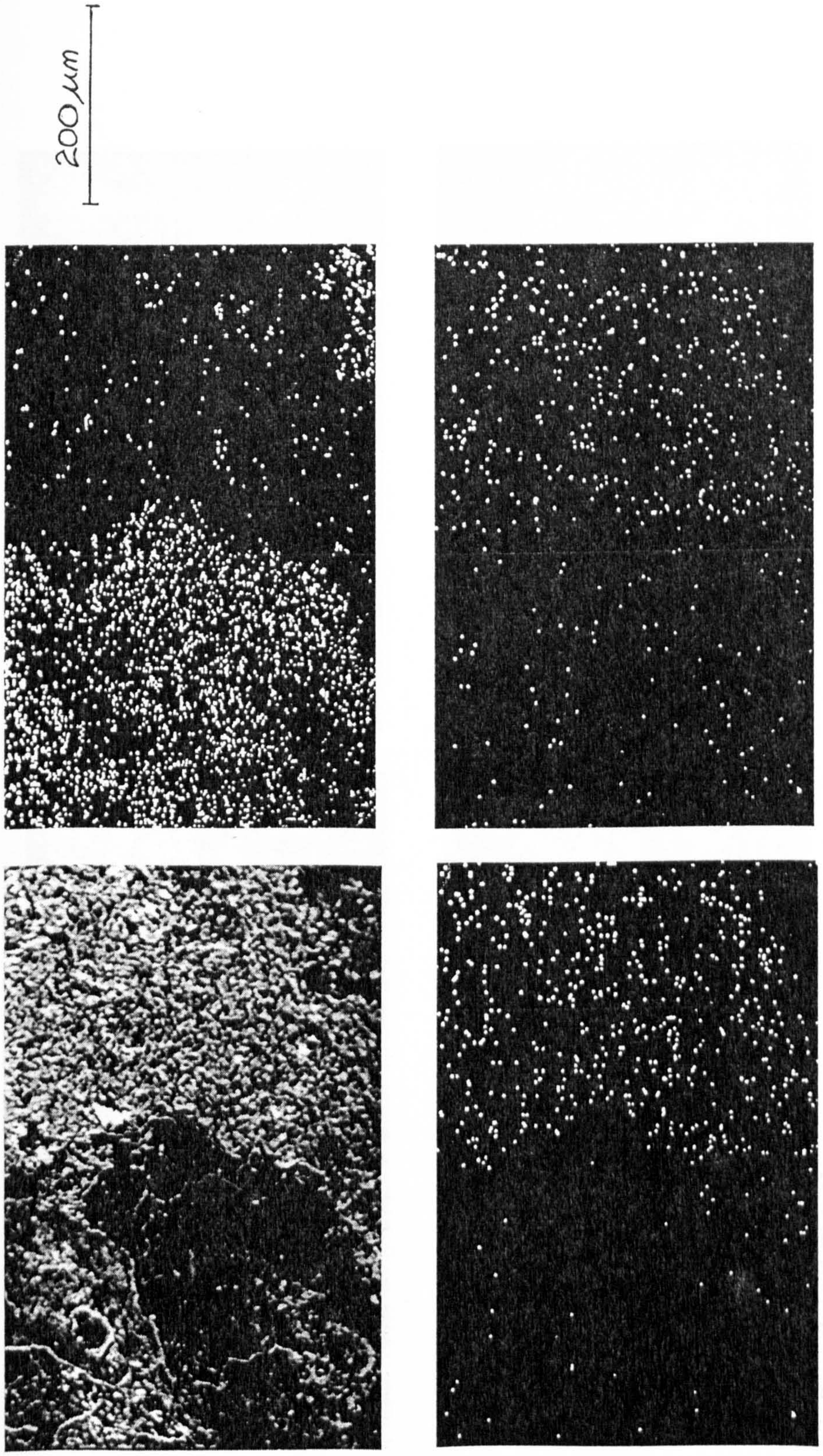

Figure 6.11: Micrographs of the natural surface of Stanford fragment H. a) secondary electron image b) the dot map for silicon c) dot map for calcium and d) dot map for sulphur.

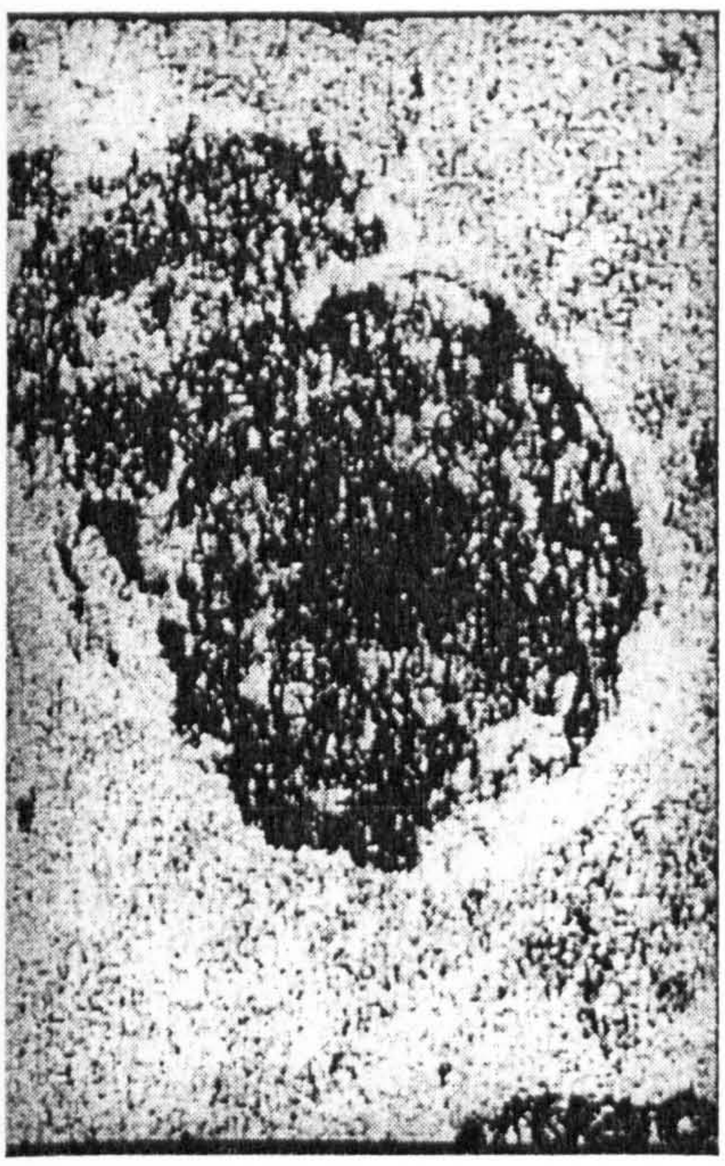

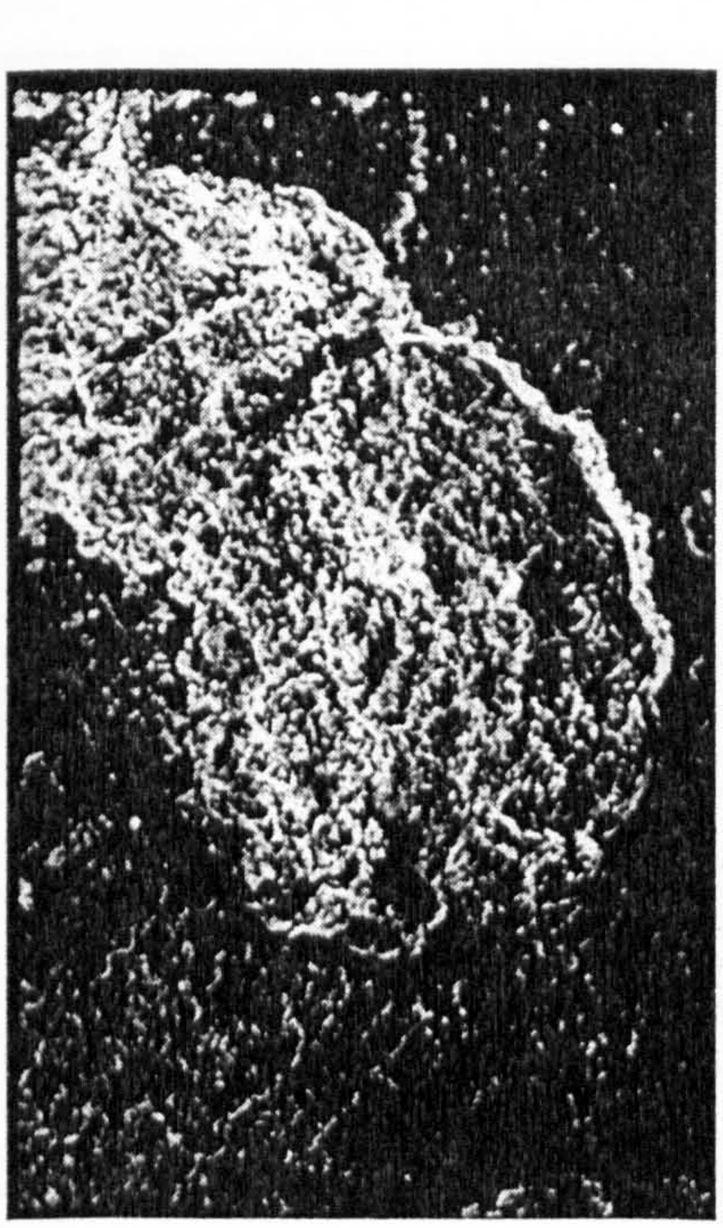

500 μm

Figure 6.12: Micrographs of the natural surface of Stanford fragment L. a) secondary electron image b) the dot map for silicon c) dot map for calcium and d) dot map for sulphur.

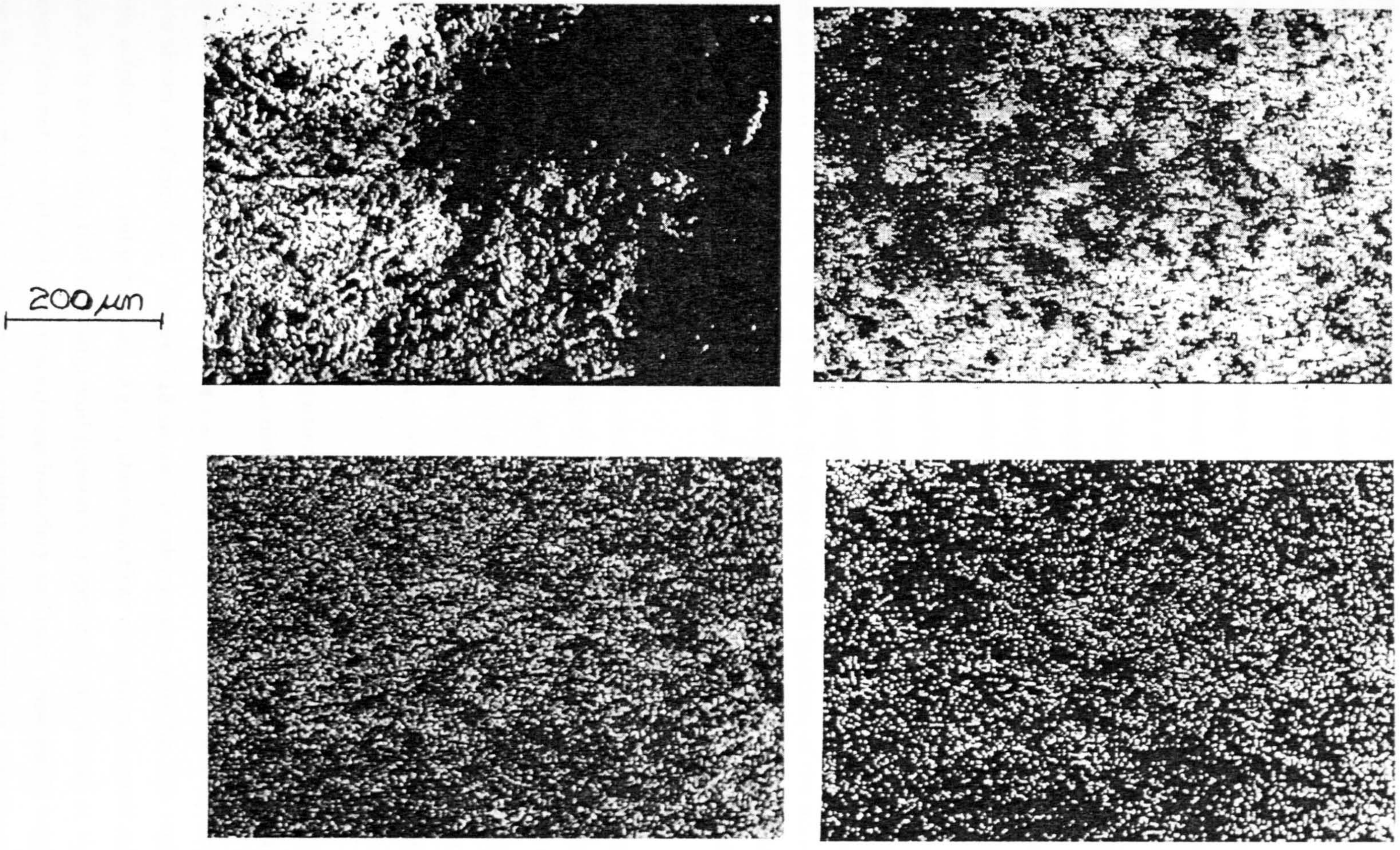

Figure 6.13: Micrographs of the natural surface of Fairford fragment A. a) secondary electron image b) the dot map for silicon c) dot map for calcium and d) dot map for sulphur.

6.2.2 The Depth Profile of the Stanford Fragments

Prior to looking at the samples in the SEM the exposed cross-sectioned surface was investigated by FT-IR spectroscopy, ie., they were analysed using the microscope facility of the FT-IR spectrometer (see chapter 4 for details). The microscope enabled an area of interest to be selected and thus correlation between the optical image and the IR spectra could be obtained.

Figure 6.14 shows the IR spectra collected from Stanford fragment A. The first spectrum, labelled glass, was taken of an area 40μm by 40μm, about 100μm from the pit edge into the glass body. The second, labelled crust, was taken at the center of a pit. The main peak in the glass spectrum was at 1047cm^{-1} whereas in the crust spectrum, this shifted to 1082cm^{-1}. This peak was identified as the Si-O-Si stretch. Also there was an associated shoulder at 1182cm^{-1} in the crust spectrum. This is characteristic of the sulphate stretch[47]. Thus the spectra indicate the leaching of the network and the presence of sulphate, as expected.

Figure 6.15 shows some of the spectra obtained for fragment L. These were taken from and around the same pit as analysed in the SEM (see Figure 6.18). In this figure four spectra have been shown. The first spectrum is that of the base glass, where the main peak is at 1033cm^{-1}. The next two spectra are taken within the 'crust' of the pit. In these a shift in position, of the major peak to wavenumber 1050cm^{-1}, can be seen. This shift is due to the introduction of the sulphate shoulder and a diminution in the height of the silica peak. The final spectrum is the background spectrum due to resin.

Given that the samples had been cross-sectioned, it was possible to determine the glass compositions. These are given in Table 6.1. The fragments compare favourably with the returned Stanford samples on a compositional basis, but some variation is present. This variation could be due to the colour of the glasses, as only colourless, complete samples were analysed from Stanford and the coloured glass there, may have quite a different composition compared to the colourless. Also the number of samples analysed was small and therefore generalising the composition was not possible.

As Stanford L was the most corroded, in particular by pitting, it proved the more interesting in cross-section, ie., it was possible to study the distribution of the elements by depth in a pit.

Figure 6.16 shows the optical micrograph of a sectioned pit; the corresponding secondary electron image is shown in Figure 6.17. Figure 6.18 shows the relevant dot maps for this region, ie. of calcium, sulphur, silicon and potassium. Again, there is a clear correlation between calcium and sulphur. It is noteworthy that the compound (presumably gypsum) only occurs at the surface. Moreover, it is not present at the corrosion/glass boundary and more importantly sulphur is not present in this region. This would suggest that sulphur is absent from the 'reaction zone'. The

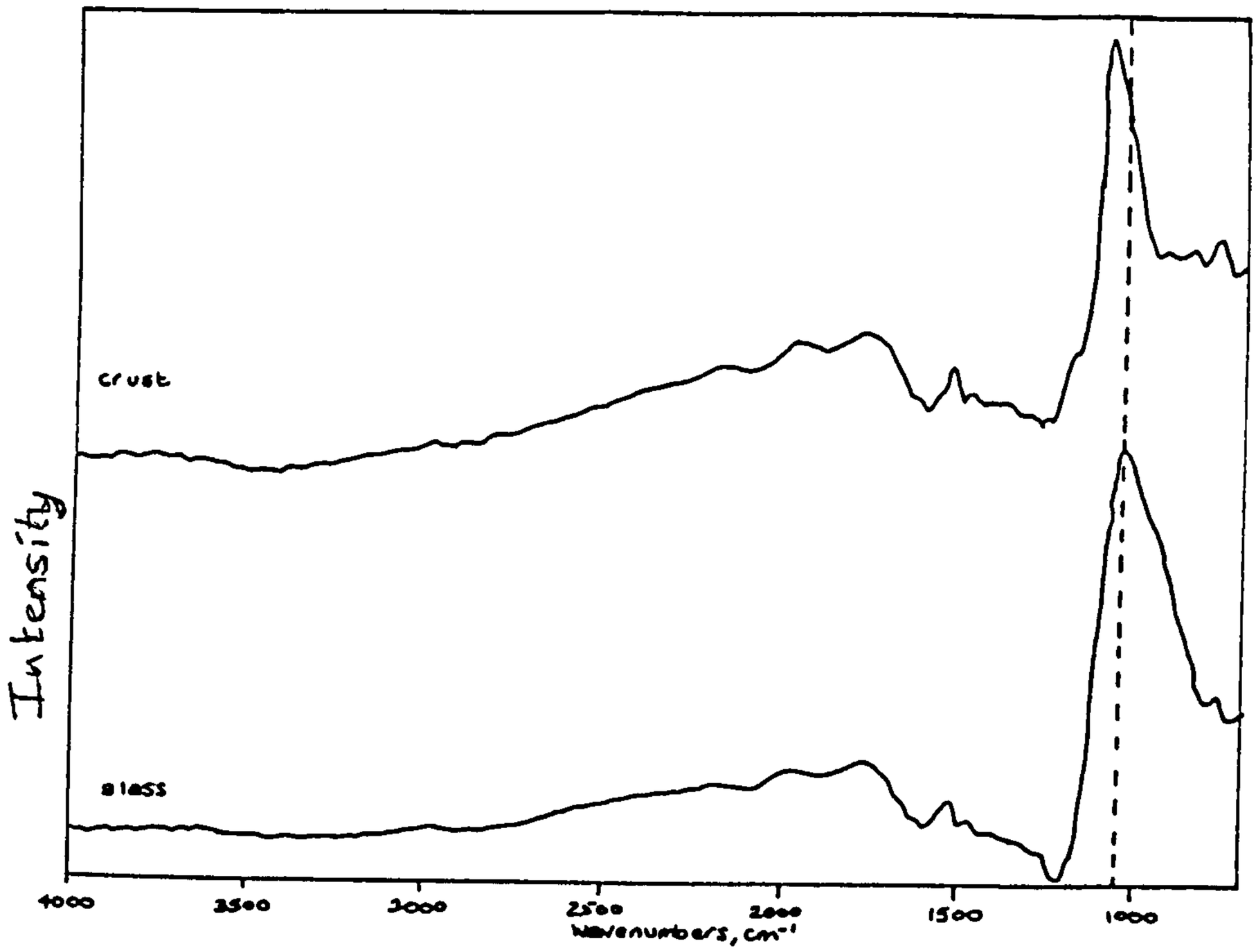

Figure 6.14: The IR spectra obtained from the cross-sectioned Stanford fragment A. a) for the crust and b) for the glass.

Oxide	Fragment		
mol%	A	H	L
Na_2O	2.5	1.6	1.6
MgO	4.8	5.6	5.9
Al_2O_3	2.2	1.8	1.3
SiO_2	53.9	52.3	50.9
K_2O	13.7	16.4	16.9
CaO	16.4	15.0	14.0
P_2O_5	4.5	4.6	4.7
Fe_2O_3	0.8	0.5	0.5
MnO_2	0.7	0.9	0.9

Table 6.1: The composition of the Stanford fragments: A, H and L.

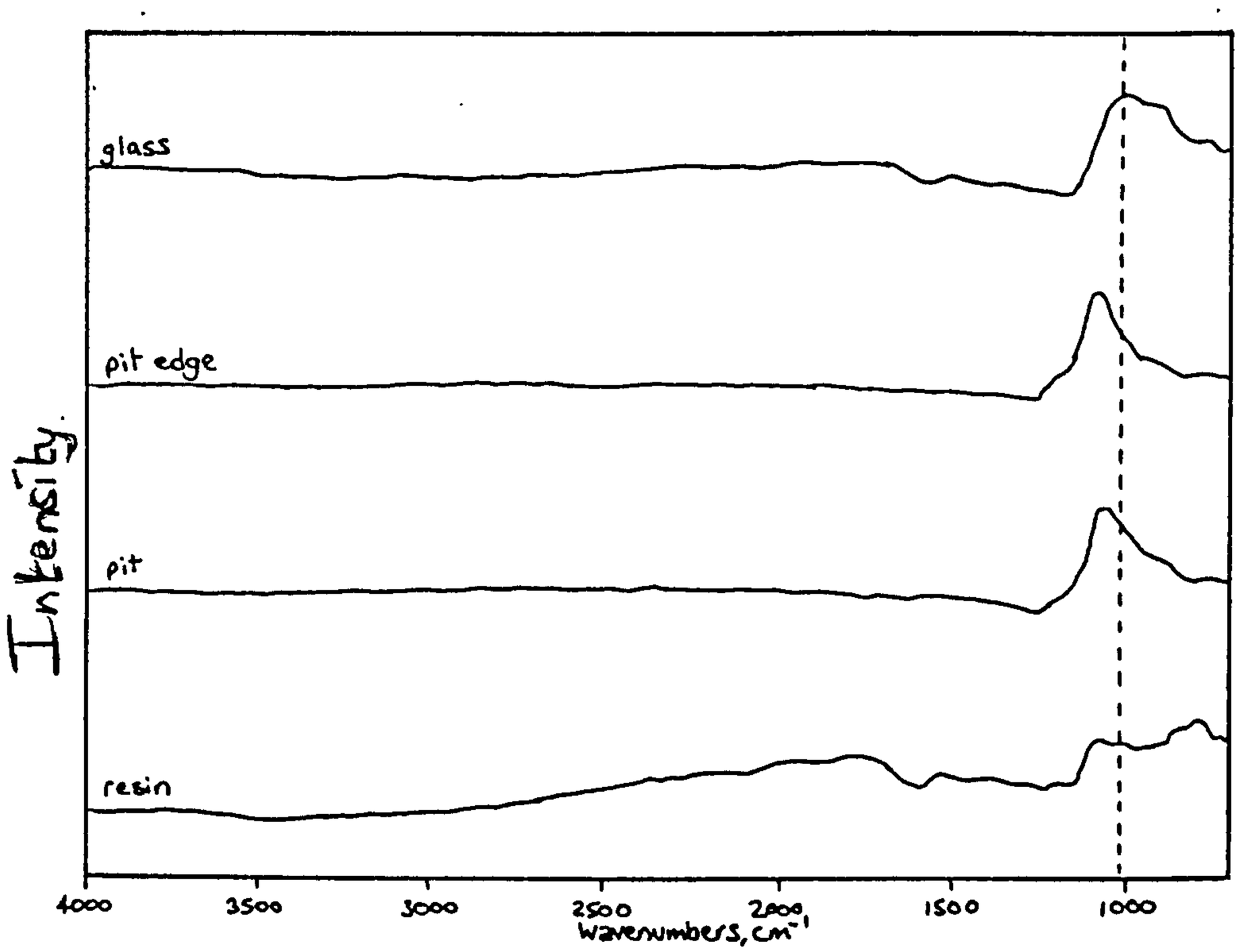

Figure 6.15: The IR spectra obtained from the cross-sectioned Stanford fragment L. a) from the base glass b) from a pit boundary c) from a pit and d) for the resin.

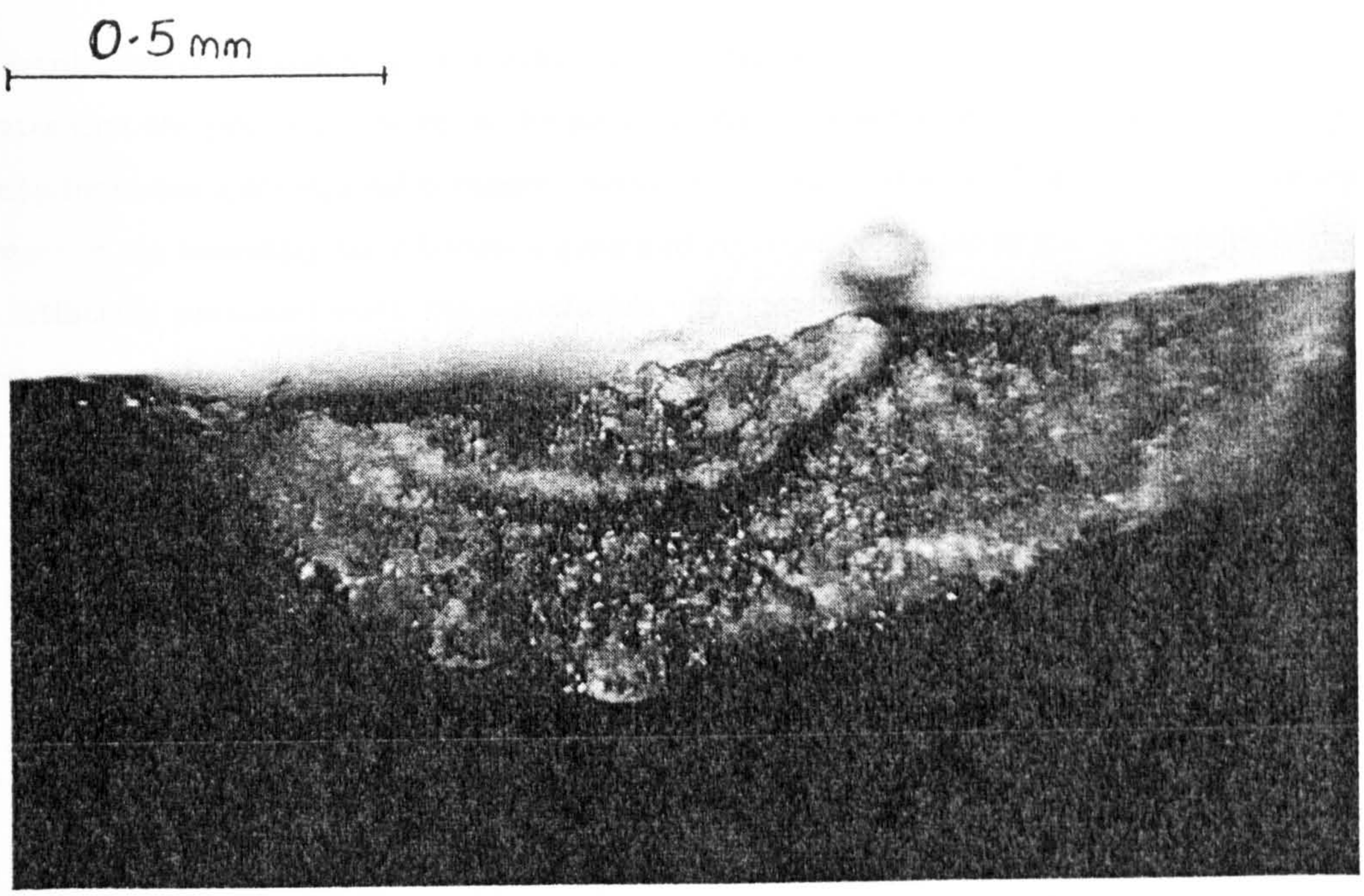

Figure 6.16: Optical micrographs of Stanford fragment L in cross-section.

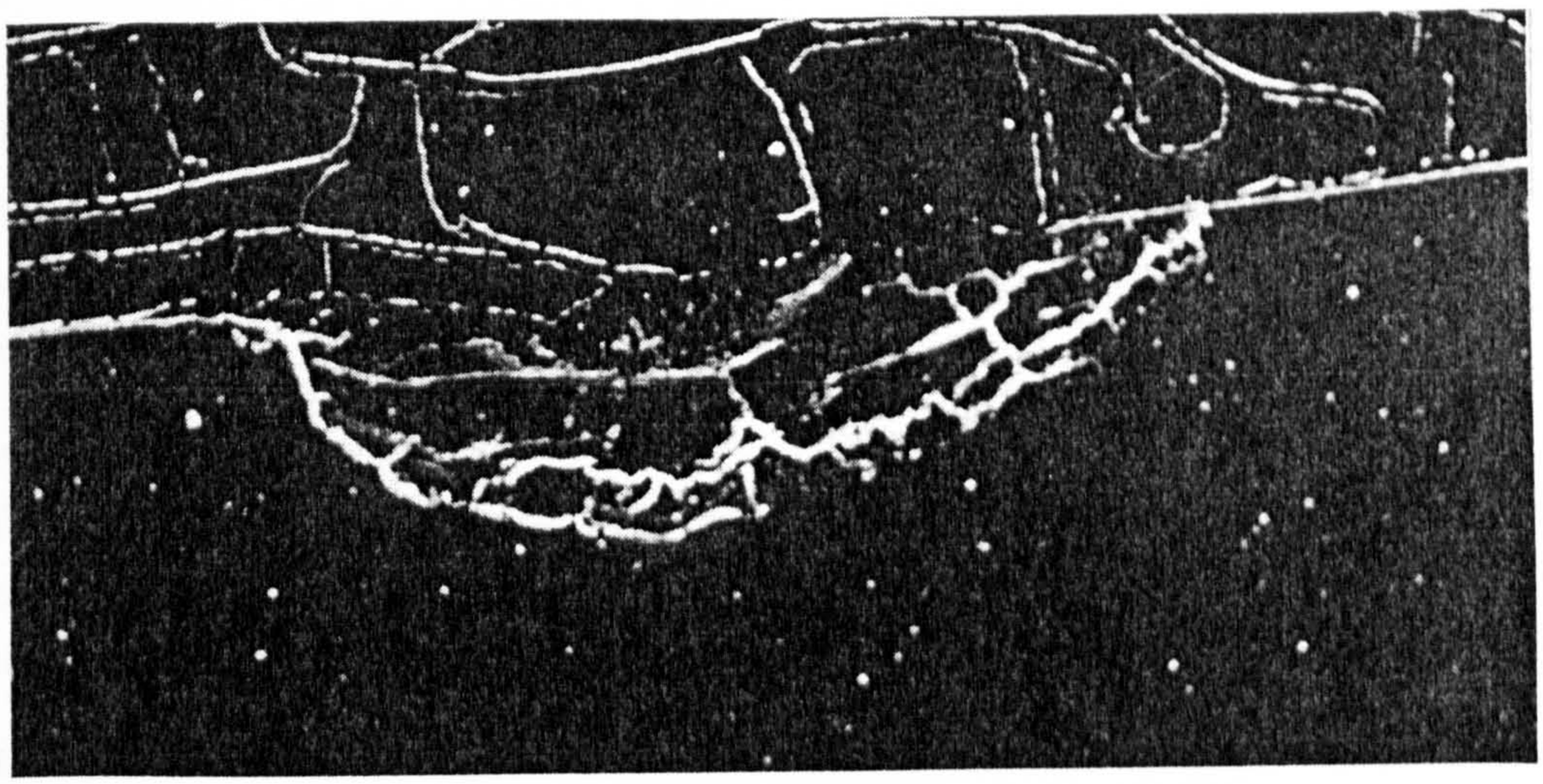

Figure 6.17: Scanning electron micrograph of a pit in Stanford fragment L, in cross-section.

zone being the area surrounding the interface between the glass and the decay products.

The distribution of potassium is clearly due to the potassium present in the base glass and therefore indicates that the product present in the pit is probably gypsum, and not syngenite. The silicon dot map indicates a widespread presence. Silicon is absent at the 'core' of the pit and appears to be absent in the boundary layer between glass and corrosion. The latter gap is more likely to have been artificially produced when the sample was embedded in resin rather than due to a break in the corrosion, as no elements are detectable in this region. Similar micrographs were produced for other regions of this specimen; all show the same correlation. Identification of the products was not possible as they were present in too small quantities.

6.3 Summary

This study investigated the distribution of the decay products on the surface of the glass. The samples have shown that sulphur was **not** present in the 'reaction zone'. That is, it was absent from the glass/corrosion boundary; described as a zone, given the actual interface is where the leaching occurs but salts are formed in the region behind this. This is in agreement with the findings of Marschner and Perez-y-Jorba *et.al.* [88, 112].

A correlation was found between calcium and sulphur in all cases; there was an associated negative correlation with silicon. Occasionally there was a correlation between the calcium and potassium distributions, suggesting the presence of a compound salt. Direct identification of these decay products was not possible due to their being coated by resin and present in only a miniscule amount.

Evidence indicates that pits form as 'altered' areas which are, perhaps under the surface as stated by Marschner (for glasses of the surface fractured nature) [88], and have an associated contrast in colour. These regions then progress by forming crystalline salts at their center, leaving the outer boundary to collapse.

The IR investigation indicated the breakdown of the silica network and the introduction of sulphates in the crust. This linked with the correlation between calcium and sulphur from the dot maps and would suggest that the decay product was gypsum.

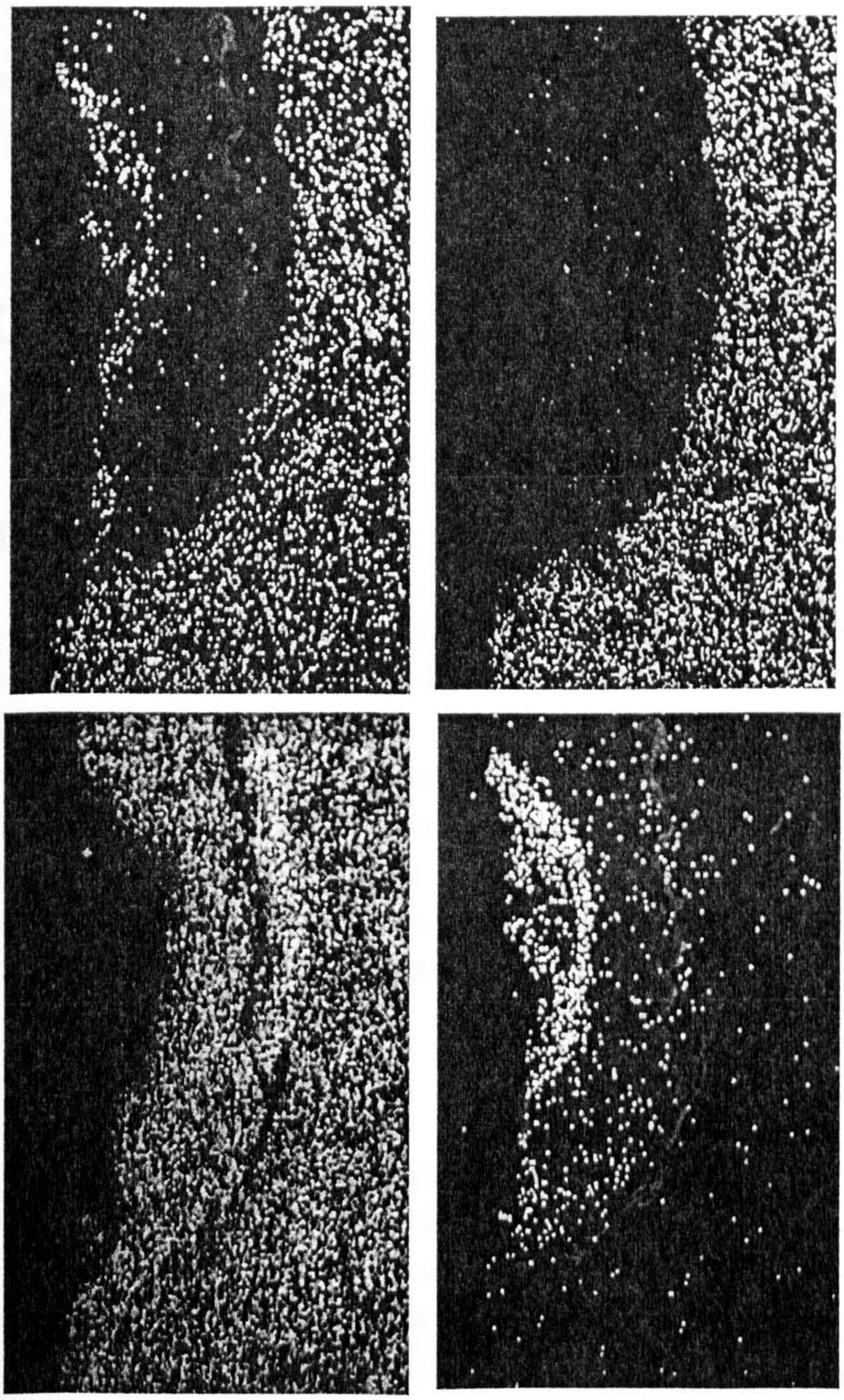

Figure 6.18: Micrographs of Stanford fragment L. A cross-sectioned pit. a) the dot map for silicon b) dot map for calcium c) dot map for sulphur and d) dot map of potassium.

Chapter 7

Results–Analytical

7.1 Correlation between Decay and Composition

In order to investigate the correlation between decay and composition, three standard procedures were undertaken, *ie.*, the compositions were first looked at to determine whether glass from different churches was comparable and to isolate the anomalous samples, *eg.* a markedly higher alumina content, within each group (see section 7.1.1). This was followed by applying the two popular methods of reducing the glass composition to a smaller set of values that are easier to handle. Sections 7.1.2 and 7.1.3 show the outcome of these trials and in these data are linked to the mode of decay. Finally multivariate statistical techniques were implemented to see if any further information could be obtained (see section 7.1.4).

7.1.1 The Compositions

Firstly, the compositions of the glasses from each of the locations were considered independently. Table 7.1 gives a summary of the chemical compositions. It contains the mean molar percentages of all the measured parameters, except copper oxide, lead oxide, sulphur and chlorine. These latter components were omitted as the deviations are comparable to the mean and they do not convey any useful information. The table shows the similarity between the compositions of the fourteenth century glasses and highlights the difference between the fourteenth century glass and the glass from Fairford. The mean amounts of iron oxide and manganese oxide in the specimens are approximately the same for all of the churches. The phosphorus oxide is $\approx$2 mol% for the fourteenth century glasses, but is slightly lower for the sixteenth century ones. The alumina content has a similar variation to that found with phosphorus oxide. The quantity of the major oxides present in the glasses, from each church, shows marked variation. Checkley appears to have a higher soda

content than the rest, with Fledborough having the lowest. Potash was expected to be present in much higher quantities than soda for the mediaeval glasses and this is shown to be true. All samples except those from Fairford have $K_2O \approx 10$ mol%. Fairford has about 5mol% potash which is indicative of the later, mixed alkali type glass (see section 2.3.4) and is consistent with the age of the glass. The mean silica content for the fourteenth century glass is about 54mol%, whereas for Fairford it is nearer 60 mol%. The vast difference is again reflecting the later date of the Fairford glass. Associated with this high silica content is increased durability, as fewer modifying ions have been incorporated. Therefore, it might be expected that the Fairford glass should be in a better state of preservation than the fourteenth century glass because of its mixed alkaline nature and high silica content–this is not the case and will be discussed more thoroughly in section 7.3. The average lime content for Checkley, Heckington, Meysey Hampton and Stanford is 15 mol%. This is normal for glass of this date when compared to that found by other workers. Newton states 17mol%[105], Perez-y-Jorba found 15.5mol%[111], and Gillies and Cox record 17mol%[58]. The lime content for Ely, Fledborough and Fairford is on average much higher, *viz.* 23mol%, which is in agreement with that found by Schreiner for Austrian mediaeval glass[130].

The range of values for magnesia (MgO) is very broad, 3–13 mol%. Referring to the work of Gillies and Cox[58] the magnesia value is usually 8-11 mol% in fourteenth century glasses. Hence the data were divided into groups, Γ_{HM} where MgO>8.0 mol%, and the low magnesia group with MgO<7.9 mol%, Γ_{LM}. Complicating this picture is the later date glass from Fairford which straddles both groups. Table 7.2 gives the mean and standard deviation of the composition for these two groups, but also gives them when the groups are subdivided into those from Fairford and those from other sites.

It can be seen that the Γ_{HM} type is composed mainly of the fourteenth century glass with only eight of the Fairford samples. This could suggest that these eight pieces of glass were re-used earlier glass or indicative of the transition to mixed-alkali glass being a slow process. On the other hand one quarter of the Γ_{LM} group is fourteenth century in date. These specimens could be explained as replacements, but this does not appear to be the case. The difference in MgO, CaO, and K_2O for Fairford suggests that a different lime source was used. The fourteenth century glass has variation in CaO, MgO, Na_2O and SiO_2, which again would suggest a different lime source, but also that if low magnesia limestone was used, more of it was necessary.

The variation in chemical composition is more easily shown graphically. Again the values of sulphur , chlorine, lead oxide and copper oxide have not been included. Figures 7.1 to 7.4 show the various molar percent oxides plotted against each other as pairs. They are presented to convey the distribution and do not necessarily imply a link. The variation of lime and silica is illustrated in Figure 7.1. Here it can be seen that the silica appears to form three clusters, whereas the lime does not divide. The monovalent alkalis, soda and potash, are shown in Figure 7.2; the group

Church → / Oxide ↓		Checkley	Ely	Fairford	Fledborough	Heckington	Meysey Hampton	Stanford
molar percentage	Na_2O	3.25 ± 1.21	1.50 ± 0.80	2.28 ± 0.81	0.93 ± 0.76	2.32 ± 0.81	2.49 ± 0.80	2.83 ± 0.85
	MgO	10.88 ± 1.36	7.74 ± 2.07	5.79 ± 1.58	7.28 ± 0.98	10.23 ± 1.34	10.06 ± 1.29	10.32 ± 1.30
	Al_2O_3	0.85 ± 0.26	0.92 ± 0.52	1.45 ± 1.42	1.21 ± 0.27	0.92 ± 0.32	0.86 ± 0.20	0.95 ± 0.18
	SiO_2	54.11 ± 1.89	51.76 ± 4.43	59.69 ± 2.24	51.51 ± 2.72	55.34 ± 1.20	55.92 ± 2.05	57.27 ± 1.67
	P_2O_5	2.30 ± 0.37	2.32 ± 0.66	1.27 ± 0.29	2.18 ± 0.42	1.94 ± 0.25	2.14 ± 0.39	2.02 ± 0.29
	K_2O	10.20 ± 2.14	10.46 ± 0.68	5.36 ± 3.02	9.59 ± 1.24	10.50 ± 1.33	9.89 ± 1.49	10.13 ± 1.64
	CaO	15.92 ± 1.18	23.42 ± 6.06	21.96 ± 3.37	25.80 ± 5.42	16.08 ± 1.61	15.95 ± 1.17	14.00 ± 1.99
	Fe_2O_3	0.24 ± 0.17	0.25 ± 0.08	0.24 ± 0.10	0.25 ± 0.05	0.24 ± 0.10	0.22 ± 0.07	0.19 ± 0.04
	MnO	0.88 ± 0.11	0.62 ± 0.25	0.85 ± 0.31	0.40 ± 0.28	0.85 ± 0.20	0.99 ± 0.32	1.04 ± 0.17
Number of samples		66	11	66	13	25	19	6
Century		14	14	16	14	14	14	14

Table 7.1: Mean and standard deviations of the chemical composition, to 2 d.p., of the glasses from each church (mol% oxide values for the major/minor components).

	Oxide	Γ_{IIM} type			Γ_{LM} type		
		All	Other	Fairford	All	Other	Fairford
molar percentage	Na_2O	2.91 ± 1.08	2.88 ± 1.11	3.33 ± 0.37	1.82 ± 0.89	0.88 ± 0.05	2.13 ± 0.75
	MgO	10.50 ± 1.37	10.55 ± 1.38	9.65 ± 0.60	5.65 ± 0.93	6.84 ± 0.53	5.26 ± 0.67
	Al_2O_3	0.92 ± 0.72	0.87 ± 0.26	1.72 ± 2.75	1.35 ± 1.04	1.15 ± 0.42	1.42 ± 1.17
	SiO_2	55.08 ± 2.12	54.87 ± 1.96	58.29 ± 2.06	57.58 ± 4.73	50.57 ± 3.18	59.88 ± 2.21
	P_2O_5	2.14 ± 0.38	2.18 ± 0.37	1.60 ± 0.15	1.49 ± 0.60	2.30 ± 0.59	1.22 ± 0.27
	K_2O	10.12 ± 1.84	10.24 ± 1.82	8.35 ± 1.01	6.14 ± 3.36	9.78 ± 1.12	4.94 ± 2.97
	CaO	15.80 ± 1.42	15.88 ± 1.38	14.59 ± 1.54	23.96 ± 3.12	26.95 ± 3.98	22.97 ± 1.99
	Fe_2O_3	0.23 ± 0.13	0.23 ± 0.14	0.23 ± 0.05	0.25 ± 0.10	0.26 ± 0.06	0.24 ± 0.10
	MnO	0.88 ± 0.19	0.89 ± 0.19	0.75 ± 0.14	0.76 ± 0.36	0.45 ± 0.30	0.86 ± 0.32
Number of samples		129	121	8	77	19	58

Table 7.2: Mean and standard deviation of the chemical composition of the specimens, when divided into groups according to age and magnesia content(to 2 d.p.).

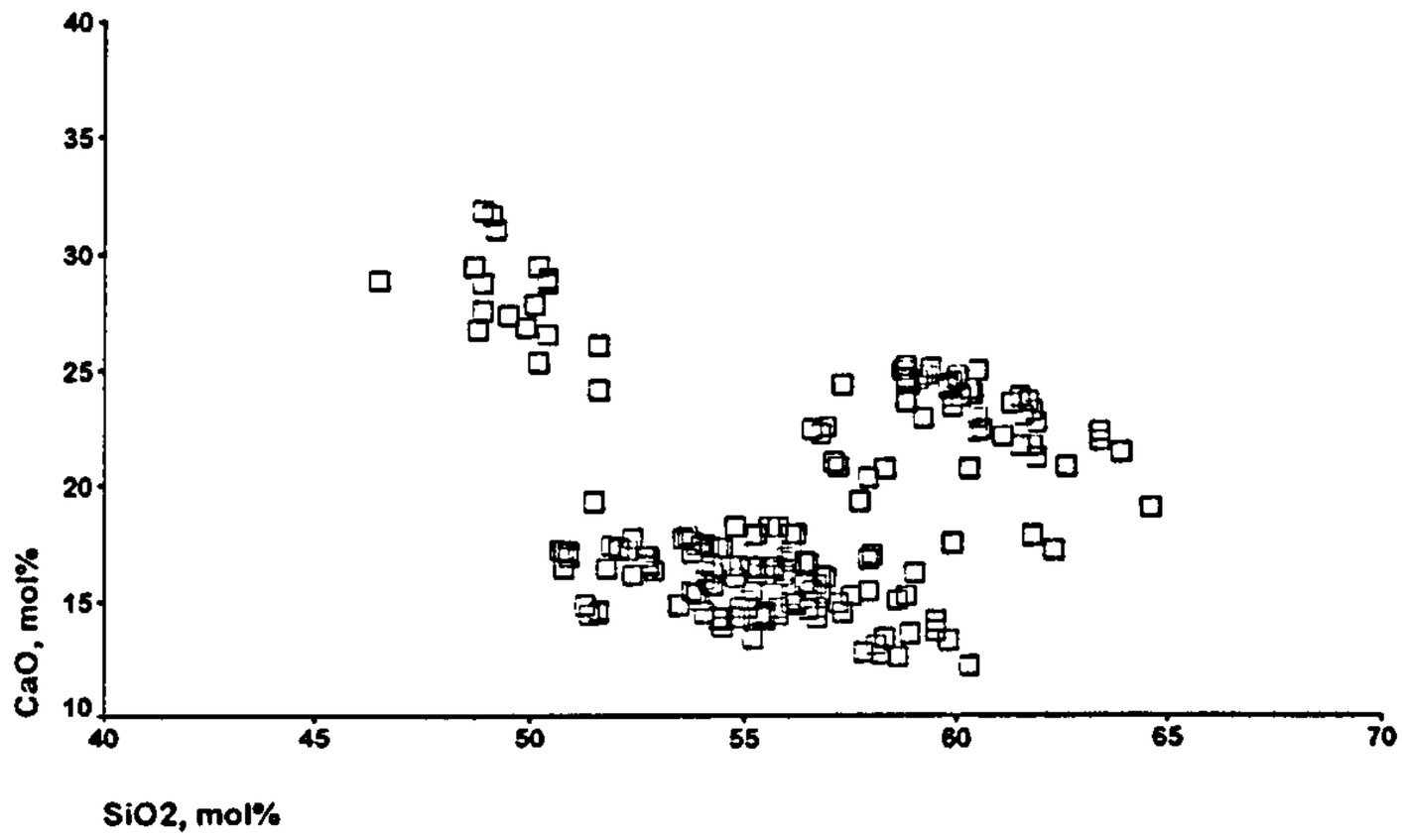

Figure 7.1: Lime-Silica scattergram of mol%.

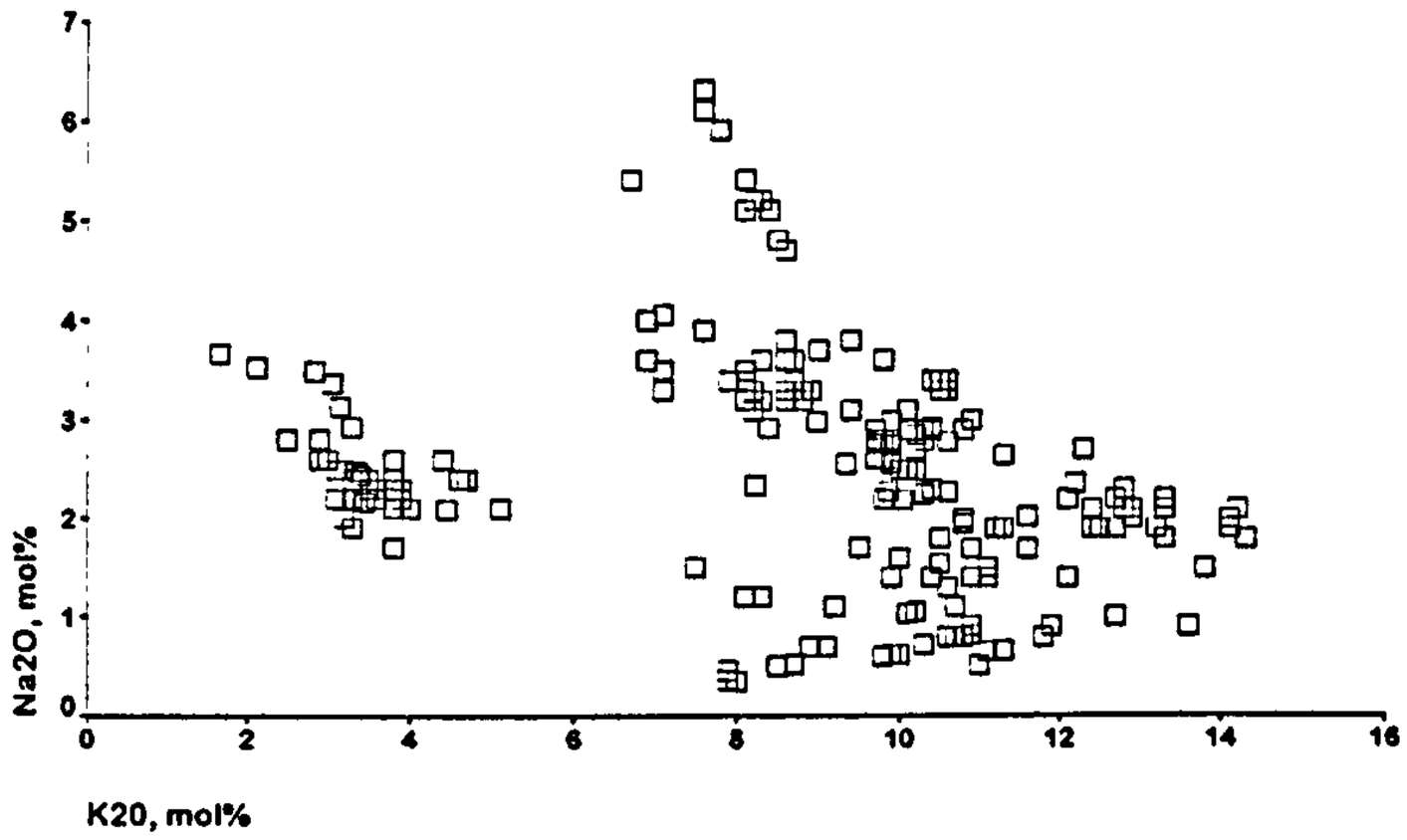

Figure 7.2: Soda-Potash scattergram of mol%.

of low K_2O glasses is immediately obvious. There maybe a tendency for the glass with $K_2O \approx 8$ mol% to have $Na_2O > 4$ mol%. When the potash content is any other value, the soda is less than 4 mol%. Any clustering within the $8 < K_2O < 14$ mol% range is masked by the scale. The distribution of phosphorus was found to be normal about 2 mol% and the alumina likewise, but centered on 1 mol% (see Figures 7.7 and 7.11). Figure 7.3 shows that the iron oxide and manganese oxide values form one cluster. As the number of oxides to be represented is an odd number the lime content was repeated so as to illustrate the magnesia variation. Figure 7.4 shows that high magnesia is associated with CaO ≈15 mol%; if 6<MgO<8mol%, then CaO>25 mol% and when MgO<6 mol%, then CaO 20–25 mol%. This suggests two or three groupings, *ie.* the two high lime groups may really be just one cluster.

When the data are separated into the two groups Γ_{LM} and Γ_{HM} the clustering is more easily

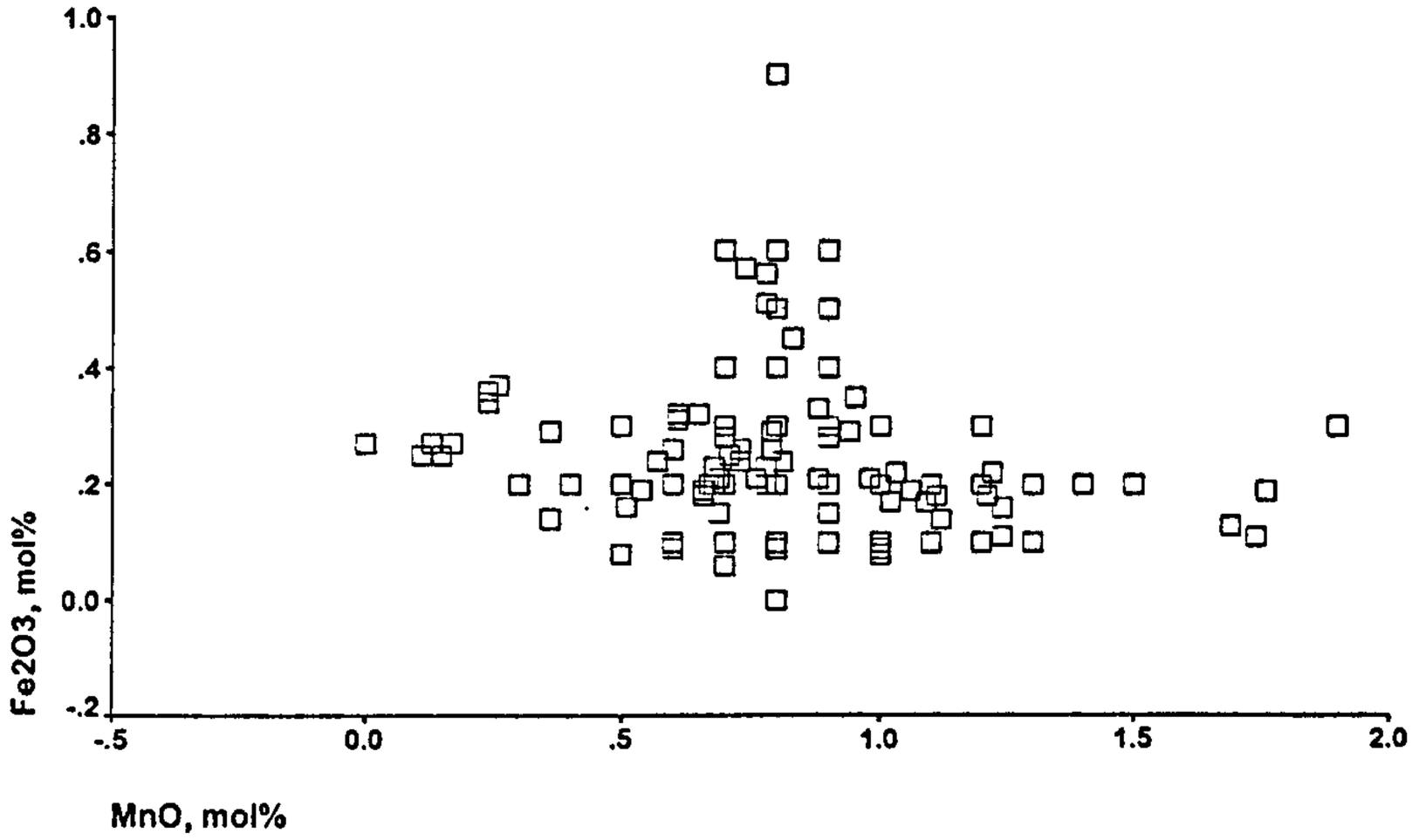

Figure 7.3: Manganese-Iron scattergram of mol%.

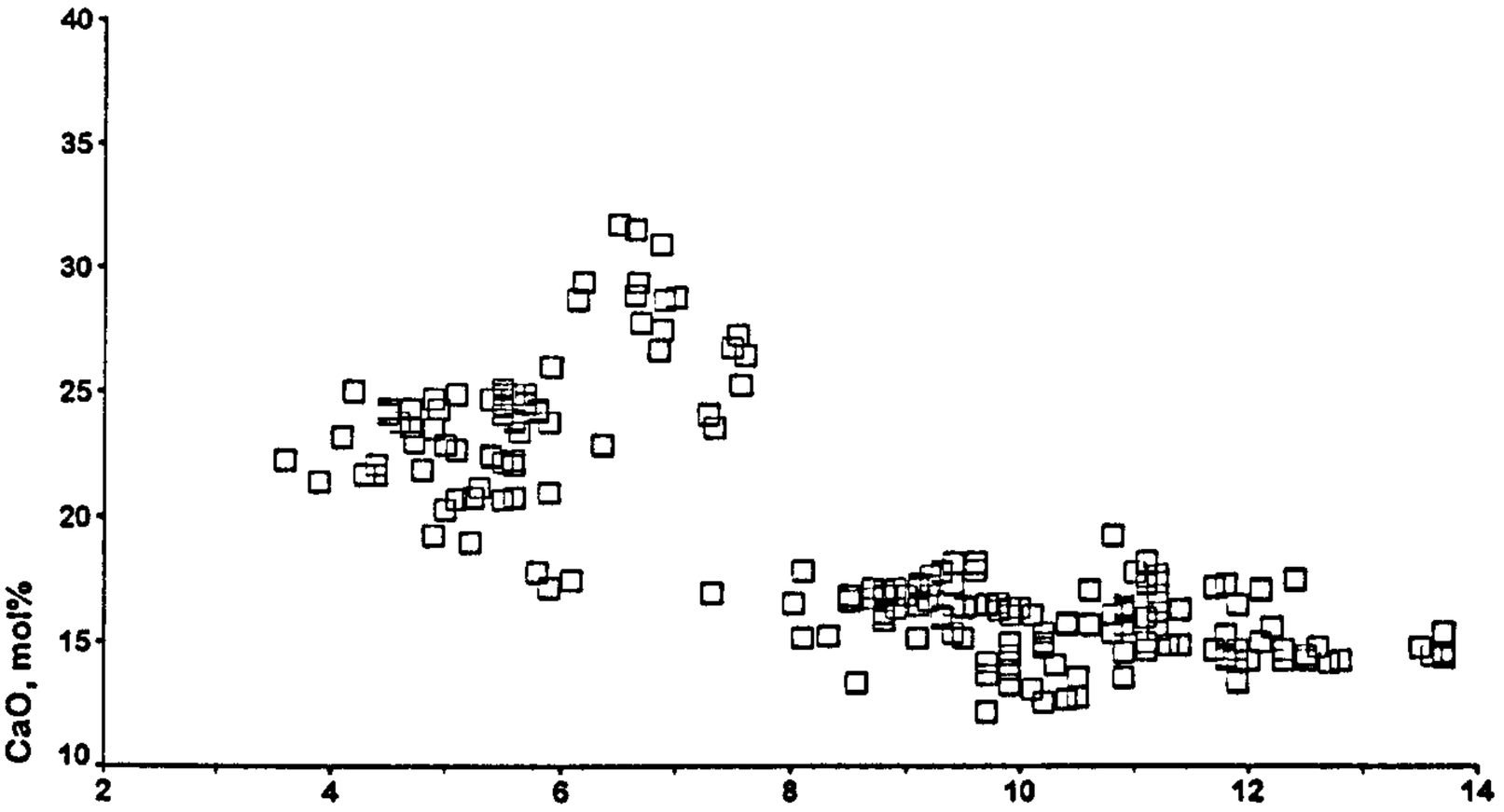

Figure 7.4: Lime-Magnesia scattergram of mol%.

Glass Corrosion

observed. These are depicted in Figures 7.5 to 7.8 for Γ_{HM} and Figures 7.9 to 7.12 for the low magnesia, Γ_{LM}, glasses.

Γ_{HM}

Generally, these glasses have a low soda content, between 1 and 3 mol%. A few outliers can be seen at $Na_2O \succeq 5$ mol% in Figure 7.6. These outliers are several samples from Checkley (CHK3, 9, 15, 18, 21, 26, 29, 32N; 3, 9, 19, 22S) and have MgO >12 mol% and K_2O between 6.7 and 8.6 mol%. They are encircled in a dotted line on the diagram. This potash level is low for fourteenth century glass and perhaps this is anticipating a shift towards the mixed-alkali glasses of the sixteenth century, or maybe a different alkali source.

The alumina, phosphorus oxide, manganese oxide and iron oxide contents were found to be normally distributed, though on these plots this distribution is hidden in the relationship between the abscissa and ordinate. The potash content is between 7 and 13 mol% and is possibly a dividing factor although the number of subgroups is difficult to determine from this graph.

A broad range of silica values is observed to split into three groups: $SiO_2 < 53$mol%, $53 < SiO_2 < 57$mol% and $SiO_2 > 57$ mol%. The lime is between 12 and 20 mol% and does not appear to divide.

Γ_{LM}

Again the manganese oxide, iron oxide and alumina are normally distributed for this group of glasses (see Figures 7.12 and 7.11).

The soda content suggests a split of this data into two clusters. This division would occur at $Na_2O \approx 1.5$mol%. Similarly two groups are suggested by the potash, splitting at K_2O=6 mol%. The lime-silica content, shown in Figure 7.9, suggests two groups $SiO_2 < 53$mol% with CaO> 24 mol% and the other with $SiO_2 > 56$mol% and CaO < 25mol%. The former cluster consists of glass from Ely, Fledborough and one sample from Fairford; the latter group is glass from Fairford, with 2 Ely samples. This division is indicative of the different dates of the glasses, *ie.*, the Fairford glass forms a distinct group. This is most marked in the silica values, FAI glass having higher silica content. Figure 7.11 suggests a division in the phosphorus oxide content at about 1.6mol%. The high lime glasses are also some of the high phosphorus oxide samples, but no correlation occurs with the potash level.

Having highlighted the compositional differences, it was now possible to consider the relationship between composition and mode of decay. As already mentioned the composition splits the data into four groups: (Γ_{LM}) and (Γ_{HM}), each of which splits into fourteenth and sixteenth century dated

Glass Corrosion

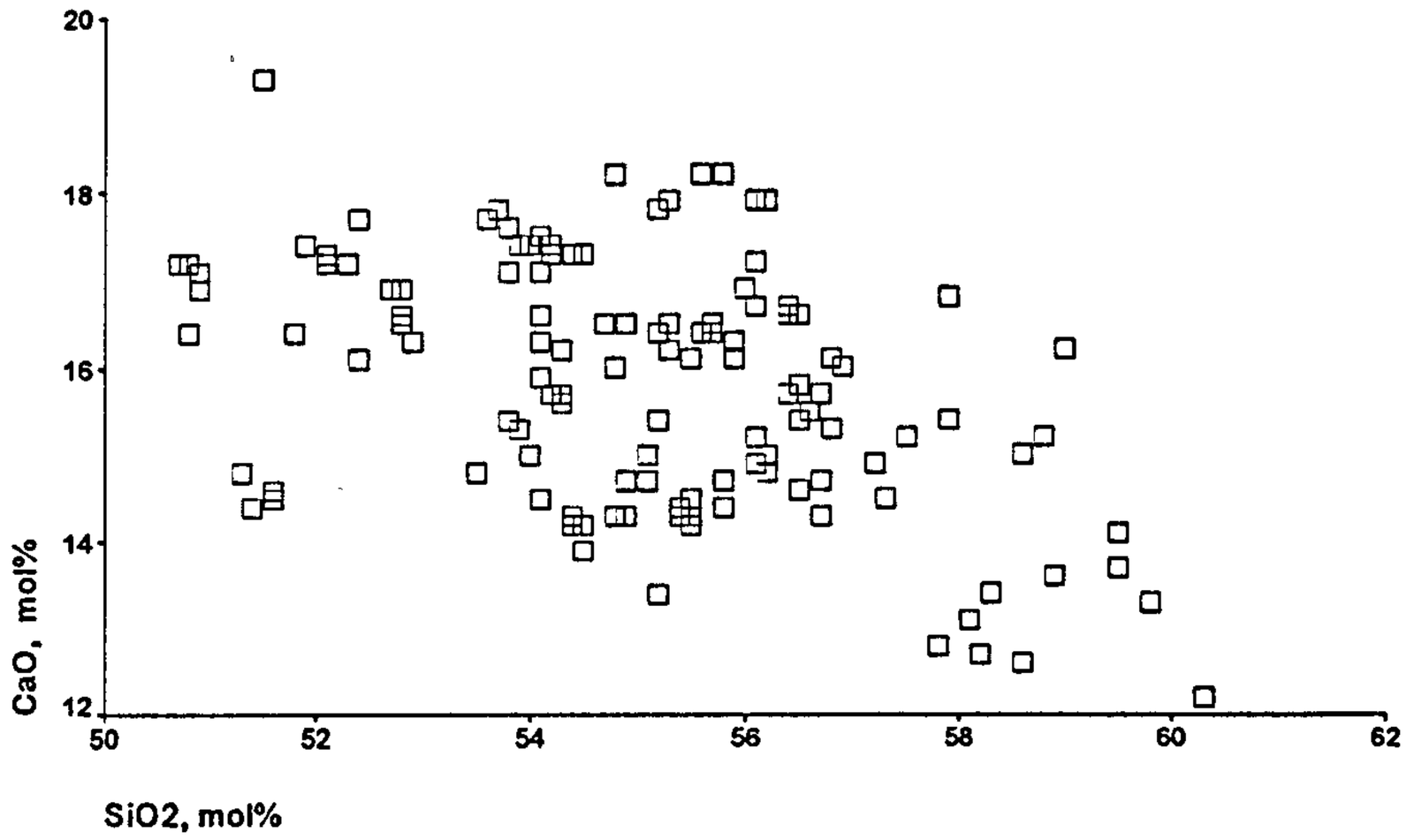

Figure 7.5: Lime-Silica scattergram of mol% for Γ_{HM}.

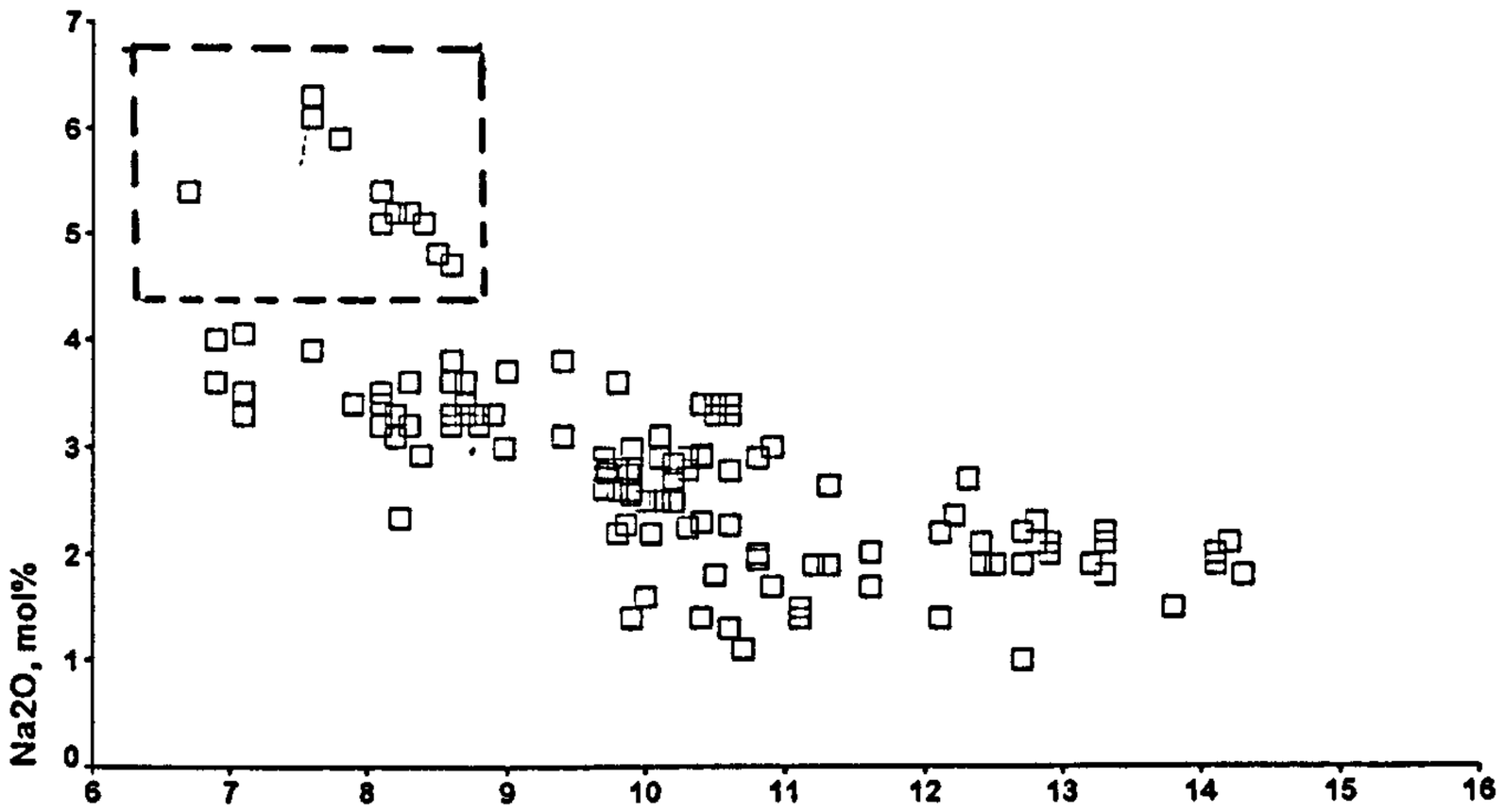

Figure 7.6: Soda-Potash scattergram of mol% for Γ_{HM}.

Glass Corrosion

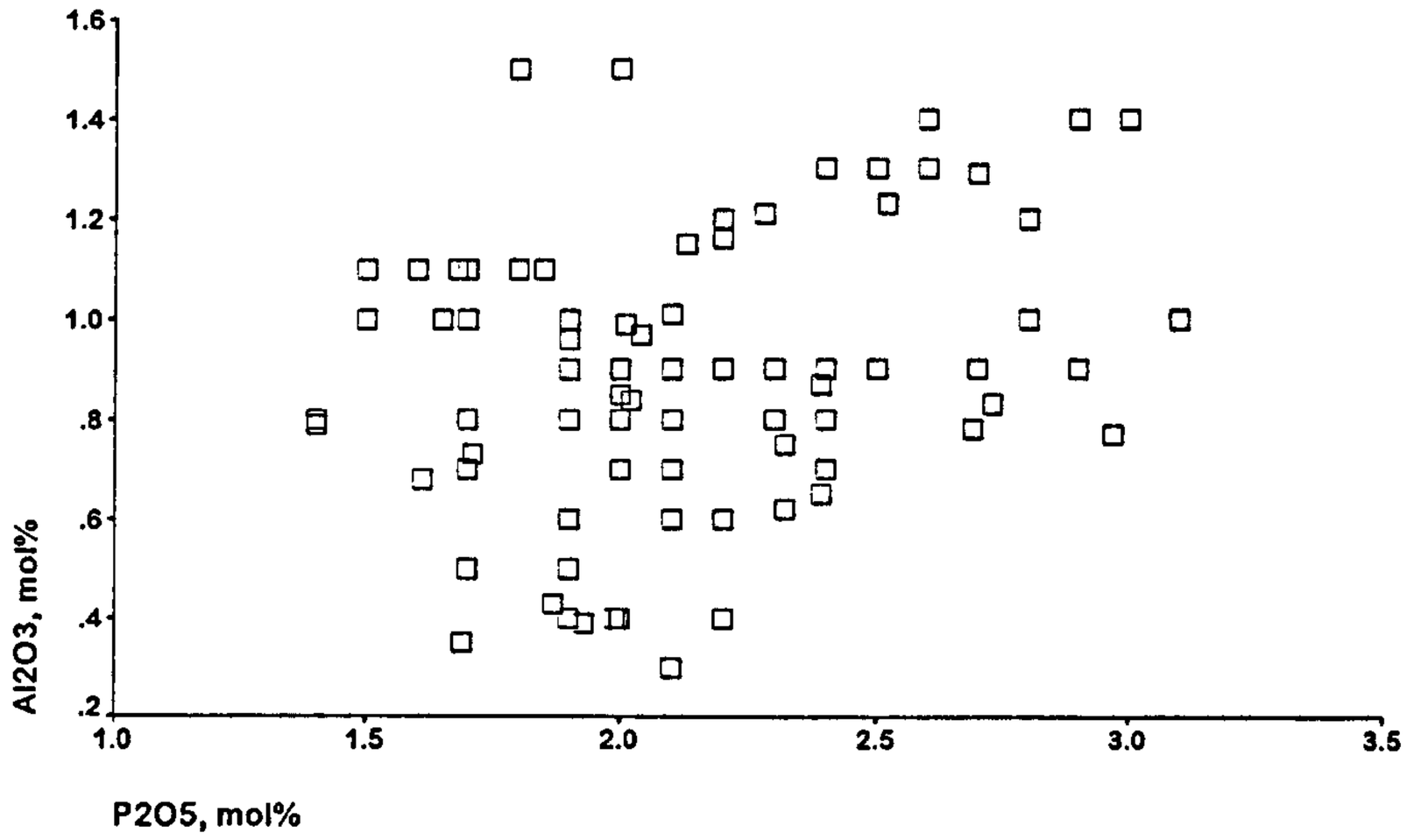

Figure 7.7: Alumina-Phosphorus scattergram of mol% for Γ_{HM}.

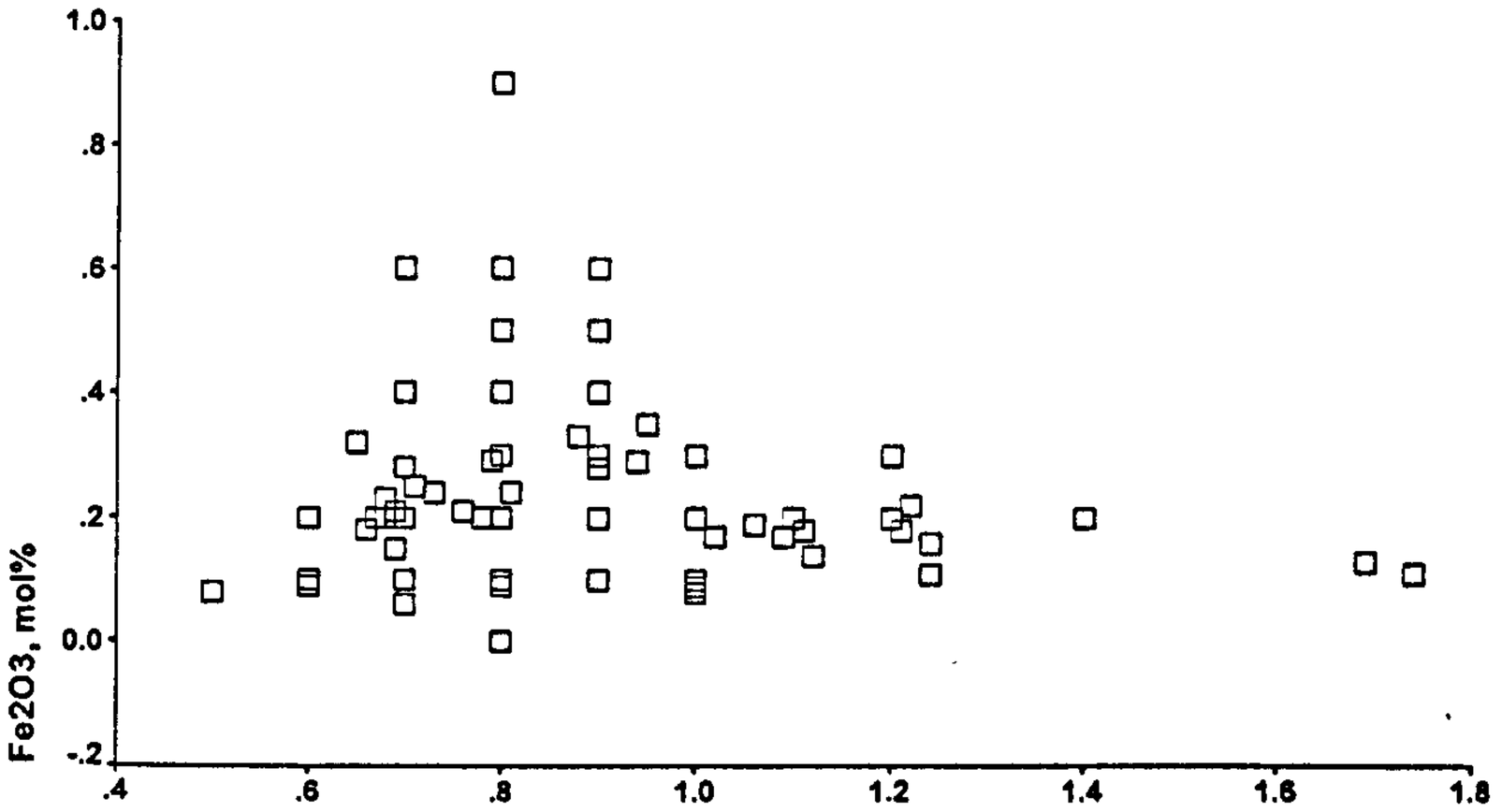

Figure 7.8: Manganese-Iron scattergram of mol% for Γ_{HM}.

Glass Corrosion

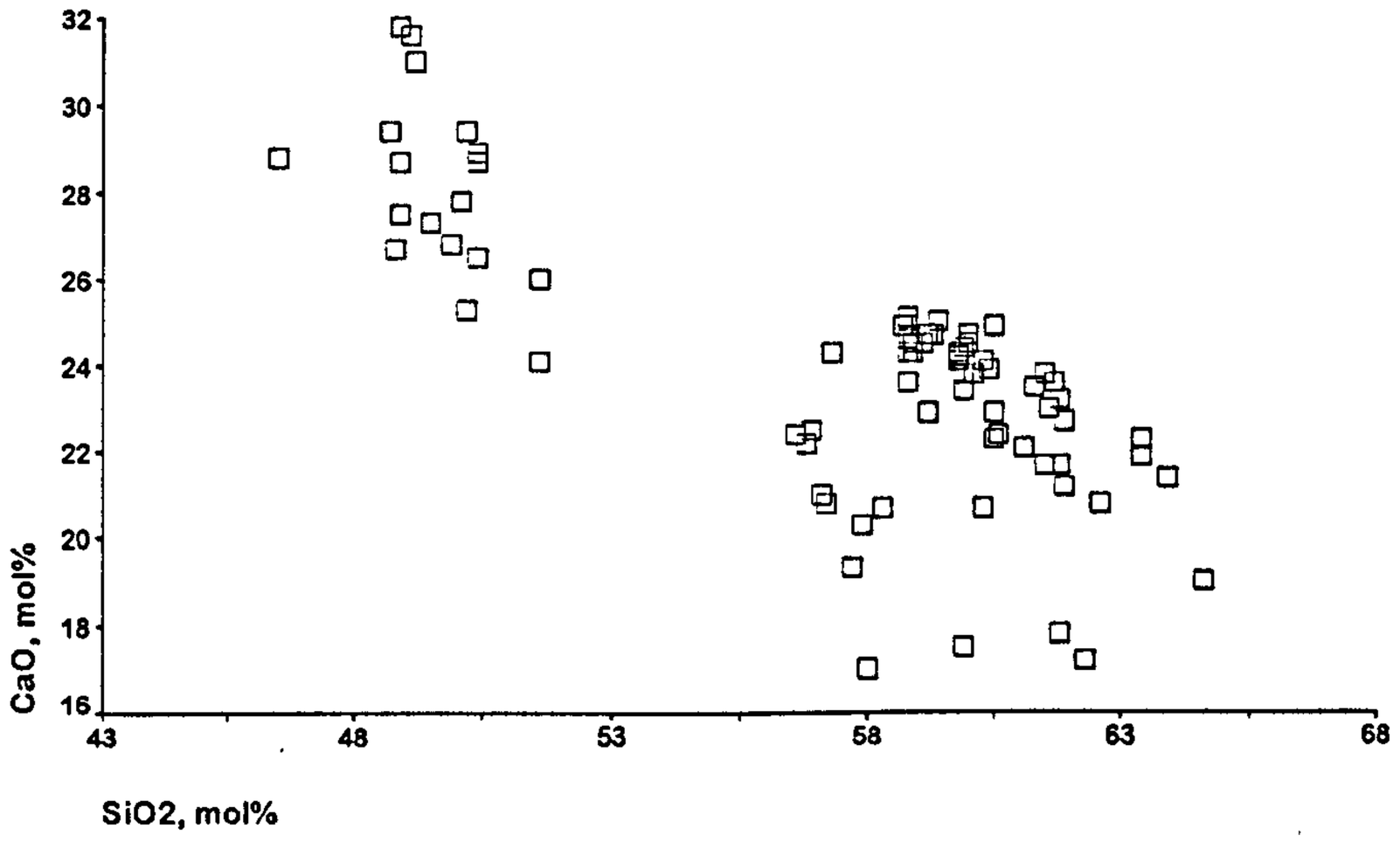

Figure 7.9: Lime-Silica scattergram of mol% for Γ_{LM}.

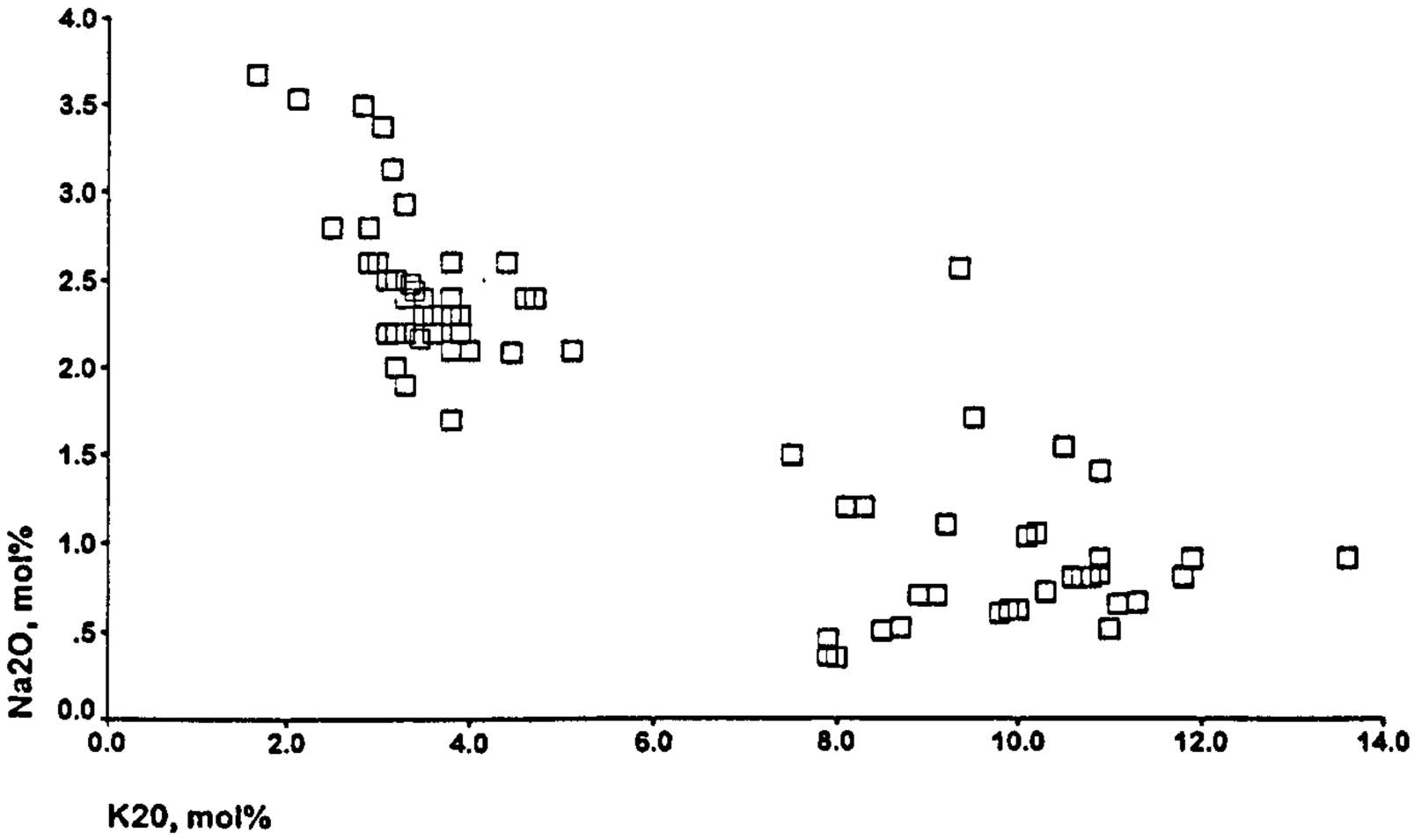

Figure 7.10: Soda-Potash scattergram of mol% for Γ_{LM}.

Glass Corrosion

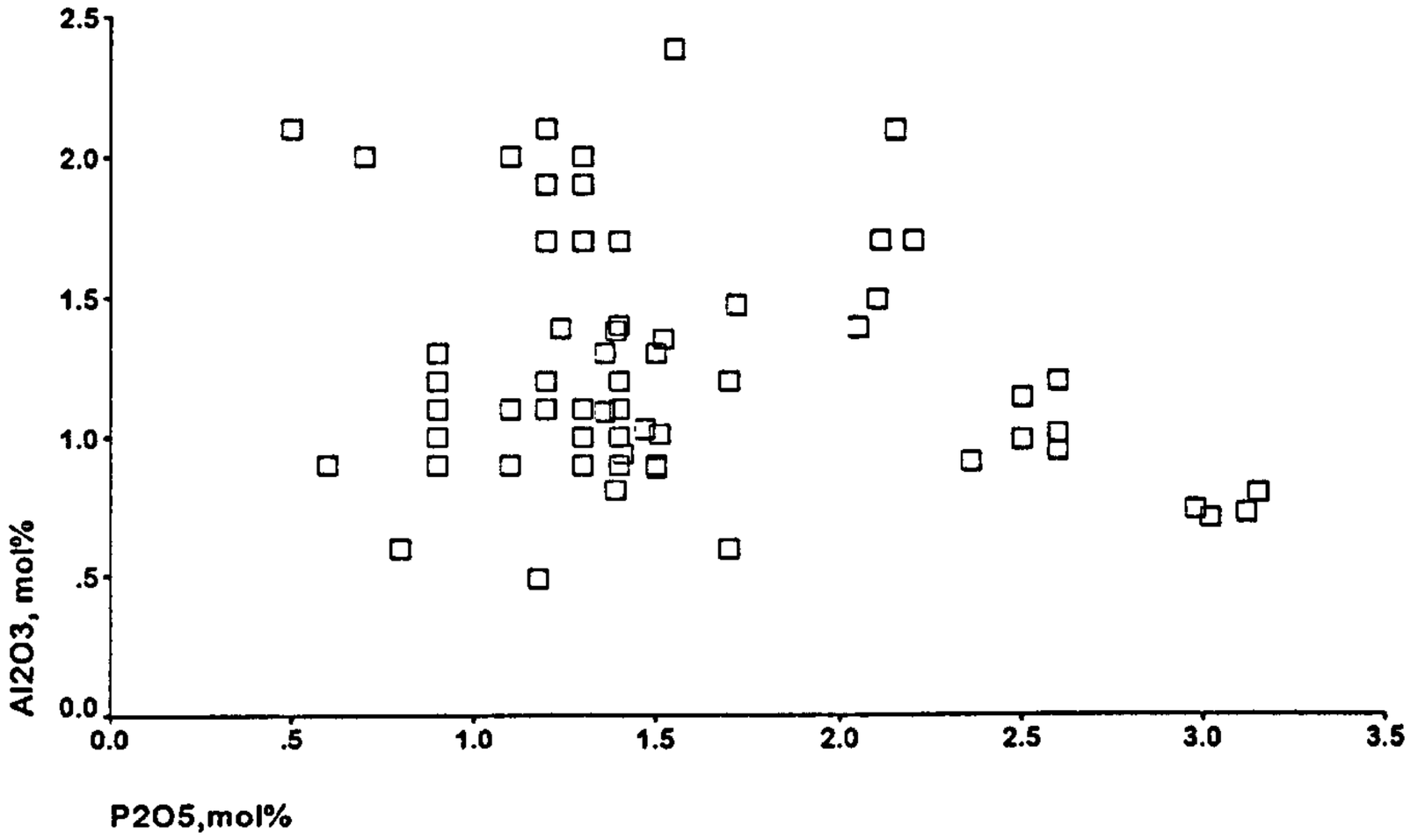

Figure 7.11: Alumina-Phosphorus scattergram of mol% for Γ_{LM}.

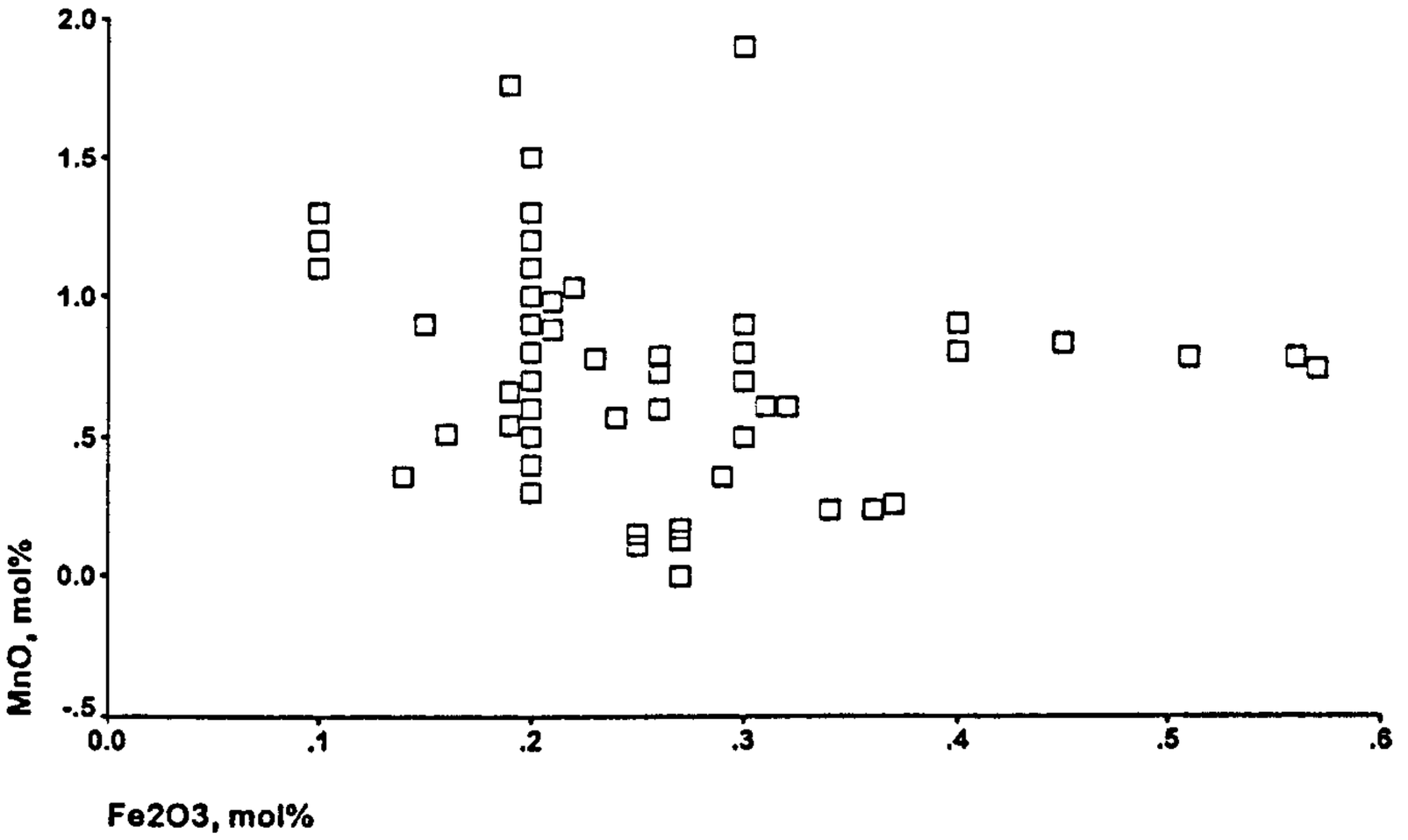

Figure 7.12: Manganese-Iron scattergram of mol% for Γ_{LM}.

Glass Corrosion

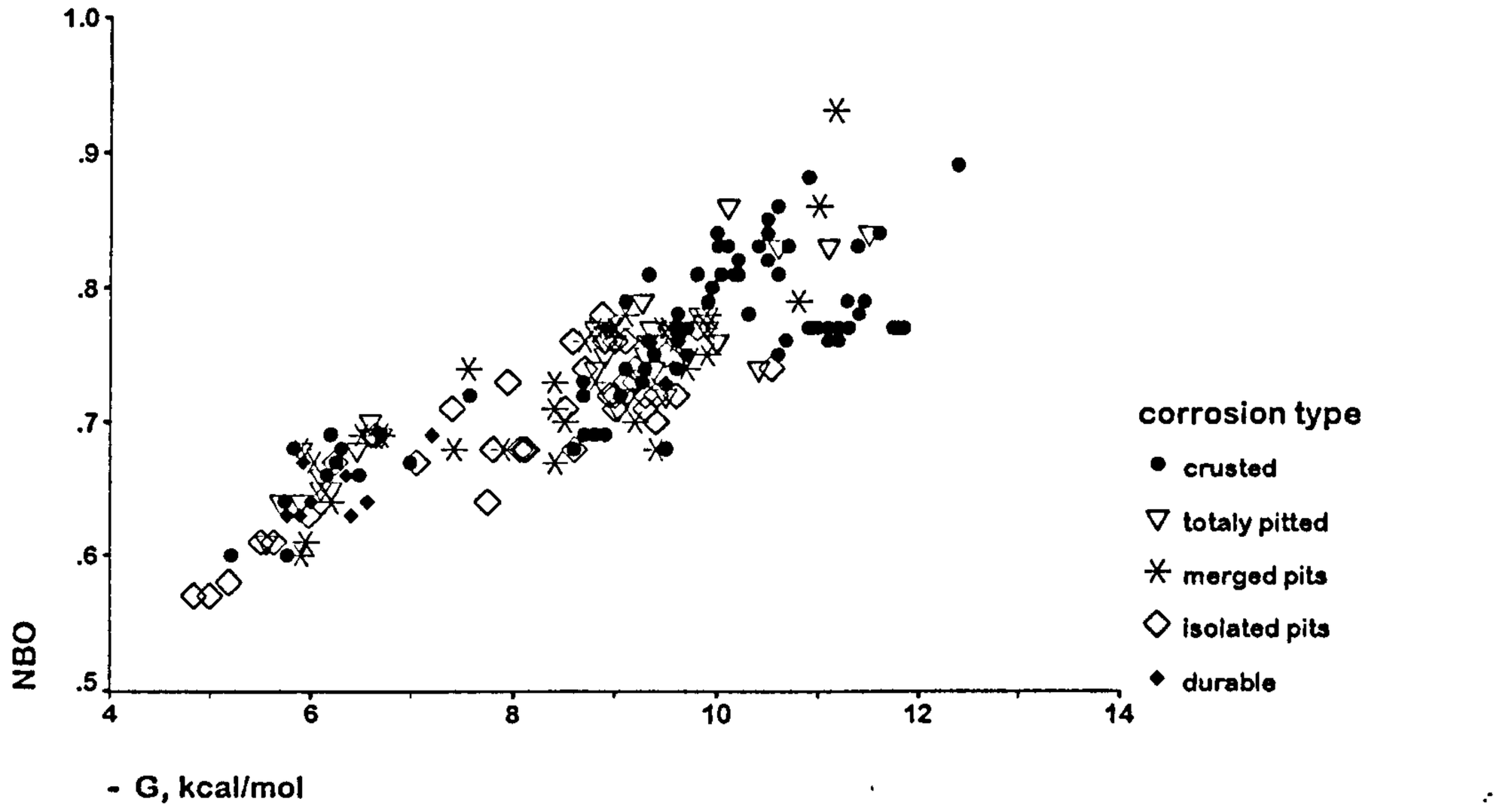

Figure 7.13: Free energy of hydration (ΔG) versus the number of non-bridged oxygens (NBO), using the extent of corrosion as markers.

glass. In the following sections the data will be considered first as a whole, and then according to these suggested four groups, where appropriate.

7.1.2 Non-bridged Oxygen Ions and Free Energy of Hydration

The value of the free energy of hydration (ΔG) and the number of non-bridged oxygen ions (NBO) are derived from the chemical composition of the glass and should therefore reflect the durability of the specimen. The closer NBO is to zero, the more durable the glass: the network has fewer modifiers breaking it up. Likewise the closer ΔG is to zero, the more durable the glass. Thus plotting the variables as abscissa and ordinate, respectively, should give the most durable species close to the origin. Figure 7.13 is the graph resulting from all the data collected, using the extent of deterioration as distinguishing markers for the glass compositions. It can be seen that the more durable glasses are closer to the origin and the uniformly weathered-crusted samples are further away.

Figures 7.14 to 7.18 illustrate the plots obtained by separating the data by corrosion type, *ie.* each plot represents glasses that have decayed to the same extent, for example, by merged pits. The markers show from which church the glass originated. Here the difference in distribution between the corrosion types can clearly be seen, *ie.* the larger number of specimens for the more decayed types. The region of the plots where ΔG>-8 kcal mol^{-1} appears to contain only specimens from

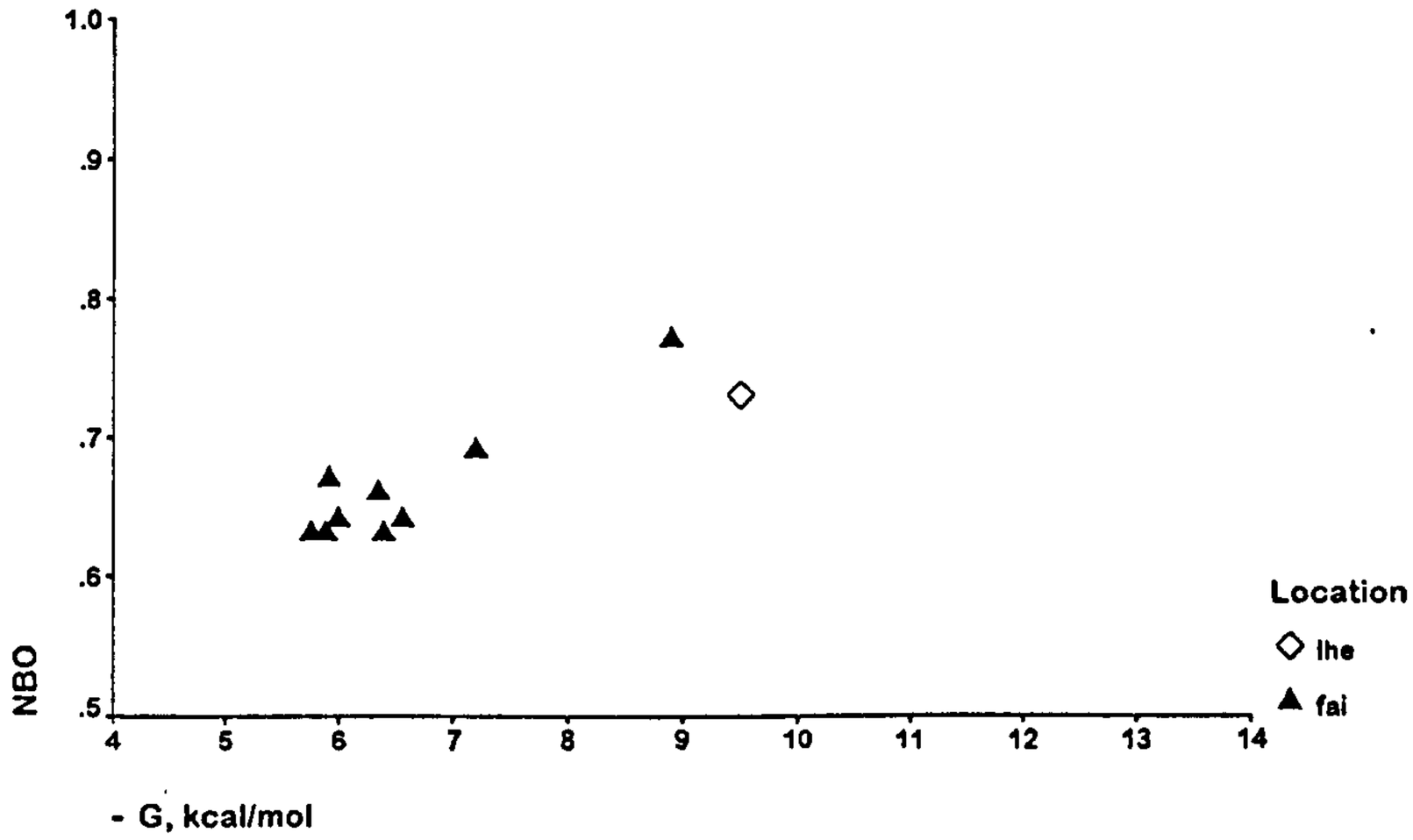

Figure 7.14: ΔG versus NBO for durable samples.

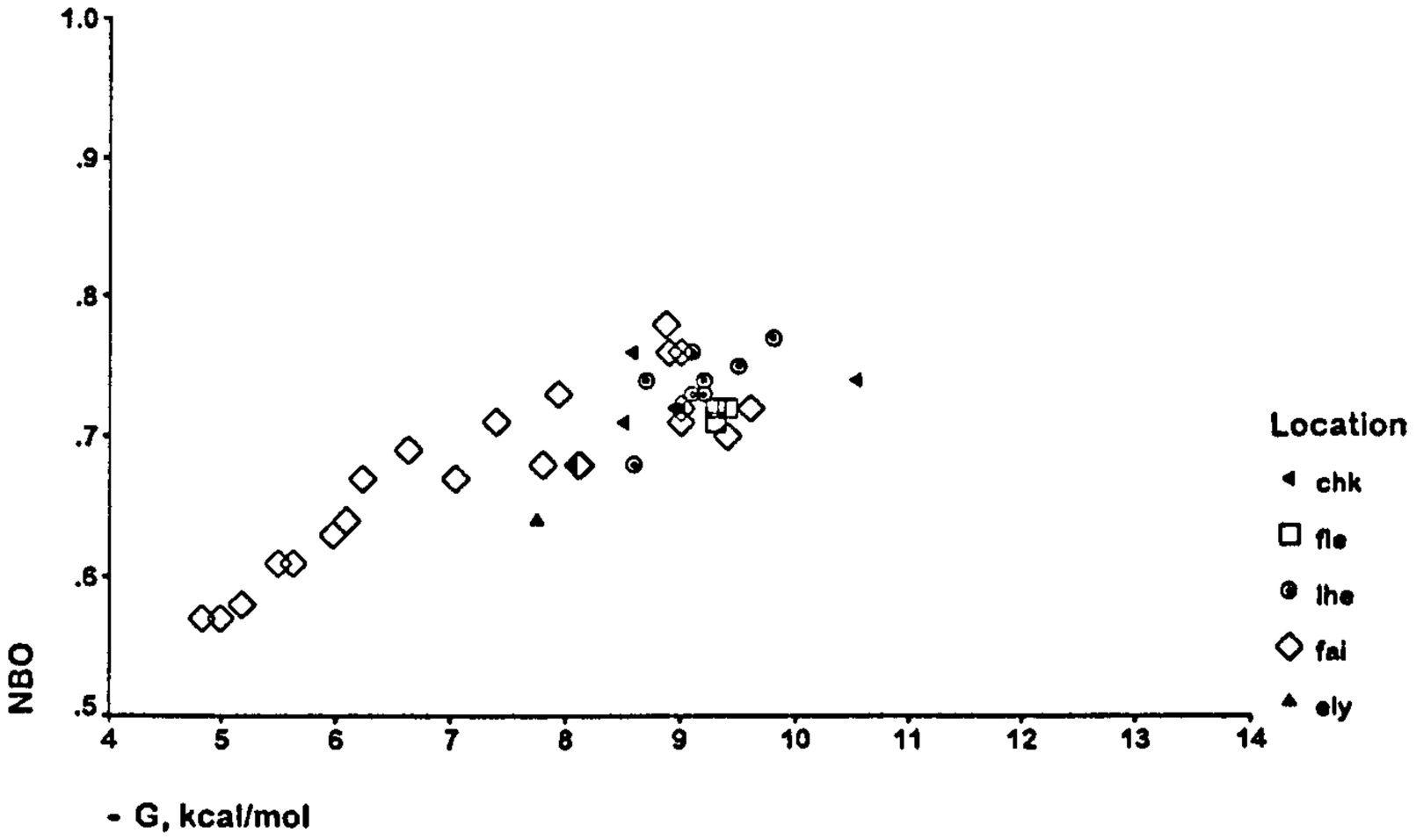

Figure 7.15: ΔG versus NBO for samples with isolated pits.

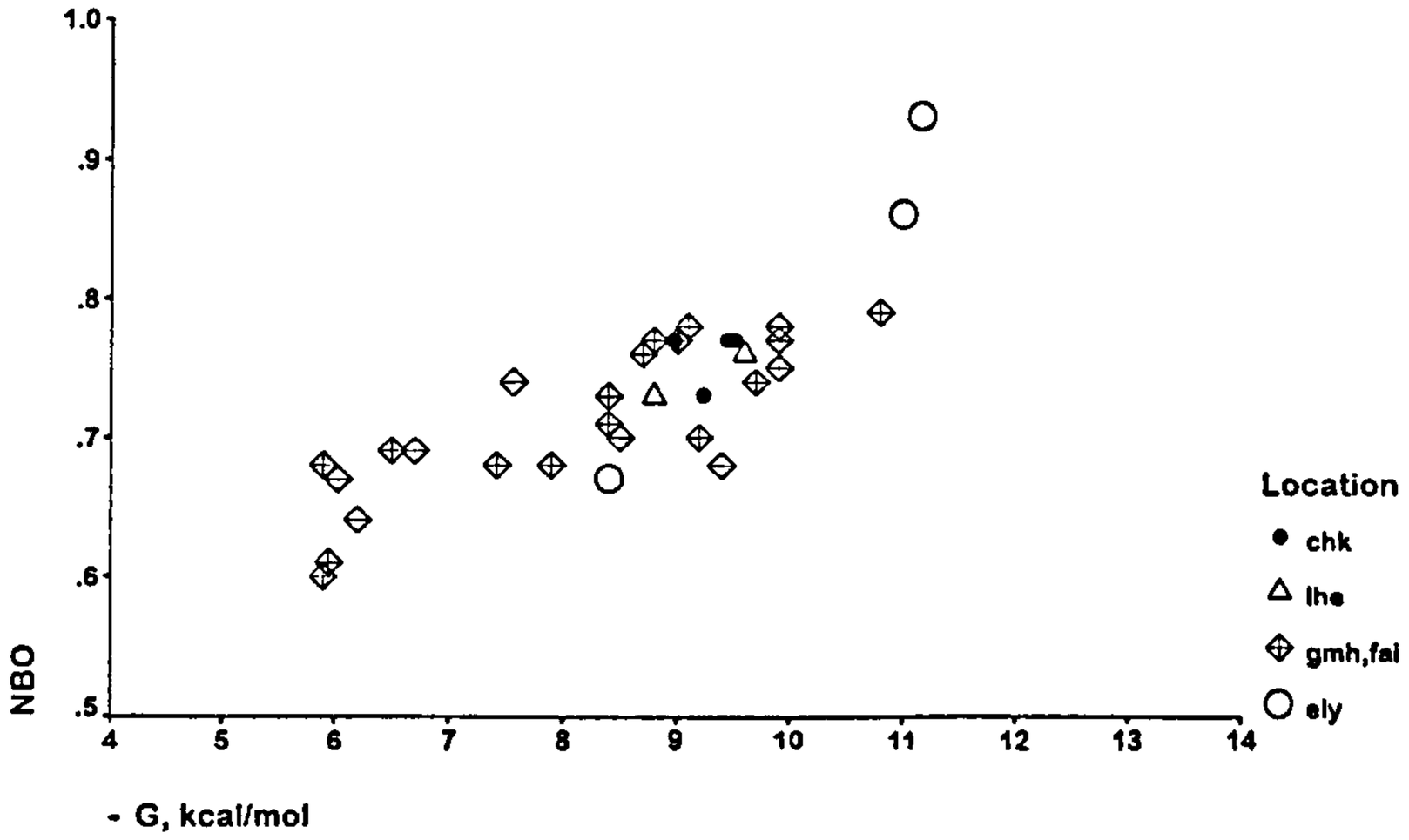

Figure 7.16: ΔG versus NBO for samples with merged pits.

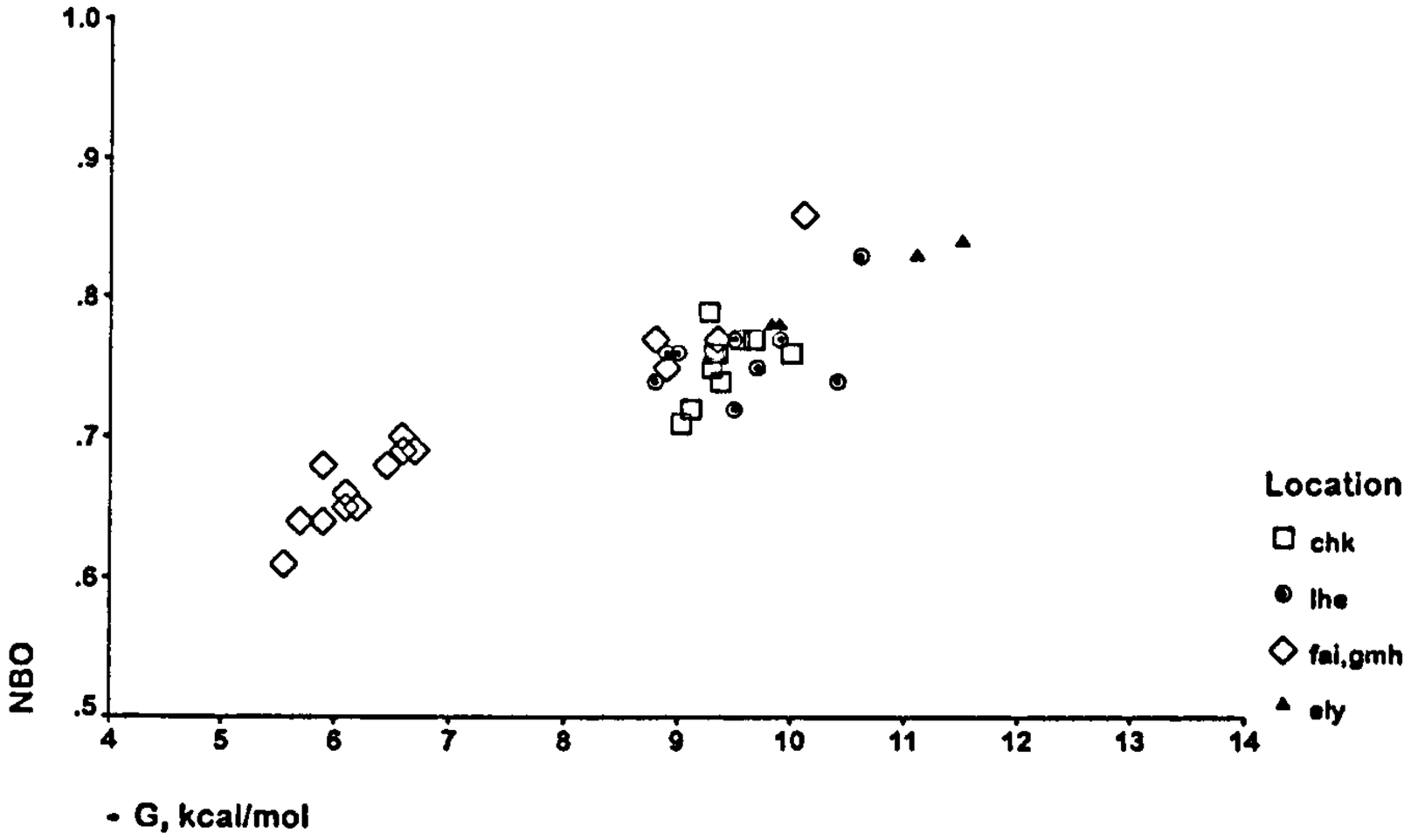

Figure 7.17: ΔG versus NBO for samples which were totally pitted.

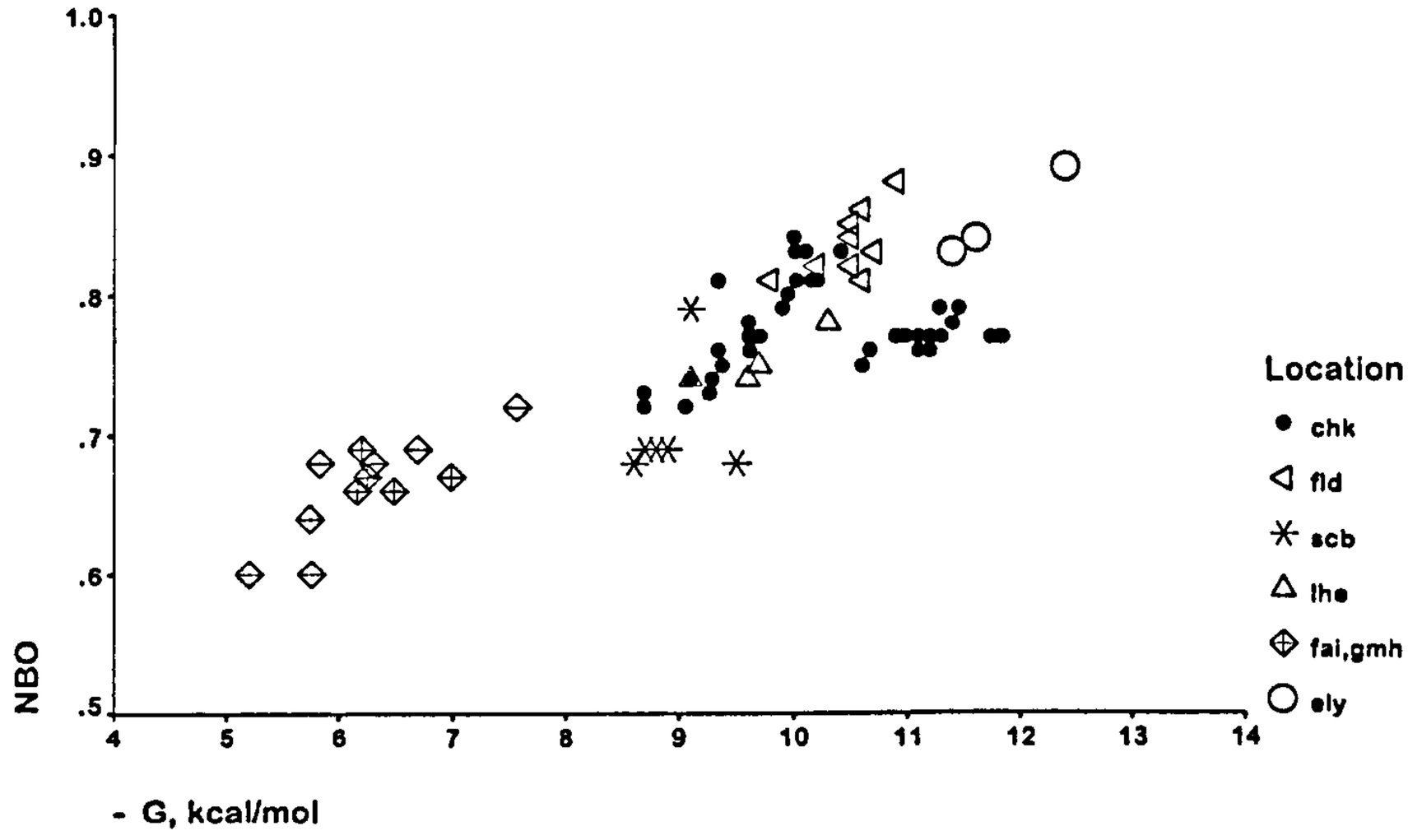

Figure 7.18: ΔG versus NBO for samples which were uniformly weathered.

Fairford. The centre for each type, except for the Fairford samples, shifts from ΔG = -8.5 kcal mol^{-1} for isolated pits to -10.3 kcal mol^{-1} for the crusted samples. This is highlighted if the data are reduced to an average NBO and its corresponding ΔG value for each of the corrosion types. Figure 7.19 is the resulting graph. The relationship is approximately linear, but that could be due to the short range of values incorporated in the analyses. Jantzen and Plodinec (1984) examined the relationship between mass loss of silica and NBO, and mass loss of silica with ΔG for various glass types undergoing artificial corrosion. Their range was much larger than that encompassed here, but this is the first use of the parameters to look at natural atmospheric corrosion. Obviously the mass loss of silica is an unknown quantity in this case and therefore the results cannot be directly compared, but they appear to be similar. On including the data of Gillies and Cox (1988a,b), a similar graph is obtained, but the actual values shift slightly. This is included in Figure 7.19 using identical symbols but with the error bars as dotted lines. The discrepancy in the position of the symbols is probably due to inconsistencies in the labelling of corrosion types, as this is subjective, but may also be due to the slightly earlier date of the glass from the York Minster or the different analytical technique.

Further insight can be gained from ΔG versus NBO plots when the markers delineate the location, as in Figure 7.20. Here it is obvious that Fairford, Gloucestershire, has remarkably durable glass. This is in part due to its late date, that is the composition is markedly different. For this reason, the results for Fairford will be discussed separately from the fourteenth century glass. The glass at Ely is the least durable and closely associated with the Fledborough glass. The other churches have comparably durable glazing when considered in this manner.

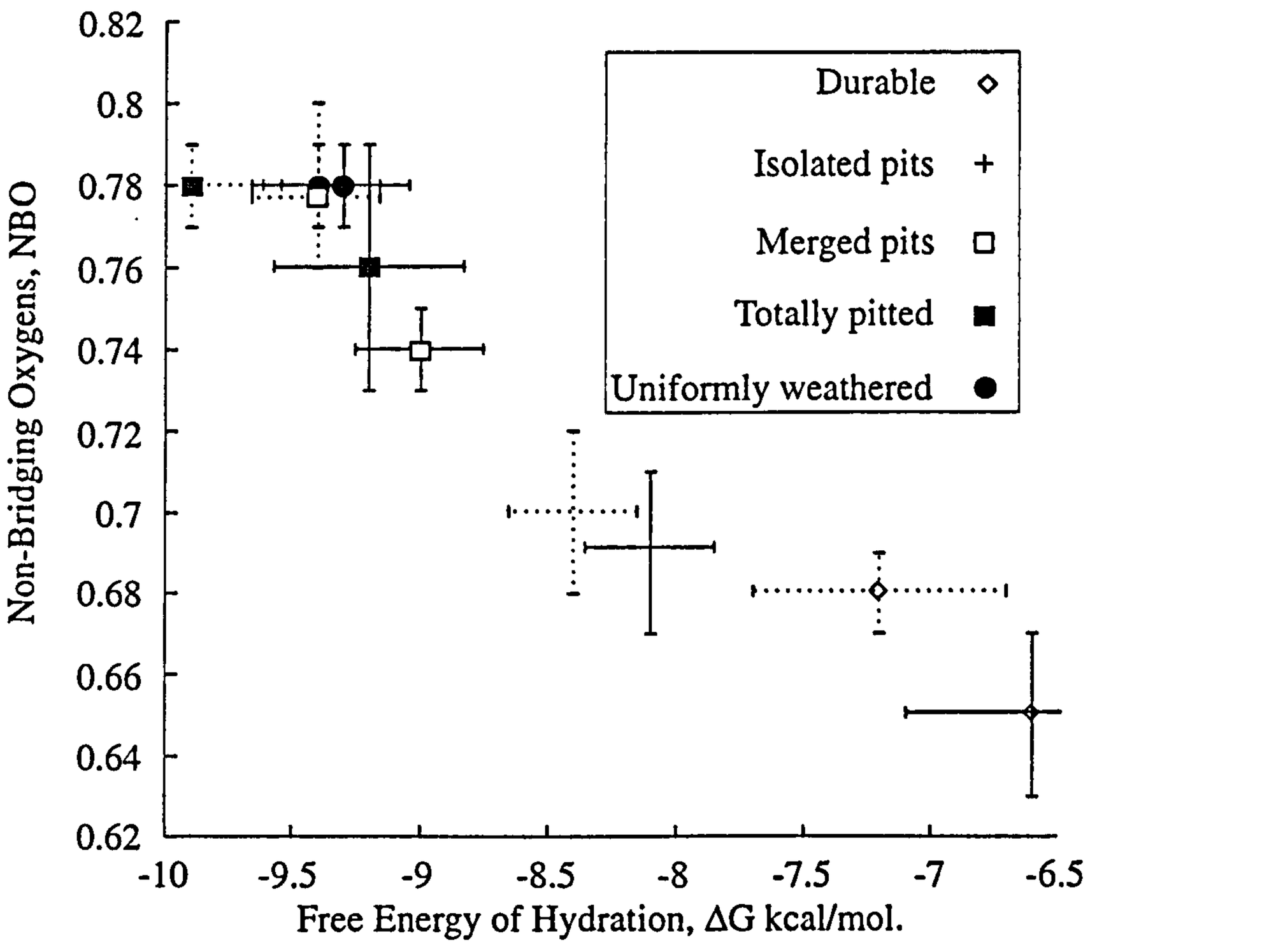

Figure 7.19: ΔG versus NBO as averages calculated for each corrosion type. The complete lines indicate the data produced from this study, whereas the dotted lines represent the data when incorporating Gillies and Cox data.

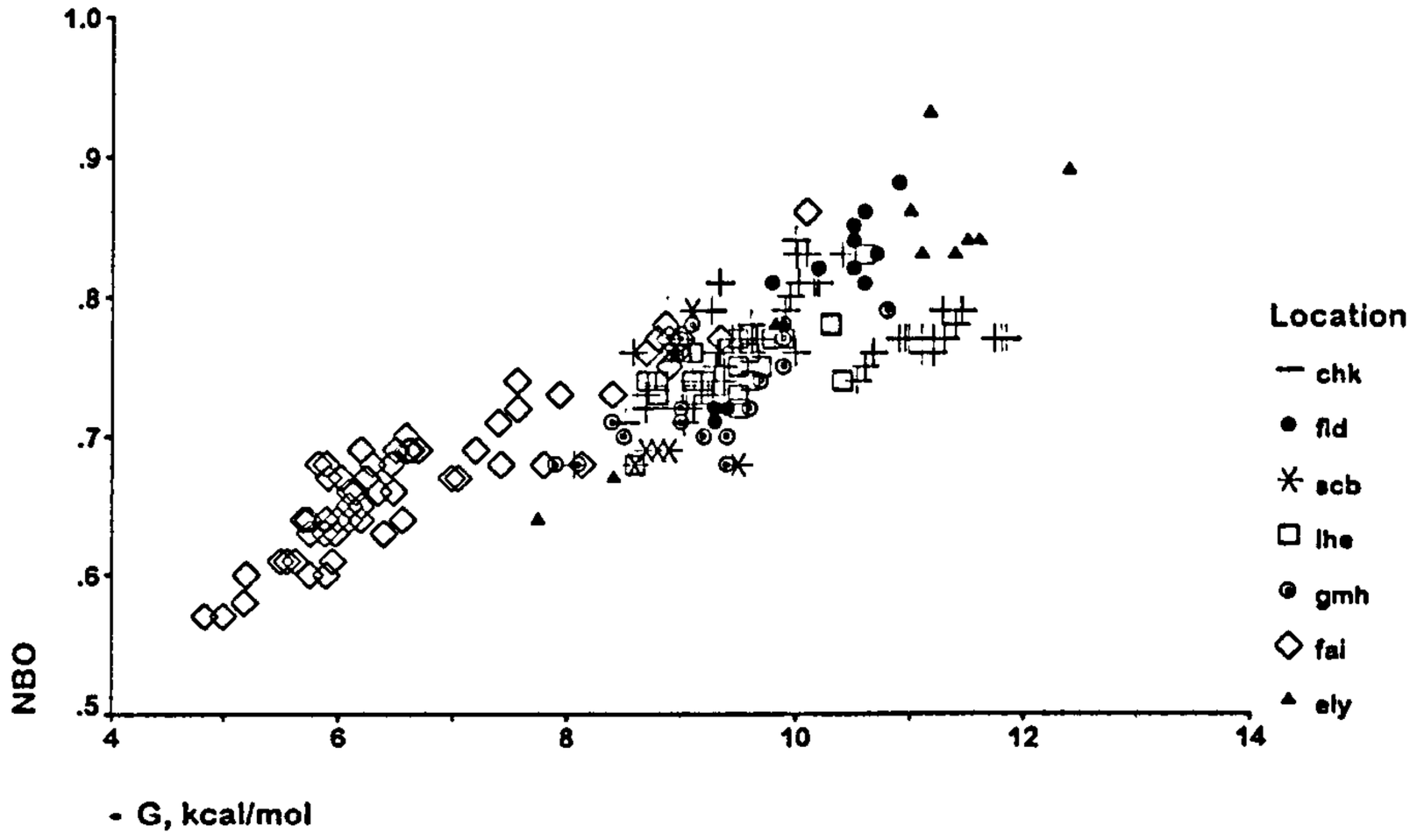

Figure 7.20: Free energy of hydration versus the number of non-bridged oxygens, using the location as markers for all data.

The clustering of the Fairford glass at ΔG >-6 kcal mol^{-1} explains the discrepancy in Figure 7.13 where some of the uniformly weathered samples appear near the origin. This glass has a low ΔG value because of its high silica content, but obviously some other factor has lead to its' decay, that is not included in this calculation.

Γ_{LM}

Figures 7.21 and 7.22 are the plots shown in 7.20 and 7.13, but eliminating the values for the Fairford glasses. A division due to location would not be expected, since that would indicate either a different date or guarding of recipes and ingredients by workshops.

Figure 7.21 illustrates the group is not divisible by the locations. It does serve as a good reference for spotting anomalous samples. The decay type is linked to the reduced composition parameters in the manner mentioned in the previous section, *ie.*, durable near the origin, most weathered at the extremes.

Fairford

Fairford requires treating separately due to its different composition, that is its mixed-alkali nature. Figure 7.23 is the ΔG/NBO plot for the Fairford samples and shows that the trend of increased ΔG associated with greater decay is no longer valid. This suggests that the calculation of ΔG needs adapting to take into account the mixed alkali effect, or that some other factor is affecting

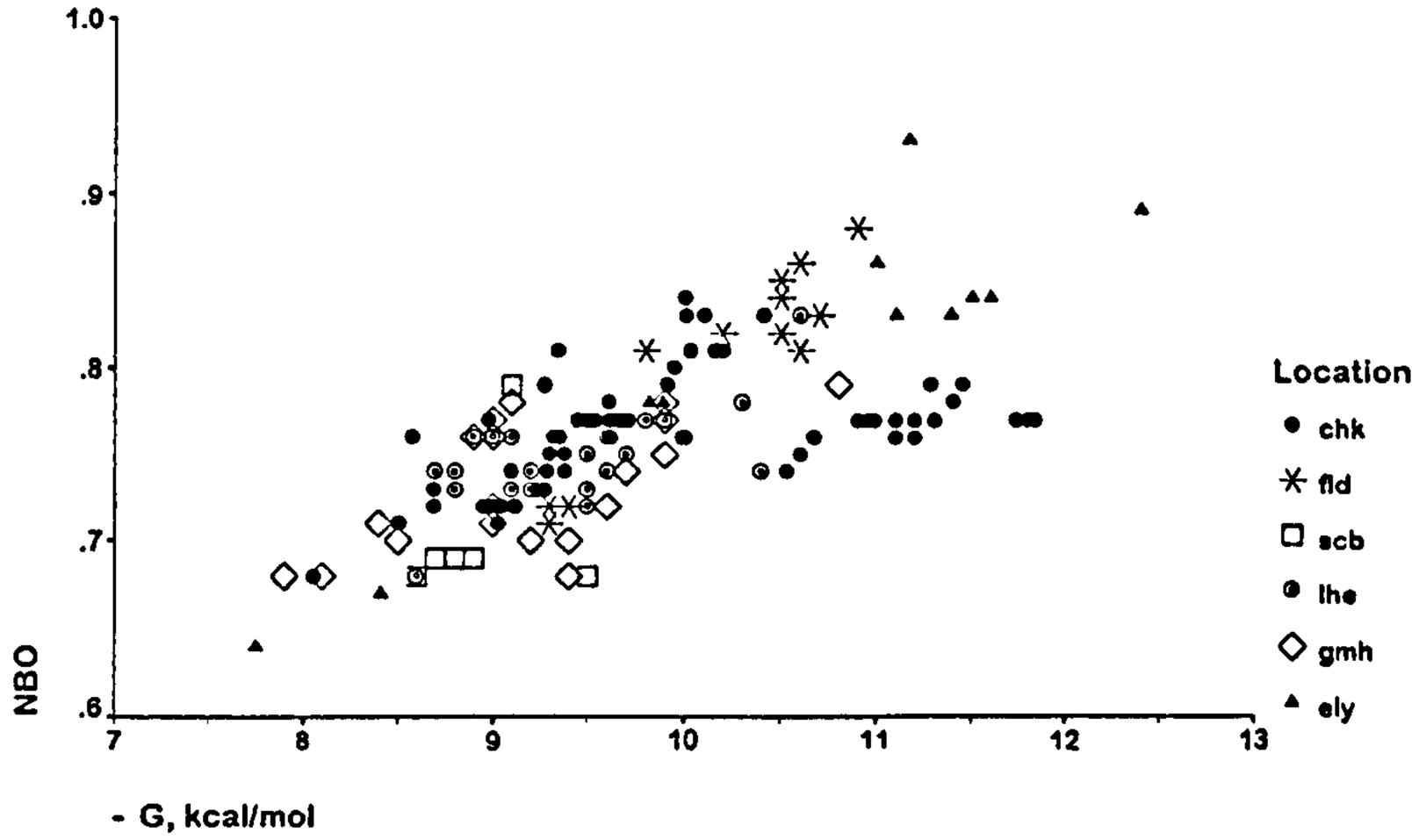

Figure 7.21: Free energy of hydration versus the number of non-bridged oxygens, excluding Fairford glasses, using location as markers.

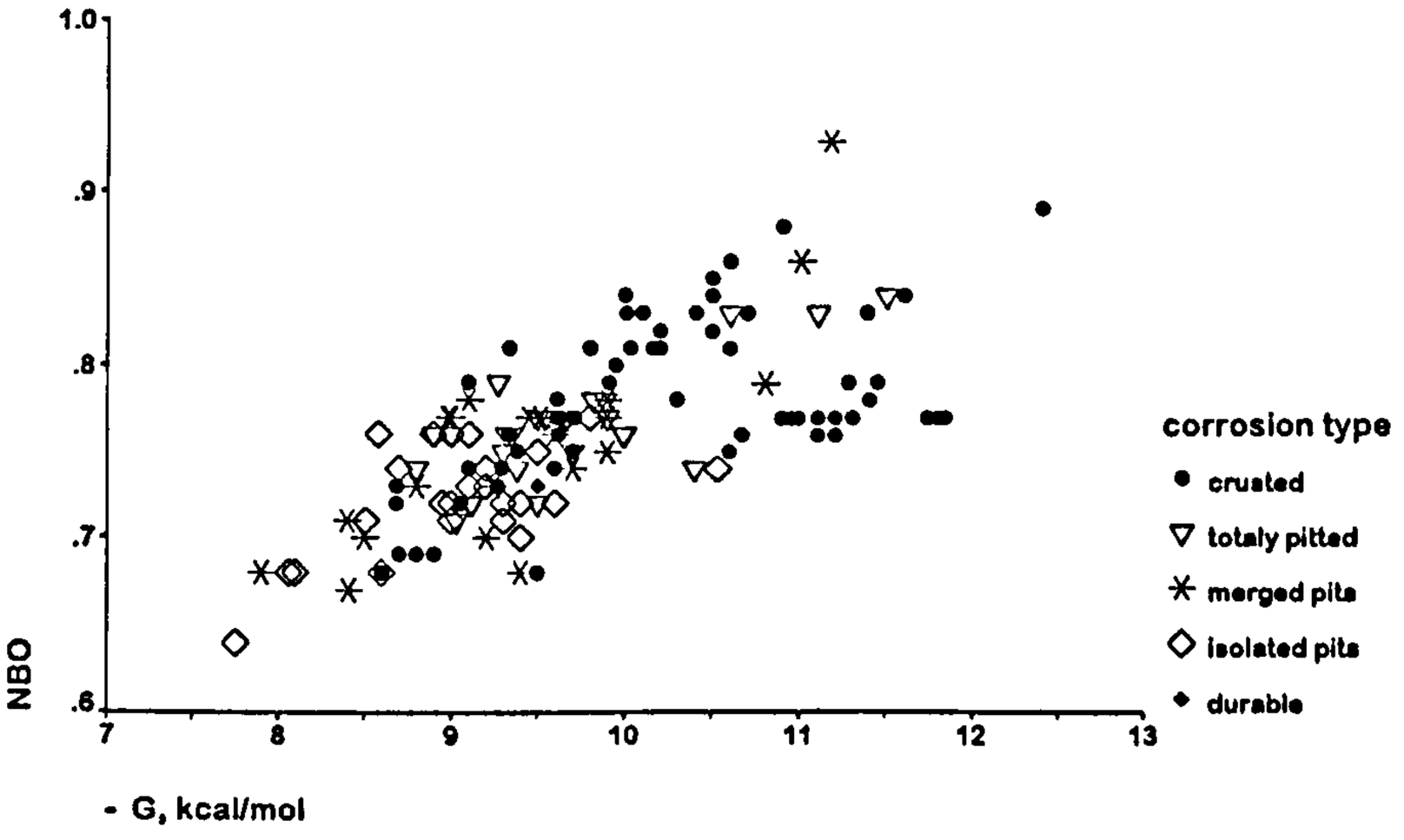

Figure 7.22: Free energy of hydration versus the number of non-bridged oxygens, excluding Fairford glasses, using corrosion type as markers.

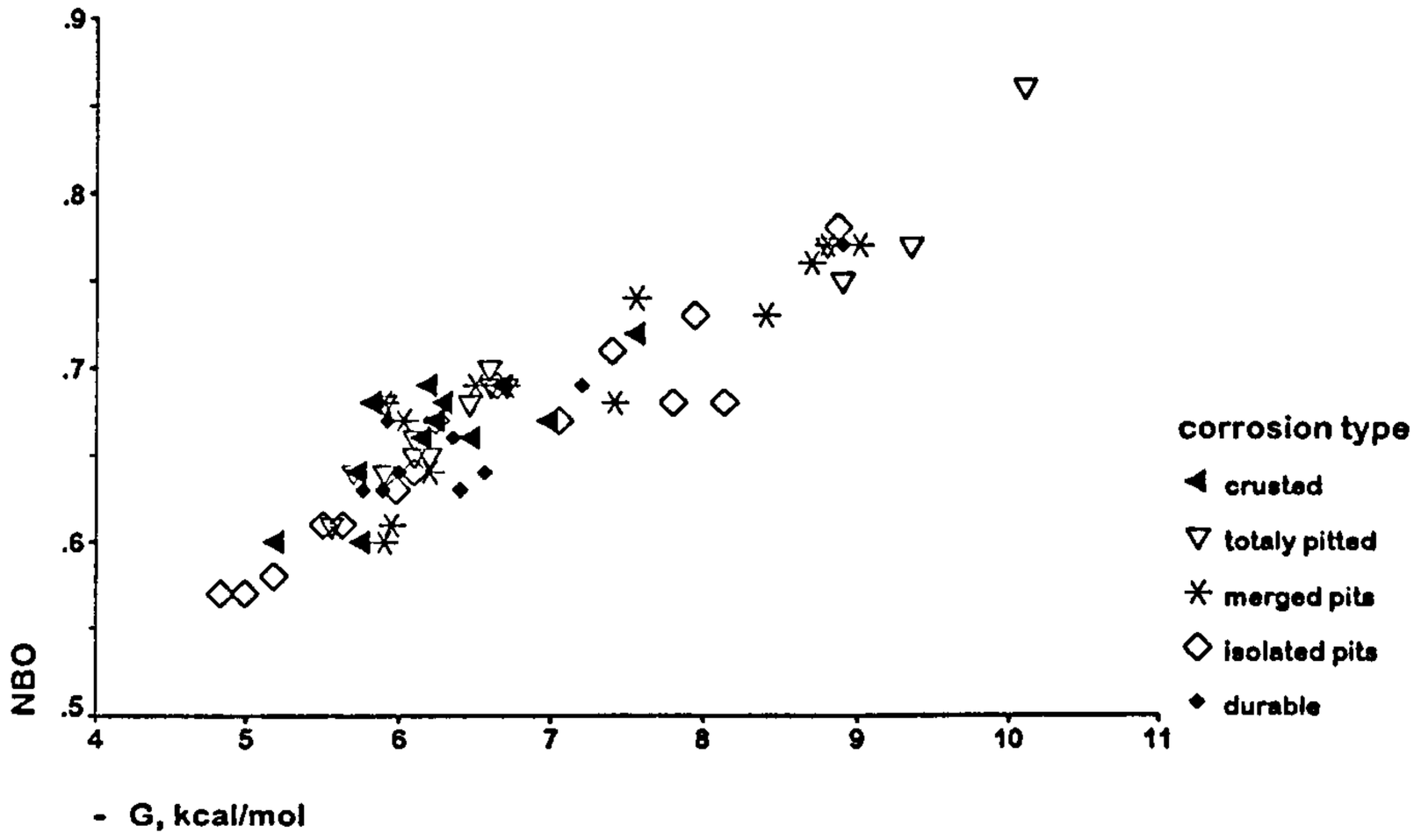

Figure 7.23: Free energy of hydration versus the number of non-bridged oxygens for Fairford glass, using extent of corrosion as markers.

the state of preservation, such as unsympathetic cleaning.

7.1.3 Ternary Co-ordinates

The usual manner of presenting ternary co-ordinates is on a "triangular diagram"; such diagrams require special software to produce computationally and therefore in this section they will be plotted as conventional graphs, with the third value implicit, since 'R_2O', 'RO' and 'SiO_2' must total to 100 mol%.

As the co-ordinates represent the composition, the markers can indicate other non-quantifiable properties, such as colour. Figure 7.24 is a general plot of 'R_2O' and 'RO' with the markers indicating the location of the church from which the glass was obtained. It is immediately obvious that three clusters form and that these are perhaps dependent on present location but more importantly suggest different workshops or source materials. That is, the cluster 25<'RO'<32 mol% and 3<'R_2O'<6 mol% is composed entirely of the glass from Fairford, though not all of the FAI glass is included. The second cluster, where 'RO'>32mol%, contains the glass from Ely and Fledborough, with one outlier from Fairford. This is sample FAI32, which is anomalous in appearance as well as composition. It is a flashed ruby glass that has decayed by pitting. These pits are in the red layer only, contain a very hard white crust and look false. This peculiar appearance would suggest that it was a replacement piece perhaps from the Victorian era (when distressing replacement glass to look comparable to the rest of the window was common practice). The third group will be given

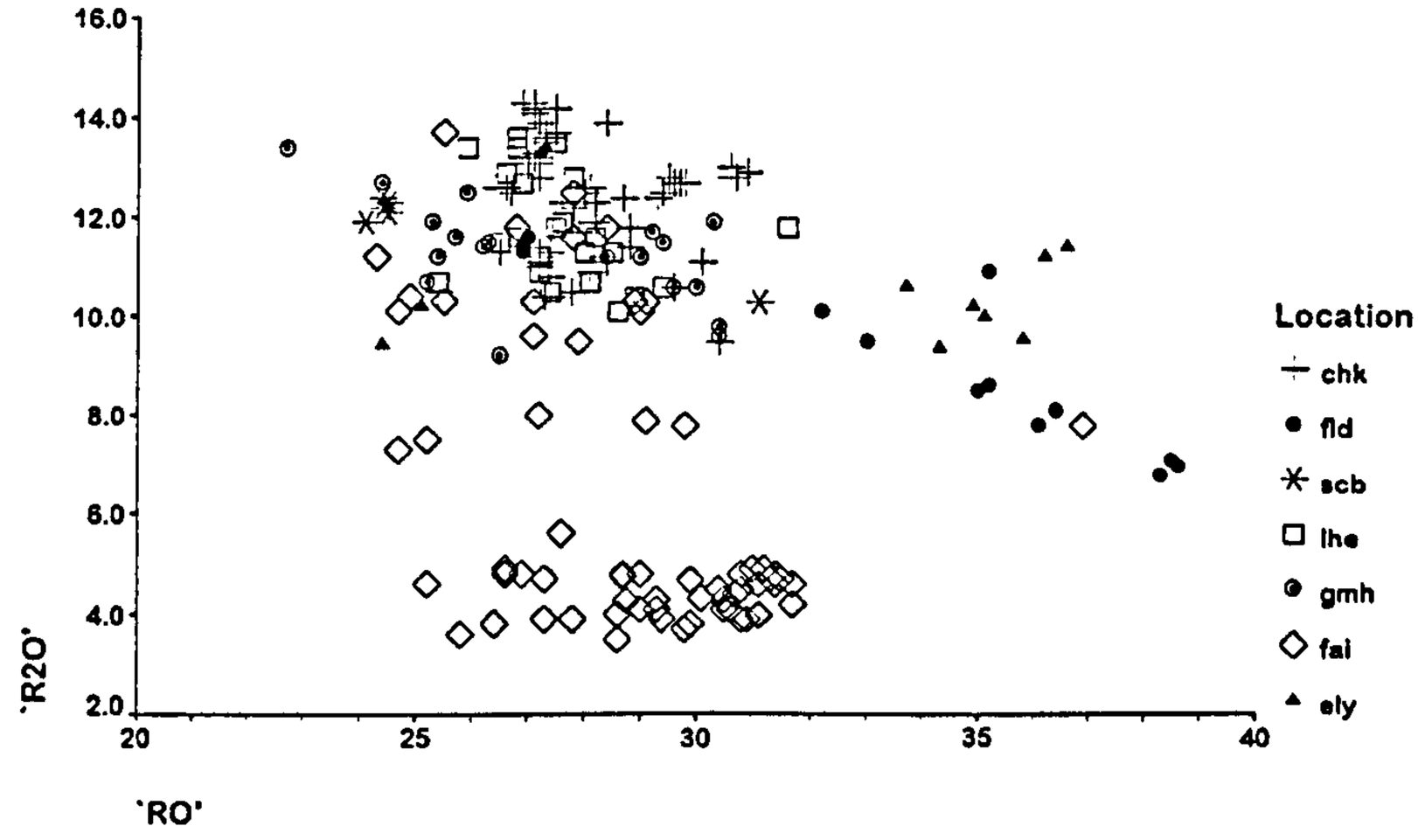

Figure 7.24: Graphical representation of the ternary co-ordinates, 'R_2O' and 'RO', using location as the marker.

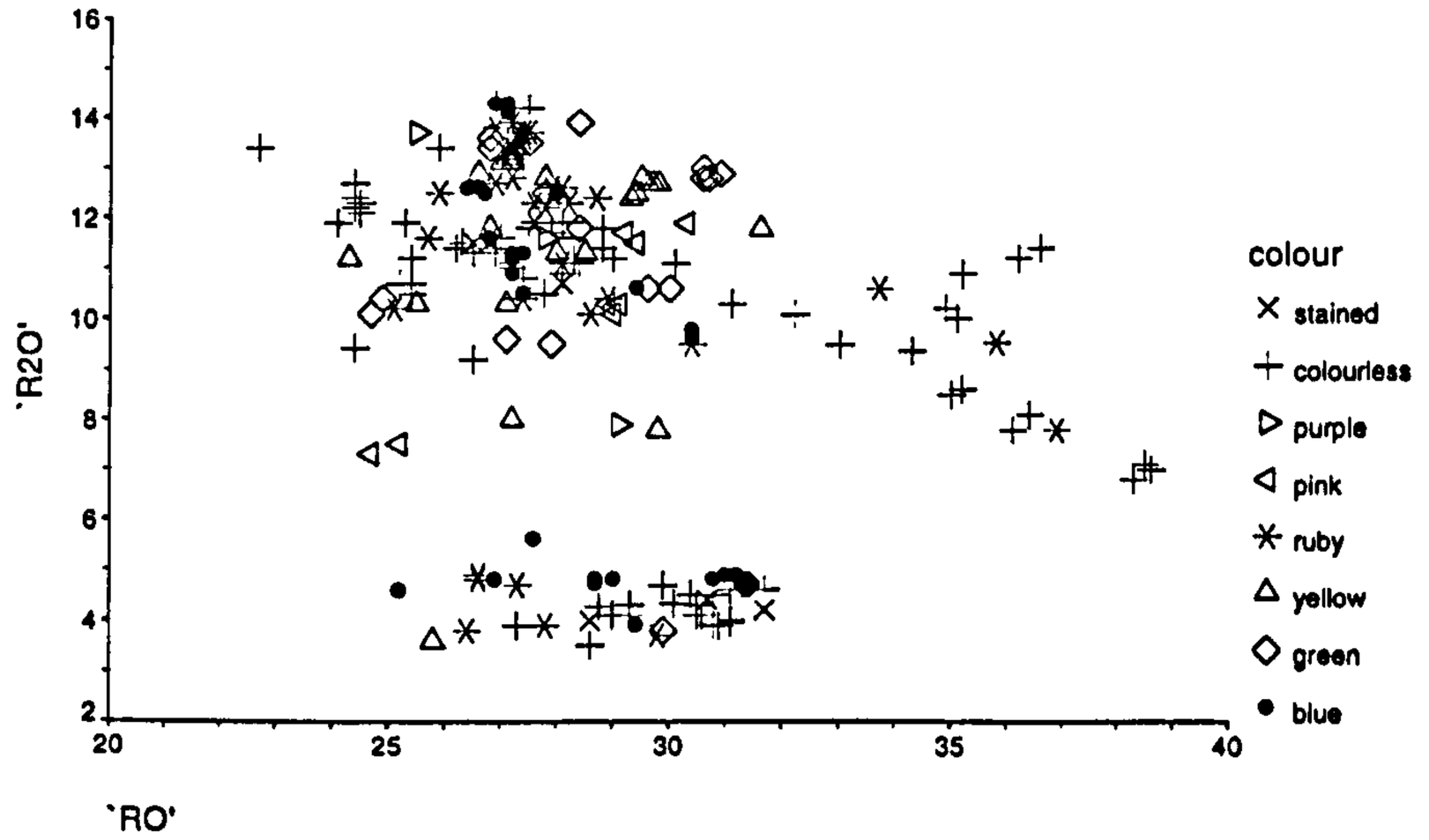

Figure 7.25: Graphical representation of the ternary co-ordinates, 'R_2O' and 'RO', using colour as a marker.

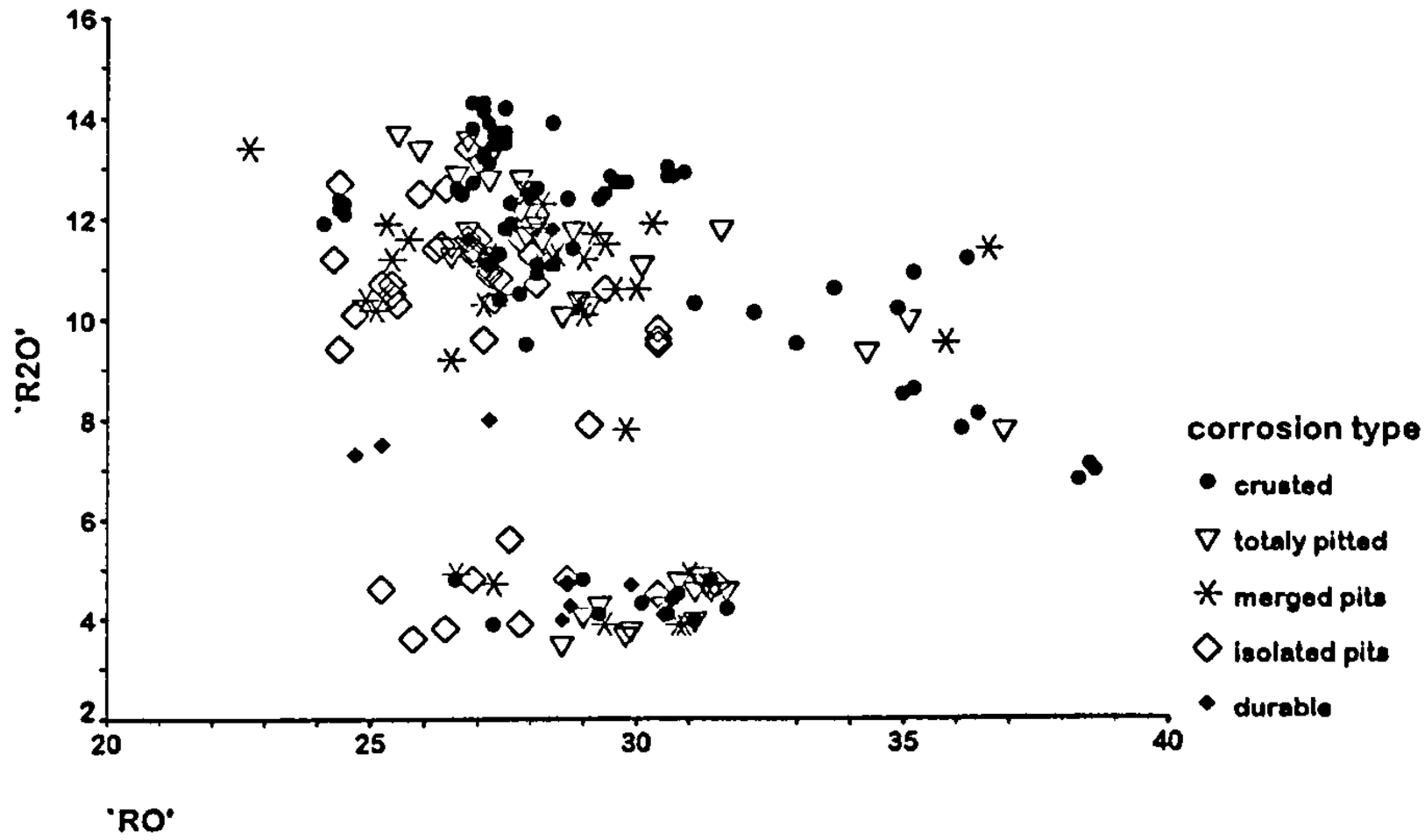

Figure 7.26: Graphical representation of the ternary co-ordinates, 'R_2O' and 'RO', using mode of corrosion as a marker.

the generic term 14C as it contains all other samples, which are mainly fourteenth century. The others group will be labelled ODD (Ely, Fledborough) and FAI (Fairford) .

Figure 7.25 is the same plot but this time the markers indicate the colour of t he particular glass. It can be seen here that the colour does not appear to be linked with the clustering. This was expected because the colouring agents have not been incorporated in the calculation of the ternary co-ordinates. The exception to this is the apparent division of the Fairford samples. The FAI group is composed of blue, colourless and ruby glasses (except for 1 yellow and 1 green sample), whereas all the other coloured samples are in the Γ_{HM} group. A similarity between ruby and colourless is likely as the red layer in a ruby glass needs only a very small amount of colloidal copper to impart the red colour[143] and so could, perhaps, have been made from the same core batch. No difference in composition was detected between the red and white layers of the ruby glasses. This, however, does not explain the blue glass—unless these incorporated an amount of Roman/Saxon blue glass as cullet (to give the necessary amount of cobalt for a blue colour). The yellow and the green samples are anomalous. They are FAI15 and FAI48 are thicker than most of the Fairford pieces, being 2.5mm and 3mm respectively compared with 2mm for the majority of the others. FAI48 is unusual in that it is a flashed green glass; these are particularly uncommon. FAI15 is the only sample which had back painting and perhaps this suggests it is a replacement. There was also no correlation found between the colour of the glass and the extent of decay.

Finally, Figure 7.26 shows the clustering with corrosion type as the marker. It can be seen that the clusters do not correlate with any particular mode of corrosion, although within the two age

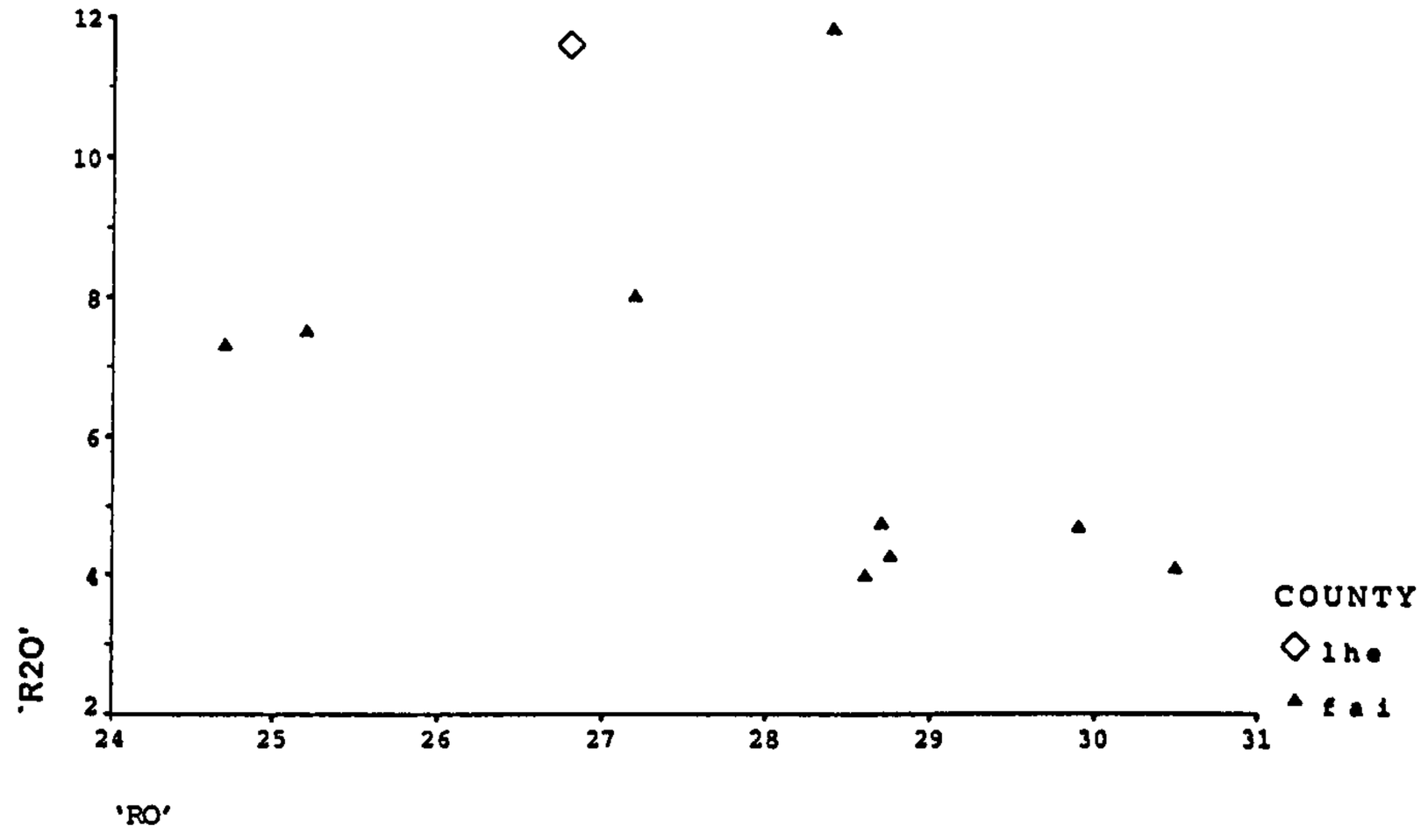

Figure 7.27: Ternary diagram for durable samples only.

categories there is a tendency for high 'R_2O' (for the fourteenth century glass) and high 'RO' (for the sixteenth century glass) to be the most decayed. Figures 7.27 to 7.31 are the same plots of 'R_2O' versus 'RO' for each of the corrosion types separately. Excluding Fairford for the moment, there are two clusters in Figure 7.24. They are divided by amount of 'RO'. The high 'RO' group is the low magnesia glasses mentioned earlier (see section 7.1.1). They are poorly durable and therefore only appear in Figure 7.31. The other compositional group, Γ_{HM}, appears on all plots 7.27 to 7.31. This group has higher 'RO' values as the extent of decay is more marked. The uniformly weathered samples of this type also have slightly higher 'R_2O'. This can be seen more clearly in Table 7.3 where the mean 'RO', 'R_2O' and 'SiO_2' have been calculated for the various modes of decay. Note that the data was first separated according to age and then the classification—Γ_{LM} or Γ_{HM}. In the low magnesia group, for both dates, the average 'RO' value increases with increased decay. For the fourteenth century glass it changes from 24.40mol% for isolated pitting (IP) to 35.64mol% for uniformly weathered (U); the Fairford glass has 27.94mol% for durable (D) and is 29.87mol% for U. This range for the Fairford glass is much tighter and may not be significant.

The Γ_{HM} type glass for both dates contains anomalously durable samples. Excluding these, there is an increase in corrosion as the 'SiO_2' decreases. That is, from 60.7mol% for IP to 58.5mol% for U in the case of the fourteenth century glass and 63.3mol% for IP and 61.4mol% for U for the Fairford glass. The other ternary co-ordinates do not show any particular trend. Figures 7.32 and 7.33 show the variation of 'R_2O' with the third parameter 'SiO_2'. These two graphs highlight that the high 'SiO_2' glass has low 'RO' and that these glasses are more durable.

Gillies and Cox[59] found that the ratio of 'R_2O'/'RO' increased as the deterioration became more

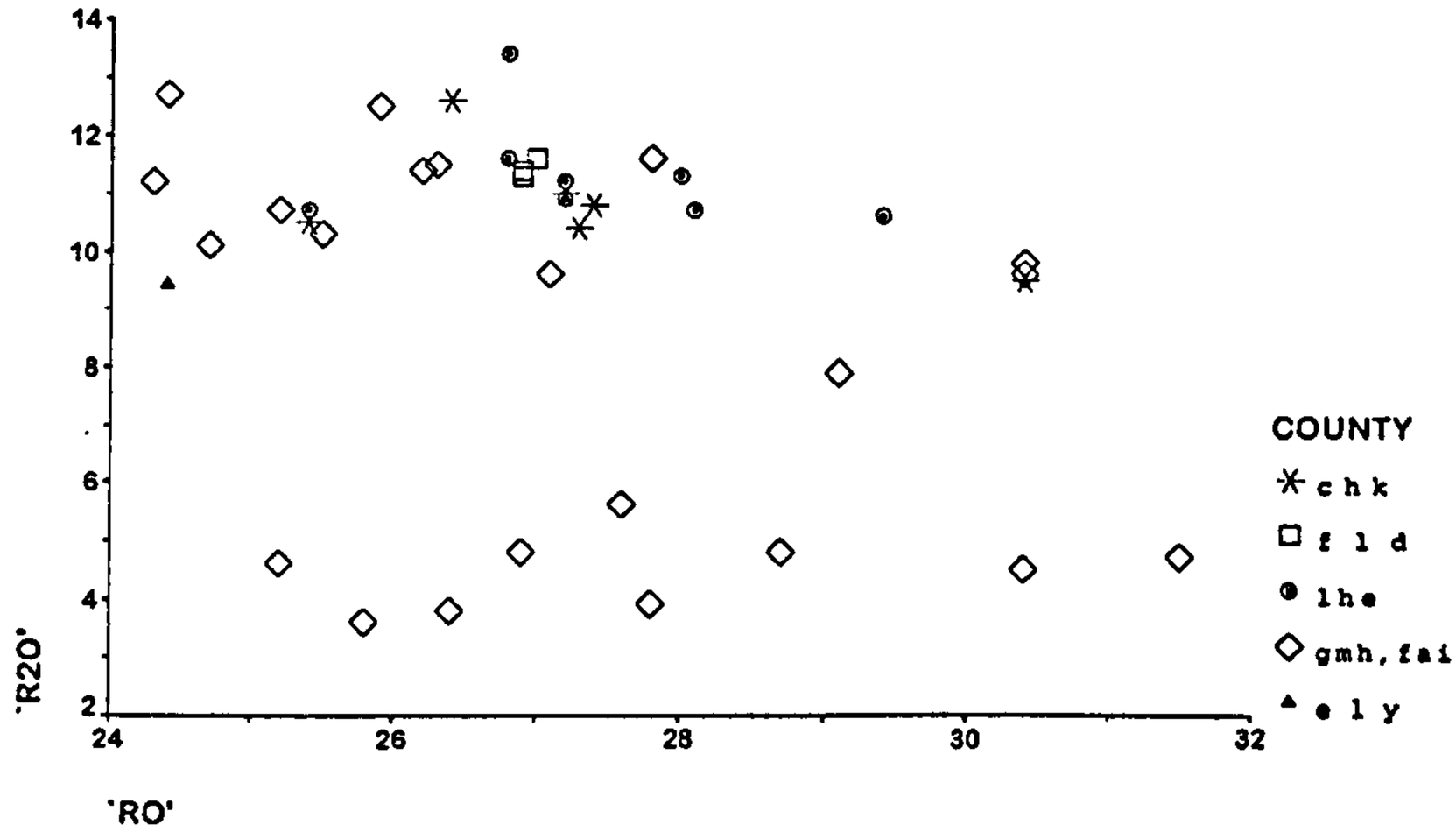

Figure 7.28: Ternary diagram for samples with isolated pits.

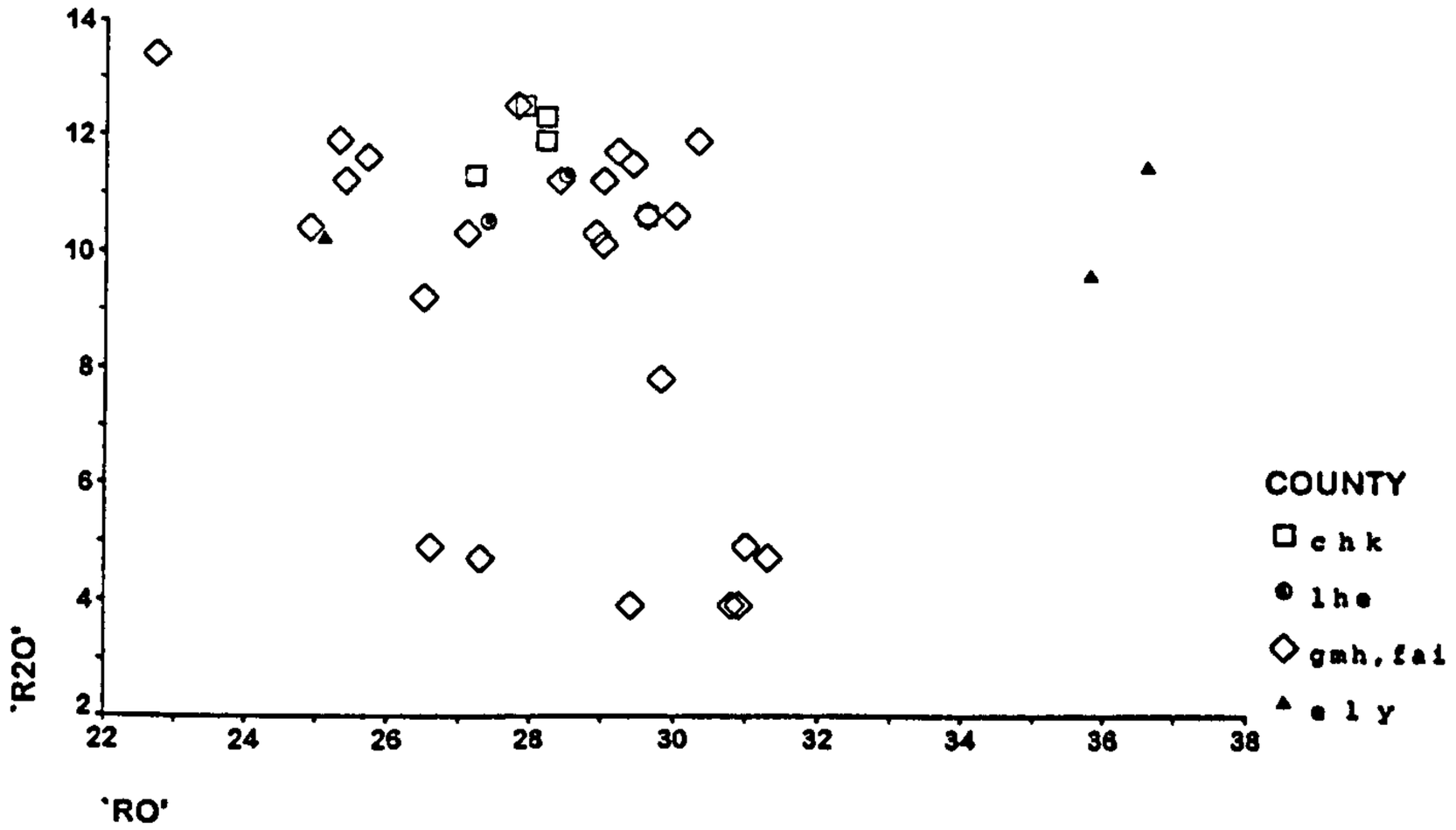

Figure 7.29: Ternary diagram for samples with merged pits.

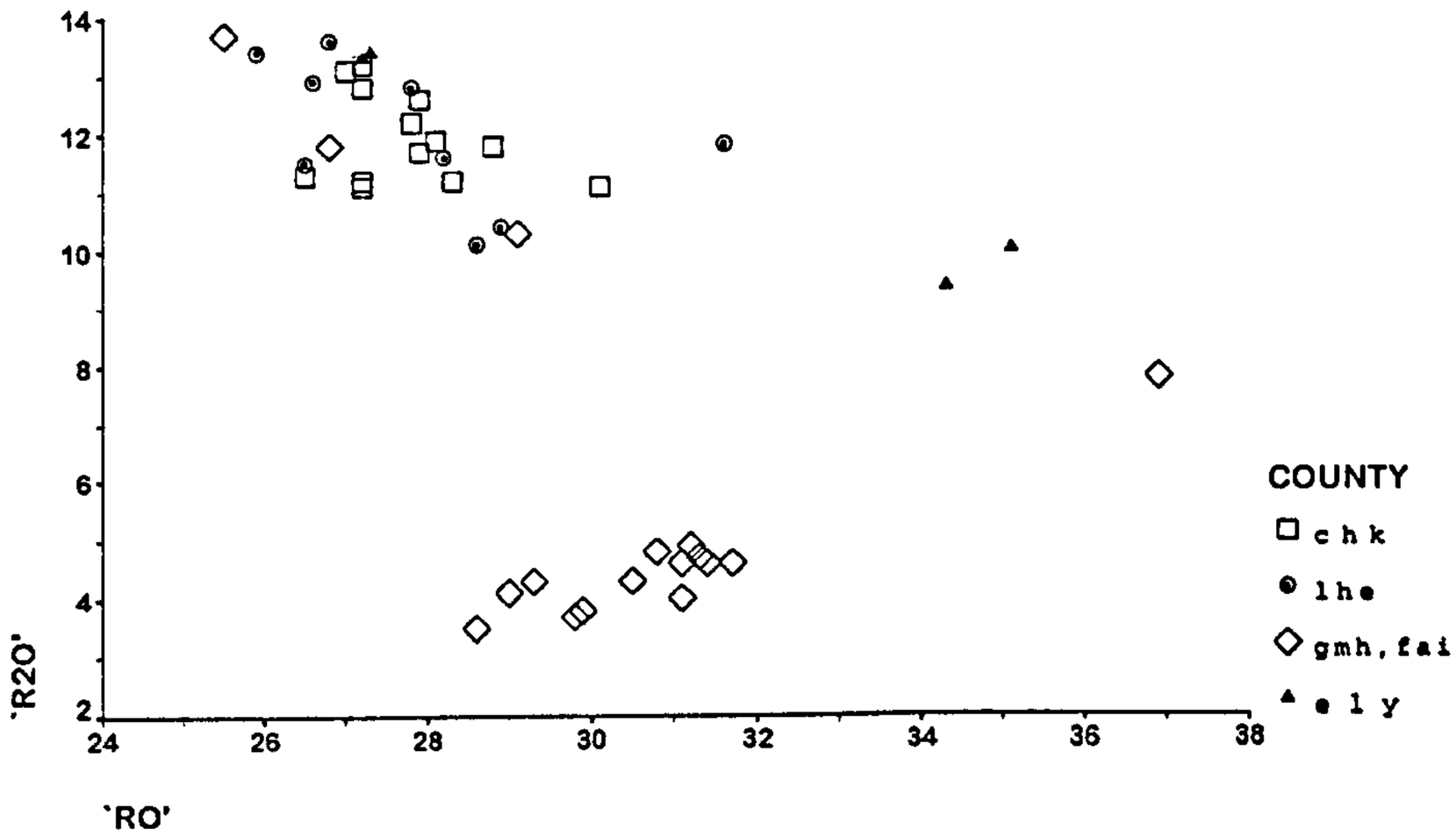

Figure 7.30: Ternary diagram for totally pitted samples.

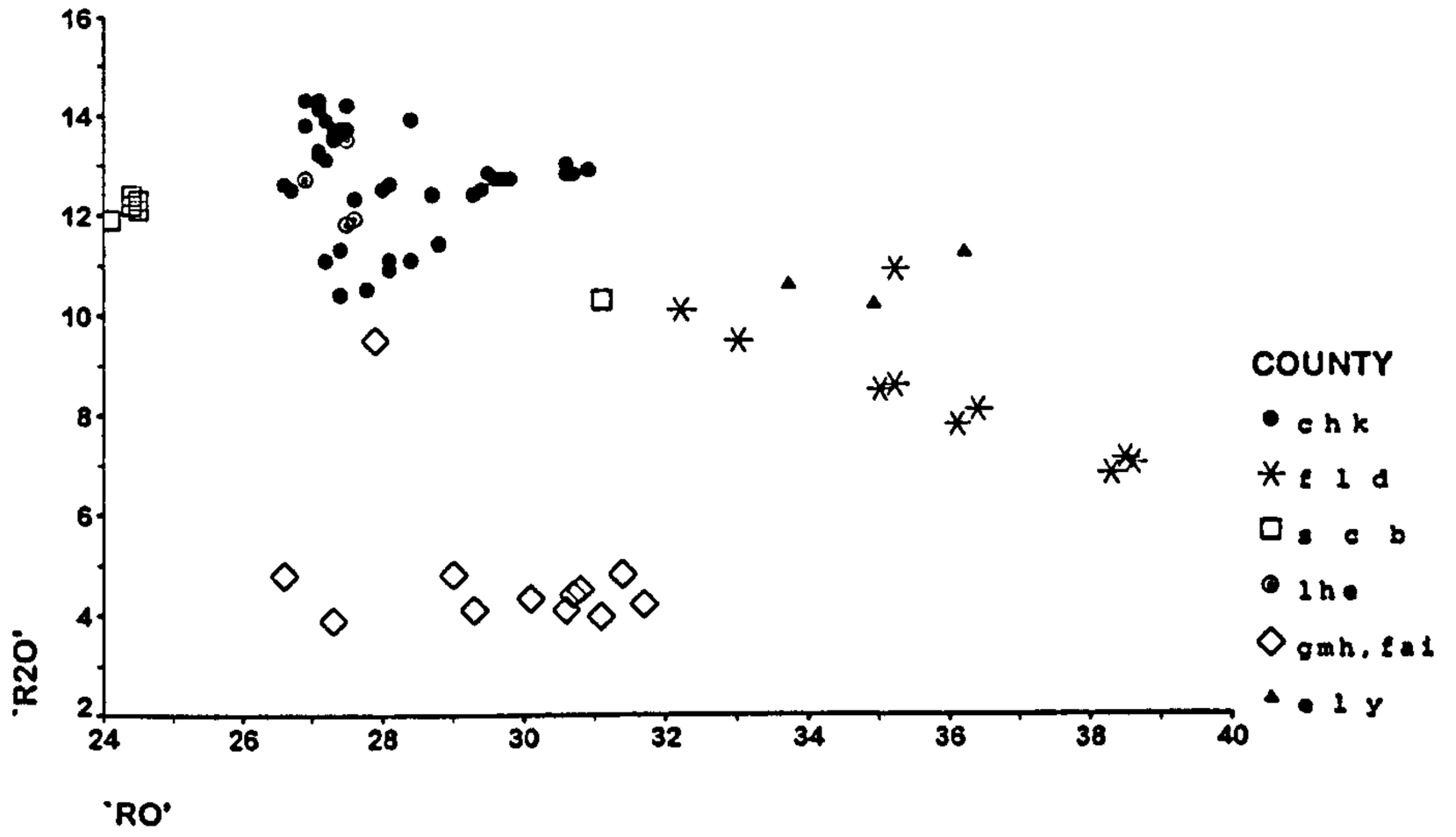

Figure 7.31: Ternary diagram for uniformly weathered samples.

	Corrosion Type	Γ_{HM}			Low Magnesia, Γ_{LM}		
		'R_2O'mol%	'RO'mol%	'SiO_2'mol%	'R_2O'mol%	'RO'mol%	'SiO_2'mol%
Fourteenth Century	Durable	11.60	26.80	60.50	–	–	–
	Isolated Pits	11.15 ± 0.96	27.19 ± 1.62	60.67 ± 1.36	9.42	24.40	65.20
	Merged Pits	11.39 ± 0.90	27.82 ± 1.96	59.71 ± 1.90	10.38 ± 0.95	32.50 ± 6.42	56.20 ± 6.39
	Totally Pitted	12.02 ± 1.04	27.82 ± 1.23	59.12 ± 1.16	9.68 ± 0.45	34.70 ± 0.57	54.85 ± 1.06
	Uniformly Weathered	12.68 ± 1.07	27.73 ± 1.63	58.54 ± 1.84	8.95 ± 1.55	35.64 ± 2.02	55.24 ± 1.61
Sixteenth Century	Durable	11.80	28.40	58.80	5.57 ± 1.71	27.94 ± 2.09	65.53 ± 1.33
	Isolated Pits	10.30 ± 0.67	25.40 ± 1.24	63.28 ± 0.73	5.44 ± 2.35	27.93 ± 1.91	65.46 ± 2.94
	Merged Pits	11.45 ±1.48	26.35 ± 2.05	60.80 ± 3.68	6.31 ± 2.74	29.28 ± 1.68	63.41 ± 2.34
	Totally Pitted	–	–	–	5.85 ± 3.11	30.24 ± 2.41	62.94 ± 2.82
	Uniformly Weathered	9.50	27.90	61.40	4.35 ± 0.34	29.87 ± 1.66	64.60 ± 1.64

Table 7.3: Mean and standard deviations of the ternary co-ordinates calculated after separating the data into date and classification as Γ_{HM} and Low Magnesia (Γ_{LM}), for the different modes of decay. Those with no standard deviation, represent only one sample; — means no sample of this type was analysed.

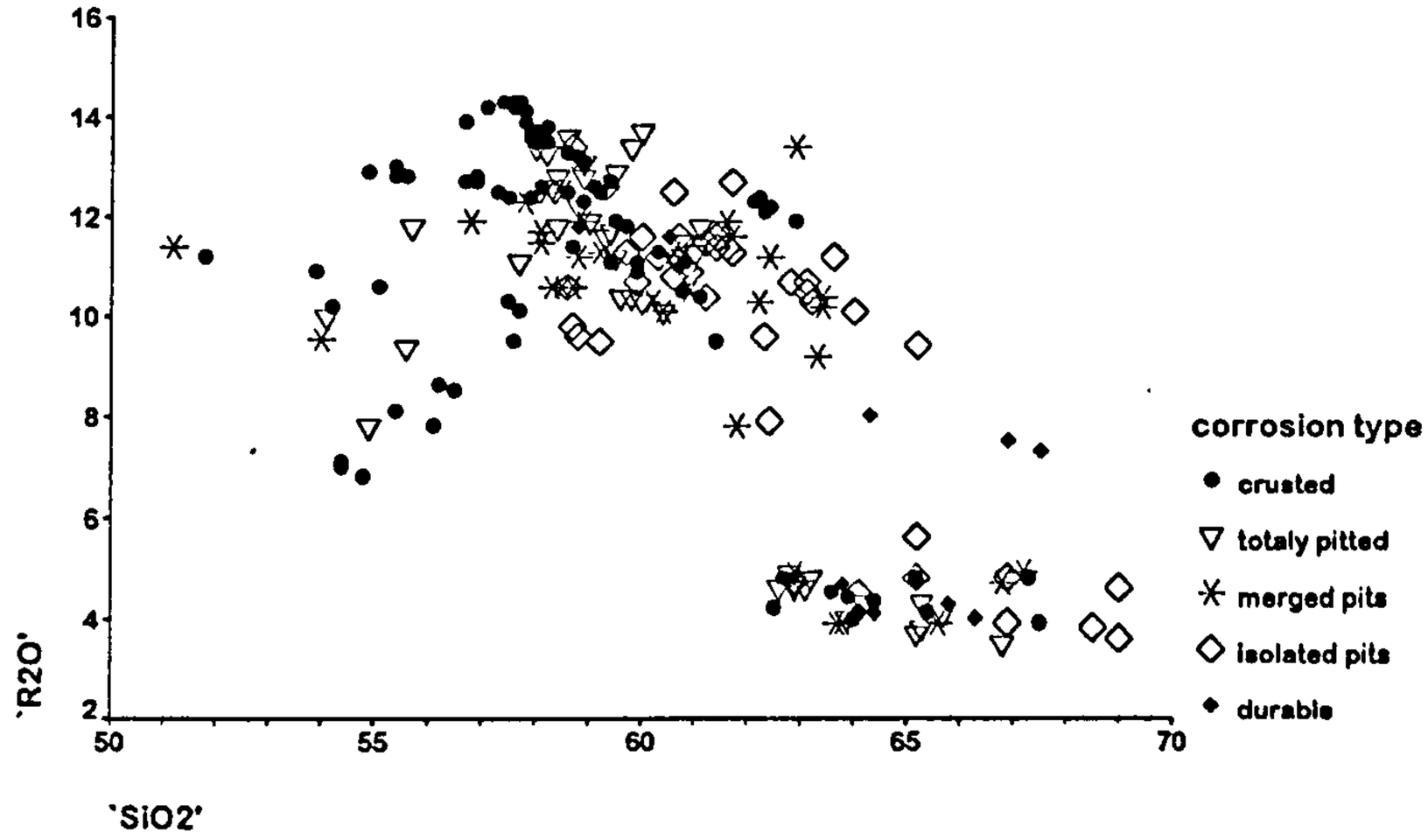

Figure 7.32: Ternary diagram of 'R_2O' and 'SiO_2' for all the glass samples, indicating the mode of corrosion.

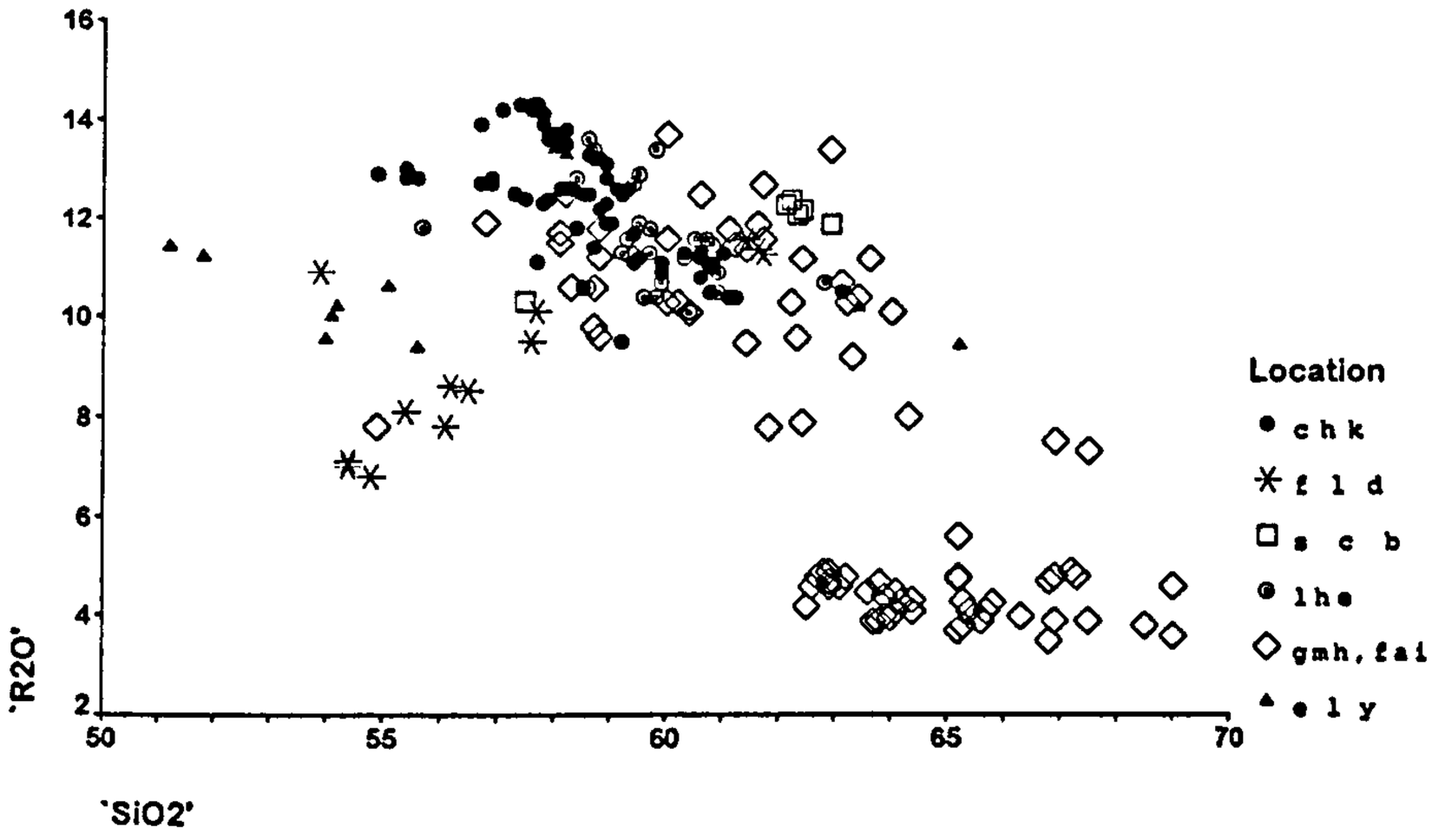

Figure 7.33: Ternary diagram of 'R_2O' and 'SiO_2' for all the glass samples, indicating the location of the church.

Date	Class	Mean ratio 'R_2O'/'RO' by corrosion type				
		Durable	Isolated Pits	Merged Pits	Totally Pitted	Uniformly Weathered
14th Century	Γ_{LM}	0.43	0.41 ± 0.05	0.41 ± 0.06	0.43 ± 0.05	0.46 ± 0.05
	Γ_{HM}	—	0.39	0.33 ± 0.07	0.28 ± 0.01	0.25 ± 0.05
16th Century	Γ_{LM}	0.42	0.41 ± 0.04	0.43 ± 0.02	—	0.34
	Γ_{HM}	0.20 ± 0.08	0.19 ± 0.08	0.22 ± 0.10	0.20 ± 0.12	0.15 ± 0.02

Table 7.4: Mean ratio values of 'R_2O'/'RO' by corrosion type, classification (Γ_{LM}/Γ_{HM}) and date.

extensive. Figures 7.35 and 7.34 show the correlation between this ratio and 'SiO_2' and mode of decay for the Γ_{HM} glass and the Γ_{LM} type respectively. Table 7.4 gives the average ratios for the dates and classifications. Here it can be seen that the trend for increasing 'R_2O'/'RO" for increased corrosion is only true for the fourteenth century glass, excluding those with low magnesia. From Figure 7.32 and 7.33 it appears that for a given 'SiO_2' content the trend is true for all fourteenth century glass, with the proviso that the lower the 'SiO_2', the lower the ratio value for the corrosion modes. That is to say the ratio value alone does not indicate the extent of decay. This is expected because the 'R_2O' parameter does not take into account the differences between Na_2O and K_2O. The low magnesia glasses have a much lower ratio value and the opposite trend occurs if the Fairford glass is excluded. This is expected from the variation in 'R_2O' and 'RO' for the two classifications. The trend implied by the Fairford glass is one which is dependent on 'SiO_2' content and independent of the ratio 'R_2O'/'RO': the 'SiO_2' content is sufficiently high that the other components make little difference.

7.1.4 Statistical Analysis

The purpose of statistical techniques of a multivariate nature is to reduce a data matrix, of n rows by p columns, to a state where a two or three dimensional summary is possible[11]. There are, however, a considerable number of techniques, each with an equally large number of methods. There is no 'best' method; each is based on different assumptions that have merits and flaws. The assumptions must be born in mind, or the conclusions obtained could be an artefact of the analysis.

The most popular multivariate techniques for dealing with chemical compositional data are Discriminant analysis (DA), Principal component analysis (PCA) and Cluster analysis (CA). Discriminant analysis is not applicable where there is no prior knowledge of grouping of the specimens and thus has not been implemented in this study. Principal component analysis complements cluster analysis as a means of displaying and interpreting the clusters identified. Cluster analysis can be problematic if the elements are highly correlated, such as in glass[11]. For this reason it is usually

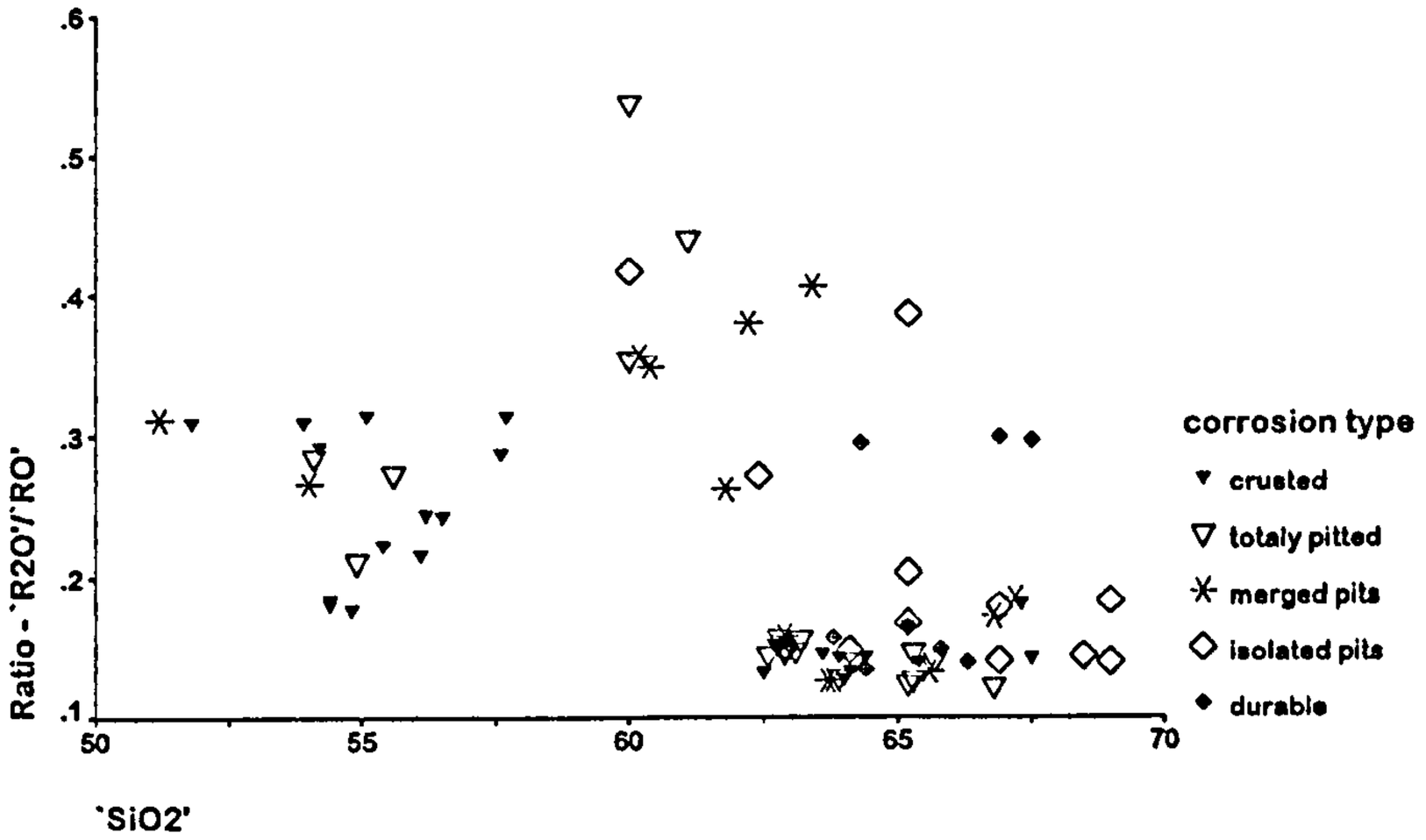

Figure 7.34: Ternary diagram of the ratio 'R_2O'/'RO' and 'SiO_2' for Γ_{LM} glasses, indicating the mode of corrosion.

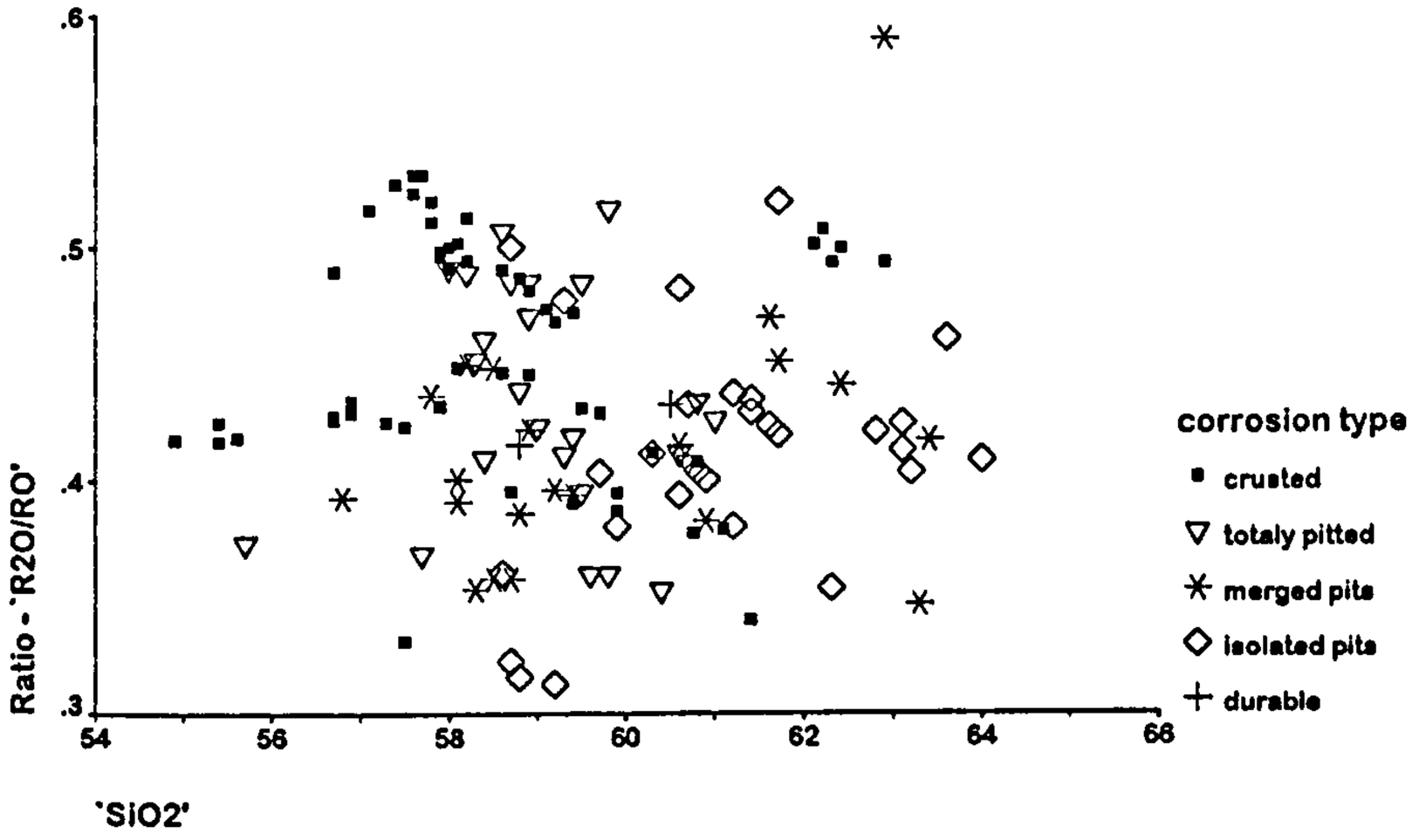

Figure 7.35: Ternary diagram of the ratio 'R_2O'/'RO' and 'SiO_2' for Γ_{HM} glasses, indicating the mode of corrosion.

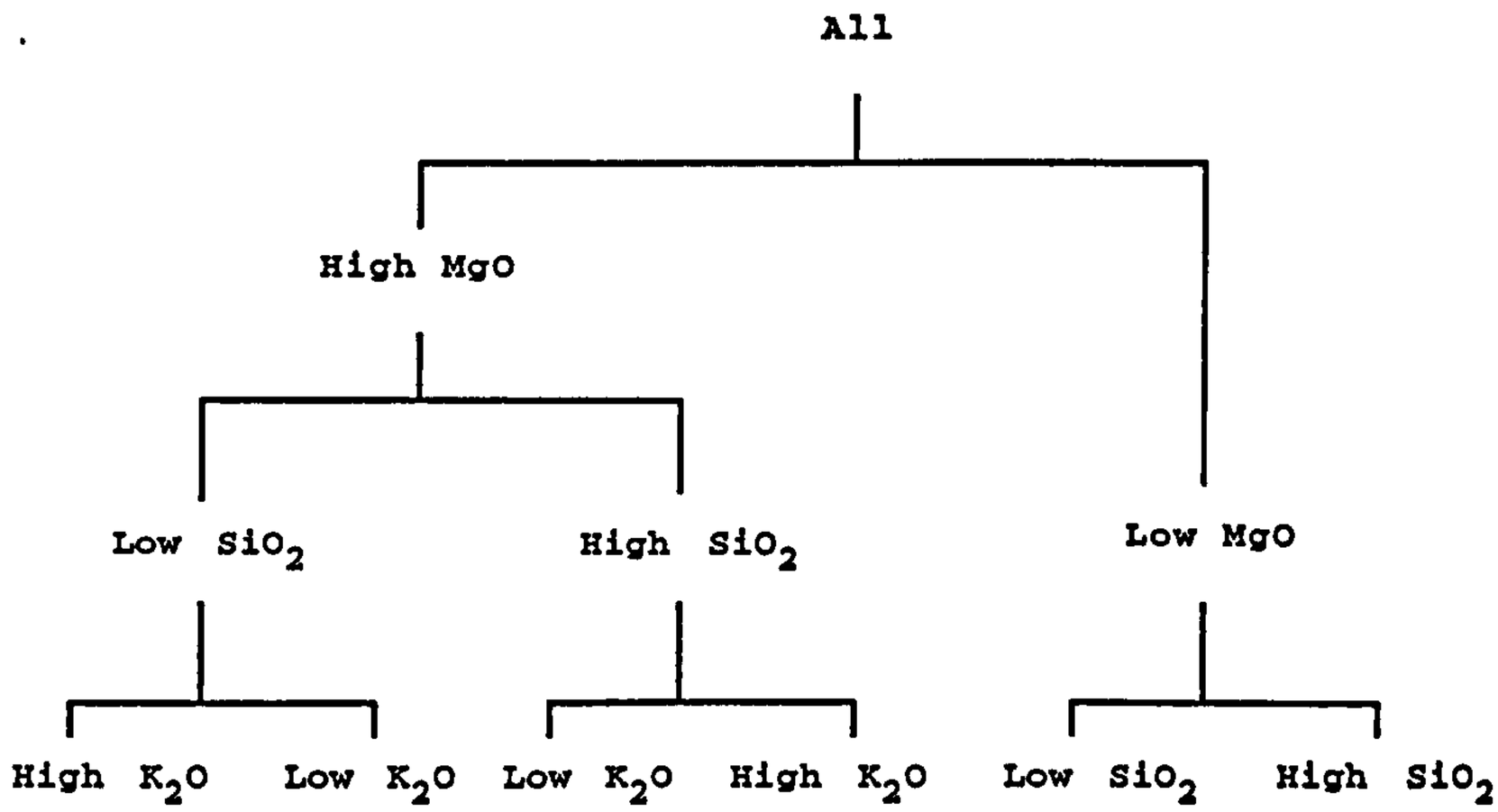

Figure 7.36: Simplified dendrogram obtained from the analysis of the all the data.

recommended that standardisation be performed on the data first.

Statistical methods such as those outlined are increasingly easier to implement through software packages such as CLUSTAN, SAS and SPSS[11]. The latter package, SPSS, was used to carry out this investigation. The method of cluster analysis implemented was Wards method using squared Euclidean distance linkage, without standardising. These options were selected because this method reduced the information lost on each pair clustering. Standardisation was not required, or useful, because it would weight the data in favour of the minor elements and for the purpose of durability studies these play a minor part. The most visual means of representing the output of cluster analysis is by plotting a dendrogram.

Figure 7.36 shows a simplified dendrogram produced from all the analytical data (excepting the highly variable sulphur, chlorine and the oxides of copper and lead). These simplifications were identified by looking for the approximate explanation for each grouping; the actual dendrogram was too long and narrow to incorporate and still be informative. As can be seen, the data were separated first by magnesia, then silica and finally by potash content to form six groups. Considering the high and low magnesia glasses (Γ_{HM} and Γ_{LM}) separately indicates the next level of splitting. Figure 7.37 shows the dendrogram for the Γ_{LM} glasses. Here the splitting according to potash levels was succeeded by a further grouping due to soda content. The cluster analysis can be seen to provide the same information as obtained from the compositional and data reduction techniques . The addition of qualitative parameters, such as colour, decay type and age, did not produce any further information.

Principal component analysis reduces the data to 'factors' and suggests the number of 'factors' that are significant. The default action of the software package is for eigenvalues, *ie.*, the total

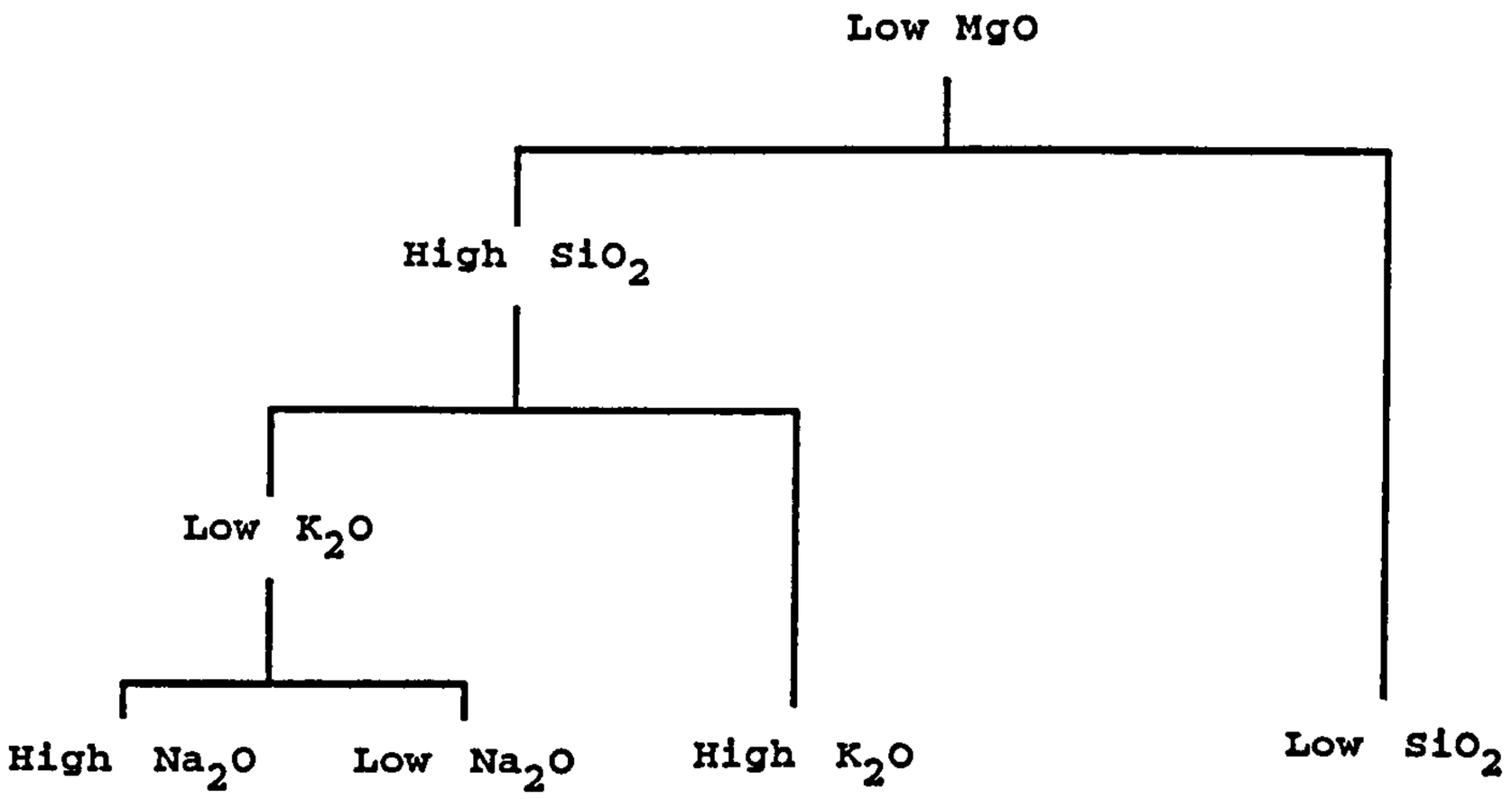

Figure 7.37: Simplified dendrogram obtained from the cluster analysis of the Γ_{LM} glasses.

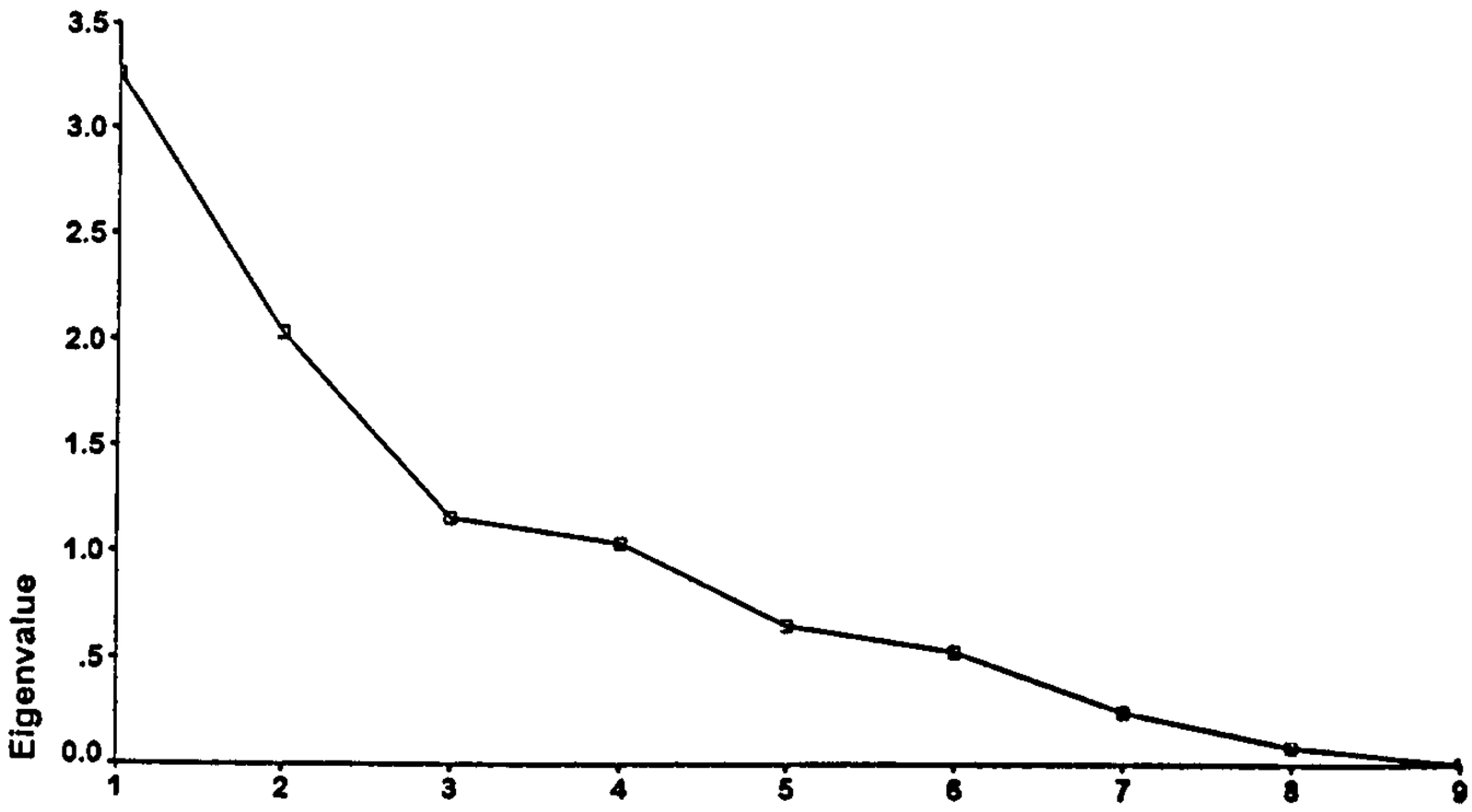

Figure 7.38: Scree plot from the factor analysis of the all the glasses.

variance explained by each factor, when greater than one to be representative of significant factors; a 'scree plot' may be drawn to investigate the validity of this assumption. Figure 7.38 shows the scree plot obtained for the PCA of all the data, as used for cluster analysis. This plot shows that three factors are significant, *ie.*, the abrupt change in gradient indicates the transition from distinct factors to ones which are redundant. The default option, in this case, would have taken four factors as significant not three as indicated by the scree plot. The factors obtained were composed of 'weighted parts' of the actual components. The coefficient matrix was interpreted to give F1(CaO, MgO, P_2O_5, SiO_2, K_2O), F2(SiO_2, Na_2O), F3(Al_2O_3) and F4(MnO) for the default case and F1(CaO, MgO, P_2O_5, SiO_2, K_2O), F2(SiO_2, Na_2O, MnO) and F3(Al_2O_3, Fe_2O_3) when set to three factors. The groupings were indicated by the weighting being greater than fifty percent, and one component can be significantly present in more than one factor. Broadly speaking, these results are expressible as F1(major components), F2(minor components) and F3(trivalent compounds).

The data were then separated into the two groups Γ_{LM} and Γ_{HM}: the resulting factor solutions changed. The Γ_{HM} group was represented by three factors F1(Na_2O, K_2O, MgO, CaO, Fe_2O_3), F2(SiO_2, P_2O_5, MnO) and F3(Al_2O_3). This compares favourably with the ternary co-ordinate reduction. On excluding the later date Fairford glass, the F1 and F3 groups merge, implying that the isolation of the alumina as a separate factor was artificial. The Γ_{LM} group was represented by three factors: F1(SiO_2, Na_2O, P_2O_5, K_2O, MgO, CaO), F2(Fe_2O_3, MnO, K_2O) and F3(Al_2O_3, Fe_2O_3). On excluding the Fairford glass, the number of factors increase to four, where the alumina is isolated, the manganese oxide and phosphorus oxide group together and the final two groups represent the major and minor components.

Thus it can be seen that PCA did not provide any more information than the established methods of reducing data for durability studies.

7.1.5 Summary

The implementation of standard statistical routines did not provide any information that was not obtainable by more readily interpretable methods. The reduction of data to three variables, 'R_2O', 'RO" and 'SiO_2', proved to be adequate for the compositional representation and investigation of how this related to the decay of the specimens. As valid but not as informative was the calculation of the one parameter, free energy of hydration (ΔG).

The composition of the glasses split them into two groups, Γ_{LM} and Γ_{HM}. These were again divisible according to age and soda content. For the Γ_{HM} group, there was a link between the composition and the decay, *ie.*, 'R_2O'/'RO' for a specific 'SiO_2' increases with increased decay. The Γ_{LM} glass was dominated by the high silica content and therefore the minor constituents played little or no part in the determination of decay mode. The ΔG value was also highly correlated

with the decay type; lower ΔG, more durable. There was, however, information lost on the data reduction which served to explain the occasional anomalous samples. That is, both techniques have no means of incorporating the mixed-alkali effect. No correlation was found between the decay and the colour of the glass.

7.2 Correlation between Composition and Decay Product

The decay of mediaeval stained glass windows is not restricted to the external surface, although this is usually the more decayed. Therefore, it is useful to consider both sides, but separately.

Windows were usually installed such that any painted decoration was on the inside. In the case of glass decorated with a yellow stain, the stain was applied to the back and thus was exposed to the elements. In this study the paintwork was taken to indicate the inner surface; where the paintwork was absent or present on both sides, the most corroded side was labelled as the outer.

Figures 7.39 to 7.42 show the frequency of the weathering products identified. These are for the outer and inner surfaces, with the additional separation of major and minor constituents. The 'no product' category contains samples which had no products and those that had unidentifiable products (perhaps being present in insufficient amounts to enable quantification). It can be seen that approximately 35% of the outer surfaces and 49% of the inner ones, fall into this group.

Quartz (crystalline silica) appears as an identified product, though this is, almost certainly, not a decay product and therefore indicates debris of an external origin. Compared with the results of other workers there was little evidence of syngenite: 4% of major outer products were syngenite, *cf* Gillies and Cox where the frequency was 20%[58]. Only 18% of the samples in this study had syngenite present at all. The relative lack of syngenite could be due to its instability in damp conditions, *ie.* it converts to gypsum. Gypsum was the most frequently found decay product, although hydrated silica was a close second. There were no unusual or unexpected compounds.

Along with this, it must be born in mind that some components could have been removed from the surface, say, by the action of rainwater. Table 7.5 gives the relative solubilities, of the identified compounds. It can be seen that gypsum and syngenite have comparable solubilities whereas calcite and silica are much less soluble. This would imply that any silica or calcite that formed would be least likely to be washed away and therefore more likely to be found *in-situ*.

In order to compare the products formed with the glass compositions, the samples were again separated into Γ_{LM} and Γ_{HM} groups *ie.*, low and high magnesia. As only a small number of samples had any syngenite present, this could not be correlated with, say, high lime and high potash contents. Within each grouping there were numerous examples of the 'no product' classification.

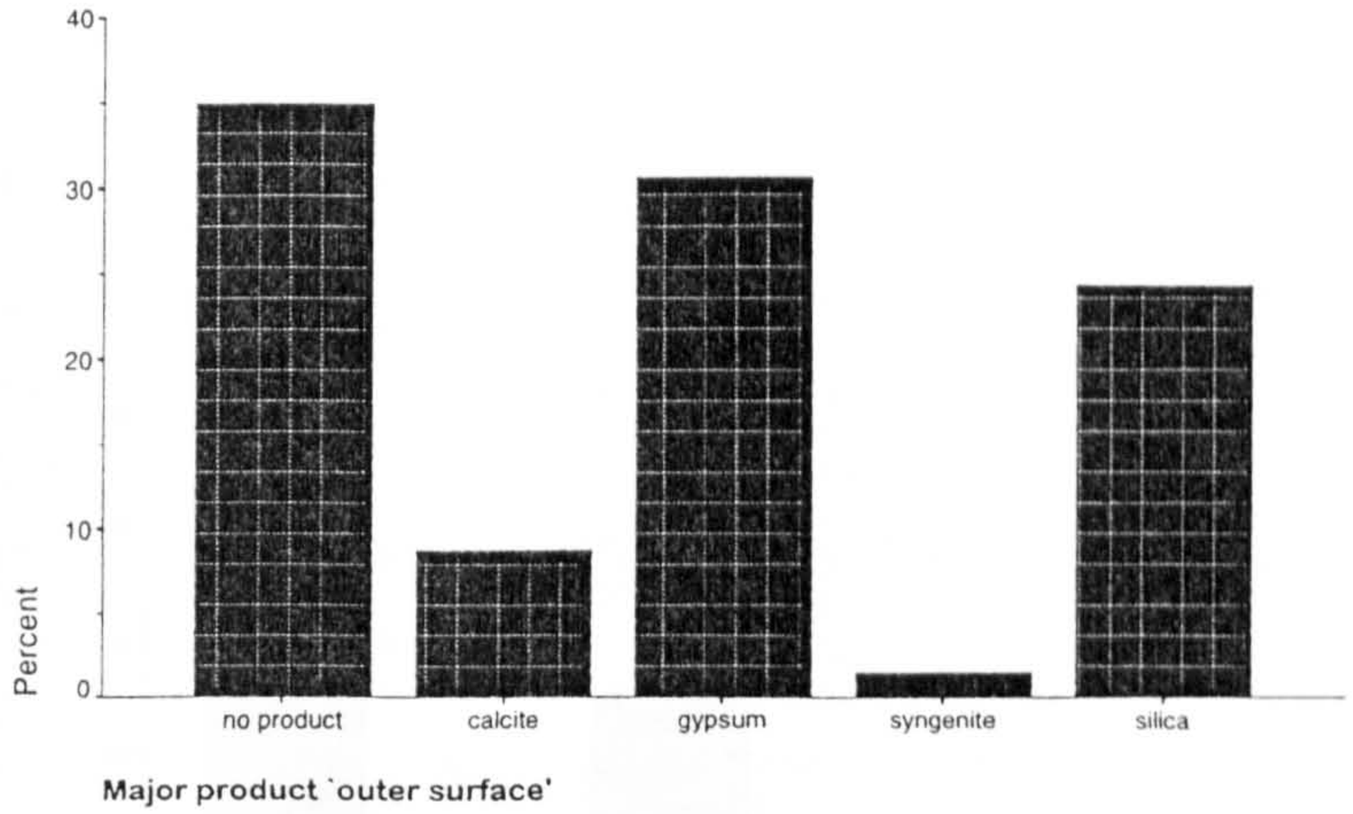

Figure 7.39: Histogram of the percentage presence of major decay products on the outer surface.

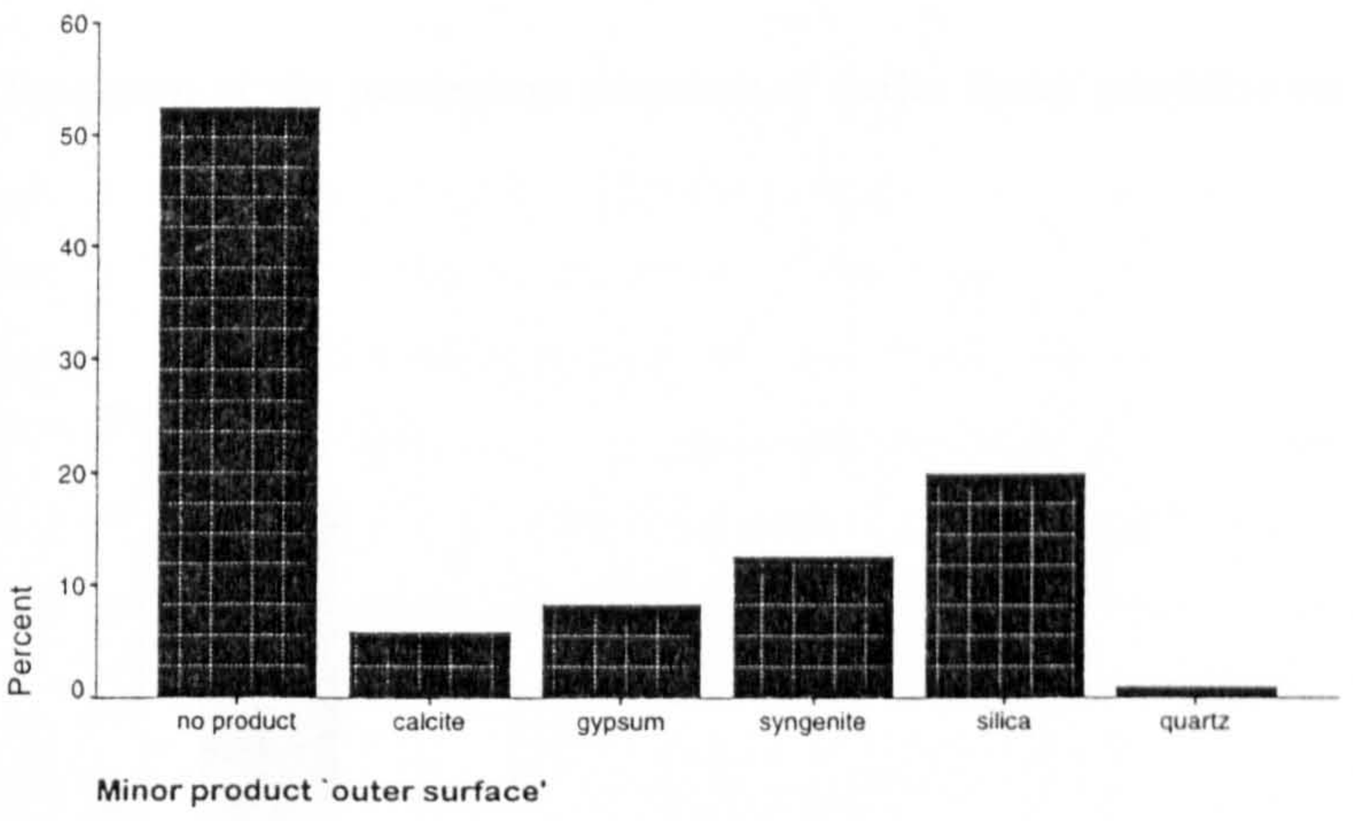

Figure 7.40: Histogram of the percentage presence of minor decay products on the outer surface.

Product	solubility in water (in g/100cm^3) at 300K
Bassanite	0.3
Calcite	0.0014
Gypsum	0.241
Hydrated Silica	sparingly soluble
Syngenite	0.25

Table 7.5: Solubilities of the minerals identified as decay products.

Glass Corrosion

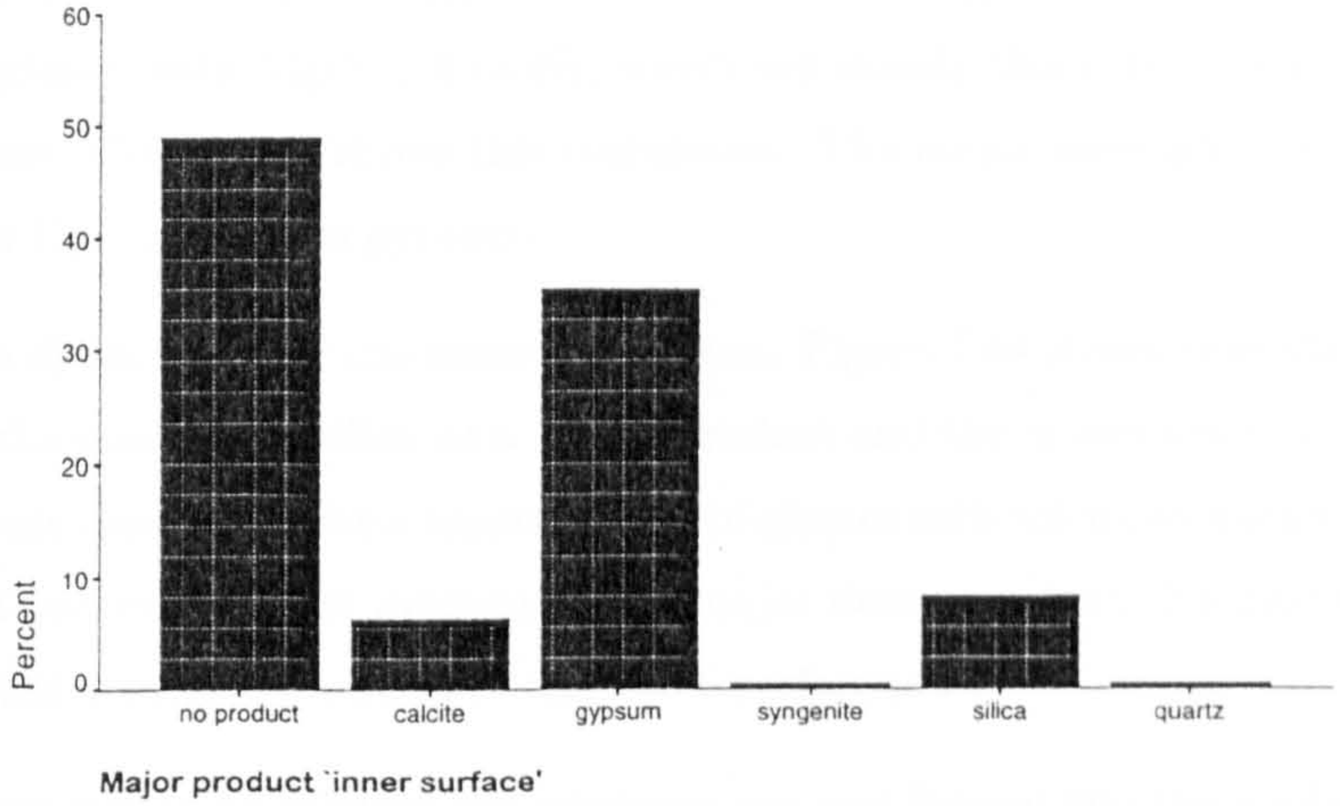

Figure 7.41: Histogram of the percentage presence of major decay products on the inner surface.

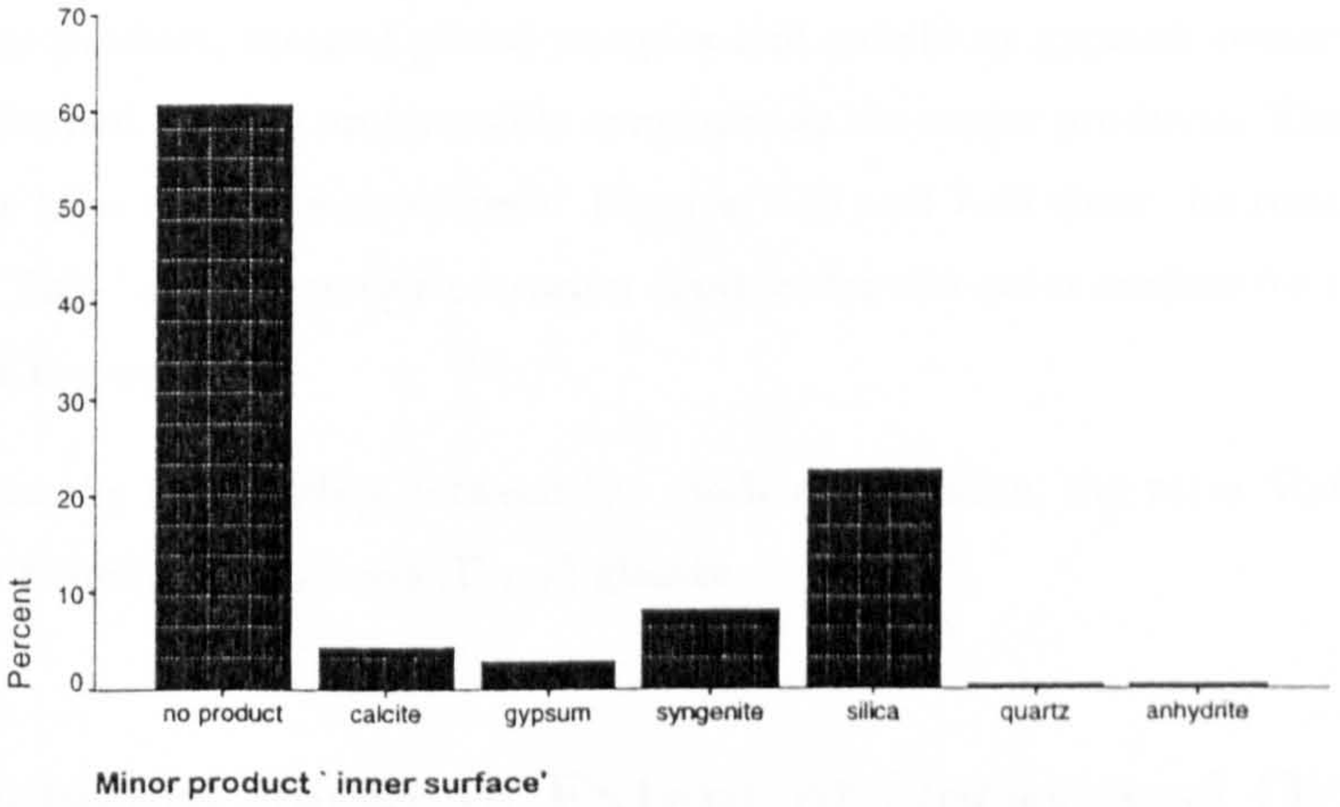

Figure 7.42: Histogram of the percentage presence of minor decay products on the inner surface.

These did not appear to correlate with any compositional parameter, the exception being the durable specimens from Fairford whose 'no product' label was due to a very high silica content. The 'no product' glasses have been eliminated from the diagrams as they hindered interpretation.

The Γ_{LM} group showed a correlation between silica as the major 'outer' product and high SiO_2 and/or low CaO content. This was also related to a lower magnesia content, within this classification, *ie.*, the glasses with MgO < 6 mol%, which are mainly those from Fairford, had silica as the major product. Figure 7.43 shows this correlation. The major inner product for all but a few specimens in the Γ_{LM} group was gypsum.

The Γ_{HM} group did not exhibit the same correlation. Figure 7.44 shows that there was no correlation between the presence of silica as a major product and the amount of CaO or SiO_2. Below 16mol% lime, there appeared to be a concentration of glasses with calcite as a major product; above this there was a concentration of gypsum as the major decay product. No pattern was observed with the minor outer surface products or the inner surface products.

There was no apparent trend relating the corrosion product formed and the mode of decay for the Γ_{LM} glasses. The Γ_{HM} group of samples, however, did exhibit a correlation. This was linked to the correlation, mentioned earlier (see section 7.1.1), between the mode of corrosion and the ratio of the ternary co-ordinates 'R_2O' and 'RO'. That is, the more corroded the sample, the higher the ratio value (for a specific 'SiO_2') and also the more likely the decay product was to be a complex salt. In more detail, this means that isolated pitting was associated with the presence of hydrated silica as a major decay product, merged pitted samples had calcite or gypsum present and uniformly weathered samples had gypsum and possibly syngenite as the major products. This correlation was only true for the high magnesia specimens. Figures 7.45 and 7.46 show the relationship between the ratio value, 'SiO_2' and the major corrosion product for the outer surface for the low and high magnesia glasses respectively.

Figure 7.47 shows the relationship between the mode of corrosion, the ratio 'R_2O'/'RO' and the decay product for the high magnesia (Γ_{HM}) glasses.

7.3 Correlation between Extent of Decay and Orientation

The number of samples obtained from the two churches, Fairford (FAI) and Checkley (CHK), were large enough to enable a good comparison of deterioration between locations to be carried out. The compositions of the glasses at the two sites were dissimilar and, therefore, the exact effect of location could not be ascertained, but the effect due to window orientation was considered. Both churches provided glass from north- and south-facing windows. Thus the difference in deterioration between north- and south-facing specimens could be looked at, for glass of equal composition, with

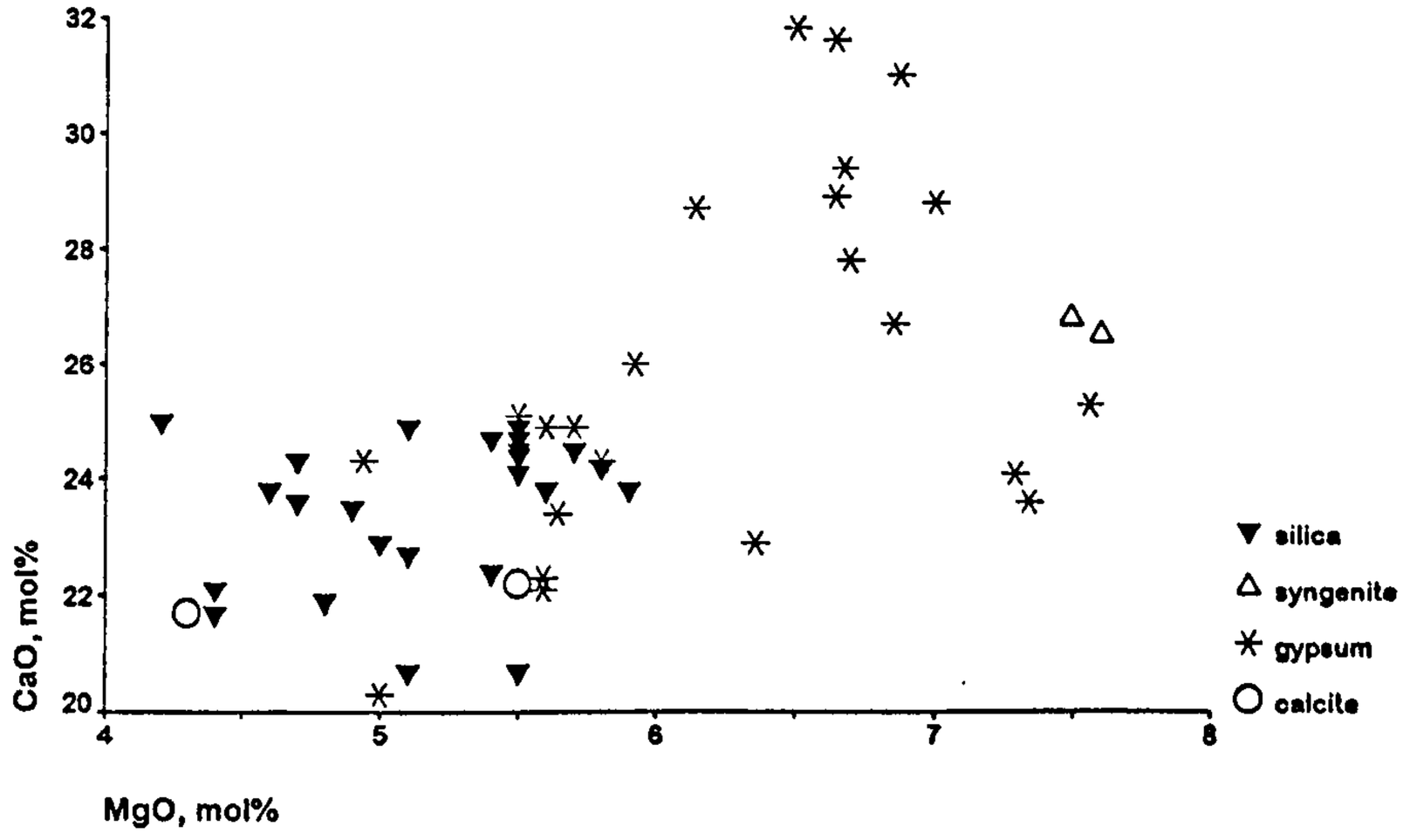

Figure 7.43: Graphical illustration of the correlation between the product formed on the outer surface and the amount of lime and magnesia in the glass for the low magnesia glasses.

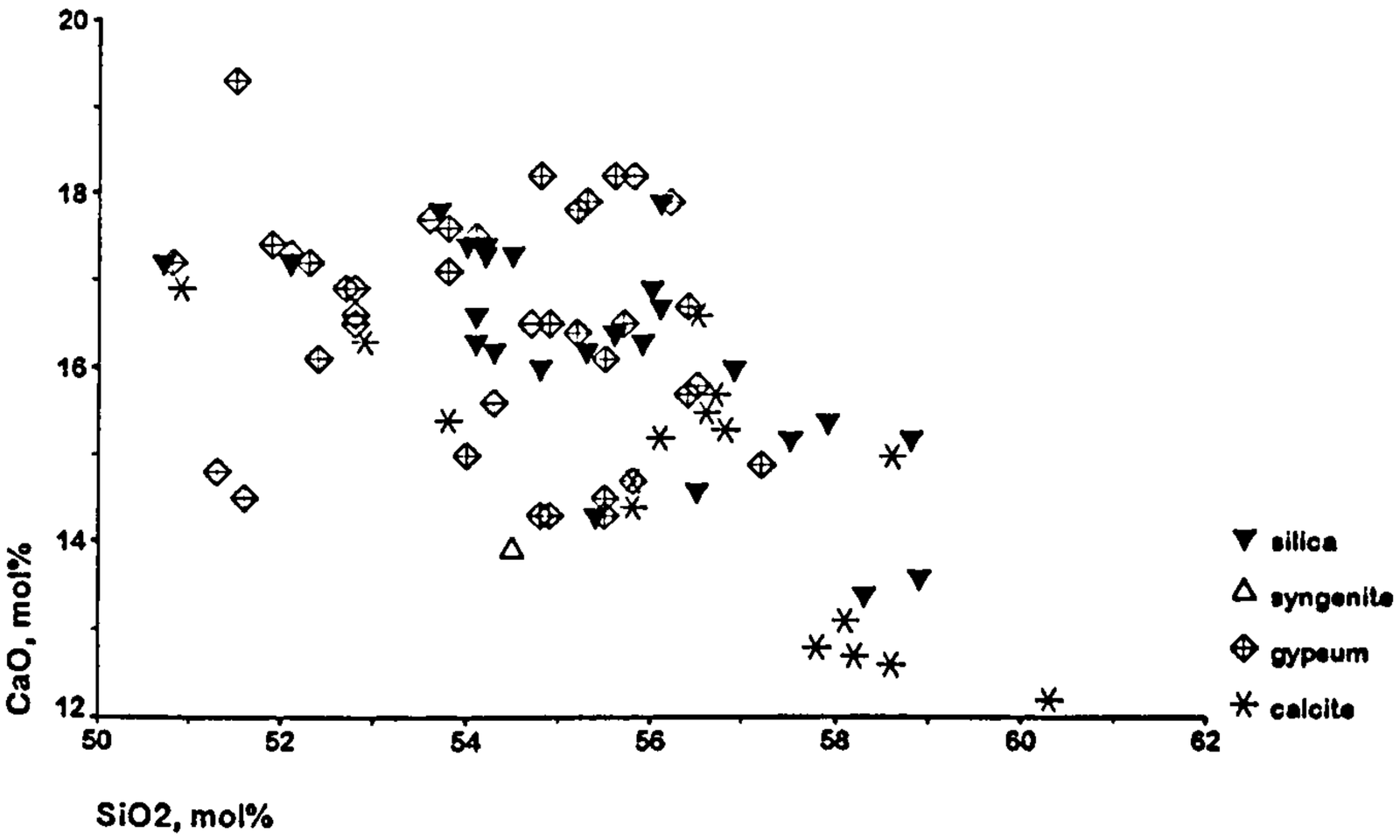

Figure 7.44: Graphical illustration of the correlation between the product formed on the outer surface and the lime and silica in the glass for the high magnesia glasses.

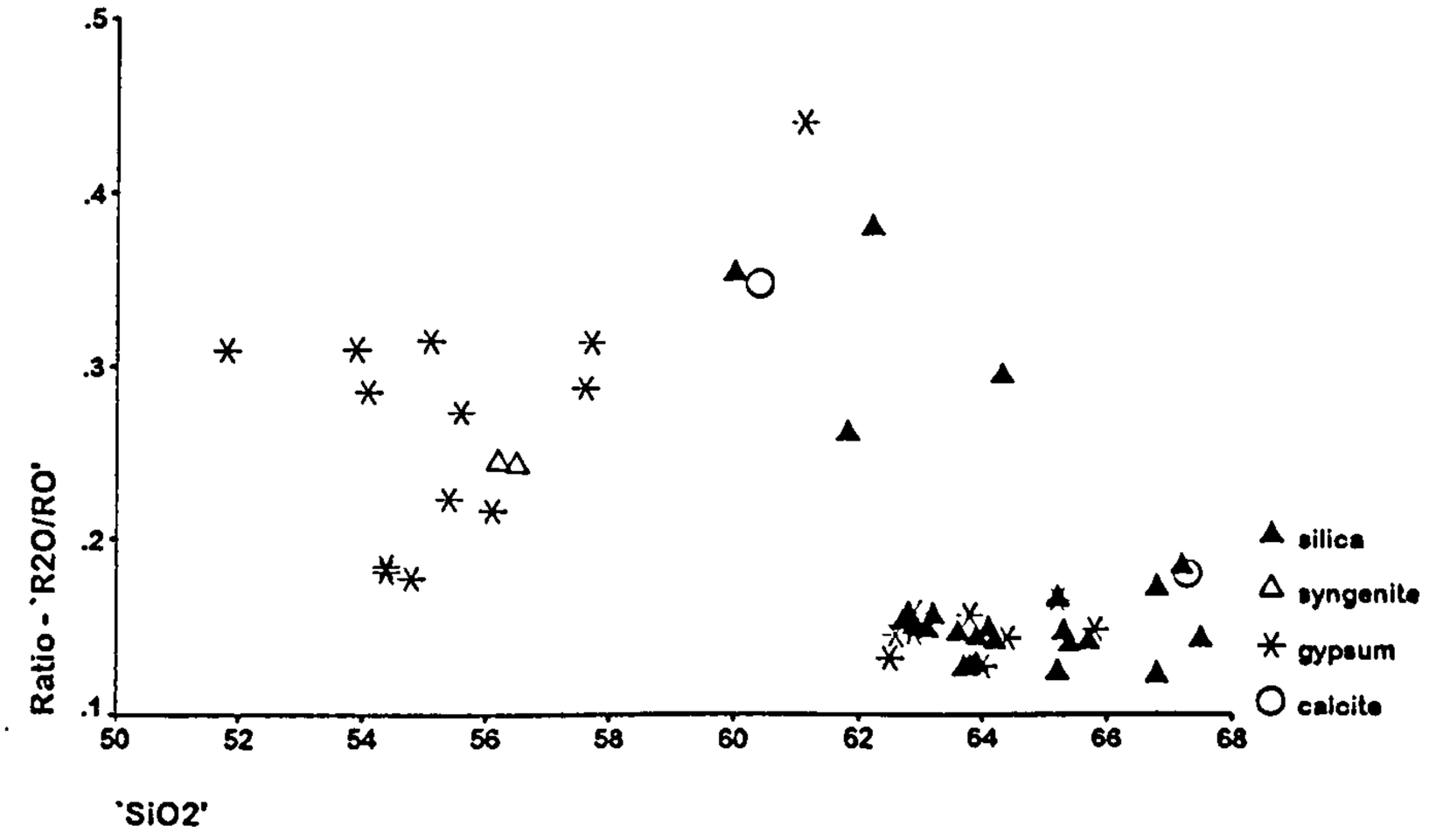

Figure 7.45: Graphical representation of the relationship between the ratio 'R_2O'/'RO', 'SiO_2' and the major corrosion product for the low magnesia glass.

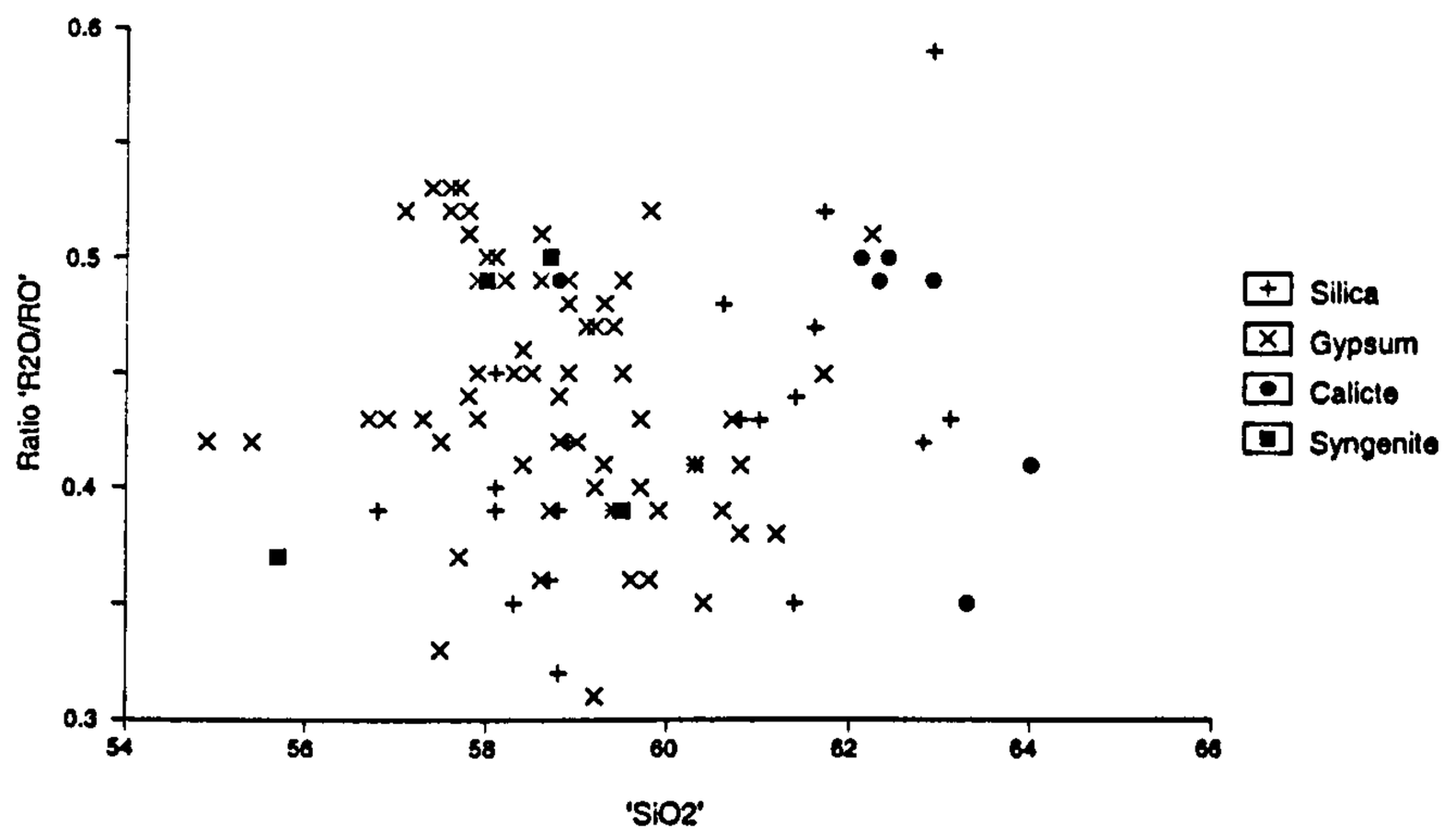

Figure 7.46: Graphical representation of the relationship between the ratio 'R_2O'/'RO', 'SiO_2' and the major corrosion product for the high magnesia glass.

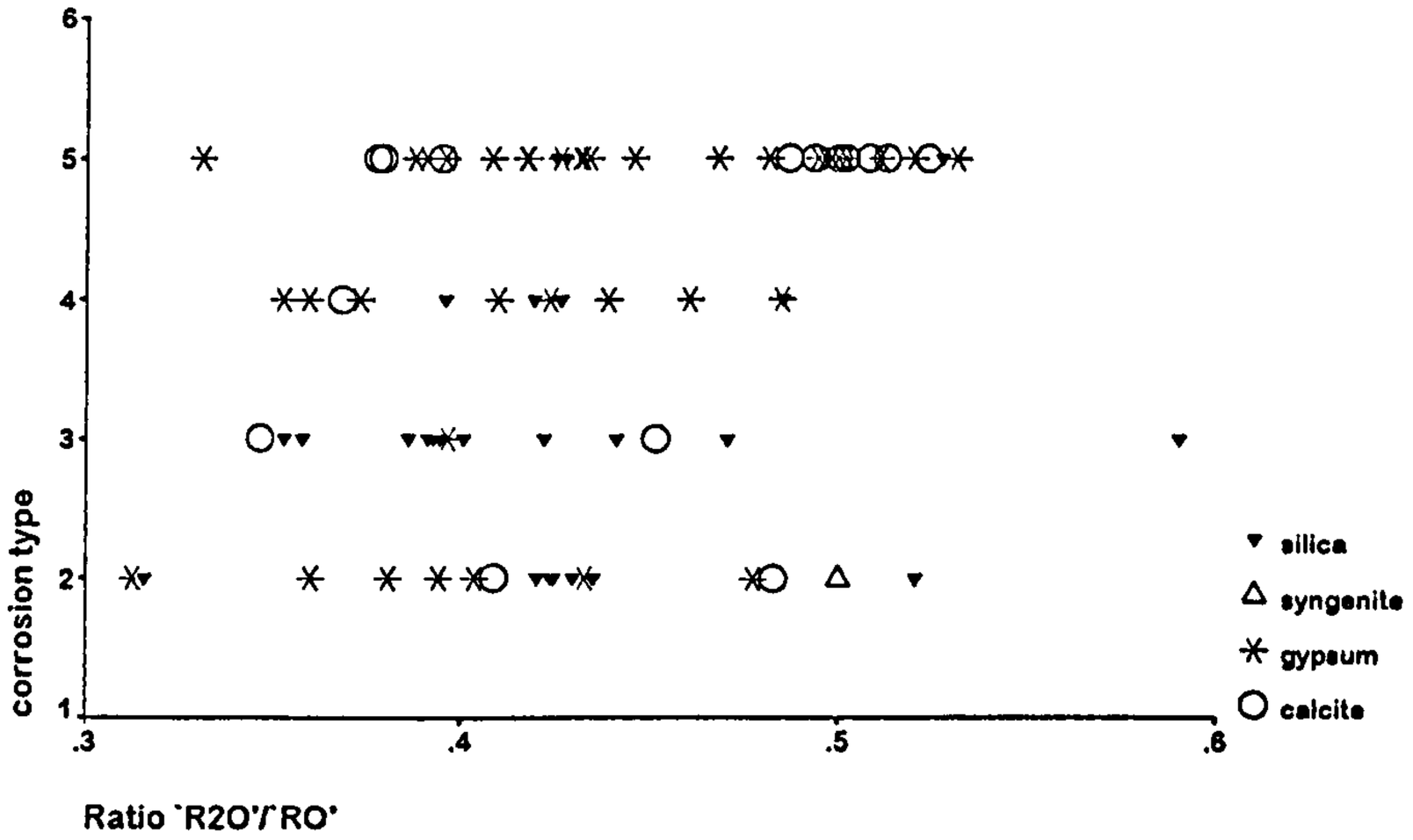

Figure 7.47: Graphical representation of the relationship between the corrosion type, the corrosion product and the ratio value for the Γ_{HM} specimens.

the effect of local environment partially removed (given there were two sites involved).

The number of samples selected from each aspect within each site was slightly different. The Fairford glass was made available at different stages of the research and the north-facing glass appeared to be more durable. There were 22 samples selected from the north panels and 44 from the south ones. The Checkley glass was a more even split of 34 from the north and 32 from the south panels. It is strongly believed by mediaeval historians and the restorer, that the glass from Fairford h as never been moved or interfered with; the Checkley glass is also believed to be 'as installed', but there is no firm evidence to indicate this.

Figure 7.48 shows the marked difference in composition between the Checkley and Fairford glass.

This divide is at $\Delta G \approx$-8kcal/mol. The corrosion type, illustrated on the y-axis, is represented by numbers as follows: 1=durable, 2=isolated pits, 3=merged pits, 4=totally pitted and 5=uniformly weathered. The x-axis shows the free energy of hydration which crudely reflects the composition. It can also be seen that the more negative the ΔG, then the less durable the glass. The CHK glass has the same distribution of corrosion types, but a much lower ΔG then FAI.

Figure 7.49 contains the same data as Figure 7.48, but with the markers now representing the window orientation. The Fairford glass is clearly more corroded on the south-facing side; the Checkley glass appears to follow the same trend, but here the glass is less durable and, therefore, more corroded.

Thus, the data available indicates that south-facing glass is more deteriorated than north-facing

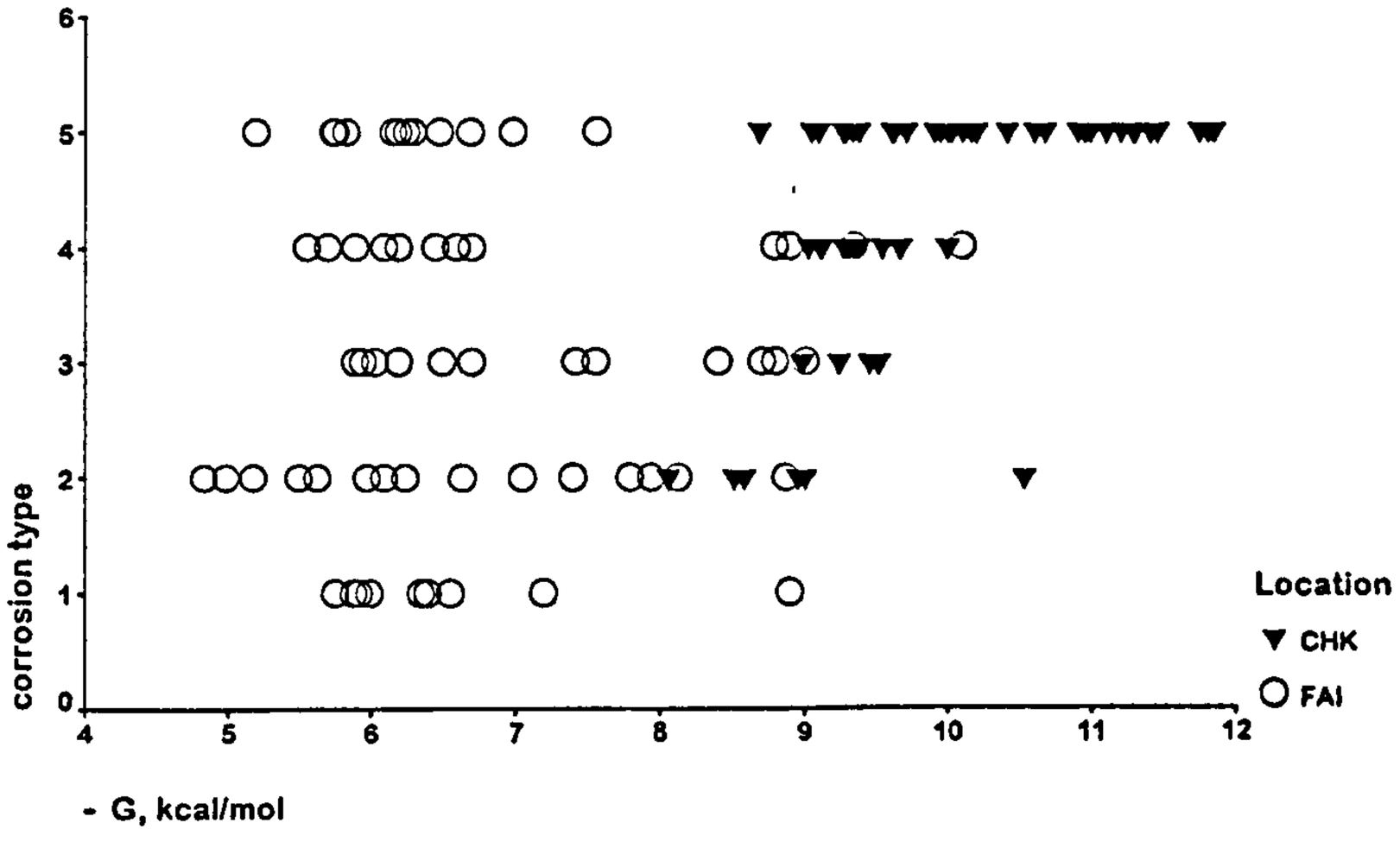

Figure 7.48: Free energy of hydration versus corrosion type for the glasses form Fairford and Checkley. The corrosion type is represented as 1=durable, 2=isolated pits, 3=merged pits, 4=totally pitted and 5=uniformly weathered.

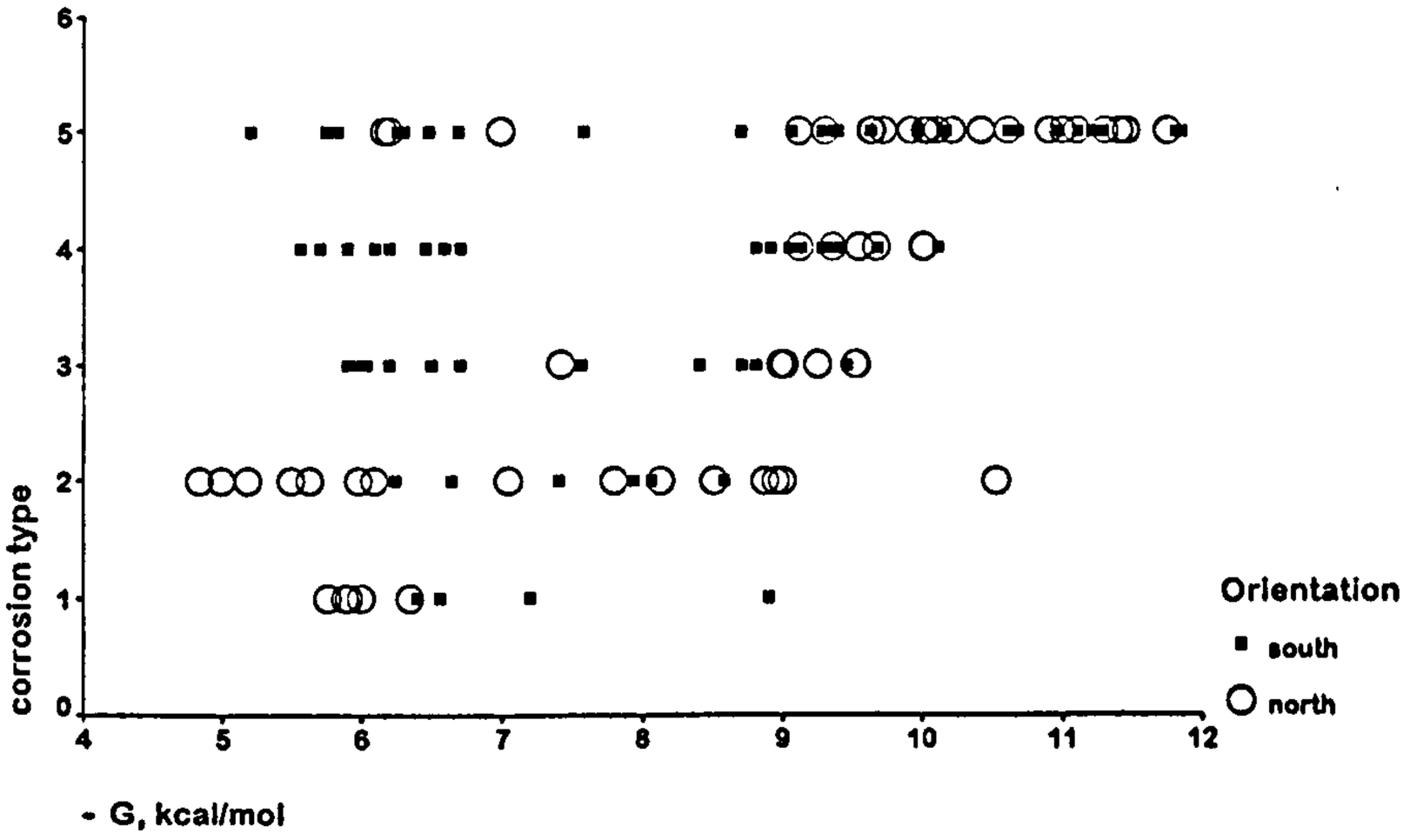

Figure 7.49: Free energy of hydration versus corrosion type, with the window orientation represented by the markers for Fairford and Checkley.

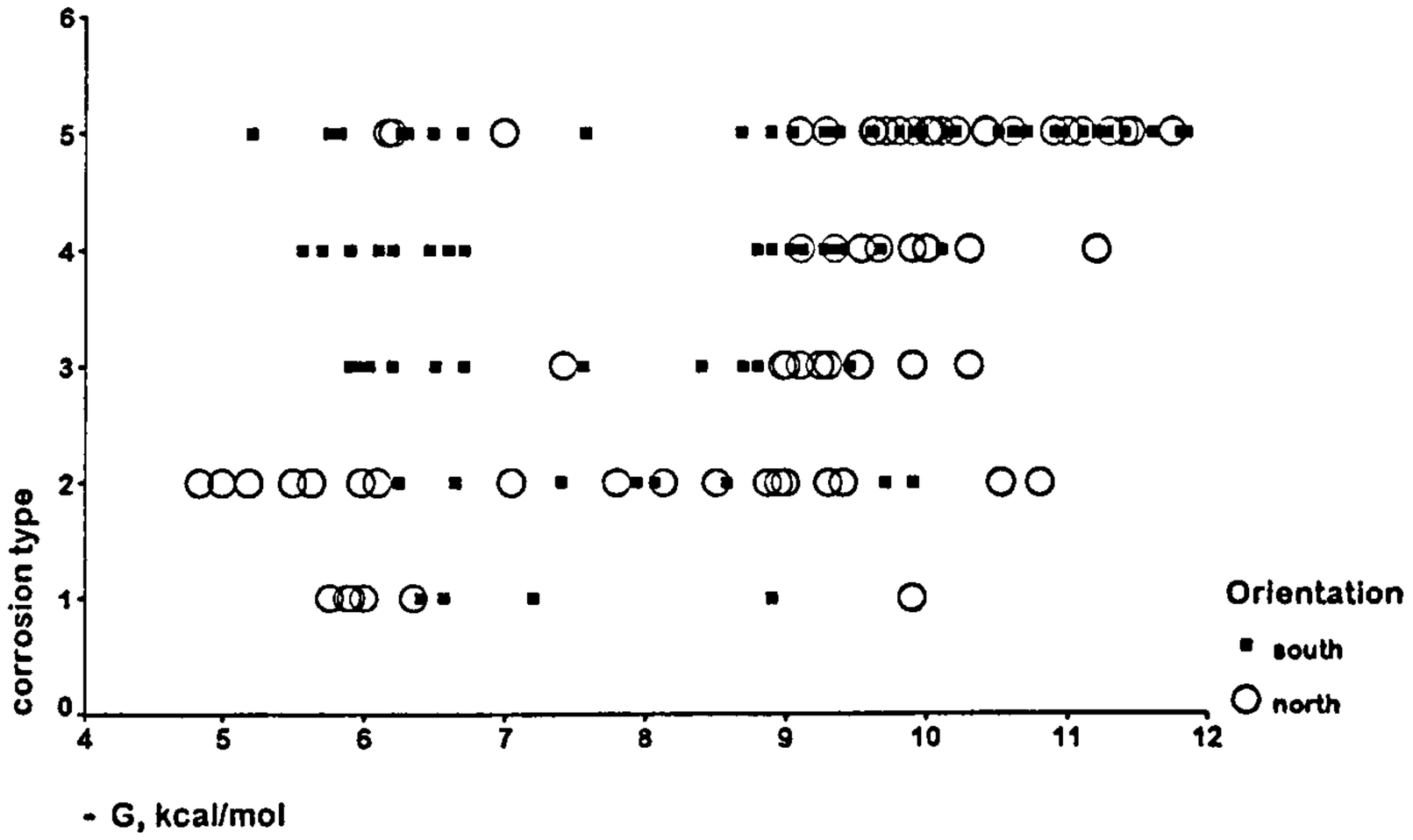

Figure 7.50: Free energy of hydration versus corrosion type, with the window orientation represented by the markers. This is for data from Fairford, Checkley, Fledborough and York Minster.

glass of the same composition. Further data were available for the church at Fledborough, although no information was provided on whether the glass had been moved around or not. These specimens were of different compositions and therefore not comparable within themselves, but when incorporated in the plots with the Checkley and Fairford data they did not contradict the trend. Figure 7.50 shows the free energy of hydration versus corrosion type plot again, but with the Fledborough and York Minster data included [58]. The same trend can be seen. As there is more data included, the other patterns, such as predominance of uniformly weathered samples, make the effect more difficult to see. Similar findings were obvious from using the number of non-bridged oxygen ions and ternary co-ordinates as means of representing the glass composition.

Chapter 8

Results-Environmental Aspects

8.1 Biological Attack

The biological deterioration of substrata has concerned the scientific community for a considerable time. The preservation of historic monuments is generally the reason for the studies of biodeterioration, but since the 1860s glass has become another substratum to suffer from the growth of lichen, moss or algae. Biodeterioration is the degradation of a substance that can be solely explained by the action of biological species, such as bacteria and fungi.

Some workers go as far as to declare that bio-deterioration is the sole reason for the decay of glass [73] whereas others state that some evidence for the action of bacteria was noted [111, 59]. In many cases, it is accepted that if lichens are present and are attacking the glass then oxalic salts should be identified amongst the decay products. This is because the organisms would excrete these and other identifiable compounds on metabolisation of the substrate.

In the course of this investigation two churches had 'green growths' on their inner glass surfaces; an attempt was made to investigate this and the following is an account of the findings. Photographs (a), (b) and (c) in Figure 8.1 show the typical appearance of the growths and (d) is a more detailed look at an area depicted in (b). The growths at the two churches concerned were very different: at Fledborough it was dark green and furry in texture; at Checkley it was of two types, one green-yellow with a light, stringy texture and the other a dark green lumpy covering.

8.1.1 Fledborough

Three of the fourteen specimens from Fledborough had material of a biological nature (that is fungi/algae/moss) present on the inner surface and these were labelled FBN1-3 (see Figure 8.1c

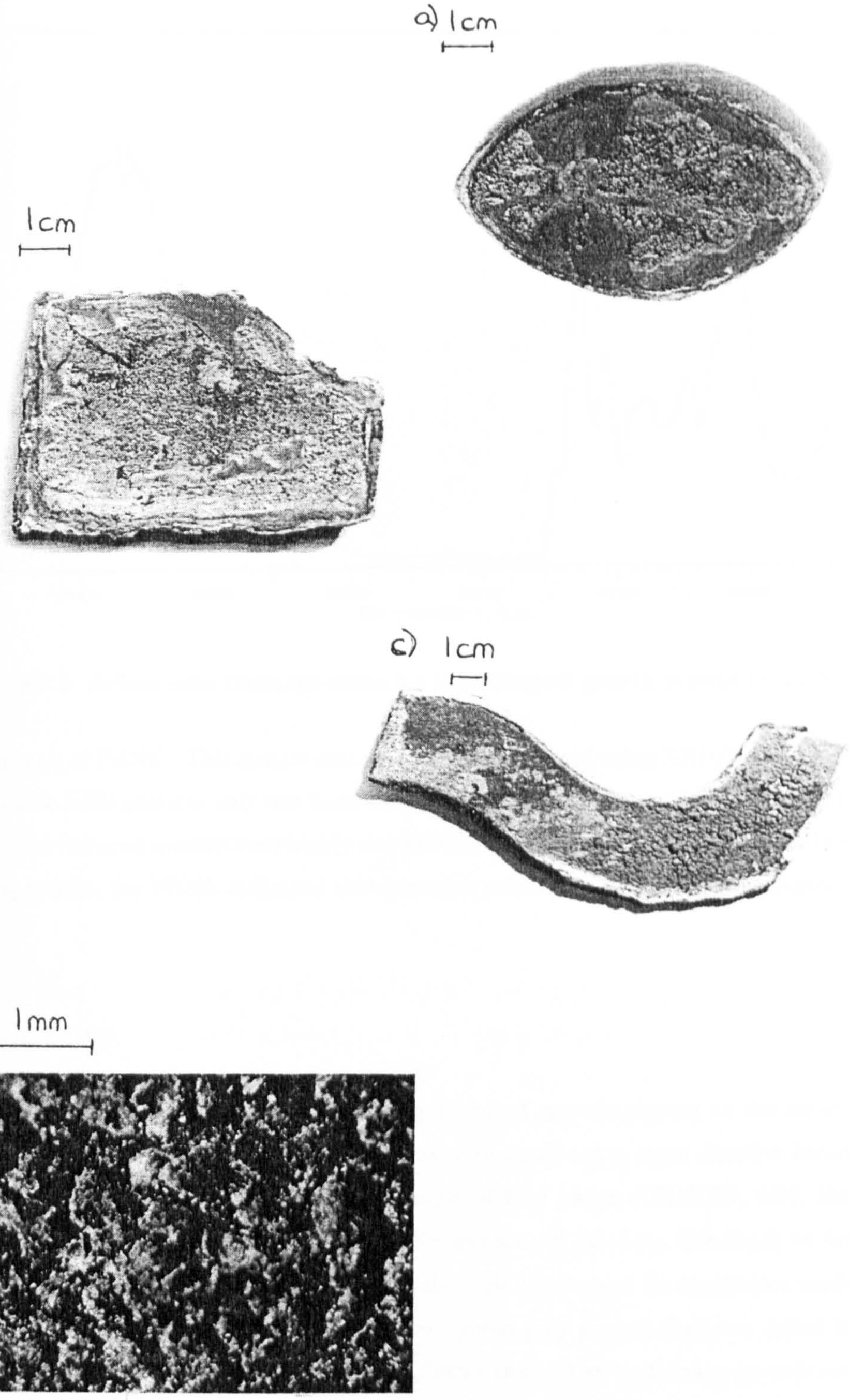

Figure 8.1: Photographs of specimens with biological growths. a) CHK16N b) CHK4N c) FBN2 and d) magnified (X21) area of CHK4N.

Glass Corrosion

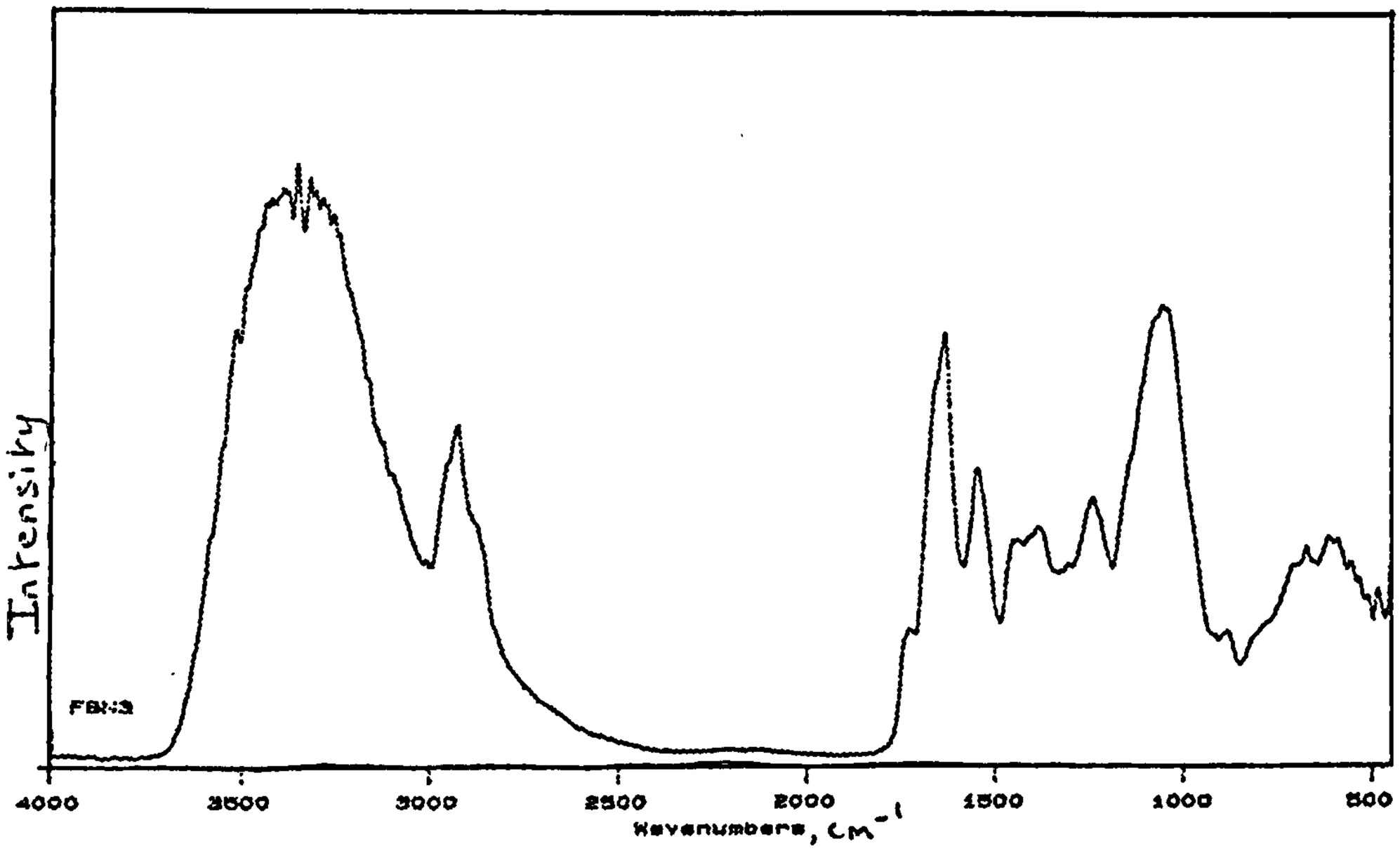

Figure 8.2: Diffuse reflectance spectrum for the biological growth present on FBN3.

for a photograph of FBN2). This matter was removed and analysed using XRD/DRIFT. There was no interpretable XRD pattern, only two lines were clear. These could have been due to the presence of gypsum. The infrared spectra were highly complex due to the organic matter present (see Figure 8.2). This spectrum, for FBN3, indicated that gypsum, calcite and some organic compounds were present.

8.1.2 Checkley

Fifty percent of the selected north-facing window pieces had growths present on the inner surface. Given the large sample size it was thought necessary to carry out a more detailed investigation than that for Fledborough. A representative sample of four pieces (CHK16N, 23N, 30N, 32N) was taken to Prof. M. Seaward (Department of Environmental Sciences, Bradford) to determine the presence or absence of any lichens and hopefully their taxonomy. As mentioned earlier there appeared to be two different growth types - a) deep green-grey growth that was raised from the surface and b) yellow-green growth that was much flatter and had an underlying green layer. These are illustrated as a) and b) respectively in Figure 8.1.

On visual examination it was decided that *Dezmococcus* algae were present, as well as what was either 'cobwebs' or lichen (depending on the sample). The yellow/green growths were the ones that were believed to have cobwebs present. In order to identify the lichen the characteristic lichen tests

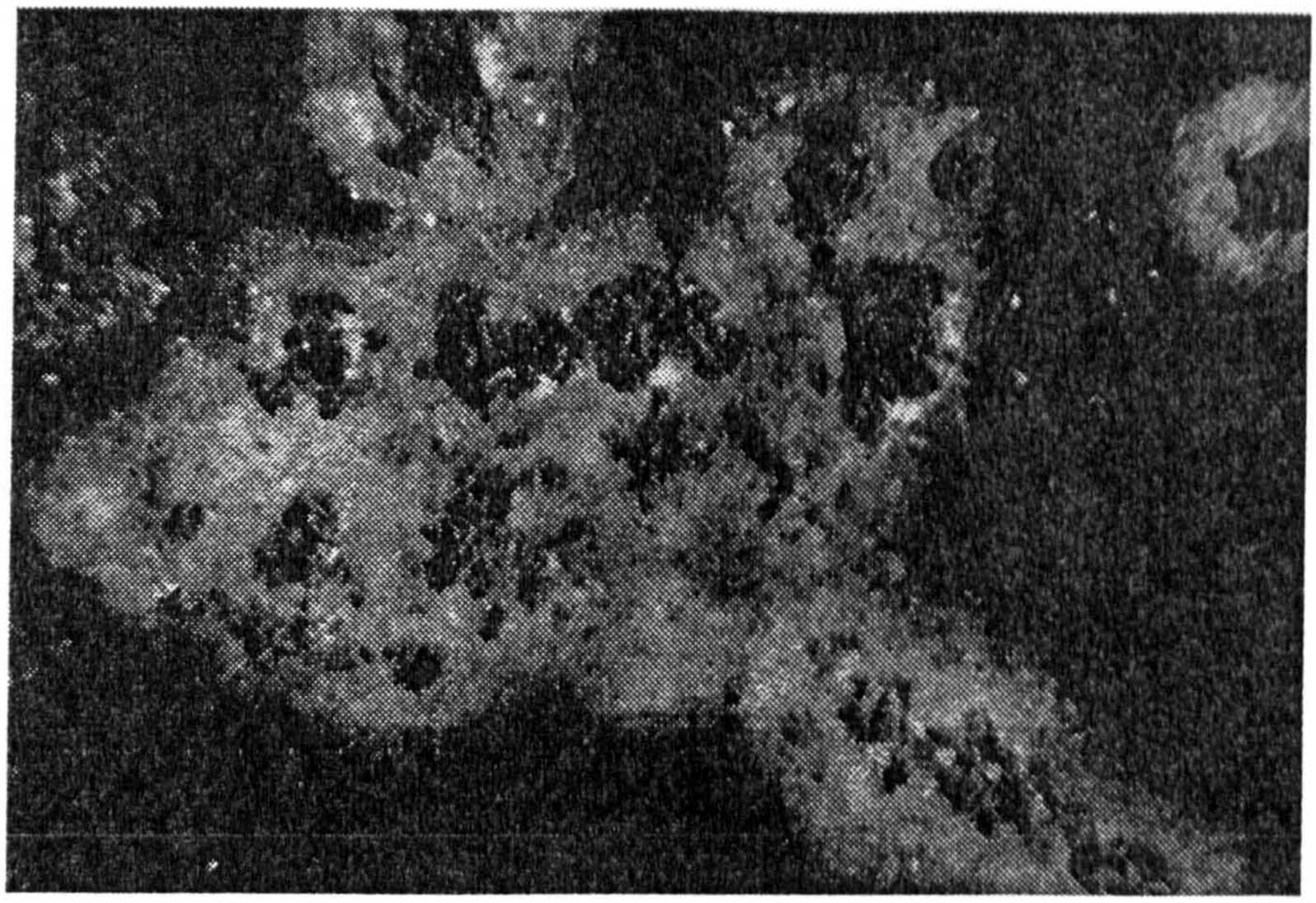

Figure 8.3: Photograph of the surface of CHK5N taken at X21, illustrating the adherence of biological matter to the centre of pits formed by atmospheric attack.

(K, C and Pd) were carried out. All four cases gave negative results, which meant that what was present was probably *Lepraria*. A more accurate characterisation could have been possible using TLC.

It appeared that the algae and lichen were not attacking the glass but were growing on it after pitting had occurred. The pits form a good base on to which the lichen can adhere. The photograph of CHK5N (taken at X21) shows the pits present, with the algae adhering only to the centre of these (see Figure 8.3). In order to state conclusively that the lichen/algae were not attacking the glass, it was suggested that the products be analysed by Raman spectroscopy and to look in particular for the oxalic salts of magnesium or potassium. This study was performed courtesy of the Chemistry Department at the University of York, with the aid of Mr. R. Girling. The operating conditions for the Raman analysis were $8cm^{-1}$ resolution with a 488nm Argon laser of power 5mW for a scan. Figure 8.4 gives the Raman spectra that were obtained from samples CHK16N and CHK23N. If an oxalate salt had been present then a band or peak should have been observed *circa* 1460-$90cm^{-1}$. In the spectrum of CHK16N three clear peaks can be seen. The peak at $1003cm^{-1}$ is identifiable as gypsum, whereas the two peaks $1156cm^{-1}$ and $1524cm^{-1}$ are due to the lichen body, the former being the carbon-carbon stretch, from the carotenoid with the latter being the carbon-carbon (double bond) stretch. The spectrum of CHK23N has the same two bands associated with the lichen body, although they are overshadowed by a peak at $1086cm^{-1}$. This

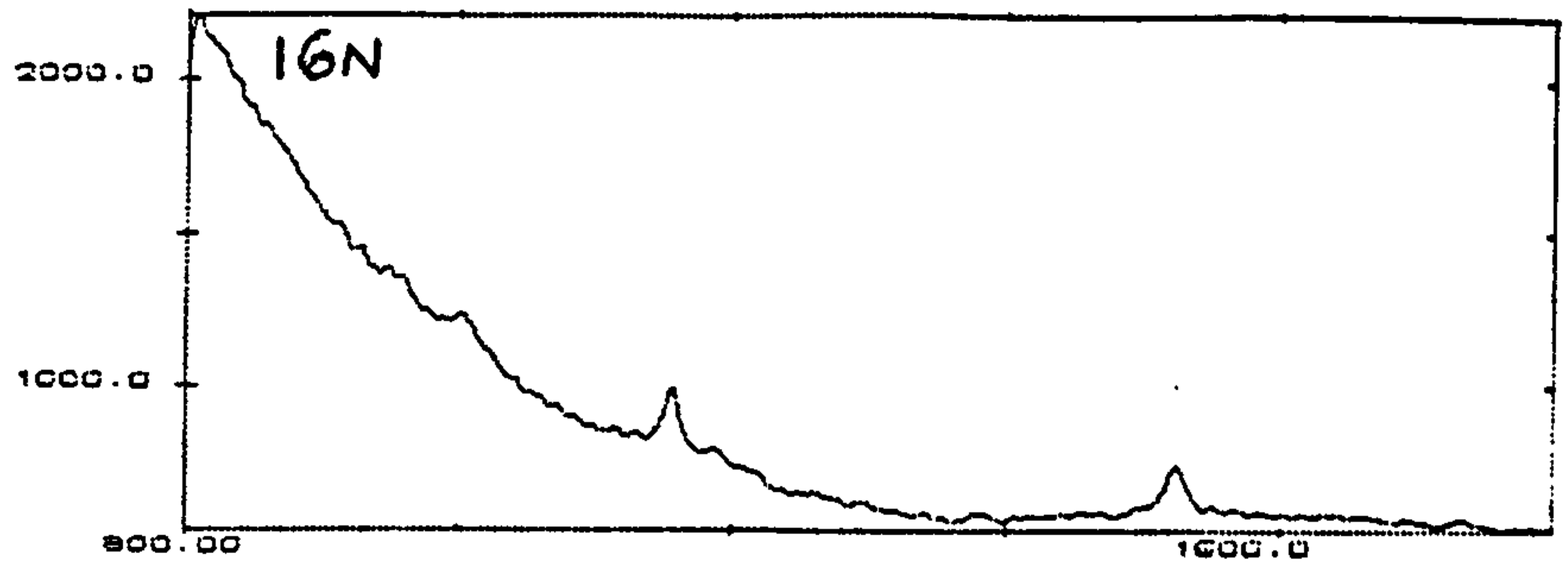

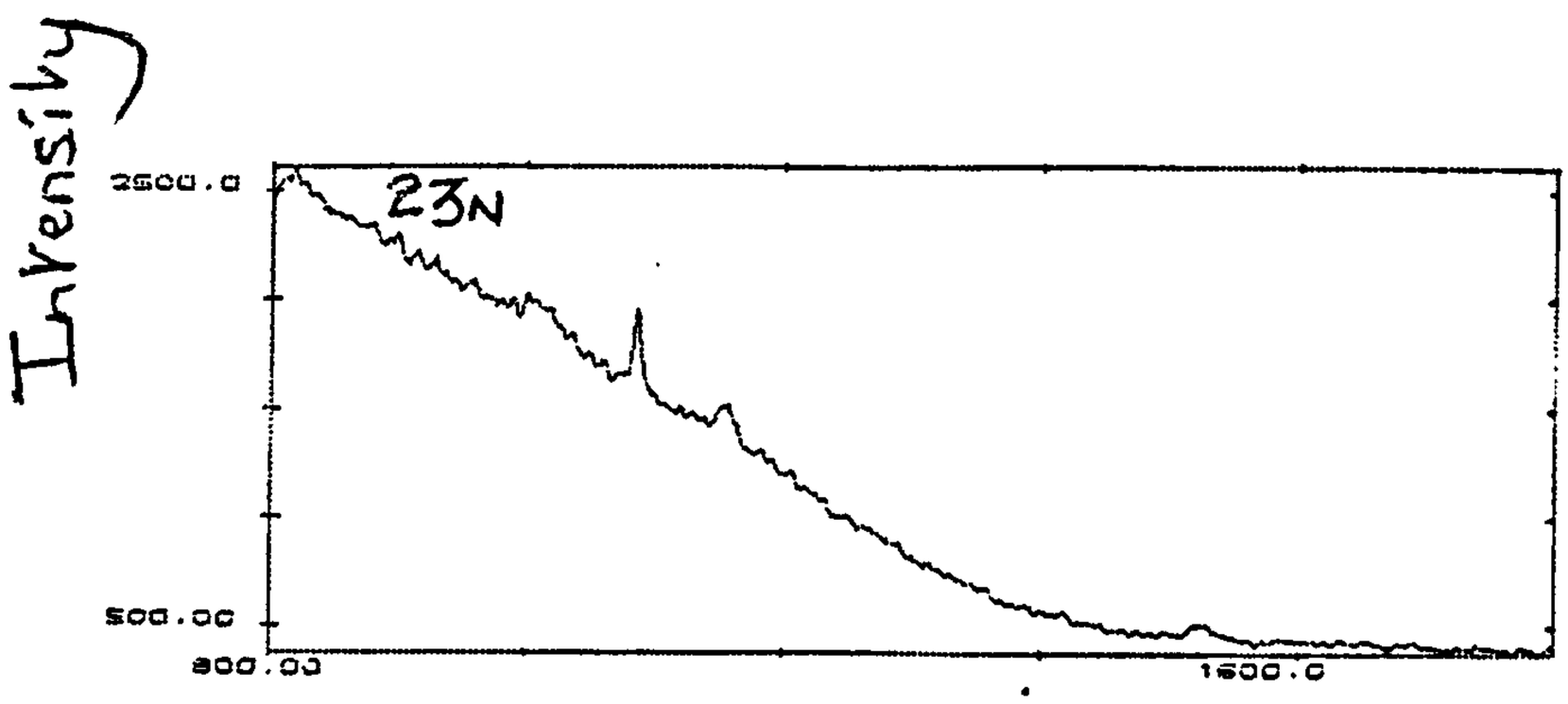

Figure 8.4: Raman spectra for the material present, probably biological, on CHK16N and CHK23N.

peak is characteristic of a carbonate, probably calcium carbonate in form of calcite. Figure 8.5 shows the respective DRIFT spectra for CHK16N and CHK23N. In the analysis of this algae/lichen, there were unidentifiable bands as well as those due to the presence of gypsum and calcite. The unknown bands were probably due to organic functional groups and OH groups that make up the body of the algae.

Therefore it is concluded that in these cases of "green growth" on north-facing samples, there appears not to have been any biodeterioration. The decay products identified were gypsum and calcite, with what is probably *Dezmococcus* and *Lepraria* growing upon it.

8.2 Environmental Considerations

In order to investigate the effect that the environment plays in the deterioration of stained glass windows it was necessary to obtain as much information on the local climate as possible. Data on temperature, precipitation and wind direction are as important as air quality (ie. the amount of smoke particles), sulphur dioxide and other noxious substances in the air. The study of climatic variations cannot be limited to just scientific measurements. This is because the recording of this sort of information was not possible prior to the sixteenth century as thermometers were

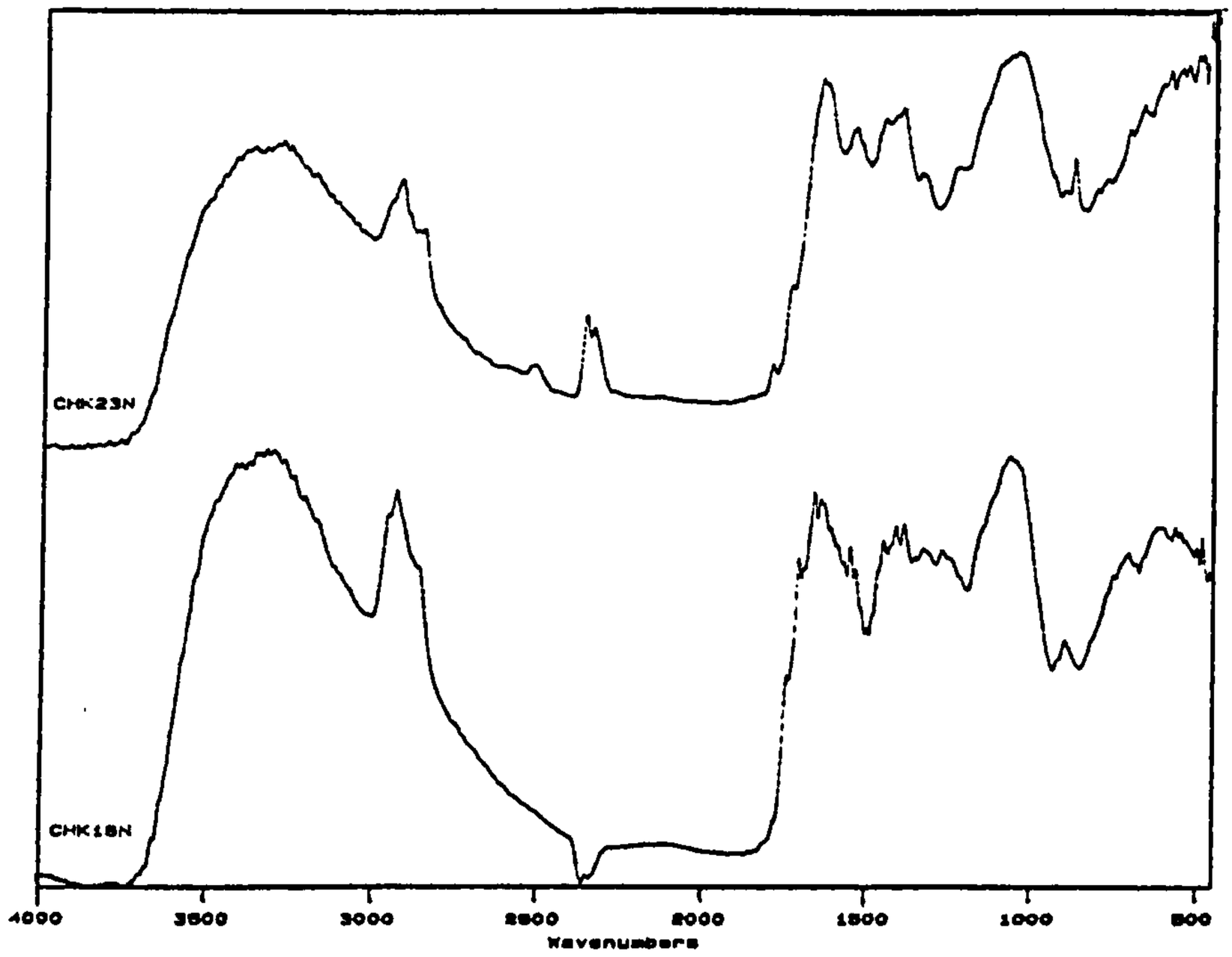

Figure 8.5: DRIFT spectra for the matter present, probably biological, on CHK16N and CHK23N.

not invented until 1597. Sulphur dioxide measurements were not carried out until well after the introduction of the Clean Air act in 1957. Therefore any information on meteorological variables for other than the recent past must come from other sources such as interpretation of tree rings. Thus a variety of data is available and each will be considered separately.

8.2.1 Climate Data

Dendroclimatology

Dendrochronology is the study of tree rings and dendroclimatology is the application of this to climate reconstruction. The latter is capable of providing meteorological data with a resolution of one year spanning a range of 10,000 years [77], although it is unusual to find a single tree ring series of longer than 500 years. The basis of tree ring analysis is that the ring-width is intimately related to the environment in which a tree grows [75]. Generally a wide ring would indicate warm, moist conditions during at least the summer months, if both high and low altitudes ringwidths agreed. Likewise a narrow ring indicates cool, dry conditions.

Several studies relating specifically to the mediaeval and post mediaeval period have been carried

Glass Corrosion

out for England and Europe [65, 19, 20, 7, 70, 25]. These essentially use oak trees and the chronologies for related areas have similar patterns. Hillam [65] studied the mediaeval oak chronology for south-west England. Her conclusion was that this chronology correlated well with those available for the rest of England, thus suggesting that independent chronologies were not necessary for each area of the British Isles.

Briffa *et al.* [19, 20] examined tree ring chronologies and successfully reconstructed temperature and precipitation information for the nineteenth century. This was verified using the records of Manley [85] and Lamb [76, 77, 78]. Extrapolation backwards should be possible, but does not yet appear to have been done.

Thus although dendroclimatology at first appears useful, it provides no more information than is already available and details of regions within a specific country are indiscernible.

Monitors and Diaries

Meteorological monitoring stations are spread throughout the world. The data obtained are published by the World Meteorological Organisation [29, 76]. In this study the climate of the British Isles is paramount and recording dates back to 1680. However, a complete record does not exist prior to 1841, when the Greenwich meteorological and magnetic observatory was established.

Manley [86] constructed a table of mean temperatures for the Midlands for the period 1698-1952. This was derived from a variety of sources:

1815+ uses average values from two sites, Oxford and Lancashire.

1771-1814 uses the average of six sites, each of which is intermittent.

1698-1770 mainly based upon London, but includes sources such as home weather diaries and estimates based on records for Utrecht.

Lamb [77, 78] took this further and created a table of temperature and rainfall data. The temperature data being that of Manley's supplemented by extrapolations from the summer and winter indices. The summer and winter indices are scales which were invented to assign values to sources such as weather diaries. A number was assigned depending upon the number of reports of mild-cold months in winter (wet-dry months in summer) in the literature. The rainfall data prior to 1740 is also based on the indices; post 1740 is derived from Nicholas and Glasspoole [107] and Meteorological Office records.

Glass Corrosion

Beetle Remains

Reasonable approximations to the mean temperature can be obtained from the 20,000 year range of climatic data that is deduced from pollen analysis and beetle remains. The premise of this work is that, if the climatic tolerance for a specific species is known, then where these species are found within the geological record as fossils, the climate is known to within that range [2].

This is too broad a temporal range for the information needed in this study.

Ice Cores

Ice cores can provide two types of information. Climate reconstruction can be achieved via oxygen isotope analysis with a resolution of years. This can extend as far back as 10,000 years ago. Alternatively the year sheets of ice can give information on the climate. These are available back to 1760 for the South Pole and 1000 for Greenland. Obviously the global climate is different to the local U.K. climate and therefore this is not a useful source of data for the mediaeval period for the British Isles.

8.2.2 The Climate of Central England since 800

The compiled evidence suggests the local climate for central England has varied as depicted in Figure 8.6. This is plotted from the precipitation and temperature data of Lamb [77] and is expressed as fifty year averages. The precipitation is expressed as percentages of the 1916-1950 average; temperature is given in °C. As the glass considered in this study is fourteenth century and later, the earlier information on climate is not needed, though it is to be noted that the twelfth and thirteenth centuries appear to have been the hottest and dampest since the advent of stained glass windows.

It is clear that the 15th to 18th centuries were particularly cool, corresponding to what was called the Little Ice Age. It is also apparent that the prevailing trend since the eighteenth century is for a warmer and wetter climate. It is this latter trend that could be suggested as being responsible for the decline in the condition of the stained glass windows. That is to say, a warm moist climate is more damaging than a cool, dry one and therefore the so called acceleration of deterioration that has been observed since the Victorian era could be due to the local climate change.

This does not mean that the temperature increase has not been heightened by the increase in chloroflurocarbons and other pollutants in the upper atmosphere, which serve to trap the ultraviolet radiation from the sun [54, 91, 136].

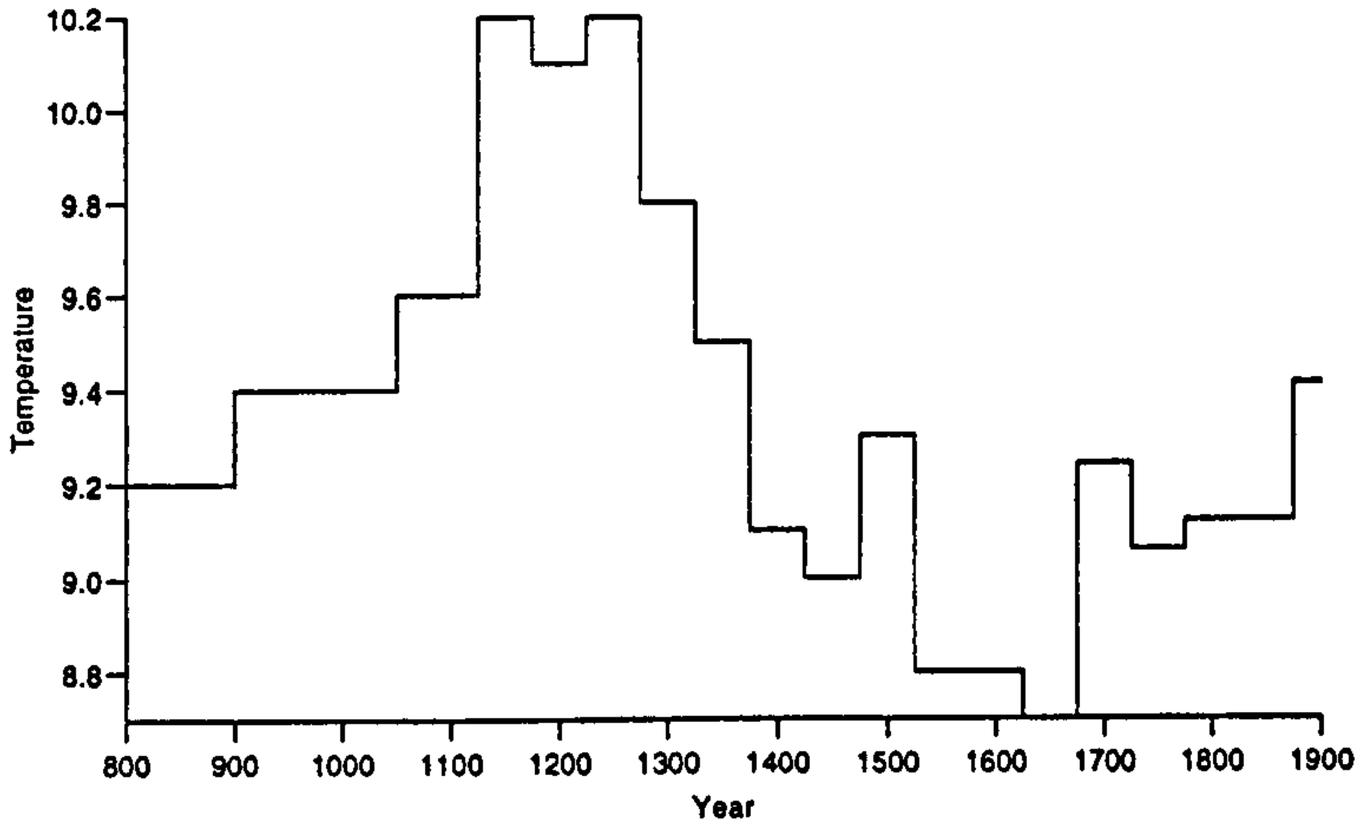

(a) Temperature

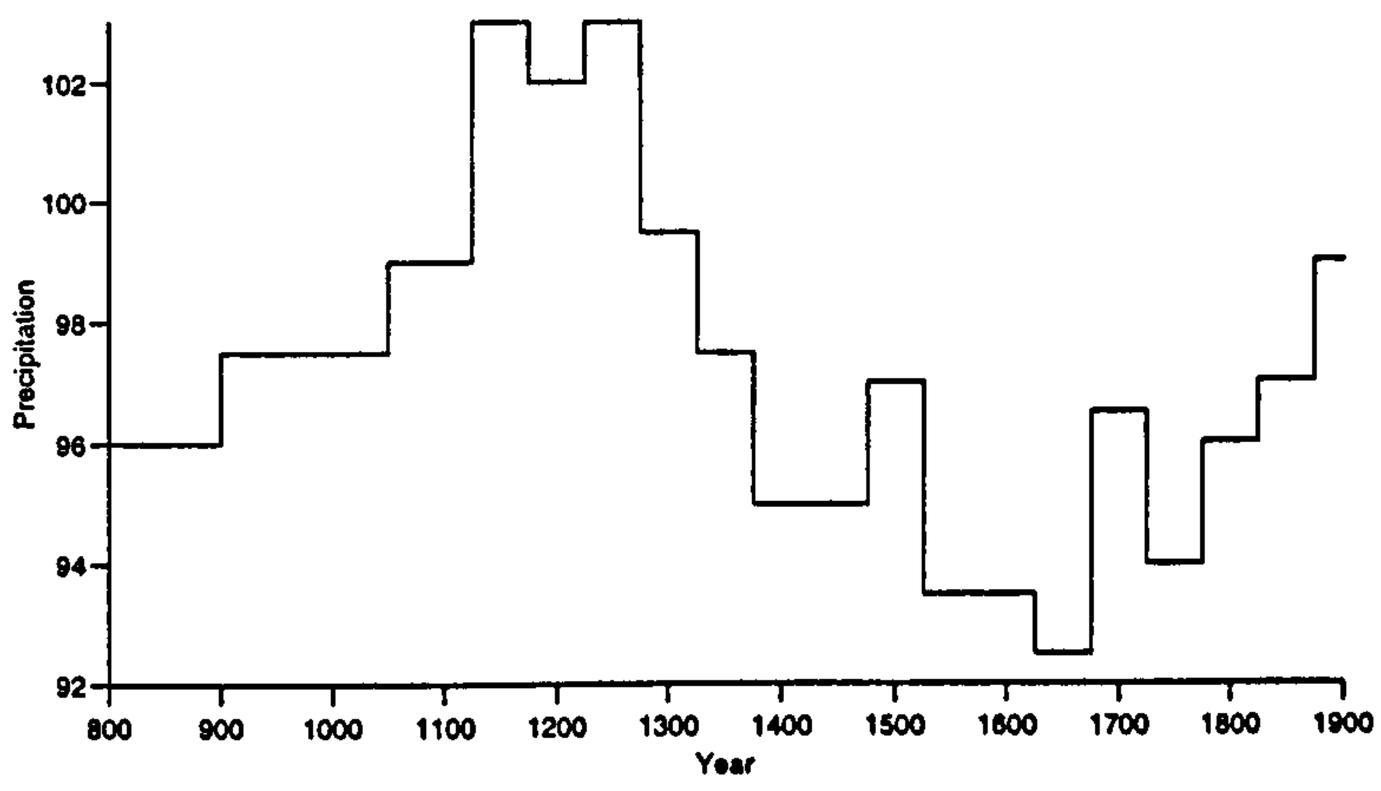

(b) Precipitation

Figure 8.6: Graphs illustrating the variation in temperature and precipitation within the United Kingdom. The data is expressed in terms of fifty year averages.

8.2.3 Pollution Data

In 1957 the government recognised the need to improve the quality of the air in major cities, such as London, by the creation of the Clean Air act. It was not until six years after this that detailed information was collected and then only for a limited number of sites [74]. Of the monitoring sites that were created in 1962 some are still functional, whereas others have been replaced or lost, and new stations established elsewhere. Thus, information on sulphur dioxide levels is sparse and intermittent. There is, however, a general trend to the levels, notably a decrease since the commencement of monitoring. The Department of Energy supplied the data on the following stations:

- Lincolnshire (LHE).
- Nottinghamshire (FBN,FBS,FLE).
- Northamptonshire (SCB).
- Gloucestershire (GMH,FAI).
- Yorkshire, Canterbury and Carlisle (for use when including the data of gillies and Cox [59]).

Unfortunately data were not available for the Cambridgeshire (ELY) and Staffordshire (CHK) regions. Graphs of the sulphur dioxide levels were plotted for each station for each region.

The graphs in Figures 8.7 and 8.8 do not illustrate all of the data supplied by the staff of the organisation, AEA Technology, but are representative of the data for each region. Figure 8.9 illustrates the locations of the sites with respect to the churches. It can be seen that there is often a marked difference in mean sulphur dioxide level for the same year within a particular county. In some cases this difference is as high as a factor of three. The following summarises the data:

- All regions have experienced a decline in mean sulphur dioxide levels.
- The mean present day level is approx. $40\mu gm^{-3}$, lower in rural areas.
- Nottinghamshire has the highest SO_2 levels.
- As the highest level recorded for these regions is $200\mu gm^{-3}$, the levels must have exceeded $300\mu gm^{-3}$ at the height of the industrial revolution (the late nineteenth century).

AEA Technology also provide an emission map of the U.K. for sulphur dioxide for 1993 on the Internet [137]. This indicates that the high emissions are centered on London, Liverpool and Birmingham, whilst the west coast and Scotland have the lowest.

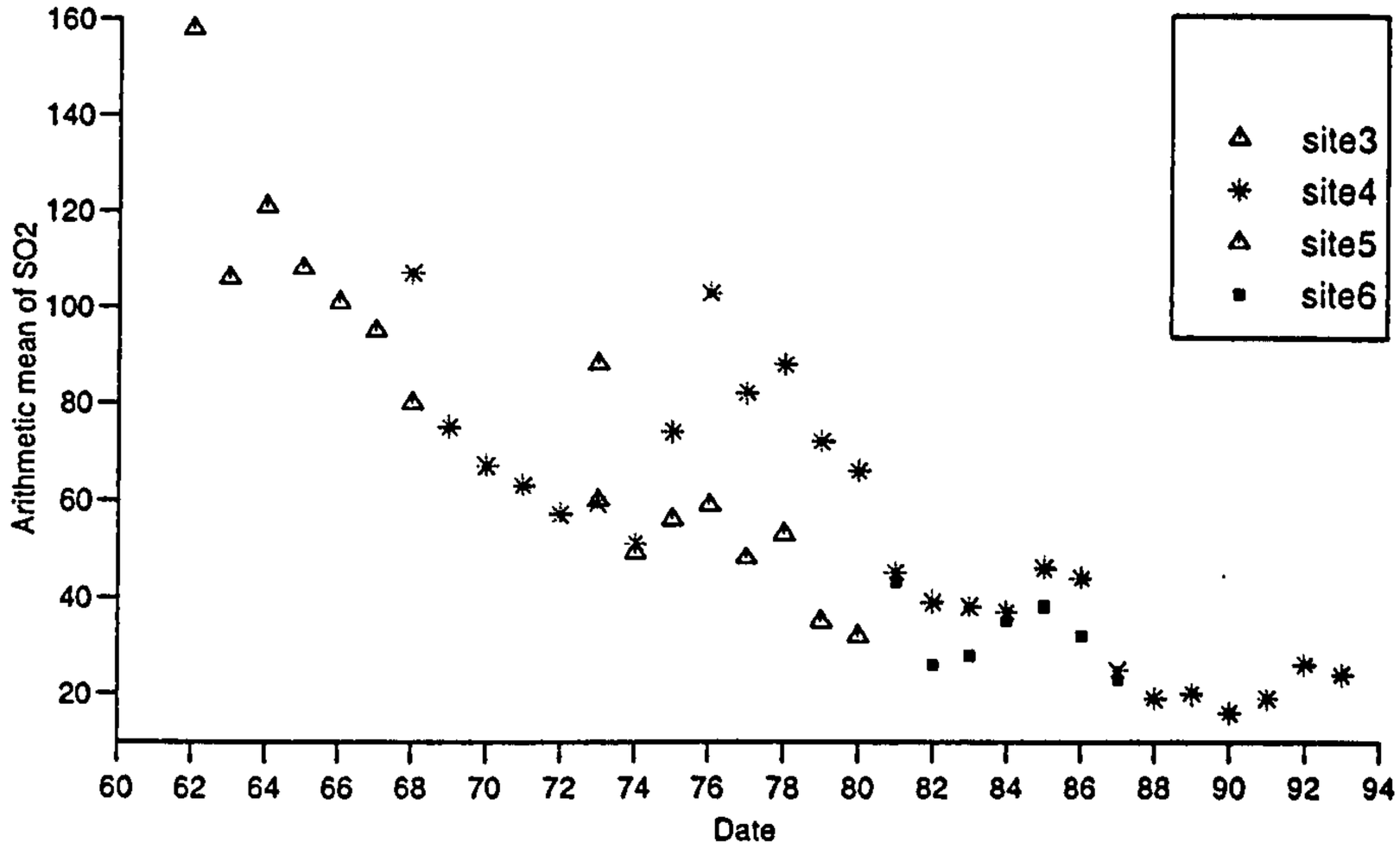

(a) Gloucestershire

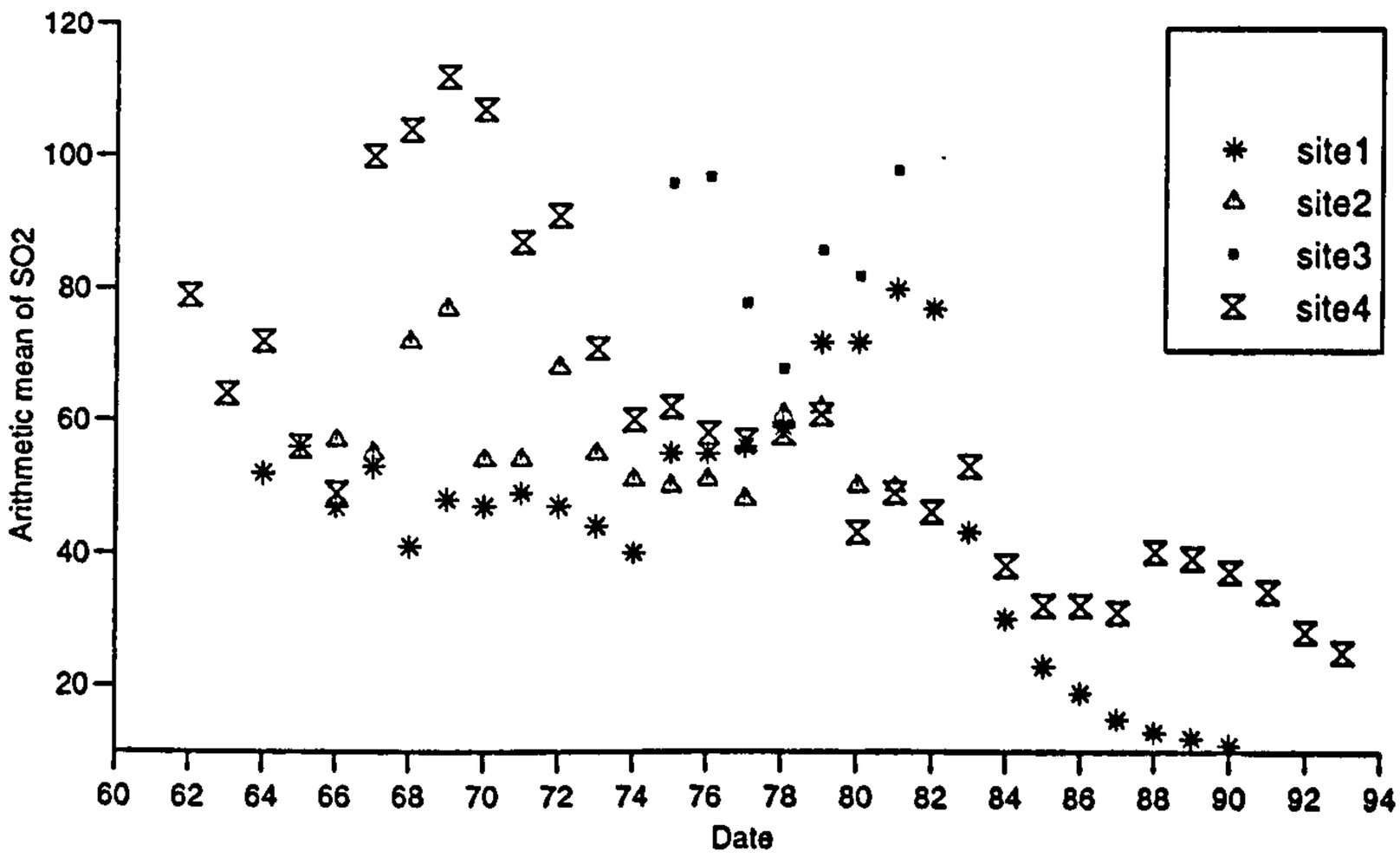

(b) Lincolnshire

Figure 8.7: Graphs illustrating the sulphur dioxide levels for the years 1962-1993 in the UK, for Gloucestershire and Lincolnshire.

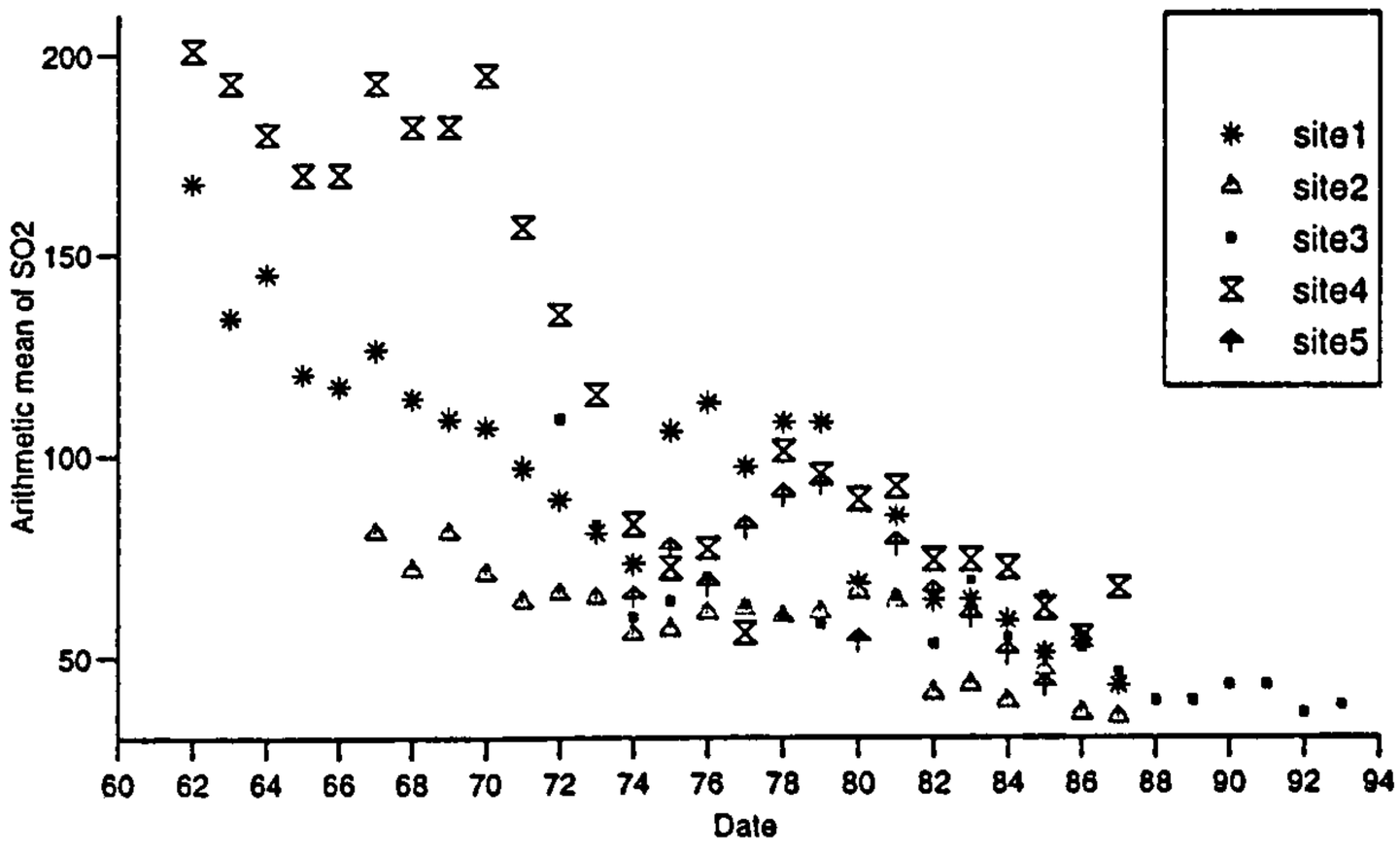

(a) Nottinghamshire

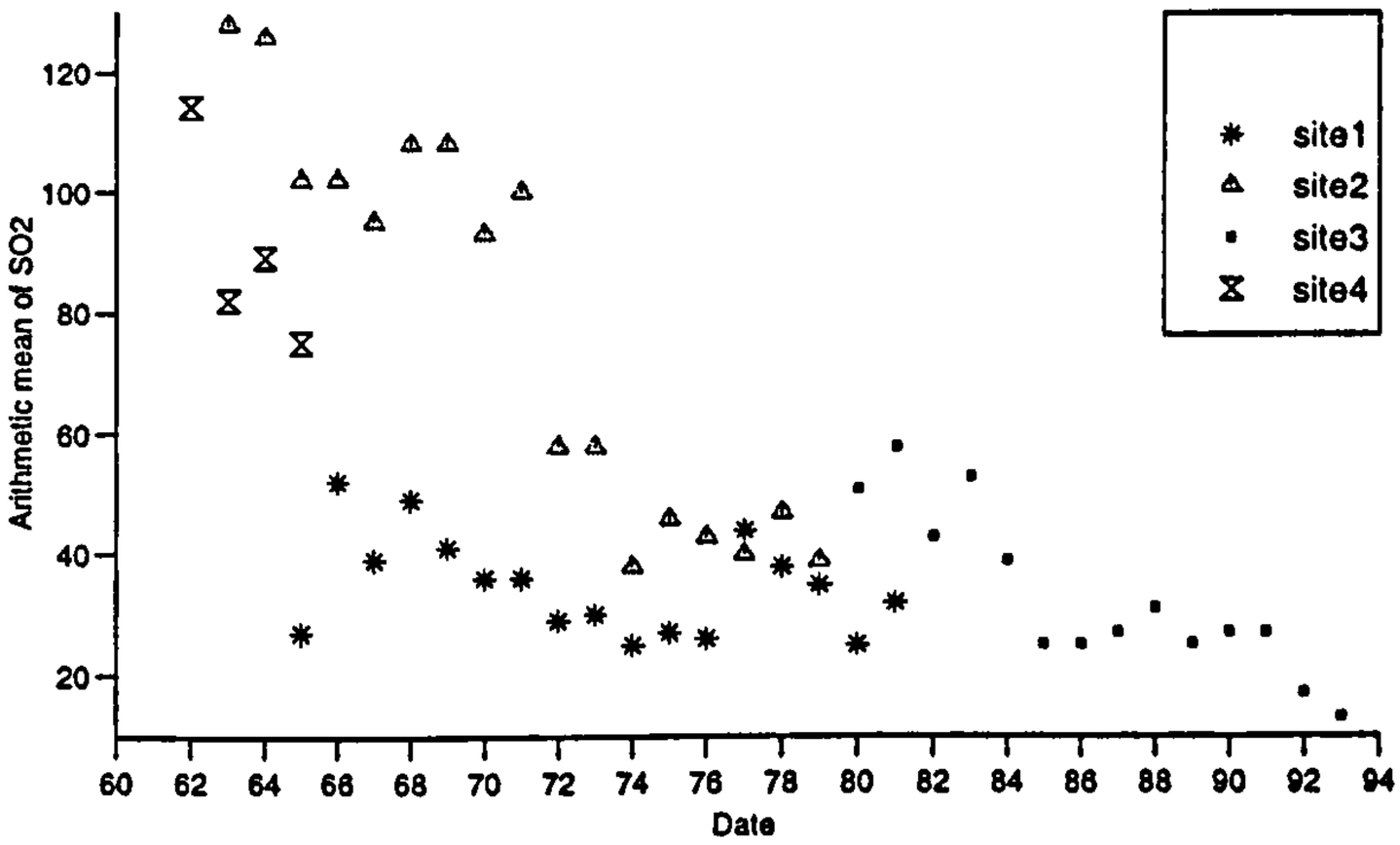

(b) Northamptonshire

Figure 8.8: Graphs illustrating the sulphur dioxide levels for the years 1962-1993 in the UK, for Nottinghamshire and Northamptonshire.

Glass Corrosion

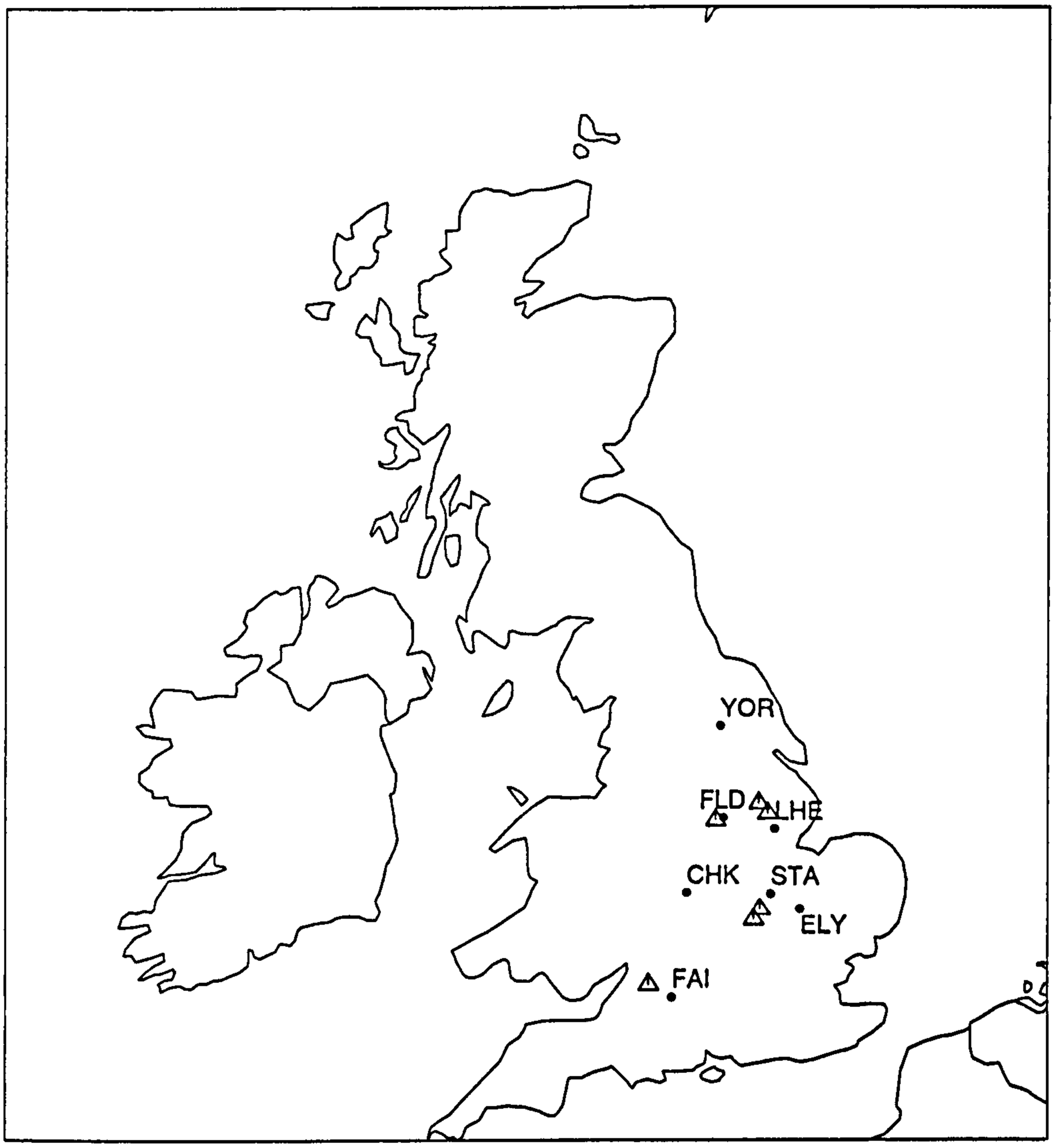

Figure 8.9: The distribution of pollution monitoring sites with respect to the church locations. The triangles represent the monitoring sites with dots and labels representing the church location.

Pollution as the cause of corrosion

There was much diversity of opinion as to whether air pollution and/or sulphur dioxide causes harm to mediaeval stained glass windows in the early 1970s [96]. Newton [102] in 1988, wrote that air pollution was not responsible for the accelerated attack since the second World War, or at the very least there was no evidence to support this claim.

Any effects due to high sulphur dioxide and/or pollution are difficult to detect because each church has a different and very individual history. Many churches had their windows removed during the second world war and this is believed, in most cases, to be the cause of increased deterioration. The recent paper of Cox and Cooper [32] shows that the mediaeval glass of York exhibited atmospheric decay prior to 1540. That is, archaeological window glass that was buried at the time of the dissolution of the monasteries had corroded in the atmosphere. This would therefore indicate that although high sulphur dioxide levels can accelerate the decay process, they are certainly not the sole cause.

There is, however, more information on the deterioration of brickwork and the contributing effect of sulphur dioxide and pollution [142]. As the majority of the churches considered were built of limestone, the degradation of which is an important consideration, they will have similar building wash. Webb [142] concluded that the pH of the run off from limestone buildings varied with rainfall intensity. Natural solubility was the most important factor in the model and the stone loss increased by less than $1\mu myr^{-1}$ for an increase in sulphur dioxide levels of 1ppb.

This study was unable to ascertain any links between the sulphur dioxide levels, climate variation and extent of corrosion due to the lack of detailed information available for the sites selected. The data presently available on climate indicates that all the sites are comparable whereas the pollution data suggests that Nottinghamshire is more polluted than the other regions considered.

Glass Corrosion

Chapter 9

Discussion

The glasses analysed in this study were fourteenth century in date except for those from Fairford which were sixteenth. All of the glasses were of later date than those previously studied by other workers: for example, Cox and Pollard studied 12-15th century glass [36]; Schreiner looked at pre14th century [132] and Perez-y-Jorba considered 13th and 14th century glass [112] to name a few of the studies.

The number of specimens considered in this study was comparable to that of Cox and Pollard but much larger than any other previously published work. In interpreting the data, information made available by previous researchers was considered although not reproduced in this volume. Most published data is incomplete, in that, if the condition of the glass is reported then either the composition or the weathering product are included but only occasionally are both characteristics mentioned. Presentation of third party data has been avoided in this thesis as the varying amounts of information available would have led to confusion.

The compositions of these glasses have been seen to divide, very clearly, into two groups by the magnesia content. This type of division was reported by Cox *et al.* [36, 59] in their study of mainly York Minster glass. The low magnesia glasses represented 20 from 203 and 5 from 67 respectively, of the samples analysed. This work has made it clear that these glasses are much more common: 129 samples from the 206 analysed. This would suggest that the importance of the magnesia content has been undervalued especially in the assessment of durability. It is likely that the magnesia content is as important as the lime content and therefore we should consider the lime-magnesia content in the same manner as we do the soda-potash.

Previous work indicated that glass with less than 62mol% silica was likely to have deteriorated by crusting (with increased likelihood the lower the value). Whilst this is the case for the mediaeval glass it was not found to be the case for the sixteenth century glass from Fairford. The Fairford

samples did not reflect the trend of increased deterioration with a decrease in the SiO_2 content.

Fairford samples exhibited a correlation between the extent of decay and the orientation of the windows from which they originated. Correlations of this sort had not been observed previously for two reasons. Firstly large numbers of samples are seldom available for study and secondly it is very unusual for glass not to have been moved during its lifetime. That is, art historians strongly believe that all of the glass at Fairford is in its original glazing, i.e., no rearrangements have taken place. Thus for example, the glass from the north side has always faced north. Previously published work has tentatively identified window orientation (if known) but has not obtained any conclusions with respect to the effect of orientation on deterioration. Incorporating this data, with that from Fairford does not affect the interpretation because very often the same composition is not present in windows of different orientation and the fourteenth century glass is generally more decayed, so distinguishing between them is often difficult. The conclusion from this, is that the south-facing window glass decays to a greater extent (or faster) than north-facing window glass of the same composition. An investigation of east/west-facing window glass was not possible, but would be a useful further study. A cursory examination of the windows of Fairford suggests that the south-east windows are the most decayed, thus implying that the wind is the reason for the difference in decay extent. The alternative explanation would be that the south-facing glass attains higher temperatures and for longer periods than windows facing in other directions.

It was initially hoped that other environmental parameters, such as location, sulphur dioxide levels, precipitation and temperature could be incorporated. The variation due to location could not be considered thoroughly due to the lack of early climatic data for the regions. The data available suggest that the locations selected were comparable and therefore the corrosion would be similar (if correlated). The corrosion correlation would only be valid if the glass at the locations was comparable in composition, age and orientation. This was not achieved for a reliable sample size.

Grouping of glasses by composition and comparing this to the extent of decay and decay products is a standard practice. Most of the sample sizes are statistically insignificant but still generalisations are made. Schreiner [132] states that crusting occurs when SiO_2 + formers < 60mol%, Bettembourg used broader parameters, 46<SiO_2 < 52mol%, 11.5<CaO<20mol% and 17<K_2O<27mol% [15] and Gillies and Cox used a ratio, 'R_2O'/'RO'>0.50 [59]. This study has found it necessary to first separate the glasses by magnesia content to elicit any trend between decay type and composition. The high magnesia group have 'SiO_2'<59mol% (slightly higher for glass of a later date) and low magnesia glasses have 'RO'>35mol% in cases of uniform weathering. This is in keeping with the Gillies and Cox correlation of 'R_2O'/'RO' with decay type but only when the data are separated as mentioned and for specific 'SiO_2'. Gillies and Cox also related the glass composition to decay product.

Glass Corrosion

Generally the major product was hydrated silica for isolated pitting, gypsum for merged pits and gypsum with syngenite for the cases of uniform weathering. This study agrees with this, with the exception that syngenite was seldom found, even on uniformly weathered samples. Perez-y-Jorba *et al.* [112], Bettembourg [15], and Gillies and Cox [58, 59] also identified more exotic sulphates such as epsomite and palmerite which were not found in this case. The work at the Deutsches Museum could not be compared as the glass composition was not determined by them.

Perez-y-Jorba *et al.* [111] reported the presence of fungi on glass, as did Fitz. In this study many examples of growing organisms were found, on the inner surface of north-facing panels. These are believed to be *Lepraria* and *Dezmococcus*. Whilst these organisms may be harbouring moisture at the surface there is no evidence to suggest that they are attacking the glass directly.

Marschner and Perez-y-Jorba investigated glass cross-sections for the purpose of understanding pit formation. This technique was used to look at glass from Fairford and Stanford, the results of which were shown in chapter six. This corroborates that sulphur is not evident in the reaction zone and therefore it is unlikely that sulphur dioxide is directly attacking the glass. Also Marschner's hypothesis on pit formation was reenforced such that it is probable that it is valid for more than the surface fractured cases.

9.1 Conclusions

The aim of this research was to investigate the extent of decay of *in-situ* mediaeval stained glass windows in the United Kingdom. To achieve this, permission to analyse mediaeval glass that would be removed for restoration during the research period was obtained. The chemical composition of glass specimens from seven locations was determined. These were fourteenth and sixteenth century in date. The sixteenth century glasses (Fairford) had distinctly different compositions compared to the others, forming an isolated group. Generally this group was the colourless, blue and ruby glasses with the other specimens being similar to the fourteenth century glass. The fourteenth century glasses divided into two classes by magnesia content. This division also partly explained the division in the Fairford samples, thus indicating that the amount of magnesia in a glass was an important consideration when determining the chemical durability.

The data were used to investigate the validity of the generally accepted means of representing the composition of a glass by reduced variables. The method of calculating triangular co-ordinates suggested three clusters in the data which correlated with the mergence of the low magnesia glasses from the two centuries. It was found that the ratio of two of the ternary co-ordinates ('R_2O' and 'RO') correlated with the extent of decay. Within the classification, i.e., low or high magnesia, the larger the ratio the more decayed the sample. The reduction via free energy of hydration (or

non-bridged oxygen) indicated a correlation between both of these values and the extent of decay. Both calculations (of free energy of hydration and non-bridged oxygen atoms) have the durability inherent in the value, but these results suggest that a linear relationship exists between them, such that the extent of corrosion of a known composition could be predicted from the plot. This relationship does not hold for the sixteenth century mixed-alkali glasses.

A link between the extent of deterioration and the orientation of the window from which the glass originated was established. That is, south-facing glass is more deteriorated than north-facing glass of the same composition, for two of the churches included in this study. This conclusion is strongly dependent upon the fact that the glass in Fairford church has always had the same aspect as present, and that the windows within the church have never been moved. The deterioration at the other churches was not in contradiction to this, although the difference in decay was not as marked. This latter fact is probably due to the earlier date of the non-Fairford glass, enabling the glass on the north side to 'catch up' with the south side in terms of decay. This variation of the extent of decay by orientation is likely to be due to a combination of prevailing wind direction and temperature.

There appeared to be no link between the glass colour and the deterioration experienced. There was, however, some correlation between the composition and the weathering product. Gypsum was the most frequently identified product, with hydrated silica being the most frequent minor product. The low magnesia glasses formed hydrated silica as the major product, namely because they were the more durable glasses and therefore had deteriorated less. There appeared to be no link between the corrosion product and the extent of decay for these low magnesia glasses. The high magnesia glasses did exhibit such a correlation. The higher the ratio 'R_2O'/'RO', the more complex the decay product. A low ratio was associated with isolated pits and hydrated silica, a higher ratio with gypsum and merged pits, and a high ratio with uniform weathering, gypsum and syngenite. There was no evidence of biodeterioration.

There was no evidence to suggest that sulphur dioxide directly attacks the glass, thus forming the sulphates on the surface. Only a few specimens were investigated and therefore this was not a statistically significant conclusion. The sulphur identified on the surface usually correlated with calcium suggesting the presence of gypsum. These two elements were normally in negative correlation with the presence of silicon. Infrared studies indicate that the sulphur is present as sulphate molecules. This agrees with the identification of sulphate weathering products. On close investigation there was evidence of the genesis of pitting. This appears to manifest itself as a modification of the network such that a hemispherical region is chemically altered (seen as a change of colour). The decay proceeds in to the glass with crystalline weathering products forming in the central region. Eventually the boundary to the pit collapses leaving a basin which may or may not retain the decay products.

References

[1] P. B. Adams. Glass corrosion: A record of the past? A predictor of the future? *Journal of Non-Crystalline Solids*, 67:193–205, 1984.

[2] J. Andersen. Beetle remains as indicators of the climate in the quaternary. *Journal of Biogeography*, 20:557–562, 1993.

[3] Anon. Chemical analyses of mediaeval window glasses-Part 1. *CVMA Newsletter*, 21:9–16, 1976.

[4] P. W. Atkins. *Physical Chemistry*. Oxford University Press, 2nd edition, 1982.

[5] E. Bacher. Visit to Britain. *CVMA Newsletter*, 11:2, 1974.

[6] E. Bacher. The decay of mediaeval stained glass: climatic and environmental influences. *International Institute of Conservation Congress*, Conservation with Historic Buildings:87–88, 1980.

[7] M. Baillie and J. Pilcher. Make a date with a tree. *New Scientist*, 117:48–51, 1988.

[8] C. Banwell and E. McCash. *Fundamentals of Molecular Spectroscopy*. McGraw-Hill, 1994. Fourth Edition.

[9] J. Barrera and B. Velde. A study of french mediaeval glass composition. *Journal of Glass Studies*, 31:48–54, 1989.

[10] W. P. Bauer. The cleaning of glass. *CVMA Newsletter*, 18:5–6, 1976.

[11] M. J. Baxter. *Exploratory Multivariate Analysis in Archaeology*. Edinburgh University Press, 1994.

[12] A. Beiser. *Concepts of Modern Physics*. McGraw-Hill, 4th edition, 1987.

[13] J. M. Bettembourg. Composition et altèration des verres de vitraux anciens. *Verres et Réfractaires*, 30:36–42, 1976.

[14] J. M. Bettembourg. Conservation problems of early stained glass windows. *Crafts Advisory Committee: Conservation Paper*, 6:9, 1977.

[15] J. M. Bettembourg. Degradation et conservation des vitraux anciens. *Les Dossiers de l'Archaeologie*, 26:102–111, 1978.

[16] J. M. Bettembourg. Climatic factors and corrosion of stained glass windows. *International Institute of Conservation Congress*, Conservation with Historic Buildings:93–95, 1980.

[17] W. L. Bragg. *Proceedings of Cambridge Philosophical Society*, 17:43–, 1913.

[18] D. Brewster. On the structure and optical phenomena of ancient decomposed glass. *Phil. Trans. R. Soc.*, 23:193–204, 1863.

[19] K. R. Briffa, P. D. Jones, T. M. L. Wigley, J. R. Pilcher, and M. G. L. Baillie. Climate reconstruction from tree rings: Part 1, Basic methodology and preliminary results for England. *Journal of Climatology*, 3:233–242, 1983.

[20] K. R. Briffa, P. D. Jones, T. M. L. Wigley, J. R. Pilcher, and M. G. L. Baillie. Climate reconstruction from tree rings: Part 2, Spatial reconstruction of summer mean sea-level pressure patterns over Great Britain. *Journal of Climatology*, 6:1–15, 1986.

[21] R. H. Brill. Ancient glass. *Scientific American*, 209:120–130, 1963.

[22] R. H. Brill. Scientific studies of stained glass. *Journal of Glass Studies*, 12:185–192, 1970.

[23] R. H. Brill. Crizzling–A problem in glass conservation. *International Institute of Conservation Congress*, Conservation in Archaeology and the Applied Arts:121–134, 1975.

[24] R. H. Brill and H. P. Hood. A new method of dating ancient glass. *Nature*, 189:12–14, 1961.

[25] N. Brown. Climate change and human history. Some indications from europe, AD400-1400. *Environmental Pollution*, 83:37–43, 1994.

[26] S. M. Budd and J. Frackiewiez. *Physics and Chemistry of Glasses*, 3:116, 1962.

[27] R. J. Charles. Static fatigue in glass. *Journal of Applied Physics*, 11:1549–1560, 1958.

[28] H. Chen and J. W. Park. Atmospheric attack at the surface of a sodium disilicate glass. *Physics and Chemistry of Glasses*, 22:39–42, 1981.

[29] H. H. Clayton. *World Weather Records*. Smithsonian Institute, 1944.

[30] R. Collongues and M. Perez-y-Jorba. Degradation of mediaeval stained glass and reactivity of solids. *Materials Science Monographs*, 28A:147–148, 1985.

[31] G. Cooper. Personal communication, 1993.

[32] G. A. Cox and G. I. Cooper. Stained glass in York in the mid-sixteenth century: analytical evbidence for its decay. *Glass Technology*, 36:129–134, 1995.

[33] G. A. Cox and B. A. Ford. The corrosion of glass on the sea bed. *Journal of Materials Science*, 24:3146–3153, 1989.

[34] G. A. Cox and B. A. Ford. The influence of inhomogeneities in glass on the morphology of the weathering layers. *Glass Technology*, 30:113–114, 1989.

[35] G. A. Cox and K. J. S. Gillies. The X-ray fluorescence analysis of mediaeval durable blue soda glass from York Minster. *Archaeometry*, 28:57–68., 1986.

[36] G. A. Cox, O. S. Heavens, R. G. Newton, and A. M. Pollard. A study of weathering behaviour of mediaeval glass from York Minster. *Journal of Glass Studies*, 21:54–75, 1979.

[37] G. A. Cox and A. R. Khooli. The natural corrosion of glass: the formation and structure of plugs. *Glass Technology*, 33:60–62, 1992.

[38] B. Cullity. *Elements of X-ray diffraction.* Addison-Wesley Inc., 1956.

[39] D'Eye and Wait. *X-ray powder photography in inorganic chemistry.* Butterworths, 1960.

[40] V. Dimbleby and W. E. S. Turner. Some experiments on the effects of humidity on the weathering of bottle glass. *Journal of Society of Glass Tcchnology*, 23:242T–252T, 1939.

[41] R. H. Doremus. *Glass Science.* John Wiley and Sons, 1973.

[42] R. W. Douglas and T. M. El-Shamy. Reactions of glasses with aqueous solutions. *Journal of American Ceramics Society*, 50:1–8, 1967.

[43] R. W. Douglas and S. O. Isard. Action of water and sulphur dioxide on glass surface. *Journal of Society of Glass Technology*, 33:289–335, 1949.

[44] T. M. El-Shamy. The rate determining step in the dealkalisation of silicate glasses. *Physics and Chemistry of Glasses*, 14:18–19, 1973.

[45] T. M. El-Shamy, J. Lewins, and R. W. Douglas. The dependence on the pH of the decomposition of glasses by aqueous solutions. *Glass Technology*, 13:81–87, 1972.

[46] F. M. Ersnberger. The role of molecular water in the diffusive transport of protons in glasses. *Physics and Chemistry of Glasses*, 21:146–149, 1980.

[47] V. C. Farmer. *The Infrared Spectra of Minerals.* Mineralogical Society, 1974.

[48] S. Fitz. Do air pollutants damage historic stained glass windows. *Proceedings of the Electrochemical Society*, 86:227–228, 1986.

[49] S. Fitz, E. Fitz-Ulrich, G. Frenzel, R. Krüger, and H. Kühn. Untersuchung der Einwirkung von Luftverunreinigungen auf Kunstwerke der Glasmalerei. *Deutsches Museum Munchen*, pages 1–48, 1983.

[50] S. Fitz, E. Fitz-Ulrich, G. Frenzel, R. Krüger, and H. Kühn. *Die Einwirkung von Luftverunreinigungen auf Ausgewählte Kunstwerke Mittelalterlicher Glasmalerei.* Bundesminister des Innern in Zusammenarbeit mit dem Deutschen Museum, 1992.

[51] I. Freestone. Theophilus and the compositon of mediaeval glass. *M.R.S.Proc.*, 267:793–746, 1993.

[52] R. W. Frei and J. D. MacNeil. *Diffuse Reflectance Spectroscopy in Environmental Problem Solving.* CRC Press, 1973.

[53] W. Friedrich, P. Knipping, and M. Laue. Interferenz-Erscheinungen bei Röntgenstrahlen. In *Biographical Memoirs of the Fellows of the Royal Society (1960)149*, pages 303–322. 1912.

[54] D. M. Gates. *Climate change and its biological consequences.* Sinauer Associates, 1993.

[55] W. V. Geilmann. Die chemische Zusammensetzung einiger alter Gläser, inbesondere deutscher Gläser des 10. bis 18. Jahrhunderts. *Glastechnische Berichte*, 28:146–156, 1955.

[56] W. V. Geilmann, H. J. Berthold, and G. Tolg. Beiträge zur Kenntnis alter Gläser V : Die Verwitterungsprodukte auf Fensterscheiben. *Glastechnische Berichte*, 33:213–219, 1960.

[57] P. Gibson. Our heritage of stained glass and its care in the C20. *Glass Technology*, 29:218–225, 1988.

[58] K. J. S. Gillies and G. A. Cox. Decay of mediaeval stained glass at York, Canterbury and Carlisle. Part 1 composition of the glass and its weathering products. *Glastechnische Berichte*, 61:75–84, 1988.

[59] K. J. S. Gillies and G. A. Cox. Decay of mediaeval stained glass at York, Canterbury and Carlisle. Part 2 relationship between the composition of the glass, its durability and the weathering products. *Glastechnische Berichte*, 61:101–107, 1988.

[60] V. M. Goldschmidt. Skrifter Norske Videnskaps Akad. *I.Math-Naturwiss. Kl.*, 1:7, 1926.

[61] J. I. Goldstein, D. E. Newbury, A. D. Ronig, C. E. Lyman, P. Echlin, D. C. Joy, C. Fiori, and E. Lifshin. *Scanning Electron Microscopy and X-Ray Microanalysis.* Plenum Press, 1992. 2nd Edition.

[62] P. R. Griffiths. *Chemical Infrared Fourier Transforn Spectroscopy.* John Wiley and Sons, 1975.

[63] J. G. Hawthorne and C. S. Smith. *Theophilus On Divers Arts.* Dover Publications, 1979.

[64] L. L. Hench, D. E. Clark, and S. Harker. A review-nuclear waste glasses. *Journal of Material Science*, 21:1457–1478, 1986.

[65] J. Hillam. A mediaeval oak tree-ring chronology from south-west England. *Tree-Ring Bulletin*, 40:13–22, 1980.

[66] A. P. Hudson and R. G. Newton. A means for the in-situ identification of mediaeval glass by the detection of its natural radioactivity. *Archaeometry*, 18:229–232, 1976.

[67] C. Iliffe and R. G. Newton. A simplified method for comparing compositions of mediaeval window glass samples from the point of view of their durability. *York Glaziers Trust Research Programme*, REF YG/74/1:1–7, 1974.

[68] C. J. Iliffe and R. G. Newton. Using triangular diagrams to understand the behaviour of mediaeval glasses. *Verres et Réfractaires*, 40:30–34, 1974.

[69] C. M. Jantzen and M. J. Plodinec. Thermodynamic model of natural, mediaeval and nuclear waste glass durability. *Journal of Non-Crystalline Solids*, 67:207–223, 1984.

[70] P. M. Kelly, M. A. R. Munro, M. K. Hughes, and C. M. Goodess. Climate and signature years in west European oaks. *Nature*, 340:57–60, 1989.

[71] C. Kittel. *Introduction to Solid State Physics*. J.Wiley and Sons, 5th edition, 1976.

[72] V. D. Korn. Causes and symptoms of the deterioration of mediaeval painted glass. *Deutsche Kunst und Denkmalpflege*, 29:58–74, 1971.

[73] W. Krumbein, C. Urzi, and C. Gehrmann. Biocorrosion and biodeterioration of antique and mediaeval glass. *Geomicrobiology*, 9:139–160, 1991.

[74] Warren Spring Laboratory. *National Survey of Air Pollution 1961-71*. HMSO, 1973. Volumes 1–5.

[75] V. C. LaMarche. Paleoclimatic inferences from long tree-ring records. *Science*, 183:1043–1048, 1974.

[76] H. H. Lamb. *Climate: Present, Past and Future. Volume 1: Fundamentals and Climate Now*. Metheun, 1977.

[77] H. H. Lamb. *Climatic History and the Future*. Metheun, 1977.

[78] H. H. Lamb. *Climate History and the Modern World*. Metheun, 1982.

[79] Lanford. Glass hydration: A method of dating glass objects. *Science*, 196:975–6, 1977.

[80] M. Laue. Eine quantitative Prüfung der Theorie fur die Interferenzerscheinungen bei Röntgenstrahlen. In *Fifty years of x-ray diffraction, P.P.Ewald (1962)48*, pages 363–373. 1912.

[81] L'Azaroff and M. J. Buerger. *The Powder Method.* McGraw-Hill, 1958.

[82] G. Libourel, P. Barbey, and M. Chaussidon. L'Àlteration des vitraux. *La Recherche*, 262, 1994.

[83] Link. *ZAF-4/FLS Operating Instructions SR2-500-Z4F-1083.* Link analytical, Halifax Road, High Wycombe, Bucks., HP12 3SE, 1989.

[84] A. K. Lyle. *Journal of American Ceramic Society*, 26:201, 1943.

[85] G. Manley. The range of variation of the british climate. *Geographical Journal*, 117:43–65, 1951.

[86] G. Manley. The mean temperature of central England, 1698-1952. *Quaternary Journal of Royal Meterological Society*, 79:242–261, 1953.

[87] R. Marks. *Stained Glass in England during the Middle Ages.* Routledge, 1993.

[88] H. Marschner. *Glaskonservierung: Historische Glasfenster und Ihre Erhaltung.* Bayerisches Landesamt fur Denkmalpflege, 1985. Arbeitsheft 32.

[89] Mattson. *Galaxy FTIR Spectrometer Series 2000, 4000, 6000 User's Manual.* Mattson Instruments, Madison, U.S.A, 1989.

[90] E. Mellor. Lichens and their action on glass. *Nature*, 112:299–300, 1923.

[91] J. L. Monteith and M. H. Unsworth. *Principles of Environmental Physics.* Edward Arnold, 2nd edition, 1990.

[92] W. V. Müller, H. Pouillon, G. Bochynek, and H. Mehner. Extreme Dunkelung von Glasmalereien. *Glastechnische Berichte*, 59:96–102, 1986.

[93] R. G. Newton. The enigma of the layered crusts on some weathered glasses; a chronological account of the investigations. *Archaeometry*, 13:1–9, 1971.

[94] R. G. Newton. Stereoscan views of weathering layers on a piece of ancient glass. *Glass Technology*, 13:54–56, 1972.

[95] R. G. Newton. The spontaneous fracturing of some mediaeval window glass. *International Congress on Glass, Kyoto (JAPAN)*, pages 1132–1138, 1974.

[96] R. G. Newton. Air pollution, sulphur dioxide and mediaeval glass. *CVMA Newsletter*, 15:9–13, 1975.

[97] R. G. Newton. The weathering of mediaeval window glass. *Journal of Glass Studies*, 17:161–168, 1975.

[98] R. G. Newton. Colouring agents used by mediaeval glassmakers. *Glass Technology*, 19:59–60, 1978.

[99] R. G. Newton. Recent views on ancient glasses. *Glass Technology*, 21:173–183, 1980.

[100] R. G. Newton. *Deterioration and Conservation of Painted Glass: A Critical Bibliography.* Oxford University Press, British Academy, 1982.

[101] R. G. Newton. The durability of glass — a review. *Glass Technology*, 26:21–38, 1986.

[102] R. G. Newton. Air pollution damage. *Professional Stained Glass*, Dec/Jan:14–21, 1988.

[103] R. G. Newton. Glass research at York Minster. *Glass*, May:181–182, 1989.

[104] R. G. Newton and S. Davison. *Conservation of Glass.* Butterworth's & Co, 1989.

[105] R. G. Newton and D. Fuchs. Chemical compositions and weathering of some mediaeval glasses from York Minster. Part 1. *Glass Technology*, 29:43–48, 1988.

[106] R. G. Newton and G. Shaw. Another unsolved problem concerning weathering layers. *Glass Technology*, 29:78–79, 1988.

[107] F. J. Nicholas and J. Glasspoole. *General monthly rainfall over England and Wales 1727 to 1931*, volume British Rainfall, pages 299–306. London, 1931.

[108] A. Paul. Chemical durability of glasses; a thermodynamic approach. *Journal of Materials Science*, 12:2246–2268, 1977.

[109] A. Paul. *Chemistry of Glasses.* Chapman Hall, 1 edition, 1982.

[110] M. Perez-y-Jorba. Corrosion atmospherique des vitraux medievaux - intervention du phosphore dans le processus d'altèration. *Glaskonservierung*, pages 56–59, 1984.

[111] M. Perez-y-Jorba, J. P. Dallas, C. Bauer, C. Bahzere, and J. C. Martin. Deterioration of stained glass by atmospheric corrosion and micro-organisms. *Journal of Materials Science*, 15:1640–1647, 1980.

[112] M. Perez-y-Jorba, J. P. Dallas, R. Collongues, C. Bahezre, and J. C. Martin. Étude de l'altération des vitraux anciens par microscopie électronique à balayage et microsonde. *Silicates Industriels*, 4:89–99, 1978.

[113] M. Perez-y-Jorba, G. Tilloca, D. Michel, and J. P. Dallas. Some aspects of the phenomena of ancient glass corrosion in french churches. *Verres et Réfractaires*, 29:53–62, 1975.

[114] N. Pevsner. *Nottinghamshire.* Penguin, 1951.

[115] N. Pevsner. *Cambridgeshire.* Penguin, 1954.

[116] N. Pevsner. *Northamptonshire.* Penguin, 1961.

[117] N. Pevsner. *Staffordshire.* Penguin, 1974.

[118] N. Pevsner and J. Harris. *Lincolnshire.* Penguin, 1964.

[119] A. M. Pollard. *X-Ray Fluorescence and Surface Studies of Glass, with Application to the Durability of Mediaeval Window Glass.* PhD thesis, University of York, 1979.

[120] E. A. Porai-Koshits. Structure of glass: The struggle of ideas and prospects. *Journal of non-Crystalline Solids*, 73:79–89, 1985.

[121] E. A. Porai-Koshits. Genesis of concepts on structure of inorganic glasses. *Journal of Non-Crystalline Solids*, 123:1–13, 1990.

[122] M. Prutton. *Introduction to Surface Physics.* Oxford Science Publications, 1994.

[123] J. C. Russ. *Fundamentals of Energy Dispersive X-Ray Analysis.* Butterworths Monographs in Materials, 1984.

[124] D. M. Sanders and L. L. Hench. Mechanisms of glass corrosion. *Journal of American Ceramics Society*, 56:373–377, 1973.

[125] D. M. Sanders, W. B. Person, and L. L. Hench. New methods for studying glass corrosion kinetics. *Applied Spectroscopy*, 26:530–536, 1972.

[126] D. C. Sanderson and J. B. Hutchings. The origins and measurement of colour in archaeolgical glasses. *Glass Technology*, 28:99–105, 1987.

[127] H. Scholze. Chemical durability of glasses. *Journal of Non-Crystalline Solids*, 52:91–103, 1982.

[128] H. Scholze. *Glass; Nature, Structure and Properties.* Springer-Verlag, 1990. Translated from German by M.J.Larkin.

[129] M. Schreiner. Analytical investigations of mediaeval glass paintings. *Recent Advances in the Conservation and Analysis of Artefacts*, pages 73–80, 1987.

[130] M. Schreiner. Deterioration of stained mediaeval glass by atmospheric attack: Part 1. Scanning electron microscopic investigations of the weathering products. *Glastechnische Berichte*, 61:197–204, 1988.

[131] M. Schreiner. Deterioration of stained mediaeval glass by atmospheric attack: Part 2. Secondary ion mass spectrometry analysis of the naturally weathered glass surfaces. *Glastechnische Berichte*, 61:223–230, 1988.

[132] M. Schreiner. Glass of the past; the degradation and deterioration of mediaeval glass artifacts. *Mikrochimica Acta*, 2:255–264, 1991.

[133] V. Scott and G. Love. *Quantitative Electron-Probe Microanalysis.* Wiley and Sons, 1983.

[134] F. G. Smith and J. H. Thomson. *Optics.* J.Wiley and Sons, 2nd edition, 1988.

[135] J. M. Stevels. New light on the structure of glass. *Phillips Technical Review*, 22:300–311, 1960.

[136] F. W. Taylor. The greenhouse effect and climatic change. *Reports on Progress in Physics*, 54:881–918, 1991.

[137] AEA Technology. Uk emissions of air pollutants 1970-1991. world wide web site: /airqual/emissions/den-naei.html, 1995.

[138] J. H. van der Maas. *Basic Infrared Spectroscopy.* Heyden and Son, 1969.

[139] D. Verey. *Gloucestershire and the Cotswolds.* Penguin, 1969.

[140] B. E. Warren. *Journal of Applied Physics*, 8:645, 1937.

[141] B. E. Warren and J. Biscoe. *Journal of American Ceramic Society*, 21:49, 1938.

[142] A. H. Webb, R. J. Bawden, A. K. Busby, and J. N. Hopkins. Studies on the effects of air pollution on limestone degradation in great britain. *Atmospheric Environment*, 26B:165–181, 1992.

[143] W. A. Weyl. Copper in copper-ruby glasses. *Journal of Society of Glass Technology*, 29:375–387, 1945.

[144] W. H. Zachariasen. The atomic arrangement in glass. *Journal of American Chemical Society*, 54:3841–3851, 1932.

Appendix A

Derivations

A.1 Kubelka-Munk Function

When a plane parallel layer of thickness d is irradiated diffusely with a monochromatic beam of intensity I_o, the radiation flow in the x-direction can be represented by I, and the radiation flow in in the negative x-direction by J[52]. An infinitesimally thin layer, dx, parallel to the surface is penetrated by the radiation in all possible directions with respect to the normal. The average path of the radiation $d\phi$, therefore is not dx but

$$d\phi_I = dx \int_0^{\frac{\pi}{2}} \frac{\delta I d\varphi}{I \delta\varphi \cos\varphi} \equiv u dx \tag{A.1}$$

or

$$d\phi_J = dx \int_0^{\frac{\pi}{2}} \frac{\delta J d\varphi}{J \delta\varphi \cos\varphi} \equiv v dx \tag{A.2}$$

where $\frac{\delta I}{\delta\varphi}$ and $\frac{\delta J}{\delta\varphi}$ stand for the angular distribution of the radiation.

Assuming conditions for ideal diffuse radiation,

$$\frac{\delta I}{\delta\varphi} = I \sin 2\varphi \tag{A.3}$$

with a similar expression for $\frac{\delta J}{\delta\varphi}$, where $u = v = 2$. This factor is included in the scattering coefficient and the absorption coefficient. The component kIdx of I is adsorbed in the layer dx while the component sIdx is scattered backward. The radiation J in the negative x-direction contributes sJdx by scattering in the positive x-direction. The change in intensity of I in the layer dx, therefore, is composed of the following elements:

$$dI = -(k+s)Idx + sJdx \tag{A.4}$$

By analogy, the decrease in intensity of J is

$$dJ = (k+s)Jdx - sIdx \tag{A.5}$$

These are the basic differential equations that describe the adsorption and scattering processes. The indefinite integrals are:

$$I = A(1-\beta)e^{\sigma x} + B(1+\beta)e^{-\sigma x} \tag{A.6}$$

$$J = A(1+\beta)e^{\sigma x} + B(1-\beta)e^{-\sigma x} \tag{A.7}$$

with

$$\sigma \equiv \sqrt{K(K+2S)} \tag{A.8}$$

and

$$\beta \equiv \frac{\sigma}{K+2S} = \sqrt{\frac{K}{(K+2S)}} \tag{A.9}$$

The constants A and B are determined by the limiting conditions. If one integrates for the entire thickness,d, of the layer the conditions

for

$$X = O : I = I_o \tag{A.10}$$

and for

$$X = d : I = I_{x=d}; J = 0 \tag{A.11}$$

are valid, and one obtains

$$A = -\frac{(1-\beta)e^{-\sigma d}}{(1+\beta)^2 e^{\sigma d} - (1-\beta)^2 e^{-\sigma d}} I_o \tag{A.12}$$

$$B = \frac{(1+\beta)e^{\sigma d}}{(1+\beta)^2 e^{\sigma d} - (1-\beta)^2 e^{-\sigma d}} I_o \tag{A.13}$$

The transmission of the layer is therefore given by

$$T = \frac{I_{x=d}}{I_o} = \frac{4\beta}{(1+\beta)^2 e^{\sigma d} - (1-\beta)^2 e^{-\sigma d}} = \frac{2\beta}{(1+\beta)^2 \sin h\sigma d + 2\beta \cos h\sigma d} \tag{A.14}$$

and the diffuse reflectance by

$$R = \frac{I_{x=0}}{I_o} = \frac{(1-\beta)^2(e^{\sigma d} - e^{-\sigma d})}{(1+\beta)^2 e^{\sigma d} - (1-\beta)^2 e^{-\sigma d}} = \frac{(1-\beta)^2 \sin h\sigma d}{(1+\beta)^2 \sin h\sigma d + 2\beta \cos h\sigma d} \tag{A.15}$$

For $s = 0$ (non-scattering layer) and $\beta = 1$, Equation A.13 becomes Bouguer-Lambert's Law $T = e^{-kd}$, and R' becomes zero.

For infinite layer thickness, d approaches 0 and one obtains R'_∞

$$R'_\infty = \frac{1-\beta)}{1+\beta} = \frac{S+K-\sqrt{K(K+2S)}}{S} \tag{A.16}$$

These conditions are achieved experimentally with 1mm layers of fine powders and R'_∞ can therefore be measured. Equation A.16 can be transformed to a more convenient form

$$\frac{(1-R'_\infty)^2}{2R'_\infty} = \frac{k}{s} \tag{A.17}$$

A.2 ZAF equation

In 1951 Castaing proposed this method of analysis, that is the comparison of unknown characteristic x-ray lines with those of a known standard. Thus if all the spectrometer parameters are fixed we need only to consider the different electron and x-ray behaviour in specimen and standard respectively. Suppose we consider a binary specimen containing elements A and B where the mass concentration of A is to be measured by reference to a standard consisting of the pure element A[133]. The intensity of the primary x-ray emission is given by:-

$$I = \phi(\Delta\rho z)\int_0^\infty \phi(\rho z)\exp(-\chi\rho z)d\rho z, \tag{A.18}$$

where $\phi(\Delta\rho z)$ corresponds to the emission from an isolated thin film of mass thickness $\Delta\rho z$. The total emitted x-ray intensity including any fluorescence contributions is then

$$I = \phi(\Delta\rho z)\int_0^\infty \phi(\rho z)\exp(-\chi\rho z)d\rho z(1+\gamma+\delta) \tag{A.19}$$

where the fluorescence correction factor $(1+\gamma+\delta)$ has γ as the ratio of the intensity of fluorescence emission to the primary characteristic x-ray emission and δ as the corresponding ratio for the continuum fluorescence contribution.

$$I = \phi(\Delta\rho z)\int_0^\infty \phi(\rho z)d\rho z f(\chi)(1+\gamma+\delta), \tag{A.20}$$

where the absorption factor is $f(\chi)$,

$$f(\chi) = \frac{\int_0^\infty \phi(\rho z)\exp(-\chi\rho z)d\rho z}{\int_0^\infty \phi(\rho z)d\rho z} \tag{A.21}$$

The ratio of x-ray intensities (characteristic A radiation) emitted from specimen AB and standard A is given by

$$\frac{I_A^{AB}}{I_A^A} = \frac{\phi(\Delta\rho z)_A^{AB}}{\phi(\Delta\rho z)_A^A}\frac{\int_0^\infty[\phi(\rho z)d\rho z]_A^{AB}}{\int_0^\infty[\phi(\rho z)d\rho z]_A^A}\frac{f(\chi)_A^{AB}}{f(\chi)_A^A}\frac{(1+\gamma+\delta)_A^{AB}}{(1+\gamma+\delta)_A^A} \tag{A.22}$$

Now it may be shown as follows that

$$\frac{\phi(\Delta\rho z)_A^{AB}}{,\phi(\Delta\rho z)_A^A} = c_A, \tag{A.23}$$

where c_A is the mass concentration of element A in specimen AB. Consider an isolated thin film of element AB of mass thickness $d\rho z$. Then the number of A atoms per unit area is $(\frac{Nc_A}{A})d\rho z$, where N is Avogadro's number. The number of ionisations produced by a given flux of electrons will be proportional to $Q(\frac{Nc_A}{A})d\rho z$ and the number of x-rays subsequently generated will be proportional to $Q\omega(\frac{Nc_A}{A})d\rho z$. Hence the intensity ratio of x-rays from isolated thin films of AB and A of the same mass thickness is given by,

$$\frac{Q\omega(\frac{Nc_A}{A})d\rho z}{Q\omega(\frac{N}{A})d\rho z} = c_A \tag{A.24}$$

The integral terms correspond to the areas under the respective $\phi(\rho z)$ curves and their ratio may be replaced by 'A' to denote the absorption correction factor while 'F' may be used to represent the ratio of the fluorescence terms, that is, $\frac{I_A^{AB}}{I_A^A} = c_A$'Z''A''F', and it may be seen that each of the correction factors for the specimen AB/ standard A can be treated separately.

Appendix B

Compositional Data Tables

This appendix contains chemical compostional data for each of the glasses analysed, in a tabular form. The tables are presented in the following order:-

- Stanford
- Fledborough
- Ely
- Meysey Hampton
- Heckington
- Fairford
- Checkley

Each table is divided into three parts; weight percent of oxide, molar percent of oxide and other. The weight and molar percent figures are quoted to one decimal place. The section labelled 'other' contains parameters calculated from the composition; the ternary co-ordinates as fractional mol% (to 1d.p.); the free energy of hydration, $-\Delta G$kcal/mol (to 1d.p.) and the number of non-bridged oxygen atoms (to 2sig.fig.).

Throughout the tables *nd* represents not determined.

	Label	scb1	scb2	scb3	scb4	scb5	scb6	fle1	fle2	fle3
weight percent	Na_2O	1.3	2.9	2.7	2.8	2.9	4.1	2.2	1.9	2.4
	MgO	5.2	6.7	6.4	6.5	6.6	8.2	5.8	5.2	5.7
	Al_2O_3	1.9	1.6	1.3	1.6	1.6	1.1	1.9	1.7	1.9
	SiO_2	52.7	54.8	55.1	55.5	55.2	53.1	53.0	52.8	52.9
	P_2O_5	5.5	4.6	4.5	4.5	4.3	3.7	4.9	4.6	4.8
	K_2O	17.6	15.5	15.8	15.2	15.5	10.9	15.2	15.9	15.1
	CaO	13.2	11.3	11.6	11.2	11.3	16.1	14.8	15.7	14.8
	MnO	0.8	1.3	1.2	1.1	1.2	1.4	0.8	0.8	0.8
	Fe_2O_3	0.6	0.3	0.5	0.4	0.4	0.6	0.6	0.5	0.6
	S	nd	nd	nd	nd	nd	nd	0.1	0.1	0.1
	Cl	nd	nd	nd	nd	nd	nd	nd	nd	nd
	CuO	nd	nd	nd	nd	nd	nd	nd	nd	nd
	PbO	nd	nd	nd	nd	nd	nd	nd	nd	nd
molar percent	Na_2O	1.4	2.93	2.78	2.85	2.93	4.06	2.25	1.95	2.49
	MgO	8.32	10.5	10.1	10.2	10.4	12.4	9.5	8.32	8.8
	Al_2O_3	1.23	0.97	0.84	0.99	0.96	0.68	1.16	1.01	1.15
	SiO_2	56.8	57.8	58.1	58.6	58.2	54.1	56.1	56.1	56.0
	P_2O_5	2.52	2.04	2.02	2.01	1.9	1.61	2.2	2.1	2.13
	K_2O	12.1	10.4	10.6	10.2	10.4	7.1	10.3	10.8	10.2
	CaO	15.3	12.8	13.1	12.6	12.7	17.5	16.7	17.9	16.9
	MnO	0.73	1.12	1.06	1.02	1.09	1.22	0.68	0.69	0.71
	Fe_2O_3	0.24	0.14	0.19	0.17	0.17	0.22	0.23	0.21	0.25
	S	nd	nd	nd	nd	nd	nd	0.22	0.18	0.25
	Cl	nd	nd	nd	nd	nd	nd	nd	nd	nd
	CuO	nd	nd	nd	nd	nd	nd	nd	nd	nd
	PbO	nd	nd	nd	nd	nd	nd	nd	nd	nd
other	'SiO_2'	62.9	62.8	62.9	63.6	63.1	58.1	61.7	61.4	61.6
	'R_2O'	12.3	12.4	12.5	12.1	12.3	10.5	11.3	11.6	11.4
	'RO'	24.8	24.8	24.6	24.3	24.6	31.4	26.9	27.0	26.9
	$-\Delta$ G	9.5	8.9	8.8	8.6	8.7	9.1	9.3	9.4	9.3
	NBO	0.68	0.69	0.69	0.68	0.69	0.79	0.71	0.72	0.72

Table B.1: Composition of the samples from Stanford and three from Fledborough. NBO is the number of non-bridged oxygen atoms and $-\Delta G$ is expressed in kcal/mol.

	Label	fbs1	fbs2	fbs3	fbs4	fbs5	fbs6	fbs7	fbs8	fbn1	fbn3
weight percent	Na_2O	0.4	0.5	0.4	0.6	0.4	0.5	0.6	0.6	0.55	0.7
	MgO	4.4	4.2	4.2	4.6	4.2	4.2	4.8	4.7	4.2	3.8
	Al_2O_3	1.9	1.5	1.8	2.4	1.7	1.6	2.7	2.7	1.5	2.3
	SiO_2	46.8	47.6	46.5	48.3	46.7	48.0	47.6	47.1	47.9	49.3
	P_2O_5	5.9	5.9	5.7	4.6	5.8	5.7	4.8	4.7	3.3	2.8
	K_2O	11.7	12.9	11.8	16.6	11.9	12.7	14.5	14.7	16.8	15.5
	CaO	27.5	26.0	28.3	21.1	28.1	25.6	23.3	23.5	24.4	23.2
	MnO	0.2	0.1	0.1	0.6	0.1	0.2	0.7	0.8	0.4	0.3
	Fe_2O_3	0.7	0.6	0.7	0.6	0.7	0.6	0.5	0.7	0.4	0.9
	S	nd	0.13	nd	0.12	nd	0.2	nd	nd	0.1	nd
	Cl	nd	nd	nd	nd	nd	0.36	nd	nd	nd	nd
	CuO	nd	nd	nd	nd	nd	nd	nd	nd	nd	nd
	PbO	nd	nd	nd	0.14	0.25	nd	nd	nd	nd	nd
molar percent	Na_2O	0.36	0.52	0.45	0.66	0.35	0.5	0.6	0.62	0.65	0.72
	MgO	6.87	6.67	6.5	7.29	6.64	6.64	7.6	7.49	6.69	5.92
	Al_2O_3	1.2	0.95	1.14	1.49	1.01	0.99	1.7	1.7	0.89	1.39
	SiO_2	49.2	50.2	48.9	51.6	49.1	50.4	50.4	49.9	50.1	51.6
	P_2O_5	2.6	2.6	2.5	2.1	2.6	2.5	2.2	2.11	1.5	1.24
	K_2O	7.9	8.7	7.9	11.3	8.0	8.5	9.8	9.9	11.1	10.3
	CaO	31.0	29.4	31.8	24.1	31.6	28.9	26.5	26.8	27.8	26.0
	MnO	0.17	0.11	0.13	0.57	nd	0.15	0.66	0.73	0.36	0.24
	Fe_2O_3	0.27	0.25	0.27	0.24	0.27	0.25	0.19	0.26	0.14	0.36
	S	nd	0.26	nd	0.23	nd	0.3	nd	nd	0.33	nd
	Cl	nd	nd	nd	nd	nd	0.64	nd	nd	nd	nd
	CuO	nd	nd	nd	nd	nd	nd	nd	nd	nd	nd
	PbO	nd	nd	nd	0.04	0.07	nd	nd	nd	nd	nd
other	'SiO_2'	54.8	55.4	54.4	57.7	54.4	56.1	56.5	56.2	53.9	57.6
	'R_2O'	6.8	8.1	7.0	10.1	7.1	7.8	8.5	8.6	10.9	9.5
	'RO'	38.3	36.4	38.6	32.2	38.5	36.1	35.0	35.2	35.2	33.0
	-Δ G	10.5	10.5	10.6	10.6	10.6	10.2	10.5	10.7	10.9	9.8
	NBO	0.85	0.84	0.86	0.81	0.86	0.82	0.82	0.83	0.88	0.81

Table B.2: Composition of the samples from Fledborough. NBO is the number of non-bridged oxygen atoms and $-\Delta G$ is expressed in kcal/mol.

	Label	ely3	ely4	ely5	ely6	ely7	ely8	ely9	ely10	ely11	ely12	ely13
weight percent	Na_2O	1.5	1.5	2.6	2.6	0.5	2.5	0.6	1.0	1.0	0.8	1.7
	MgO	4.0	4.4	7.7	7.5	4.7	4.6	4.5	4.3	3.9	4.3	3.9
	Al_2O_3	0.8	1.1	0.6	0.7	1.1	2.2	1.5	1.3	1.2	3.3	2.4
	SiO_2	46.8	43.4	52.6	52.7	46.9	54.9	46.8	45.7	45.8	45.5	36.4
	P_2O_5	2.7	6.9	4.4	4.2	6.6	4.6	5.3	6.9	6.6	4.7	3.8
	K_2O	15.8	15.9	16.9	16.9	16.1	13.8	14.9	14.9	14.8	16.0	14.0
	CaO	26.4	25.1	13.1	13.2	22.0	15.0	24.1	24.0	23.1	23.3	15.4
	MnO	1.1	0.3	0.7	0.4	0.9	0.7	1.1	0.4	0.9	0.3	0.1
	Fe_2O_3	0.4	0.9	0.5	0.2	0.5	0.2	0.3	0.3	0.3	0.2	0.1
	S	0.4	0.2	0.2	0.5	0.2	0.2	0.3	0.3	0.3	0.2	0.1
	Cl	nd	0.2	0.5	nd	nd	0.44	nd	nd	nd	nd	0.38
	CuO	nd	nd	nd	nd	nd	nd	nd	nd	nd	nd	nd
	PbO	nd	nd	nd	nd	nd	nd	nd	nd	nd	nd	nd
molar percent	Na_2O	1.5	1.4	2.6	2.6	0.5	2.6	0.6	1.1	1.0	0.8	1.7
	MgO	6.2	7.0	11.9	11.7	7.6	7.3	7.5	6.9	6.1	6.9	6.1
	Al_2O_3	0.5	0.7	0.4	0.4	0.7	1.4	0.9	0.8	0.7	2.1	1.5
	SiO_2	48.7	46.5	54.9	55.1	50.2	58	49.5	48.9	48.9	48.8	39.9
	P_2O_5	1.2	3.1	1.9	1.9	3.0	2.1	2.4	3.2	2.9	2.2	1.7
	K_2O	10.5	10.9	11.3	11.3	11.0	9.3	10.0	10.2	10.1	10.9	9.5
	CaO	29.4	28.8	14.7	14.7	25.3	17.0	27.3	27.5	28.7	26.7	17.5
	MnO	0.9	0.3	0.7	0.7	0.9	0.6	0.9	0.4	0.2	0.6	0.6
	Fe_2O_3	0.2	0.4	0.2	0.1	0.2	0.3	0.2	0.3	0.3	0.3	0.3
	S	0.8	0.5	0.4	0.3	0.5	0.4	0.5	0.5	0.6	0.5	0.3
	Cl	nd	0.3	0.8	nd	nd	0.8	nd	nd	nd	nd	0.7
	CuO	nd	nd	nd	nd	nd	nd	nd	nd	nd	nd	nd
	PbO	nd	nd	nd	nd	nd	nd	nd	nd	nd	nd	nd
other	'SiO_2'	51.6	52.2	58.5	58.9	55.4	64.2	54.4	54.6	54.5	56.0	63.9
	'R_2O'	11.5	11.3	13.5	13.5	10.6	10.4	9.6	10.3	10.1	9.5	9.5
	'RO'	36.9	36.5	27.9	27.6	33.9	25.4	35.9	35.0	35.1	34.5	24.6
	$-\Delta G$	11.17	12.4	9.89	9.82	11.39	8.41	11.0	11.6	11.5	11.1	7.75
	NBO	0.93	0.89	0.78	0.78	0.83	0.67	0.86	0.84	0.84	0.83	0.64

Table B.3: Composition of the samples from Ely. NBO is the number of non-bridged oxygen atoms and $-\Delta G$ is expressed in kcal/mol.

	Label	gmh1	gmh2	gmh3	gmh4	gmh5	gmh6	gmh7	gmh8	gmh9	gmh10
weight percent	Na_2O	2.3	1.9	2.6	2.9	2.1	2.2	2.7	2.2	2.2	2.5
	MgO	6.6	5.9	7.3	5.8	7.2	5.4	7.2	7.0	7.4	6.8
	Al_2O_3	1.8	1.2	1.0	1.8	1.3	1.4	1.0	1.3	1.2	0.6
	SiO_2	56.2	52.5	51.6	56.3	51.3	54.3	51.8	51.9	49.3	36.6
	P_2O_5	4.1	5.2	5.4	3.8	6.2	5.3	5.2	6.1	6.6	3.8
	K_2O	12.4	17	14.5	13.5	14.9	17.8	14.5	14.7	15.7	14.9
	CaO	13.4	13.3	14.5	13.6	14.7	11.6	14.5	14.2	15.2	12.2
	MnO	0.9	1.0	1.9	0.8	1.4	0.8	1.9	1.4	1.4	1.3
	Fe_2O_3	0.8	0.9	0.4	0.5	0.4	0.5	0.3	0.5	0.3	0.5
	S	0.07	0.09	0.09	0.08	0.15	nd	nd	0.12	0.11	0.09
	Cl	nd	nd	0.4	0.5	0.3	0.4	0.4	0.4	0.4	0.5
	CuO	0.44	nd	nd	nd	nd	nd	nd	nd	nd	nd
	PbO	nd	nd	nd	nd	nd	nd	nd	nd	nd	nd
molar percent	Na_2O	2.34	2.02	2.61	2.99	2.19	2.36	2.76	2.28	2.27	2.56
	MgO	10.2	9.49	11.4	9.09	11.2	8.56	11.2	11.1	11.7	10.5
	Al_2O_3	1.1	0.75	0.65	1.1	0.83	0.87	0.62	0.78	0.77	0.35
	SiO_2	58.6	56.1	54.1	58.8	54.1	58.3	54.3	54.8	52.1	58.9
	P_2O_5	1.85	2.32	2.39	1.68	2.73	2.39	2.32	2.69	2.97	1.69
	K_2O	8.23	11.6	9.7	8.98	10.04	12.2	9.72	9.86	10.6	9.89
	CaO	15.0	15.2	16.3	15.2	16.6	13.4	16.2	16.0	17.2	13.6
	MnO	0.88	0.95	1.69	0.68	1.24	0.76	1.74	1.21	1.24	1.11
	Fe_2O_3	0.33	0.35	0.13	0.2	0.16	0.21	0.11	0.18	0.11	0.18
	S	0.14	nd	0.18	0.16	0.28	0.12	0.11	0.24	0.21	0.19
	Cl	0.82	nd	0.69	0.9	0.05	0.8	0.65	0.7	nd	0.87
	CuO	0.35	nd	nd	nd	nd	nd	nd	nd	nd	nd
	PbO	nd	nd	nd	nd	nd	nd	nd	nd	nd	nd
other	'SiO_2'	63.9	61.2	58.7	63.7	59.4	63.5	58.7	59.9	57.3	62.2
	'R_2O'	9.3	12.8	11.7	10.9	11.4	13.6	11.8	11.4	12.1	12.0
	'RO'	26.8	26.1	29.6	25.6	29.2	23.1	29.5	28.7	30.6	23.6
	-ΔG	7.9	9.6	9.9	8.1	9.9	9.4	9.9	9.7	10.8	8.4
	NBO	0.68	0.72	0.77	0.68	0.73	0.68	0.78	0.74	0.79	0.71

Table B.4: Composition of the samples from Meysey Hampton. NBO is the number of non-bridged oxygen atoms and $-\Delta G$ is expressed in kcal/mol.

	Label	gmh11	gmh12	gmh13	gmh14	gmh15	gmh16	gmh17	gmh18	gmh19
weight percent	Na_2O	2.7	1.1	1.2	1.0	2.8	3.1	2.7	4.0	4.0
	MgO	5.0	5.8	5.9	5.0	5.9	6.0	5.9	7.7	7.9
	Al_2O_3	1.9	1.6	1.6	1.2	1.6	1.8	1.6	1.5	1.5
	SiO_2	53.1	51.2	50.7	53.5	53.9	55.4	54.0	52.7	52.5
	P_2O_5	5.1	3.8	3.7	4.6	4.6	3.8	4.6	4.6	4.8
	K_2O	15.1	15.8	15.6	18.6	14.6	14.0	14.7	10.5	10.6
	CaO	14.6	15.2	15.3	13.2	14.3	13.7	14.2	15.7	15.5
	MnO	0.9	0.9	0.8	1.1	0.8	0.8	0.7	1.2	1.1
	Fe_2O_3	0.6	0.7	0.7	0.7	0.5	0.6	0.6	0.9	0.9
	S	0.07	nd	nd	nd	nd	0.05	nd	0.09	0.09
	Cl	0.5	0.4	0.4	0.5	0.4	0.4	0.4	0.5	0.5
	CuO	0.4	2.8	2.9	nd	nd	nd	nd	nd	nd
	PbO	nd	0.6	0.8	0.2	nd	nd	nd	0.3	0.3
molar percent	Na_2O	2.79	1.1	1.3	1.0	2.8	3.1	2.75	4.0	4.0
	MgO	8.02	9.2	9.4	8.1	9.3	9.4	9.3	11.8	12.1
	Al_2O_3	1.21	1.0	1.0	0.8	0.9	1.0	0.9	0.8	0.9
	SiO_2	56.5	54.5	54.0	57.5	56.8	57.9	56.9	54.2	54.1
	P_2O_5	2.28	1.7	1.65	2.1	2.0	1.7	2.1	2.0	2.1
	K_2O	10.3	10.7	10.6	12.7	9.8	9.4	9.88	6.9	6.9
	CaO	16.6	17.3	17.4	15.2	16.1	15.4	16.0	17.3	17.1
	MnO	0.81	0.7	0.79	0.9	0.78	0.67	0.6	1.0	1.0
	Fe_2O_3	0.24	0.28	0.29	0.28	0.2	0.2	0.2	0.3	0.3
	S	0.15	nd	nd	nd	nd	0.1	nd	0.1	0.2
	Cl	0.82	0.68	0.73	0.9	0.79	0.8	0.8	0.9	0.9
	CuO	nd	2.3	2.4	nd	nd	nd	nd	nd	nd
	PbO	nd	0.1	0.2	0.08	nd	nd	nd	0.09	0.09
other	'SiO_2'	62.3	59.3	58.9	62.3	61.8	62.9	62.0	59.4	59.3
	'R_2O'	11.8	10.8	10.6	12.9	11.6	11.4	11.5	9.8	9.9
	'RO'	25.9	29.8	30.4	24.6	26.6	25.7	26.5	30.6	30.7
	$-\Delta G$	9.2	9.0	9.1	9.4	9.0	8.5	9.0	8.9	9.0
	NBO	0.70	0.77	0.78	0.70	0.72	0.70	0.71	0.76	0.76

Table B.5: Composition of the samples from Meysey Hampton. NBO is the number of non-bridged oxygen atoms and $-\Delta G$ is expressed in kcal/mol.

	Label	lhe1	lhe2	lhe3	lhe4	lhe5	lhe6	lhe7	lhe8	lhe9
weight percent	Na_2O	3.9	1.7	1.9	2.7	1.5	2.4	1.6	1.4	1.9
	MgO	7.7	6.0	5.8	5.5	6.0	6.3	6.1	6.1	6.1
	Al_2O_3	1.1	1.7	2.3	2.1	1.7	2.4	1.7	1.7	1.3
	SiO_2	52.9	52.6	51.9	50.1	51.9	54.3	53.4	53.7	50.8
	P_2O_5	4.9	4.2	4.5	5.4	3.9	4.2	3.4	3.5	4.3
	K_2O	11.5	16.1	16.6	17.8	16.5	14.9	15.1	14.9	18.5
	CaO	14.9	14.5	14.4	13.7	16.1	12.8	16.3	15.9	12.3
	MnO	0.9	1.1	0.9	0.9	0.9	1.0	0.9	0.9	1.3
	Fe_2O_3	0.7	0.7	0.7	0.7	0.6	0.8	0.5	0.6	0.5
	S	0.1	0.1	0.1	0.1	0.07	0.07	0.09	0.06	nd
	Cl	0.5	0.4	0.5	0.4	0.4	0.5	0.4	0.4	0.4
	CuO	nd	0.3	nd	nd	nd	nd	nd	0.4	2.2
	PbO	0.5	0.3	nd	nd	0.2	nd	nd	nd	nd
molar percent	Na_2O	3.9	1.7	1.9	2.7	1.5	2.5	1.6	1.4	1.9
	MgO	11.9	9.5	9.1	8.8	9.4	9.9	9.6	9.6	9.7
	Al_2O_3	0.6	1.1	1.5	1.3	1.1	1.5	1.0	1.1	0.8
	SiO_2	54.7	55.7	55.3	54.1	54.8	57.3	55.8	56.2	54.5
	P_2O_5	2.1	1.8	2.0	2.4	1.7	1.8	1.5	1.5	1.9
	K_2O	7.6	10.9	11.3	12.3	11.1	10.0	10.0	9.9	12.7
	CaO	16.5	16.5	16.5	15.9	18.2	14.5	18.2	17.9	14.2
	MnO	0.8	0.9	0.8	0.8	0.8	0.9	0.9	0.8	1.2
	Fe_2O_3	0.3	0.3	0.3	0.3	0.3	0.3	0.2	0.3	0.2
	S	0.2	0.3	0.2	0.2	0.2	0.1	0.2	0.1	nd
	Cl	0.9	0.8	0.9	0.6	0.8	0.9	0.7	0.7	0.8
	CuO	nd	0.2	nd	nd	nd	nd	nd	0.4	1.7
	PbO	0.1	0.1	nd	nd	0.06	nd	nd	nd	nd
other	'SiO_2'	59.4	61.2	61.7	60.6	59.8	63.5	60.3	60.9	59.2
	'R_2O'	10.8	11.4	11.7	13.5	11.5	10.8	10.6	10.3	13.8
	'RO'	29.8	27.4	26.5	25.9	28.7	25.7	29.1	28.8	26.9
	-Δ G	9.1	9.2	9.5	10.4	9.6	8.6	8.9	8.8	9.9
	NBO	0.76	0.74	0.72	0.74	0.76	0.68	0.76	0.74	0.77

Table B.6: Composition of the samples from Heckington. NBO is the number of non-bridged oxygen atoms and $-\Delta G$ is expressed in kcal/mol.

	Label	lhe10	lhe11	lhe12	lhe13	lhe14	lhe15	lhe16	lhe17
weight percent	Na_2O	1.7	1.9	2.0	2.3	3.4	1.4	3.5	1.8
	MgO	5.9	5.6	6.9	5.4	8.2	5.9	7.6	6.3
	Al_2O_3	1.7	1.8	1.6	1.6	0.7	1.8	1.2	1.4
	SiO_2	51.5	51.5	49.0	53.1	54.6	52.3	52.5	49.6
	P_2O_5	4.3	4.8	4.3	4.5	4.6	3.5	5.5	5.0
	K_2O	17.0	16.4	16.2	15.4	13.3	15.5	14.7	18.5
	CaO	14.5	14.3	17.2	14.7	13.4	15.8	11.9	12.8
	MnO	0.9	1.0	1.4	1.3	0.7	0.9	0.9	1.1
	Fe_2O_3	0.7	1.0	0.5	0.5	0.2	0.7	0.4	0.6
	S	nd	nd	nd	nd	nd	nd	nd	nd
	Cl	0.3	0.4	0.4	0.4	0.5	0.4	0.5	0.4
	CuO	1.1	0.4	nd	nd	nd	1.2	0.9	1.9
	PbO	nd	0.5	0.3	nd	0.1	0.4	0.3	0.5
molar percent	Na_2O	1.7	1.9	2.0	2.3	3.4	1.4	3.6	1.9
	MgO	9.4	8.9	10.8	8.5	12.6	9.3	11.9	10.2
	Al_2O_3	1.0	1.2	0.9	0.9	0.4	1.1	0.7	0.9
	SiO_2	54.9	55.2	51.5	56.4	56.2	55.2	55.2	53.5
	P_2O_5	1.9	2.2	1.9	2.0	1.9	1.6	2.4	2.3
	K_2O	11.6	11.2	10.8	10.4	8.7	10.4	9.8	12.7
	CaO	16.5	16.4	19.3	16.7	14.8	17.8	13.4	14.8
	MnO	0.8	0.9	1.4	1.1	0.6	0.8	0.8	0.9
	Fe_2O_3	0.3	0.4	0.2	0.2	0.09	0.3	0.2	0.2
	S	nd	nd	nd	nd	nd	nd	nd	nd
	Cl	0.7	0.8	0.7	0.7	0.8	0.7	0.9	0.7
	CuO	0.9	0.4	nd	nd	nd	0.98	0.7	1.5
	PbO	nd	0.1	0.08	nd	0.03	0.1	0.09	0.2
other	'SiO_2'	59.9	60.9	56.3	61.3	59.6	60.3	60.0	58.6
	'R_2O'	11.9	11.8	11.9	11.8	11.7	10.8	12.9	13.6
	'RO'	28.0	27.1	31.8	26.9	28.7	28.9	27.1	27.8
	-Δ G	9.7	9.5	10.6	9.2	9.0	9.0	9.6	10.3
	NBO	0.75	0.73	0.83	0.73	0.76	0.76	0.74	0.78

Table B.7: Composition of the samples from Heckington. NBO is the number of non-bridged oxygen atoms and $-\Delta G$ is expressed in kcal/mol.

	Label	lhe18	lhe19	lhe20	lhe21	lhe22	lhe23	lhe24	lhe25
weight percent	Na_2O	3.8	2.2	2.9	2.0	3.3	3.3	1.8	1.4
	MgO	8.2	6.2	7.1	6.2	8.4	7.9	5.7	5.9
	Al_2O_3	5.4	1.7	1.0	1.3	0.9	0.6	1.7	1.7
	SiO_2	53.7	53.6	53.1	50.8	55.2	54.9	52.9	52.4
	P_2O_5	4.8	3.7	4.9	4.4	4.4	4.9	3.9	3.9
	K_2O	14.3	14.6	16.1	18.1	12.5	13.6	15.6	16.6
	CaO	13.1	14.7	13.1	12.1	13.0	13.3	15.1	15.9
	MnO	0.7	0.9	0.7	1.3	0.9	0.6	0.9	0.8
	Fe_2O_3	0.2	1.0	0.3	0.6	0.4	0.2	1.0	0.6
	S	0.04	nd	nd	0.1	0.1	0.1	0.1	0.1
	Cl	0.5	0.4	0.4	0.4	0.5	0.4	0.4	0.4
	CuO	nd	nd	nd	2.15	nd	0.03	nd	nd
	PbO	nd	0.6	nd	nd	nd	nd	0.5	nd
molar percent	Na_2O	3.8	2.2	2.9	2.1	3.3	3.3	1.8	1.4
	MgO	12.5	9.7	11.1	9.9	12.8	12.3	9.1	9.3
	Al_2O_3	0.3	1.0	0.6	0.85	0.6	0.4	1.1	1.1
	SiO_2	55.5	56.4	55.8	54.5	56.7	56.7	56.1	55.3
	P_2O_5	2.1	1.7	2.2	2.0	1.9	2.2	1.7	1.8
	K_2O	9.4	9.8	10.8	12.4	8.2	8.9	10.3	11.1
	CaO	14.5	16.6	14.7	13.9	14.3	14.7	17.2	17.9
	MnO	0.7	0.8	0.6	1.2	0.8	0.5	0.8	0.7
	Fe_2O_3	0.06	0.4	0.1	0.3	0.1	0.08	0.4	0.2
	S	0.08	nd	nd	0.2	0.2	0.2	0.2	0.2
	Cl	0.9	0.8	0.7	0.8	0.9	0.8	0.7	0.7
	CuO	nd	nd	nd	1.74	nd	0.02	nd	nd
	PbO	nd	0.2	nd	nd	nd	nd	0.1	nd
other	'SiO_2'	58.9	61.6	60.1	59.3	60.6	60.3	61.5	60.3
	'R_2O'	13.2	10.6	13.1	13.5	10.8	11.8	10.9	11.3
	'RO'	27.9	27.8	26.9	27.1	28.4	27.9	27.5	28.4
	-Δ G	9.5	8.8	9.7	9.8	8.7	9.1	9.1	9.5
	NBO	0.77	0.73	0.75	0.77	0.74	0.74	0.73	0.75

Table B.8: Composition of the samples from Heckington. NBO is the number of non-bridged oxygen atoms and $-\Delta G$ is expressed in kcal/mol.

	Label	fai1	fai2	fai3	fai4	fai5	fai6	fai7	fai8	fai9	fai10
weight percent	Na_2O	2.2	3.6	3.5	3.1	2.9	2.5	2.1	2.5	3.8	2.9
	MgO	3.2	4.3	3.7	6.2	6.7	3.7	3.2	3.7	4.9	3.4
	Al_2O_3	2.2	1.4	1.7	1.4	1.2	2.2	3.9	2.2	1.6	1.8
	SiO_2	60.3	60.4	59.4	57.7	57.4	59.1	55.4	59.9	59.0	63.2
	P_2O_5	3.2	3.3	3.4	3.3	3.9	3.2	3.5	3.5	3.3	3.2
	K_2O	5.3	3.3	4.3	12.3	12.7	5.2	6.7	5.2	2.6	5.0
	CaO	21.0	21.4	20.4	10.9	12.7	21.5	21.9	20.2	22.1	17.4
	MnO	0.9	0.5	0.9	0.8	1.1	0.9	2.0	1.2	0.6	0.9
	Fe_2O_3	0.7	0.4	1.5	0.8	0.8	0.5	0.5	0.5	0.5	1.18
	S	0.18	0.3	nd	nd	0.1	nd	nd	nd	0.3	0.08
	Cl	0.39	0.6	0.6	0.4	0.4	0.5	0.4	0.6	0.5	0.5
	CuO	nd	nd	nd	2.7	nd	nd	nd	nd	nd	nd
	PbO	nd	0.2	nd	nd	nd	nd	nd	nd	0.24	0.13
molar percent	Na_2O	2.17	3.53	3.49	3.09	2.92	2.48	2.09	2.44	3.67	2.93
	MgO	4.73	6.36	5.59	9.7	10.3	5.64	4.94	5.59	7.34	5.22
	Al_2O_3	1.38	0.81	1.03	0.85	0.73	1.3	2.38	1.35	0.94	1.09
	SiO_2	61.6	60.5	60.5	60.3	59.5	59.9	57.3	61.1	58.8	64.6
	P_2O_5	1.38	1.38	1.47	1.4	1.7	1.4	1.6	1.5	1.4	1.4
	K_2O	3.46	2.12	2.84	8.2	8.38	3.36	4.45	3.4	1.66	3.29
	CaO	23	22.9	22.3	12.2	14.1	23.4	24.3	22.1	23.6	19.0
	MnO	0.79	0.51	0.74	0.65	0.94	0.78	1.76	1.03	0.54	0.83
	Fe_2O_3	0.26	0.16	0.57	0.32	0.29	0.23	0.19	0.22	0.19	0.45
	S	0.35	0.53	nd	nd	0.2	nd	nd	nd	0.6	0.15
	Cl	0.67	1.01	1.17	0.86	0.77	0.98	0.78	0.98	0.98	0.89
	CuO	nd	nd	nd	2.14	nd	nd	nd	nd	nd	nd
	PbO	nd	0.05	nd	nd	nd	nd	nd	nd	0.06	0.03
other	'SiO_2'	66.7	64.4	65.8	64.6	63.8	65.0	64.6	66.4	63.1	69.6
	'R_2O'	4.19	4.88	4.94	10.3	10.5	4.52	4.17	4.47	4.4	4.8
	'RO'	29.0	30.3	29.1	25.1	25.9	30.5	31.5	29.15	32.1	25.6
	$-\Delta G$	5.76	5.92	6.03	7.05	7.79	6.16	6.99	5.89	4.20	4.99
	NBO	0.63	0.67	0.64	0.67	0.68	0.66	0.67	0.63	0.69	0.57

Table B.9: Composition of the samples from Fairford. NBO is the number of non-bridged oxygen atoms and $-\Delta G$ is expressed in kcal/mol.

	Label	fai11	fai12	fai13	fai14	fai15	fai16	fai17	fai18	fai19	fai20
weight percent	Na_2O	3.4	3.2	3.7	2.6	2.7	2.4	0.8	2.2	2.7	3.2
	MgO	3.6	3.5	6.4	3.5	2.6	2.6	3.6	2.4	6.3	6.4
	Al_2O_3	1.7	1.6	0.8	1.0	2.9	2.8	1.5	2.8	1.6	1.1
	SiO_2	59.4	61.5	52.8	60.8	62.9	60.5	54.4	61.9	56.8	57.5
	P_2O_5	3.5	3.2	3.9	3.9	2.7	3.2	1.4	2.9	3.7	3.7
	K_2O	4.7	4.9	14.1	5.8	4.6	5.3	17.7	5.5	14.5	12.1
	CaO	20.5	19.1	13.4	19.5	19.7	21.2	18.4	20.3	12.3	11.9
	MnO	0.9	0.9	0.9	1.0	0.4	0.4	1.4	0.4	0.7	1.7
	Fe_2O_3	1.5	1.3	0.4	0.4	0.5	0.5	0.4	0.6	0.6	0.6
	S	nd	0.1	0.2	0.2	0.2	0.1	0.2	0.1	0.1	0.2
	Cl	0.6	0.6	0.5	0.6	0.7	0.6	0.1	0.6	0.4	0.4
	CuO	nd	nd	2.4	nd	nd	nd	nd	nd	nd	1.4
	PbO	nd	nd	nd	nd	nd	nd	nd	nd	nd	0.6
molar percent	Na_2O	3.37	3.13	3.8	2.6	2.6	2.3	0.8	2.2	2.8	3.2
	MgO	5.4	5.24	9.9	5.3	3.9	4.1	5.6	3.6	9.7	9.9
	Al_2O_3	1.01	0.95	0.5	0.6	1.7	1.7	0.9	1.7	1	0.7
	SiO_2	60.6	62.6	55.1	61.9	63.9	61.8	57.2	63.4	59.5	59.8
	P_2O_5	1.51	1.38	1.7	1.7	1.2	1.4	0.6	1.3	1.7	1.7
	K_2O	3.05	3.15	9.4	3.8	2.9	3.5	11.8	3.6	9.7	8.1
	CaO	22.4	20.8	15.0	21.2	21.4	23.2	20.8	22.3	13.7	13.3
	MnO	0.78	0.78	0.9	0.9	0.3	0.4	1.3	0.4	0.6	0.6
	Fe_2O_3	0.56	0.51	0.2	0.2	0.2	0.2	0.2	0.2	0.2	0.2
	S	nd	0.2	0.4	0.4	0.3	0.2	0.4	0.2	0.1	0.4
	Cl	1.07	1.1	0.9	1.0	1.3	1.1	0.2	1.0	0.8	0.7
	CuO	nd	nd	1.9	nd	nd	nd	nd	nd	nd	1.1
	PbO	nd	nd	nd	nd	nd	nd	nd	nd	nd	0.1
other	' SiO_2'	65.8	67.5	58.8	65.8	69.6	67.5	60.6	69.1	64.2	64.0
	'R_2O'	5.0	5.0	12.7	5.8	3.8	4.1	11.8	4.0	11.4	10.6
	'RO'	29.1	27.3	28.2	28.0	26.2	28.2	28.2	26.8	24.7	25.3
	$-\Delta G$	6.10	5.50	9.01	5.98	4.83	5.63	8.87	5.18	8.13	7.42
	NBO	0.64	0.61	0.77	0.63	0.57	0.61	0.78	0.58	0.68	0.68

Table B.10: Composition of the samples from Fairford. NBO is the number of non-bridged oxygen atoms and $-\Delta G$ is expressed in kcal/mol.

	Label	fai21	fai22	fai23	fai24	fai25	fai26	fai27	fai28	fai29	fai30
weight percent	Na_2O	0.9	1.7	3.6	1.9	2.1	2.5	2.8	3.4	2.4	0.7
	MgO	3.1	3.2	5.7	3.3	3.3	3.6	3.8	5.6	2.8	3.7
	Al_2O_3	1.0	2.1	1.3	2.3	3.4	1.7	1.9	1.3	3.4	3.4
	SiO_2	54.1	58.8	57.3	60.8	57.2	59.4	59.5	55.9	59.4	59.1
	P_2O_5	1.8	3.6	3.1	3.2	2.6	3.2	2.9	3.2	2.8	1.1
	K_2O	19.9	5.9	10.6	5.1	7.7	5.2	3.9	10.7	6.9	13.6
	CaO	16.9	22.6	14.7	20.8	20.7	22.2	22.5	15.2	20.0	15.8
	MnO	0.3	0.5	0.8	0.9	1.1	0.9	1.0	0.8	0.6	1.7
	Fe_2O_3	0.2	0.2	0.4	0.8	1.0	0.4	0.5	0.5	0.5	0.4
	S	0.2	0.2	nd	0.2	nd	0.8	0.1	0.7	nd	0.1
	Cl	nd	0.3	0.4	0.4	0.4	0.4	0.6	0.5	0.7	nd
	CuO	nd	nd	1.6	nd	nd	nd	nd	2.1	nd	nd
	PbO	nd	nd	0.3	nd	0.2	nd	nd	0.4	nd	nd
molar percent	Na_2O	0.9	1.7	3.6	1.9	2.1	2.4	2.8	3.5	2.4	0.7
	MgO	4.9	4.9	8.8	5.1	5.0	5.5	5.8	8.7	4.4	5.8
	Al_2O_3	0.6	1.3	0.79	1.4	2.0	1.0	1.1	0.8	2.1	2.1
	SiO_2	57.7	60.0	59.0	61.9	59.2	60.3	59.8	57.9	61.1	61.8
	P_2O_5	0.8	1.5	1.4	1.4	1.1	1.4	1.2	1.4	1.2	0.5
	K_2O	13.6	3.8	6.9	3.3	5.1	3.3	2.5	7.1	4.6	9.1
	CaO	19.3	24.7	16.2	22.7	22.9	24.1	24.2	16.8	22.1	17.8
	MnO	1.3	0.8	0.7	0.7	0.9	0.8	0.8	0.7	0.5	1.5
	Fe_2O_3	0.1	0.2	0.2	0.3	0.4	0.2	0.2	0.2	0.2	0.2
	S	0.5	0.5	nd	0.3	nd	0.2	0.3	0.1	nd	0.3
	Cl	nd	0.5	0.8	0.8	0.8	0.7	1.0	0.8	1.1	nd
	CuO	nd	nd	1.3	nd	nd	nd	nd	1.7	nd	nd
	PbO	nd	nd	0.08	nd	0.06	nd	nd	0.01	nd	nd
other	' SiO_2'	60.5	64.9	62.9	67.4	65.8	64.6	64.6	62.0	67.4	66.9
	'R_2O'	13.7	4.3	9.7	3.8	4.9	4.6	4.1	9.7	4.9	7.5
	'RO'	25.7	30.8	27.4	28.8	29.3	30.7	31.3	28.3	27.7	25.4
	-ΔG	9.35	6.35	7.40	5.56	6.48	6.24	6.03	7.57	5.95	6.56
	NBO	0.77	0.66	0.71	0.61	0.66	0.67	0.67	0.72	0.61	0.64

Table B.11: Composition of the samples from Fairford. NBO is the number of non-bridged oxygen atoms and $-\Delta G$ is expressed in kcal/mol.

	Label	fai31	fai32	fai33	fai34	fai35	fai36	fai37	fai38	fai39	fai40
weight percent	Na_2O	2.3	1.1	2.7	1.5	2.4	1.1	2.6	2.3	2.2	2.6
	MgO	3.7	4.4	3.7	3.0	3.7	3.8	2.8	3.0	3.7	3.6
	Al_2O_3	1.8	2.0	1.9	1.5	1.7	3.3	3.2	1.9	1.5	1.7
	SiO_2	57.8	48.4	60.1	56.9	58.0	54.3	60.1	60.5	57.9	59.3
	P_2O_5	2.9	3.8	2.3	2.0	3.1	1.6	2.8	2.9	3.1	3.3
	K_2O	5.8	12.1	4.5	11.3	5.4	13.7	6.7	4.9	6.0	4.7
	CaO	22.8	25.7	22.2	22.0	23.2	18.7	19.7	21.9	22.9	22.6
	MnO	0.9	1.4	1.1	0.8	1.1	2.1	0.5	0.9	0.9	0.8
	Fe_2O_3	0.8	0.5	0.6	0.5	0.5	0.7	0.6	0.6	0.9	0.6
	S	nd	0.1	0.1	nd	0.1	0.1	nd	0.2	0.2	0.1
	Cl	0.5	nd	0.5	0.3	0.5	0.2	0.7	0.5	0.5	0.5
	CuO	nd	nd	nd	nd	nd	nd	nd	nd	nd	nd
	PbO	0.3	0.2	nd	nd	nd	0.1	nd	0.3	0.1	nd
molar percent	Na_2O	2.3	1.2	2.6	1.5	2.3	1.1	2.6	2.2	2.2	2.6
	MgO	5.7	6.9	5.6	4.7	5.5	5.9	4.3	4.6	5.3	5.3
	Al_2O_3	1.1	1.2	1.1	0.9	1.0	2.0	1.9	1.1	0.9	0.9
	SiO_2	58.8	50.4	60.4	58.8	58.8	57.1	61.8	61.5	58.8	60.0
	P_2O_5	1.3	1.7	0.9	0.9	1.3	0.7	1.2	1.2	1.3	1.4
	K_2O	3.8	8.1	2.9	7.5	3.5	9.2	4.4	3.2	3.9	3.0
	CaO	24.9	28.7	23.9	24.3	25.1	21.0	21.7	23.8	24.9	24.3
	MnO	0.8	1.2	0.9	0.7	0.9	1.9	0.4	0.8	0.8	0.7
	Fe_2O_3	0.3	0.2	0.2	0.2	0.2	0.3	0.2	0.2	0.4	0.2
	S	nd	0.2	0.3	nd	0.2	0.1	nd	0.3	0.3	0.2
	Cl	0.8	nd	0.9	0.5	0.8	0.4	1.1	0.8	0.8	0.8
	CuO	nd	nd	nd	nd	nd	nd	nd	nd	nd	nd
	PbO	0.09	0.05	nd	nd	nd	0.04	nd	0.07	0.03	nd
other	' SiO_2'	63.2	54.9	64.7	62.4	63.0	62.6	67.9	66.0	63.2	64.3
	'R_2O'	4.9	8.1	4.3	7.8	4.8	7.9	5.1	4.3	4.8	4.6
	'RO'	31.8	36.9	31.0	29.8	31.9	29.4	26.9	29.7	31.8	30.9
	-ΔG	6.64	10.1	5.83	7.56	6.59	7.94	5.76	5.74	6.69	6.25
	NBO	0.69	0.86	0.68	0.74	0.7	0.73	0.6	0.64	0.69	0.67

Table B.12: Composition of the samples from Fairford. NBO is the number of non-bridged oxygen atoms and $-\Delta G$ is expressed in kcal/mol.

	Label	fai41	fai42	fai43	fai44	fai45	fai46	fai47	fai48	fai49
weight percent	Na_2O	2.9	2.3	3.7	2.6	2.1	2.3	2.3	2.3	2.3
	MgO	3.7	2.7	6.6	3.6	2.8	3.6	3.7	2.9	3.2
	Al_2O_3	2.1	1.8	1.2	1.5	3.4	1.7	1.9	3.1	2.0
	SiO_2	59.3	57.8	52.7	59.1	57.9	58.1	57.8	58.4	62.4
	P_2O_5	3.3	3.2	3.9	3.3	2.9	3.1	2.9	2.9	2.8
	K_2O	4.5	5.9	13.6	4.8	5.9	5.9	5.9	5.5	4.9
	CaO	21.9	22.6	13.7	22.5	22.8	22.5	22.8	22.2	20.2
	MnO	0.7	1.0	0.9	0.9	0.6	0.9	0.9	0.6	0.9
	Fe_2O_3	0.5	0.9	0.6	0.6	0.6	0.8	0.9	0.6	0.7
	S	0.2	0.1	0.1	0.1	nd	0.2	0.1	nd	0.1
	Cl	0.6	0.5	0.4	0.5	0.6	0.4	0.5	0.6	0.5
	CuO	nd	nd	2.4	nd	nd	nd	nd	nd	nd
	PbO	0.2	nd	0.1	nd	nd	nd	nd	nd	nd
molar percent	Na_2O	2.8	2.3	3.7	2.5	2.1	2.2	2.3	2.3	2.2
	MgO	5.6	5.7	10.2	5.5	4.2	5.5	5.6	4.5	4.8
	Al_2O_3	1.2	1.0	0.7	0.9	2.0	1.0	1.1	1.9	1.2
	SiO_2	59.9	58.8	55.2	59.9	59.4	59.1	58.7	59.8	63.4
	P_2O_5	1.4	1.4	1.7	1.4	1.3	1.3	1.3	1.2	1.2
	K_2O	2.9	3.8	9.0	3.1	3.8	3.9	3.8	3.6	3.1
	CaO	23.8	24.6	15.4	24.4	25.0	24.5	24.9	24.3	21.9
	MnO	0.6	0.9	0.9	0.7	0.5	0.8	0.8	0.5	0.8
	Fe_2O_3	0.2	0.3	0.2	0.2	0.3	0.3	0.3	0.2	0.3
	S	0.3	0.2	0.2	0.2	nd	0.4	0.2	nd	0.3
	Cl	1.0	0.8	0.7	0.9	1.1	0.7	0.8	0.9	0.8
	CuO	nd	nd	1.9	nd	nd	nd	nd	nd	nd
	PbO	0.05	nd	0.03	nd	nd	nd	nd	nd	nd
other	'SiO_2'	64.6	63.4	59.4	64.2	66.1	63.8	63.4	63.7	68.4
	'R_2O'	4.6	4.9	11.9	4.9	3.7	5.0	4.8	3.9	4.3
	'RO'	30.6	31.6	28.6	30.9	30.2	31.2	31.8	30.3	27.3
	$-\Delta G$	6.1	6.7	8.9	6.3	6.2	6.6	6.6	6.1	5.2
	NBO	0.66	0.69	0.77	0.68	0.65	0.69	0.69	0.65	0.60

Table B.13: Composition of the samples from Fairford. NBO is the number of non-bridged oxygen atoms and $-\Delta G$ is expressed in kcal/mol.

	Label	fai50	fai51	fai52	fai53	fai54	fai55	fai56	fai57	fai58
weight percent	Na_2O	2.5	0.8	0.9	0.9	0.8	2.9	2.1	2.1	0.7
	MgO	3.7	3.4	3.2	3.2	3.4	3.9	3.4	2.9	3.8
	Al_2O_3	1.7	1.9	1.6	2.0	1.7	1.9	1.6	3.2	3.5
	SiO_2	58.4	53.8	54.6	55.0	54.1	59.9	60.0	58.1	59.5
	P_2O_5	3.1	2.0	1.9	2.2	1.9	2.5	2.4	3.0	1.1
	K_2O	5.4	16.0	17.7	16.1	16.0	3.9	4.9	6.1	13.4
	CaO	22.8	19.9	17.9	18.2	19.9	22.1	23.1	21.8	15.3
	MnO	1.1	1.3	1.5	1.3	1.2	1.0	1.0	0.8	1.7
	Fe_2O_3	0.5	0.3	0.3	0.6	0.3	0.5	0.5	0.8	0.4
	S	0.1	0.2	nd	nd	0.1	0.1	0.2	nd	0.1
	Cl	0.5	0.1	nd	0.1	0.1	0.6	0.4	0.6	0.1
	CuO	0.09	0.2	nd	nd	nd	nd	0.1	nd	nd
	PbO	nd	nd	nd	0.2	nd	nd	nd	nd	0.1
molar percent	Na_2O	2.4	0.8	0.9	0.9	0.8	2.8	2.0	2.1	0.7
	MgO	5.5	5.4	5.0	5.1	5.4	5.9	5.1	4.5	5.9
	Al_2O_3	0.9	1.1	1.0	1.3	1.1	1.1	0.9	1.9	2.1
	SiO_2	59.2	56.6	57.9	58.3	56.9	60.1	60.5	59.8	62.3
	P_2O_5	1.3	0.9	0.9	0.9	0.9	1.1	1.1	1.3	0.5
	K_2O	3.5	10.7	11.9	10.9	10.8	2.5	3.2	4.0	8.9
	CaO	24.7	22.4	20.3	20.7	22.5	23.8	24.9	24.1	17.2
	MnO	0.9	1.2	1.3	1.1	1.1	0.9	0.9	0.7	1.5
	Fe_2O_3	0.2	0.1	0.1	0.2	0.1	0.2	0.2	0.3	0.2
	S	0.2	0.4	nd	nd	0.3	0.3	0.4	nd	0.3
	Cl	0.9	0.2	nd	0.2	0.2	0.1	0.7	1.0	0.2
	CuO	0.06	0.2	nd	nd	nd	nd	0.1	nd	nd
	PbO	nd	nd	nd	0.05	nd	nd	nd	nd	0.04
other	'SiO_2'	63.5	60.4	61.3	62.3	60.6	64.5	64.4	66.3	67.8
	'R_2O'	4.9	10.3	11.8	10.3	10.5	4.4	4.2	3.9	7.5
	'RO'	31.7	29.3	26.8	27.4	28.9	31.1	31.4	29.7	24.7
	-ΔG	6.5	8.8	8.9	8.4	8.8	5.9	5.9	6.2	6.4
	NBO	0.69	0.77	0.75	0.73	0.77	0.68	0.68	0.64	0.63

Table B.14: Composition of the samples from Fairford. NBO is the number of non-bridged oxygen atoms and $-\Delta G$ is expressed in kcal/mol.

	Label	fai59	fai60	fai61	fai62	fai63	fai64	fai65	fai66
weight percent	Na_2O	1.2	2.6	2.3	2.2	2.4	2.4	0.8	2.5
	MgO	3.5	3.6	3.8	3.1	3.2	2.8	3.5	3.8
	Al_2O_3	2.1	1.6	1.5	1.8	1.9	3.2	1.9	1.6
	SiO_2	57.9	58.6	58.0	60.7	60.3	59.6	54.0	57.9
	P_2O_5	2.1	3.4	3.1	3.0	3.2	3.1	1.9	3.1
	K_2O	12.5	4.9	5.9	5.1	5.1	7.2	15.8	5.9
	CaO	18.6	22.8	22.5	21.7	21.6	19.6	19.7	22.3
	MnO	1.1	0.9	0.9	0.8	0.9	0.5	1.4	0.9
	Fe_2O_3	0.6	0.5	0.9	0.5	0.5	0.6	0.3	0.9
	S	0.1	0.3	0.1	0.2	0.1	nd	0.2	0.1
	Cl	0.1	0.5	0.5	0.5	0.5	0.6	nd	0.5
	CuO	nd	nd	nd	nd	nd	nd	nd	nd
	PbO	nd	0.1	nd	0.1	nd	nd	0.2	nd
molar percent	Na_2O	1.2	2.5	2.3	2.2	2.4	2.4	0.8	2.4
	MgO	5.5	5.4	5.7	4.7	4.9	4.4	5.5	5.8
	Al_2O_3	1.3	0.9	0.9	1.1	1.1	1.9	1.2	0.9
	SiO_2	60.3	59.3	58.9	61.7	61.3	61.5	56.8	58.9
	P_2O_5	0.9	1.5	1.3	1.3	1.4	1.3	0.9	1.3
	K_2O	8.3	3.2	3.9	3.3	3.3	4.7	10.6	3.8
	CaO	20.7	24.7	24.5	23.6	23.5	21.7	22.2	24.3
	MnO	1.0	0.8	0.8	0.7	0.7	0.4	1.2	0.8
	Fe_2O_3	0.2	0.2	0.4	0.2	0.2	0.2	0.1	0.4
	S	0.2	0.5	0.3	0.3	0.3	nd	0.4	0.2
	Cl	0.2	0.8	0.8	0.8	0.8	1.1	nd	0.9
	CuO	nd	nd	nd	nd	nd	nd	nd	nd
	PbO	nd	0.04	nd	0.03	nd	nd	0.05	nd
other	'SiO_2'	64.5	63.6	63.4	66.3	65.9	67.8	60.6	63.5
	'R_2O'	8.3	4.8	5.0	4.3	4.3	4.9	10.4	4.9
	'RO'	27.2	31.5	31.5	29.4	29.7	26.9	29.0	31.4
	$-\Delta G$	7.2	6.46	6.6	5.7	5.9	5.9	8.7	6.7
	NBO	0.69	0.68	0.69	0.64	0.64	0.6	0.76	0.69

Table B.15: Composition of the samples from Fairford. NBO is the number of non-bridged oxygen atoms and $-\Delta G$ is expressed in kcal/mol.

	Label	chn1	chn2	chn3	chn4	chn5	chn6	chn7	chn8	chn9	chn10
weight percent	Na_2O	3.3	2.0	5.3	2.0	3.6	3.2	3.4	2.0	4.8	1.9
	MgO	7.7	6.2	8.2	6.1	7.9	7.6	7.4	6.0	7.6	5.9
	Al_2O_3	1.0	1.4	1.3	1.5	1.3	1.0	1.4	1.5	1.2	1.5
	SiO_2	53.1	47.7	52.6	48.3	53.9	53.1	55.2	48.9	52.0	48.8
	P_2O_5	4.3	6.3	4.9	6.2	5.4	4.2	4.8	5.9	4.7	5.9
	K_2O	15.7	19.2	12.3	19.2	12.5	15.9	12.1	18.6	12.8	18.7
	CaO	12.7	14.1	12.8	13.8	13.2	12.8	13.4	14.3	13.7	14.2
	MnO	0.9	0.9	1.1	0.9	1.1	1.0	1.0	0.9	1.0	0.9
	Fe_2O_3	0.3	0.7	0.5	0.5	0.2	0.3	0.3	0.7	0.5	0.7
	S	0.1	0.1	nd	nd	nd	0.1	0.1	0.1	0.3	0.1
	Cl	0.4	0.4	0.5	0.4	0.5	0.4	0.5	0.4	0.5	0.3
	CuO	nd	nd	nd	nd	nd	nd	nd	nd	nd	nd
	PbO	0.3	0.6	nd	0.6	nd	0.2	nd	nd	0.4	nd
molar percent	Na_2O	3.4	2.1	5.4	2.2	3.6	3.3	3.4	2.1	4.8	2.0
	MgO	11.9	9.99	12.7	9.9	12.3	11.8	11.4	9.7	11.8	9.6
	Al_2O_3	0.6	0.9	0.8	0.9	0.8	0.6	0.8	0.9	0.7	0.9
	SiO_2	55.5	51.8	54.4	52.4	55.8	55.5	57.2	52.8	53.9	52.8
	P_2O_5	1.9	2.9	2.1	2.9	2.4	1.9	2.1	2.7	2.0	2.7
	K_2O	10.5	13.3	8.1	13.3	8.3	10.6	7.9	12.8	8.5	12.9
	CaO	14.2	16.4	14.2	16.1	14.7	14.3	14.9	16.5	15.3	16.5
	MnO	0.9	0.9	0.9	0.9	1.0	0.9	0.9	0.8	0.9	0.9
	Fe_2O_3	0.1	0.3	0.2	0.2	0.08	0.1	0.1	0.3	0.2	0.3
	S	0.1	0.2	nd	nd	nd	0.1	0.2	0.2	0.6	0.2
	Cl	0.8	0.8	0.9	0.7	0.9	0.7	0.8	0.6	0.9	0.6
	CuO	nd	nd	nd	nd	nd	nd	nd	nd	nd	nd
	PbO	0.1	0.2	nd	0.2	nd	0.1	nd	nd	0.1	nd
other	'SiO_2'	59.5	57.7	59.1	58.2	60.5	59.5	61.8	58.6	58.4	58.7
	'R_2O'	13.3	14.5	12.7	14.5	11.3	13.3	10.6	13.9	12.5	13.9
	'RO'	27.4	27.9	28.3	27.3	28.5	27.6	27.6	27.8	28.5	27.7
	$-\Delta G$	9.66	11.40	9.52	11.30	9.10	9.62	8.51	10.90	9.51	10.99
	NBO	0.77	0.78	0.77	0.77	0.74	0.77	0.71	0.77	0.77	0.77

Table B.16: Composition of the samples from Checkley. NBO is the number of non-bridged oxygen atoms and $-\Delta G$ is expressed in kcal/mol.

	Label	chn11	chn12	chn13	chn14	chn15	chn16	chn17	chn18	chn19	chn20
weight percent	Na_2O	2.5	3.1	2.5	1.8	5.2	3.6	2.8	5.1	3.2	2.9
	MgO	6.3	7.2	6.4	5.1	8.2	7.2	7.1	8.1	6.8	6.7
	Al_2O_3	1.3	0.7	1.5	1.9	1.2	1.5	0.6	1.3	1.3	1.5
	SiO_2	52.6	51.7	52.8	47.4	52.7	53.7	51.5	52.3	54.0	50.9
	P_2O_5	4.7	4.4	4.6	5.8	4.8	5.6	4.5	4.8	5.3	5.4
	K_2O	14.7	15.1	14.9	17.7	12.6	12.9	15.5	12.8	12.9	14.8
	CaO	14.4	15.6	14.2	14.2	12.9	13.4	15.9	13.1	13.9	15.2
	MnO	0.9	0.9	0.9	0.9	1.1	1.0	0.9	1.0	1.1	1.0
	Fe_2O_3	1.0	nd	0.9	1.3	0.4	0.4	0.3	0.4	0.4	1.0
	S	nd	0.07	0.08	0.1	0.1	nd	0.1	0.1	0.1	0.08
	Cl	0.3	0.4	0.4	0.3	0.5	0.4	0.3	0.5	0.5	0.4
	CuO	nd	0.2	nd	0.3	0.2	nd	nd	0.2	0.1	nd
	PbO	0.7	nd	0.4	3.1	nd	nd	nd	nd	0.2	nd
molar percent	Na_2O	2.6	3.1	2.5	1.9	5.2	3.6	2.9	5.1	3.3	2.99
	MgO	9.9	11.2	10.1	8.5	12.5	11.3	11.0	12.5	10.6	10.6
	Al_2O_3	0.8	0.5	0.9	1.29	0.7	0.9	0.4	0.8	0.8	0.9
	SiO_2	55.7	53.9	55.9	52.7	54.4	56.1	53.7	54.1	56.4	53.8
	P_2O_5	2.1	1.9	2.1	2.7	2.1	2.5	1.9	2.1	2.3	2.4
	K_2O	9.9	10.1	10.1	12.5	8.3	8.6	10.3	8.4	8.6	9.9
	CaO	16.4	17.4	16.1	16.9	14.3	14.9	17.8	14.5	15.7	17.1
	MnO	0.8	0.8	0.8	0.8	0.9	0.9	0.8	0.9	0.9	0.9
	Fe_2O_3	0.4	nd	0.4	0.6	0.2	0.2	0.1	0.2	0.2	0.2
	S	nd	0.15	0.2	0.2	0.2	nd	0.3	0.2	0.2	0.2
	Cl	0.6	0.6	0.6	0.6	0.9	0.8	0.6	0.9	0.8	0.8
	CuO	nd	0.2	nd	0.3	0.1	nd	nd	0.2	0.1	nd
	PbO	0.02	nd	0.1	0.9	nd	nd	nd	nd	0.07	nd
other	'SiO_2'	60.9	57.5	61.2	59.7	58.9	61.3	57.3	58.7	61.2	59.0
	'R_2O'	11.4	12.8	11.4	12.7	12.7	11.2	12.8	12.7	10.9	11.9
	'RO'	27.7	29.9	27.5	26.9	28.2	27.5	30.0	28.4	27.8	29.0
	$-\Delta G$	9.29	10.03	9.24	10.6	9.54	9.11	10.20	9.61	8.95	9.99
	NBO	0.74	0.81	0.73	0.75	0.77	0.72	0.81	0.77	0.72	0.76

Table B.17: Composition of the samples from Checkley. NBO is the number of non-bridged oxygen atoms and $-\Delta G$ is expressed in kcal/mol.

	Label	chn21	chn22	chn23	chn24	chn25	chn26	chn27	chn28	chn29	chn30
weight percent	Na_2O	6.1	2.7	2.0	3.1	3.2	6.3	3.3	1.4	5.9	3.3
	MgO	8.8	7.1	6.0	6.9	7.6	8.9	6.9	5.8	8.9	7.6
	Al_2O_3	1.1	0.7	1.6	1.5	0.8	1.3	1.3	1.6	1.1	0.9
	SiO_2	49.8	52.2	48.8	51.6	53.4	49.9	54.2	46.3	50.1	53.0
	P_2O_5	4.6	4.5	6.2	4.7	4.3	4.8	5.3	6.6	4.8	4.2
	K_2O	11.6	15.4	18.8	12.9	15.8	11.6	13.0	19.8	11.8	15.9
	CaO	13.4	15.5	14.1	13.9	12.9	12.9	13.8	13.9	13.2	12.9
	MnO	1.4	0.9	0.8	1.1	0.9	1.3	1.0	0.7	1.5	0.9
	Fe_2O_3	0.4	0.3	0.6	0.6	0.2	0.4	0.4	0.9	0.5	0.3
	S	0.2	0.1	nd	0.2	nd	nd	nd	0.1	0.1	0.1
	Cl	0.5	0.3	0.4	0.4	0.4	0.4	0.5	0.3	0.5	0.4
	CuO	1.7	nd	nd	2.5	nd	1.7	nd	2.3	1.6	nd
	PbO	0.3	nd	nd	0.5	nd	nd	nd	0.4	0.2	nd
molar percent	Na_2O	6.1	2.7	2.1	3.2	3.3	6.3	3.3	1.5	5.9	3.4
	MgO	13.5	11.1	9.8	10.9	11.8	13.7	10.8	9.5	13.6	11.8
	Al_2O_3	0.7	0.4	1.0	0.9	0.5	0.8	0.8	1.0	0.7	0.6
	SiO_2	51.3	54.4	52.9	54.2	55.8	51.4	56.5	50.8	51.6	55.4
	P_2O_5	2.0	1.99	2.8	2.1	1.9	2.1	2.3	3.1	2.1	1.9
	K_2O	7.6	10.2	12.9	8.6	10.5	7.6	8.7	13.8	7.8	10.6
	CaO	14.8	17.3	16.3	15.7	14.4	14.4	15.4	16.4	14.5	14.4
	MnO	1.2	0.8	0.8	1.0	0.8	1.2	0.9	0.7	1.2	0.8
	Fe_2O_3	0.2	0.1	0.2	0.2	0.9	0.2	0.1	0.4	0.2	0.1
	S	0.3	0.3	nd	0.4	nd	nd	nd	0.2	0.2	0.1
	Cl	0.8	0.6	0.8	0.8	0.7	0.8	0.8	0.6	0.8	0.7
	CuO	0.1	nd	nd	2.0	nd	1.3	nd	1.9	1.3	nd
	PbO	0.08	nd	nd	0.1	nd	nd	nd	0.1	0.05	nd
other	'SiO_2'	55.4	58.0	58.7	59.0	59.3	55.9	61.3	57.2	55.9	59.1
	'R_2O'	13.0	12.5	13.9	10.7	13.3	13.1	11.1	14.0	12.9	13.4
	'RO'	31.2	29.6	27.2	29.9	27.4	30.9	27.5	28.7	31.0	27.4
	$-\Delta G$	10.00	9.91	11.10	8.98	9.63	10.10	9.00	11.45	10.01	9.71
	NBO	0.84	0.79	0.76	0.77	0.77	0.83	0.72	0.79	0.83	0.77

Table B.18: Composition of the samples from Checkley. NBO is the number of non-bridged oxygen atoms and $-\Delta G$ is expressed in kcal/mol.

	Label	chn31	chn32	chn33	chn34	chs1	chs2	chs3	chs4	chs5	chs6
weight percent	Na_2O	2.9	6.1	1.9	1.9	2.8	2.9	5.1	3.4	2.6	3.3
	MgO	6.6	8.9	5.1	5.4	7.1	7.2	8.1	7.7	6.9	7.3
	Al_2O_3	1.6	1.2	2.0	2.2	0.9	0.8	1.3	0.9	0.9	1.3
	SiO_2	51.3	50.1	47.6	46.0	53.4	52.1	53.1	53.2	53.6	54.4
	P_2O_5	4.9	4.8	5.5	6.4	4.5	4.4	4.7	4.3	4.5	3.9
	K_2O	16.3	11.6	17.6	19.9	14.8	15.3	12.2	15.7	14.7	10.9
	CaO	13.9	13.2	14.2	14.5	15.8	15.6	12.9	12.8	14.6	16.6
	MnO	1.1	1.4	0.8	0.8	0.9	0.9	1.1	0.9	0.8	0.9
	Fe_2O_3	0.6	0.5	1.4	1.4	0.3	nd	0.4	0.3	0.4	0.3
	S	0.1	nd	nd	0.9	0.1	nd	nd	0.6	0.1	nd
	Cl	0.4	0.5	0.4	0.3	0.4	0.4	0.6	0.5	0.4	0.5
	CuO	nd	1.4	0.3	nd	nd	nd	nd	nd	nd	0.4
	PbO	0.2	0.2	3.1	0.7	nd	nd	0.1	nd	nd	nd
molar percent	Na_2O	3.0	6.1	2.1	2.0	2.8	2.9	5.1	3.4	2.6	3.3
	MgO	10.4	13.7	8.5	8.9	10.9	11.1	12.5	12.0	10.9	11.1
	Al_2O_3	0.9	0.7	1.3	1.4	0.6	0.5	0.8	0.6	0.6	0.8
	SiO_2	54.3	51.6	52.8	50.8	55.6	54.2	54.9	55.4	55.9	55.6
	P_2O_5	2.2	2.1	2.6	2.9	1.9	1.9	2.1	1.9	1.9	1.7
	K_2O	10.9	7.6	12.4	14.1	9.9	10.1	8.1	10.4	9.8	7.1
	CaO	15.7	14.6	16.9	17.2	16.4	17.4	14.3	14.3	16.3	18.2
	MnO	0.9	1.2	0.7	0.7	0.8	0.8	1.1	0.9	0.7	0.8
	Fe_2O_3	0.2	0.2	0.6	0.6	0.09	nd	0.2	0.1	0.2	0.1
	S	0.2	nd	nd	0.2	0.1	nd	nd	0.1	0.2	nd
	Cl	0.7	0.8	0.7	0.6	0.8	0.6	0.9	0.8	0.8	0.8
	CuO	nd	1.1	0.3	nd	nd	nd	nd	nd	nd	0.3
	PbO	0.05	0.05	0.9	0.2	nd	nd	0.1	nd	nd	nd
other	'SiO_2'	59.4	56.1	59.8	58.3	59.4	57.8	59.3	59.2	59.9	59.7
	'R_2O'	12.9	12.9	12.7	14.2	12.0	12.6	12.3	13.3	11.8	9.6
	'RO'	27.5	30.9	26.7	27.4	28.5	29.7	28.1	27.5	28.2	30.7
	$-\Delta G$	10.00	10.41	10.53	11.74	9.45	9.95	9.32	9.67	9.30	8.58
	NBO	0.76	0.83	0.74	0.77	0.77	0.80	0.76	0.77	0.75	0.76

Table B.19: Composition of the samples from Checkley. NBO is the number of non-bridged oxygen atoms and $-\Delta G$ is expressed in kcal/mol.

	Label	chs7	chs8	chs9	chs10	chs11	chs12	chs13	chs14	chs15	chs16
weight percent	Na_2O	1.9	3.3	4.7	2.1	2.9	1.9	3.2	3.2	3.2	1.7
	MgO	5.3	6.9	7.8	5.7	7.2	5.4	6.7	7.1	6.7	5.3
	Al_2O_3	2.2	1.5	1.2	2.0	0.7	2.1	1.5	1.4	1.4	2.1
	SiO_2	47.5	53.1	52.1	48.4	51.4	46.0	54.3	52.9	54.1	45.9
	P_2O_5	5.6	5.4	4.7	5.4	4.4	6.4	5.0	5.3	5.2	6.5
	K_2O	17.5	13.1	12.9	17.5	15.6	20.1	12.5	13.2	13.3	20.3
	CaO	14.3	14.4	13.5	15.3	15.8	14.5	14.0	14.6	14.1	14.5
	MnO	0.9	1.1	1.1	2.0	0.8	0.9	1.0	1.2	0.9	0.9
	Fe_2O_3	1.2	0.3	0.3	1.4	0.3	1.3	0.5	0.2	0.3	1.1
	S	nd	nd	nd	0.9	nd	nd	nd	0.1	nd	0.1
	Cl	1.2	0.3	0.3	0.3	0.3	0.4	0.5	0.4	0.4	0.4
	CuO	0.2	nd	0.8	0.1	nd	nd	nd	nd	nd	nd
	PbO	3.0	0.2	nd	0.6	0.2	0.8	0.4	nd	0.1	0.2
molar percent	Na_2O	1.9	3.3	4.7	2.2	2.9	2.1	3.2	3.2	3.2	1.8
	MgO	8.8	10.8	12.1	9.2	11.2	8.8	10.4	10.9	10.4	8.7
	Al_2O_3	1.4	0.9	0.8	1.3	0.5	1.4	0.9	0.8	0.8	1.4
	SiO_2	52.7	55.5	54	52.4	53.6	50.9	56.7	55.2	56.5	50.7
	P_2O_5	2.6	2.4	2.1	2.5	1.9	3.0	2.2	2.4	2.3	3.0
	K_2O	12.4	8.7	8.6	12.1	10.4	14.2	8.3	8.8	8.8	14.3
	CaO	16.9	16.1	15.0	17.7	17.7	17.1	15.7	16.4	15.8	17.2
	MnO	0.8	0.9	0.9	0.9	0.7	0.8	0.9	1.0	0.9	0.9
	Fe_2O_3	0.5	0.1	0.1	0.6	0.1	0.5	0.2	0.09	0.1	0.5
	S	nd	nd	nd	0.2	nd	nd	nd	0.2	nd	0.2
	Cl	0.6	0.8	0.8	0.5	0.6	0.6	0.9	0.8	0.8	0.7
	CuO	0.2	nd	0.6	0.1	nd	nd	nd	nd	nd	nd
	PbO	0.9	0.07	nd	0.2	0.06	0.2	0.1	nd	0.04	0.2
other	'SiO_2'	59.6	60.3	58.3	59.0	57.1	58.1	61.5	59.8	61.2	57.8
	'R_2O'	12.5	10.9	12.4	12.5	12.7	14.3	10.4	11.1	11.1	14.3
	'RO'	26.9	28.3	28.9	28.2	30.0	27.1	27.6	28.6	27.4	27.3
	$-\Delta G$	10.60	9.27	9.61	10.67	10.16	11.80	8.69	9.38	9.05	11.84
	NBO	0.75	0.73	0.78	0.76	0.81	0.77	0.72	0.75	0.72	0.77

Table B.20: Composition of the samples from Checkley. NBO is the number of non-bridged oxygen atoms and $-\Delta G$ is expressed in kcal/mol.

	Label	chs17	chs18	chs19	chs20	chs21	chs22	chs23	chs24	chs25	chs26
weight percent	Na_2O	2.8	1.9	5.2	3.6	1.7	5.4	2.2	1.8	3.4	3.5
	MgO	7.1	5.5	7.9	7.0	5.6	9.0	6.0	5.6	7.1	7.0
	Al_2O_3	0.7	2.1	1.3	1.4	1.9	1.3	1.5	1.9	1.3	1.6
	SiO_2	51.6	46.2	53.1	54.1	47.8	52.8	49.0	48.0	53.8	56.7
	P_2O_5	4.6	6.4	4.7	5.5	6.2	4.5	5.9	5.9	5.5	4.6
	K_2O	15.7	20.1	12.4	13.1	19.2	10.3	18.7	19.0	13.1	12.2
	CaO	15.8	14.4	12.9	13.0	14.9	14.1	14.4	14.9	13.4	12.2
	MnO	0.9	0.9	1.1	1.0	0.9	1.1	0.9	0.9	1.0	0.9
	Fe_2O_3	0.2	1.1	0.5	0.4	0.9	0.4	0.4	0.7	0.4	0.3
	S	0.1	0.2	0.1	nd	0.2	nd	nd	0.1	0.1	nd
	Cl	0.3	0.3	0.6	0.5	0.4	nd	0.4	0.5	0.4	0.5
	CuO	nd	nd	nd	nd	nd	0.1	nd	nd	nd	nd
	PbO	nd	nd	nd	nd	nd	nd	nd	nd	nd	0.2
molar percent	Na_2O	2.9	1.9	5.2	3.6	1.8	5.4	2.3	1.9	3.4	3.5
	MgO	11.1	9.0	12.3	10.9	9.1	13.7	9.7	9.1	11.1	10.9
	Al_2O_3	0.4	1.4	0.8	0.9	1.2	0.8	0.9	1.2	0.8	0.9
	SiO_2	53.8	50.9	54.8	56.5	51.9	53.8	52.8	52.1	56.2	58.9
	P_2O_5	2.0	2.9	2.0	2.4	2.8	1.9	2.7	2.8	2.4	2.0
	K_2O	10.4	14.1	8.2	8.7	13.3	6.7	12.8	13.2	8.7	8.1
	CaO	17.6	16.9	14.3	14.6	17.4	15.4	16.6	17.3	15	13.6
	MnO	0.8	0.9	0.9	0.9	0.8	0.9	0.8	0.8	0.9	0.8
	Fe_2O_3	0.1	0.5	0.2	0.2	0.4	0.2	0.2	0.3	0.2	0.1
	S	0.2	0.3	0.2	nd	0.3	nd	nd	0.2	0.2	nd
	Cl	0.6	0.6	0.9	0.9	0.7	nd	0.07	0.8	0.8	0.8
	CuO	nd	nd	nd	nd	nd	0.1	nd	nd	nd	nd
	PbO	nd	nd	nd	nd	nd	nd	nd	nd	nd	0.1
other	'SiO_2'	57.3	58.0	59.3	61.4	58.3	58.1	58.2	58.3	61.0	63.5
	'R_2O'	12.9	14.3	12.4	11.4	13.7	11.2	14.0	13.7	11.3	10.6
	'RO'	29.8	27.4	27.9	26.8	27.7	30.4	27.5	27.6	27.5	25.7
	$-\Delta G$	9.34	11.8	9.34	9.03	11.28	9.27	11.10	11.2	9.12	8.06
	NBO	0.81	0.77	0.76	0.71	0.79	0.79	0.77	0.77	0.72	0.72

Table B.21: Composition of the samples from Checkley. NBO is the number of non-bridged oxygen atoms and $-\Delta G$ is expressed in kcal/mol.

	Label	chs27	chs28	chs29	chs30	chs31	chs32
weight percent	Na_2O	3.8	1.8	3.3	2.8	2.1	3.4
	MgO	7.9	5.6	7.1	7.0	6.1	7.2
	Al_2O_3	1.3	1.9	1.2	0.9	1.5	1.5
	SiO_2	52.2	48.2	52.9	53.6	49.0	54.7
	P_2O_5	5.5	6.0	5.5	4.4	5.9	4.6
	K_2O	13.0	19.1	13.2	14.6	18.4	12.3
	CaO	13.9	14.8	14.5	14.8	14.4	13.9
	MnO	1.0	0.9	1.2	0.8	0.9	1.1
	Fe_2O_3	0.4	0.7	0.3	0.3	0.5	0.4
	S	0.1	0.1	nd	0.1	0.1	0.1
	Cl	0.5	0.3	0.5	0.4	0.3	0.4
	CuO	nd	nd	nd	nd	nd	nd
	PbO	nd	0.2	nd	nd	0.3	nd
molar percent	Na_2O	3.8	1.9	3.3	2.9	2.2	3.4
	MgO	12.2	9.1	10.9	10.9	9.8	11.2
	Al_2O_3	0.8	1.2	0.8	0.6	0.9	0.9
	SiO_2	54.3	52.3	55.3	55.7	52.8	56.6
	P_2O_5	2.4	2.8	2.4	1.9	2.7	2.0
	K_2O	8.6	13.2	8.8	9.7	12.7	8.1
	CaO	15.6	17.2	16.2	16.5	16.6	15.5
	MnO	0.9	0.8	1.0	0.7	0.9	0.9
	Fe_2O_3	0.2	0.3	0.1	0.1	0.2	0.2
	S	0.1	0.3	nd	0.2	0.3	0.1
	Cl	0.9	0.6	0.8	0.7	0.6	0.8
	CuO	nd	nd	nd	nd	nd	nd
	PbO	nd	0.06	nd	nd	0.09	nd
other	'SiO_2'	59.2	58.7	60.0	59.5	58.4	61.2
	'R_2O'	11.5	13.6	11.3	12.0	13.8	10.6
	'RO'	29.1	27.6	28.6	28.4	27.8	28.1
	$-\Delta G$	9.62	11.20	9.38	9.35	10.95	8.69
	NBO	0.76	0.76	0.74	0.76	0.77	0.73

Table B.22: Composition of the samples from Checkley. NBO is the number of non-bridged oxygen atoms and $-\Delta G$ is expressed in kcal/mol.

Appendix C

Sample Description Tables

This appendix contains descriptions of each of the samples analysed. The following abbreviations are used to identify the decay product:

G gypsum

C calcite

S hydrated silica

Y syngenite

Q quartz

A anhydrous calcium sulphate

– unknown

and these abbreviations represent the decay type:

P micropitted

IP isolated pits

MP merged pits

TP totally pitted

U uniformly weathered

D durable

A altered (artificial deterioration)

L biological organisms present.

If the glass was of unknown date then this is represented by a ? in the century column.

Label	Century	Colour	Description	Outer Surface		Inner Surface	
				Type	Product	Type	Product
scb1	14	pale green-/colourless	thick white deposit on one side	U	C,S	P	none
scb2	14	pale green-/colourless	both sides are crusted (though it has the appearance of plaster)	U	C,G	U	C,G
scb3	14	pale green-/colourless	as for scb2	U	C,G	U	C,G
scb4	14	pale green-/colourless	as for scb2	U	C,S	U	C,G
scb5	14	pale green-/colourless	as for scb2	U	C,Q,G	U	C,G
scb6	14	pale green-/colourless	unusual sample with a shiny crust that looks false	U	S	U	S,G
ely1	?	amber	very large, one side covered in strongly adhered white powder;other polished	A	none	U	S,A,C
ely2	?	colourless	a thick white crust on both sides	U	G,Y,S	U	G,S
ely3	?	colourless	one surface highly polished	A	none	MP	G
ely4	?	colourless	the surfaces have an etched look	U	S	U	S
ely5	?	yellow	paint work in good condition	TP	G,Y	U	none
ely6	?	yellow	one side has been polished	A	none	TP	none
ely7	?	ruby	one surface looks etched	U	none	U	none
ely8	?	ruby	a very thick uneven piece, with smooth shiny surface	MP	none	A	none
ely9	?	ruby	outer surface has an etched look	MP	G,S	U	none
ely10	?	pale green-/colourless	white crust on both surfaces	U	G,Y	U	none

Label	Century	Colour	Description	Outer Surface		Inner Surface	
				Type	Product	Type	Product
ely11	?	pale green-/colourless	very thick sample, no products	TP	none	U	none
ely12	?	pale green-/colourless-with stain	most of the natural surface has been removed	TP	C,S	U	none
ely13	?	pale green-/colourless	one side highly polished, the other micropitted	A	none	IP	none
gmh1	14	pale green-/colourless	shallow pits containing loose white powder on one side, no evidence of paintwork	U	C	MP	S,C
gmh2	14	ruby	paintwork intact, isolated deep pits on other surface	IP	G,S	D	none
gmh3	14	pink	a dull white coating on painted side, deep small but merged pits on the other	MP	C,S	U	none
gmh4	14	pale green-/colourless	shallow pits on outer surface, pitting along the edge of paint lines on the inner surface	IP	S	MP	C,S
gmh5	14	colourless	the outer surface mainly pitted with yellow deposits; the inner surface has well preserved paintwork	MP	S	P	none
gmh6	14	pale yellow	deep pits, 1-2mm in diameter, on the outer surface;inner paintwork intact	IP	S	D	none
gmh7	14	pink	the deposit is a golden colour, with the inner surface having micropits present	MP	S	P	none
gmh8	14	pink	as for sample gmh7	MP	S	P	none

Label	Century	Colour	Description	Outer Surface		Inner Surface	
				Type	Product	Type	Product
gmh9	14	pink	this is a foot-shaped piece with the ankle showing particularly extensive decay. A white deposit is present on the inner surface	MP	S	IP	none
gmh10	14	colourless	some of the pits have merged into lines	MP	S	P	S
gmh11	14	ruby	as for gmh10	MP	S	MP	none
gmh12	14	green	some iridescence present on outer surface	MP	S	P	none
gmh13	14	green	the outer surface has a region of isolated and shallow pits	MP	S	P	none
gmh14	14	colourless	white deposit on inner surface near paint lines	MP	S,C	P	S
gmh15	14	colourless	specimen appears to have been painted on both sides, both have only micropitting present	IP	none	P	none
gmh16	14	colourless	as for gmh15	IP	S	P	none
gmh17	14	colourless	as for gmh15, but also the outer surface is dulled	MP	S	P	none
gmh18	14	blue	shiny inner surface; micropits in the back paint	IP	S	P	none
gmh19	14	blue	as for gmh18	IP	none	P	none
lhe1	14	blue	deep pits 2mm in diameter in outer surface	IP	G,S	P	none
lhe2	14	blue	inner surface dulled, whereas the outer has a frosted look	IP	S,G	P	none
lhe3	14	colourless	inner surface has an orange deposit in the paint work; the other side is dulled	D	none	TP	S

Label	Century	Colour	Description	Outer Surface		Inner Surface	
				Type	Product	Type	Product
lhe4	14	colourless	outer surface pitted becoming more isolated as the surface is traversed. The inner surface has only the paint intact	TP	none	TP	G,S
lhe5	14	yellow	deep pits (3mm in diameter) on outer surface containing grey deposit	MP	G,S	U	none
lhe6	14	colourless	inner surface is dulled; the outer has a white deposit	IP	S,Y	P	none
lhe7	14	ruby	great loss of surface, the pits up to 3 mm deep	TP	G,S	U	none
lhe8	14	ruby	as for lhe7	TP	G,S	P	none
lhe9	14	green	pits are 2mm deep and up to 3mm in diameter and contain white deposit	TP	G,S	P	none
lhe10	14	ruby	one surface eaten away completely and covered in dust;the other coated in cream deposit	U	G,S	U	none
lhe11	14	blue	one surface shiny	D	none	D	none
lhe12	14	yellow	no original inner surface remaining; outer surface covered in white deposit	TP	Y,G,S	U	none
lhe13	14	ruby	inner pits cluster round paint edge; outer ones up to 1mm in diameter	IP	G,S	MP	none
lhe14	14	colourless	pits are 1mm deep	TP	G,S	TP	none
lhe15	14	ruby	pits contain white deposit	TP	G,S	U	none
lhe16	14	ruby	red glass more decayed than the colourless	U	G,S	U	none
lhe17	14	green	inner surface is frosted; the outer is a flaky crust	U	G,S	A	none

Label	Century	Colour	Description	Outer Surface		Inner Surface	
				Type	Product	Type	Product
lhe18	14	yellow	paint work in good condition; extensive white deposit on the outer surface	TP	G,S	TP	none
lhe19	14	blue	the inside shiny; some of the paint has decayed	MP	none	A	none
lhe20	14	yellow	deep pits on inner surface contain unremovable white deposit	TP	G,S	TP	none
lhe21	14	green	small region of micropits on inner surface; the outer having pits up to 1mm in diameter beginning to merge	IP	Y,G,S	P	none
lhe22	14	colourless	small white deposit on inner surface, too little to enable identification	IP	none	MP	none
lhe23	14	colourless	outer surface had a slight frosted look	U	none	TP	G,S
lhe24	14	blue	a shiny inner surface; micropitting on the outer	IP	none	TP	none
lhe25	14	yellow	white deposit from near the paint edges on outer surface	IP	G,S	P	none
fai1	16	colourless	inner surface is shallow pitted	D	none	IP	G,C
fai2	16	colourless	micropitting on both sides	P	G,C	P	C,S
fai3	16	colourless	glossy surfaces with scratches	P	G,Y,S	D	none
fai4	16	green	most of the surface is pitted or covered in white deposits	MP	C,G	U	C,S
fai5	16	yellow	white deposits in pits	IP	none	P	G,S
fai6	16	colourless	badly deteriorated at one edge due to water retention	U	G,C	U	none

Label	Century	Colour	Description	Outer Surface		Inner Surface	
				Type	Product	Type	Product
fai7	16	colourless	covered in loose brown powder	U	G,Y	U	G,Y
fai8	16	colourless	shallow pits	MP	G,Y	D	none
fai9	16	colourless	pits are deep in the stained area, shallow elsewhere	U	G,Y	P	G,Y,S
fai10	16	blue	outer surface still glossy	IP	none	MP	G,S
fai11	16	blue	shallow pits with white irremivable, deposit within	IP	none	MP	none
fai12	16	blue	as for fai11	IP	none	U	none
fai13	16	green	merged pits 1mm in diameter	MP	none	P	none
fai14	16	blue	much of the paint work is missing	IP	none	P	none
fai15	16	yellow	back painted and both surfaces dulled	IP	none	U	none
fai16	16	ruby	inner surface appears etched	IP	none	P	none
fai17	16	purple	shallow pits containing irremovable white dcposit	IP	none	IP	none
fai18	16	ruby	many surface scratches	IP	none	U	none
fai19	16	yellow	pits cluster around lead edge	IP	none	IP	none
fai20	16	green	paints on inner surface are within paint only	MP	none	TP	none
fai21	16	purple	outer surface has deep pits (1-2mm in diameter)	TP	G,S	P	none
fai22	16	colourless	no evidence of decay	D	none	D	none
fai23	16	green	shallow pitting on both sides	MP	S,C	P	none
fai24	16	colourless	white/yellow deposit in the pits	TP	S	P	S,G
fai25	16	blue	micropitting near paint; grey crust on other side	U	G,S	P	none
fai26	16	colourless	deep pits with yellow deposit on outer surface	IP	G	P	S

Label	Century	Colour	Description	Outer Surface		Inner Surface	
				Type	Product	Type	Product
fai27	16	colourless	flaking paint and beginnings of micropits on inner surface	MP	S,Y	P	none
fai28	16	green	white crust on outer, micropits and dulling to inner	U	none	TP	S,C
fai29	16	ruby	grey crust and deep pits with yellow deposit	MP	S	U	G,S
fai30	16	murray	both surfaces dulled	D	none	P	none
fai31	16	blue	as for fai30	P	none	U	G,Y
fai32	16	ruby	deep pits through to the colourless base from red flashed glass	TP	G	U	none
fai33	16	colourless	grey crust on painted side	IP	none	U	G
fai34	16	yellow	2mm deep pits on outer; thick grey crust on other	MP	S	U	C,G
fai35	16	colourless	pits 1mm deep; crust is grey	TP	G	U	C
fai36	16	purple	surface scratches; shiny inner surface where there is no crust	IP	none	U	G
fai37	16	ruby	crust is flaky, inner surface slightly iridescent	U	C,S	MP	G,S
fai38	16	colourless	totally pitted with occasional deposit	TP	S,C	U	G,Y
fai39	16	blue	flaky crust, yellow deposit in the pits	U	S,C	TP	G,S
fai40	16	colourless	as above	TP	S,C	U	G
fai41	16	colourless	as above except inner surface is dulled	TP	S,C	P	none
fai42	16	blue	as for fai41	D	none	U	G
fai43	16	green	grey crust, one side flakly green matter– could be paintwork	U	G	U	none
fai44	16	colourless	crust is grey, pits contain yellow powder	TP	S	U	G

Label	Century	Colour	Description	Outer Surface		Inner Surface	
				Type	Product	Type	Product
fai45	16	ruby	deep pits, grey crust	TP	S	U	G,S
fai46	16	blue	as above	TP	S	U	G,Y
fai47	16	blue	as above	TP	G	U	G,Y
fai48	16	green	flashed glass, burnt look to green surface layer	U	G	U	none
fai49	16	colourless	grey crust, isolated pits are deep-merged ones shallow	MP	S	U	G,Y
fai50	16	colourless	thick white deposit on outer surface	TP	S	P	none
fai51	16	pink	iridescent outer surface; thin grey crust on other	TP	S	U	G,Y
fai52	16	yellow	grey crust, 1-3mm diameter pits on other	MP	S	U	G,Y
fai53	16	yellow	as above	MP	S,Y	U	G
fai54	16	pink	no deposit in pits, thick grey crust	MP	none	U	G,Y
fai55	16	colourless	no natural outer surface left	TP	S,Y	U	none
fai56	16	colourless	merged pits run along a paint line	MP	S,Y	U	none
fai57	16	pale blue	some iridescence to outer surface	D	none	U	S,C,Y
fai58	16	pink	thin grey crust, iridescent outer surface	D	none	U	G
fai59	16	amber	deep pits in outer; 2mm crust on other	TP	S	U	G,Y
fai60	16	colourless	thin grey crust on inner, covering the paint	TP	S	U	G
fai61	16	pale blue	deep pits form a channel	TP	S,Y	U	G
fai62	16	colourless	thick white deposit in pits,crust is thin and grey	TP	S,Y	U	G,Y
fai63	16	colourless	as above	TP	S,Y	U	G,Y
fai64	16	ruby	decay as above, flashed red but appears false	MP	S,Y	U	G,Y

Label	Century	Colour	Description	Outer Surface		Inner Surface	
				Type	Product	Type	Product
fai65	16	pink	sparse amount of decay products	MP	G,C	U	C,G
fai66	16	pale blue	inner is shiny in places; merged pits form channels	MP	S	U	S,Y
chk1n	14	yellow	orange/white deposit on outer; pits on inner almothst form a crust	TP	G	TP	none
chk2n	14	colourless	yellow/green coating on inner; etched look to outer	U	G	L	G,S,C,-
chk3n	14	ruby	pits 1mm in dianeter, with white deposit	MP	G,S	P	none
chk4n	14	colourless	yellow/green covering on inner; white deposit in pits	U	G,S	L	G,S,C,-
chk5n	14	ruby	green coating on top of pits	U	G,S	L	C,G,S,-
chk6n	14	yellow	outer surface covered in loose orange powder; inner has shallow micropits	U	G,S	TP	none
chk7n	14	colourless	inner surface is dulled; white deposit in pits	IP	G	P	none
chk8n	14	ruby	fine white crust on both sides	U	G,S	U	none
chk9n	14	ruby	green coating on inner; thick white deposits on outer	MP	G,C	L	G,S,C,-
chk10n	14	ruby	fine grey crust on outer, orange on inner	U	G	U	none
chk11n	14	blue	inner has samll region of undecayed surface; inner covered in grey/yellow growth	U	none	U	G
chk12n	14	yellow	yellow/green coating to inner, orange powder on outer	U	G,S	L	G,S,C,-
chk13n	14	blue	inner as above; outer dulled	MP	none	L	none

Label	Century	Colour	Description	Outer Surface		Inner Surface	
				Type	Product	Type	Product
chk14n	14	turquoise	inner as above; outer thick with white deposit	U	G,S	L	G,S,C,-
chk15n	14	ruby	very little natural surface left; yellow/green growth	TP	G,S	L	G,C,S,-
chk16n	14	colourless	dark green on inner; outer looks as though crust removed	TP	none	L	none
chk17n	14	yellow	green/yellow growth on inner; orange powder on outer	U	S	L	S
chk18n	14	ruby	as above	U	S,G	L	G,S,C,-
chk19n	14	colourless	outer has a worn-smooth appearance, small amount of white deposit	P	G,S	L	G,S,C,-
chk20n	14	colourless	yellow/green growth on inner, orange/white deposit on outer	TP	G,S	L	G,S,C,-
chk21n	14	green	grey crust on both sides	U	G,S	U	none
chk22n	14	yellow	yellow/green growth, orange powder on outer	U	S	L	G,S,C,-
chk23n	14	ruby	as above	U	C,G	L	C,S,-
chk24n	14	green	no product in the pits; dulled inner	MP	none	L	G,S,C,-
chk25n	14	yellow	orange powder on outer	TP	C,S	U	none
chk26n	14	green	grey/green growth on inner, grey crust onouter	U	none	L	none
chk27n	14	colourless	yellow/green growth on inner; white deposit in deep pits	IP	G,Y,S	P	none
chk28n	14	green	loosely attached fine powder on both sides, but not enough for analysis	U	none	U	none
chk29n	14	green	grey crust on both sides	U	G	U	none

Label	Century	Colour	Description	Outer Surface		Inner Surface	
				Type	Product	Type	Product
chk30n	14	yellow	yellow/green growth on inner; orange powder on outer	U	G,S	L	G,S,C,-
chk31n	14	ruby	deep pits with white deposit in them	TP		L	G,S,C,-
chk32n	14	green	yellow/green growth on inner; no natural outer surface left	U	none	L	none
chk33n	14	blue	green growth on inner; dulled outer	TP	G,S	L	none
chk34n	14	turquoise	green growth on inner, grey crust onouter	U	G,S	L	none
chk1s	14	colourless	paint is proud of inner surface, orange deposit in pits	MP	S	TP	none
chk2s	14	yellow	paint beginning to decay, fine orange crust on outer	U	C,S	IP	S,G
chk3s	14	ruby	white deposit in pits	TP	S,G	TP	G,Y
chk4s	14	yellow	micropitting on inner; no natural outer surface left	TP	S	P	none
chk5s	14	colourless	inner is shiny in parts; deep pits in outer	TP	S,G	MP	none
chk6s	14	ruby	inner is dulled	IP	G,S	IP	none
chk7s	14	blue	paint is intact, pits shallow	U	S,G	TP	C
chk8s	14	colourless	inner surface has a frosted look; outer covered in flaky orange crust	U	G,C	U	none
chk9s	14	ruby	orange crust on both sides	U	G	U	none
chk10s	14	blue	grey powder on both sides	U	none	U	none
chk11s	14	yellow	as for chk9s	U	G	U	C
chk12s	14	blue	grey crust on inner; orange on outer	U	none	U	G,Y,S
chk13s	14	ruby	white deposit in pits	IP	C,G	U	S,C
chk14s	14	colourless	grey crust on outer, inner paint decayed	U	G,Y	U	none

Label	Century	Colour	Description	Outer Surface		Inner Surface	
				Type	Product	Type	Product
chk15s	14	ruby	micropits on inner; grey crust on other	U	G	MP	none
chk16s	14	blue	cream coating on outer, dulled inner surface	U	G,S	U	none
chk17s	14	yellow	most of paint removed; orange crust on outer	U	G	TP	none
chk18s	14	blue	grey dust on inner; thick cream crust on outer	U	G,C	U	none
chk19s	14	ruby	flaky orange crust on outer	U	G	U	none
chk20s	14	colourless	inner pits filled with green growth	TP	S	TP	none
chk21s	14	ruby	outer crust appeared to be plaster	U	S,G	U	none
chk22s	14	colourless	crust on inner runs along centre of sample	TP	G,S	U	S
chk23s	14	ruby	orange crust on outer; fine dust on inner	U	G,S	U	none
chk24s	14	ruby	as above	U	G,S	U	none
chk25s	14	colourless	conchoidal fracture at one end; frost like outer surface	TP	none	MP	none
chk26s	14	colourless	micropitting on inner; iridescent outer	IP	none	P	none
chk27s	14	colourless	orange crust on outer; paint intact on inner	U	G,S	TP	G,C,S
chk28s	14	ruby	greyish dust on inner; white crust on outer	U	G,S	U	none
chk29s	14	colourless	paint 2mm proud of surface, white deposit in pits	TP	S,Y	MP	none
chk30s	14	colourless	white and yellow deposit in pits	TP	G,S	TP	G,S
chk31s	14	ruby	grey dust on inner; orange crust on outer	U	G,S	U	none
chk32s	14	colourless	inner surface dulled, white crust on outer	U	C,G	D	none
fle1	14	colourless	average pit diameter 3mm	TP	S	P	none

Label	Century	Colour	Description	Outer Surface		Inner Surface	
				Type	Product	Type	Product
fle2	14	colourless	white deposit in pits	TP	S,Y	P	none
fle3	14	colourless	as above	TP	S,Y	P	none
fbn1	14	grey	outer covered in green growth	L	G,S,-	U	G,Y
fbn2	14	grey	as above	L	G,S,-	U	G,S
fbn3	14	grey	as above	L	G,S,-	U	G,S
fbs1	14	colourless	grey/white crust on outer; orange on inner, but broken into four pieces	U	G,S	U	G
fbs2	14	colourless	as above, eight pieces	U	G,S	U	G
fbs3	14	colourless	as above,two pieces	U	G,Y	U	G,S
fbs4	14	colourless	as above, not broken	U	G,Y	U	G,S
fbs5	14	colourless	as above	U	G,Y	U	G,S
fbs6	14	colourless	as above	U	G,Y	U	G,S
fbs7	14	colourless	as above	U	S,Y	U	G,S
fbs8	14	colourless	as above	U	G,Y,S	U	G,S

Table C.1: Description of the samples.

Glass Corrosion